



Ecole doctorale 398 - Géosciences, ressources naturelles et environnement
(GRNE)

THÈSE DE DOCTORAT DE SORBONNE UNIVERSITÉ

Spécialité : Géophysique

Sujet de la thèse :

Monitoring the remediation of coal tar in contaminated soil using electro-geophysical methods

**(Surveillance de la dépollution du goudron de houille dans le sol contaminé à
l'aide de méthodes électro-géophysiques)**

Présentée par

Mohammad Ali IRAVANI

Soutenue le 30 janvier 2020

Devant le jury composé de :

Myriam SCHMUTZ	Professeure à Bordeaux INP	Rapporteure
Frédéric NGUYEN	Professeur à l'Université de Liège	Rapporteur
Loïc LABROUSSE	Professeur à Sorbonne Université	Examineur
Vincent ALLEGRE	Maître de Conférences à l'Université de Bordeaux	Examineur
Roger GUÉRIN	Professeur à Sorbonne Université	Directeur
Alexis MAINEULT	Chargé de Recherche au CNRS	Co-directeur
Jacques DEPARIS	Ingénieur de Recherche au BRGM	Co-encadrant
Hossein DAVARZANI	Ingénieur de Recherche au BRGM	Co-encadrant

Résumé étendu

Au cours des deux dernières décennies, la dépollution et la surveillance des sites pollués sont devenus une question sociétale importante. Les réglementations sanitaires et environnementales dans les pays développés et en développement sont plus restrictives en ce qui concerne les sites pollués. L'étude des facteurs contribuant à la pollution et à la dépollution est utile pour la protection de l'environnement et de la santé. Les techniques classiques de surveillance par piézomètres et piézajirs ne suffisent pas pour suivre les changements caractéristiques dans le sous-sol de ces sites en raison de leur caractère ponctuel. Par conséquent, des techniques géophysiques permettant notamment un maillage spatial fin, sont nécessaires pour caractériser et suivre ces sites.

Ainsi l'interprétation de données géophysiques acquises lors de la surveillance de tels sites est un outil pour la dépollution de leurs sols. Les propriétés géophysiques sont des paramètres clés dans la validation des méthodes de dépollution des sols contaminés par des produits chimiques organiques et industriels, comme les hydrocarbures lourds, DNAPL ('Dense Non-Aqueous Phase Liquids' en anglais). Parmi les techniques géophysiques pouvant être utilisées pour suivre les propriétés physiques des sites contaminés, les méthodes électriques et électromagnétiques se sont révélées être des techniques de surveillance fiables fournissant des informations sur la résistivité électrique et la permittivité diélectrique reliées aux propriétés physiques et hydrodynamiques du milieu. Les méthodes électromagnétiques ont déjà été utilisées dans de nombreuses études, pour la caractérisation du milieu environnant peu profond et pour la détection des hydrocarbures légers, LNAPL ('Light Non-Aqueous Phase Liquids' en anglais).

L'objectif principal de cette thèse est d'évaluer la capacité des méthodes électromagnétiques afin de suivre le processus de dépollution dans des sols contaminés par des DNAPL, via l'utilisation en laboratoire des méthodes de SIP ('Spectral Induced Polarization' en anglais, polarisation provoquée spectrale ou dans le domaine fréquentiel en français) et TDR ('Time Domain Reflectometry' en anglais) dans des milieux poreux contaminés, ces méthodes mesurant ces propriétés électromagnétiques.

Les principales questions posées sont :

- Q1 : Est-ce que les méthodes électromagnétiques peuvent suivre la dynamique de DNAPL ?

- Q2 : Quels sont les impacts de la température sur la résistivité électrique complexe et sur la permittivité diélectrique relative des milieux poreux saturés avec un écoulement multi-phasique non isotherme ? La réponse à cette question peut permettre d'évaluer l'efficacité des mesures électromagnétiques pour suivre la remédiation d'un sol contaminé au DNAPL avec une technique de récupération des polluants améliorée par la chaleur.
- Q3 : Comment la résistivité électrique et la permittivité diélectrique d'un milieu poreux multi-phasique changent-elles lorsque la saturation d'une phase change dans un système isotherme ? La réponse à cette question doit permettre d'évaluer lors de l'assainissement des sols, la qualité de l'élimination des DNAPL en raison de leur résistivité électrique élevée et de leur faible permittivité diélectrique qui entraîne une variation de ces deux propriétés électromagnétiques du milieu.

Pour atteindre les objectifs de cette étude, il est important de comprendre les aspects environnementaux et théoriques de la dépollution ainsi que leurs avantages et limites. L'utilisation de la géophysique permet d'accroître la précision du processus d'assainissement et de réduire les coûts de dépollution. Dans de nombreux travaux précédents, les interactions entre les DNAPL et différents fluides ont été étudiées et une étude des effets de la température et de la saturation sur les paramètres géophysiques peut être très utile pour caractériser les propriétés du sol au cours du processus de remédiation. Les variations de température dans un sol contaminé modifient la résistivité électrique complexe et la permittivité diélectrique relative du sol en raison de leurs effets sur les propriétés physico-chimiques du sol, de l'eau et des polluants dans le sol. En prenant en compte les variations et les effets de ces paramètres, on peut améliorer la précision de la méthode en abordant les questions susmentionnées.

Des modèles empiriques sont proposés afin d'estimer la teneur en DNAPL en fonction de la saturation et de la température, avant, pendant et après le processus de dépollution. En utilisant la méthode de SIP basée sur les mesures des variations de résistivité complexe dans le sol, la procédure de remédiation sera validée. L'autre méthode géophysique utilisée est la TDR qui a été développée pour mesurer la permittivité diélectrique relative, la teneur en eau dans des milieux poreux homogènes ou hétérogènes.

La méthode de dépollution que nous considérons ici est la récupération améliorée du CT ('coal tar' en anglais, goudron de houille en français) par chauffage par conduction, au moyen de la technique de « pompage et traitement » pour extraire et éliminer le CT des sols pollués. Selon les principes rhéologiques, lorsque la température augmente, la viscosité diminue et la mobilité des polluants augmente. L'excavation, le transport et le chauffage du sol en font une

technique coûteuse mais abordable dans de nombreux projets de restauration des sols contaminés.

Les résultats de nos mesures de laboratoire utilisés pour modéliser la dépendance en température de la résistivité complexe et de la permittivité relative, pourront ainsi être appliqués aux mesures de terrain. La gamme de température utilisée en laboratoire englobe la gamme qui sera mise en œuvre sur le terrain : 50°C comme température maximale correspondant à la température maximale de chauffage sur le terrain, 20°C comme température minimale correspondant à une valeur inférieure à celle employée sur le terrain. Les variations de saturation en eau et en DNAPL ont un impact plus important sur la résistivité et la permittivité que la température. Après le pompage des DNAPL dans les sols contaminés, les variations de résistivité et de permittivité du sol sont dues aux variations de température et de saturation.

Les différents dispositifs expérimentaux ont été conçus pour étudier les effets de la température (chauffage) et de la saturation (drainage et imbibition) sur la résistivité électrique complexe et la permittivité diélectrique relative d'un milieu poreux saturé en conditions isothermes sur différentes colonnes 1D (Fig. I). Les mesures ont été effectuées avec différents couples de polluants et de fluides : CT+water ('water' en anglais), CS ('chlorinated solvent' en anglais, solvant chloré en français)/eau, et CO ('canola oil' en anglais, huile de colza en français)/SE ('salty ethanol' en anglais, éthanol salé en français) dans un milieu poreux simulé avec des GB ('glass beads' en anglais, billes de verre en français) de 1 mm de diamètre.

Les résultats montrent que la composante réelle de la permittivité diélectrique relative de l'eau (respectivement des deux types de DNAPL, CT et CS) diminue (respectivement augmente) linéairement lorsque la température augmente que ce soit en présence ou en absence de phase solide (Fig. II). Sur la figure II, l'effet de la variation de température sur la permittivité relative des DNAPL dans un milieu poreux (GB+CT et GB+CS) est le même que pour les DNAPL purs. Cependant, après l'imbibition (92% d'eau et 8% de DNAPL), la permittivité relative des échantillons de CS n'est pas la même que celle de CS pur, contrairement au CT.

L'amplitude et le déphasage de la résistivité électrique de l'eau et des deux types de DNAPL diminue avec l'augmentation de la température, que ce soit en présence ou en absence de phase solide (Fig. III). Les données expérimentales sur la résistivité électrique complexe et la permittivité diélectrique relative sont cohérentes avec les modèles empiriques. Les modifications des paramètres Cole-Cole en fonction de la température ont également été abordées dans cette étude. Les spectres montrent qu'avec une augmentation de température, la résistivité du CT diminue, en présence ou en absence de phase solide. Il a été constaté que la différence de résistivité était plus significative pour les basses fréquences que pour les hautes

fréquences. Les spectres de phase avec et sans phase solide montrent que l'augmentation de la température décale la courbe en cloche du spectre à une fréquence plus élevée.

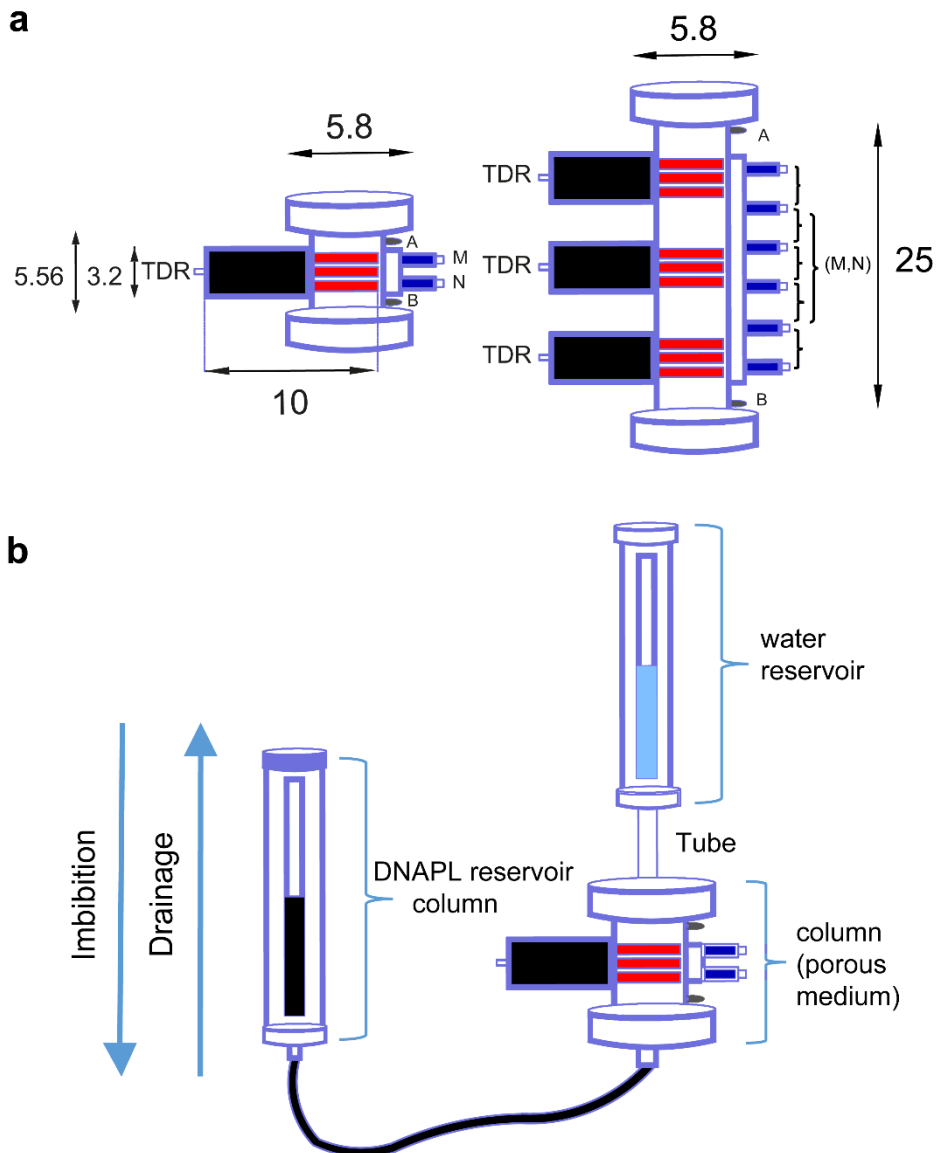


Fig. 1 : Schéma du montage expérimental (les longueurs sont en cm). a) Géométrie d'une cellule et d'une colonne avec la position des électrodes : TDR, d'injection de courant (A et B) et de mesure du potentiel (M et N). Chaque accolade indique une mesure dans un échantillon. b) Montage expérimental comprenant des réservoirs et des échantillons d'eau et de DNAPL

Le chauffage du milieu réduit la viscosité des polluants, ce qui augmente le taux de récupération des polluants dans un sol saturé. L'étude des paramètres géophysiques au cours de cette opération est influencée par deux paramètres environnementaux : la température due au réchauffement du sol et le changement de saturation dû au pompage des polluants. Dans un premier temps, les paramètres géophysiques sont corrigés des effets de la température. L'étape suivante consiste à trouver la relation entre les paramètres géophysiques et la saturation. Les

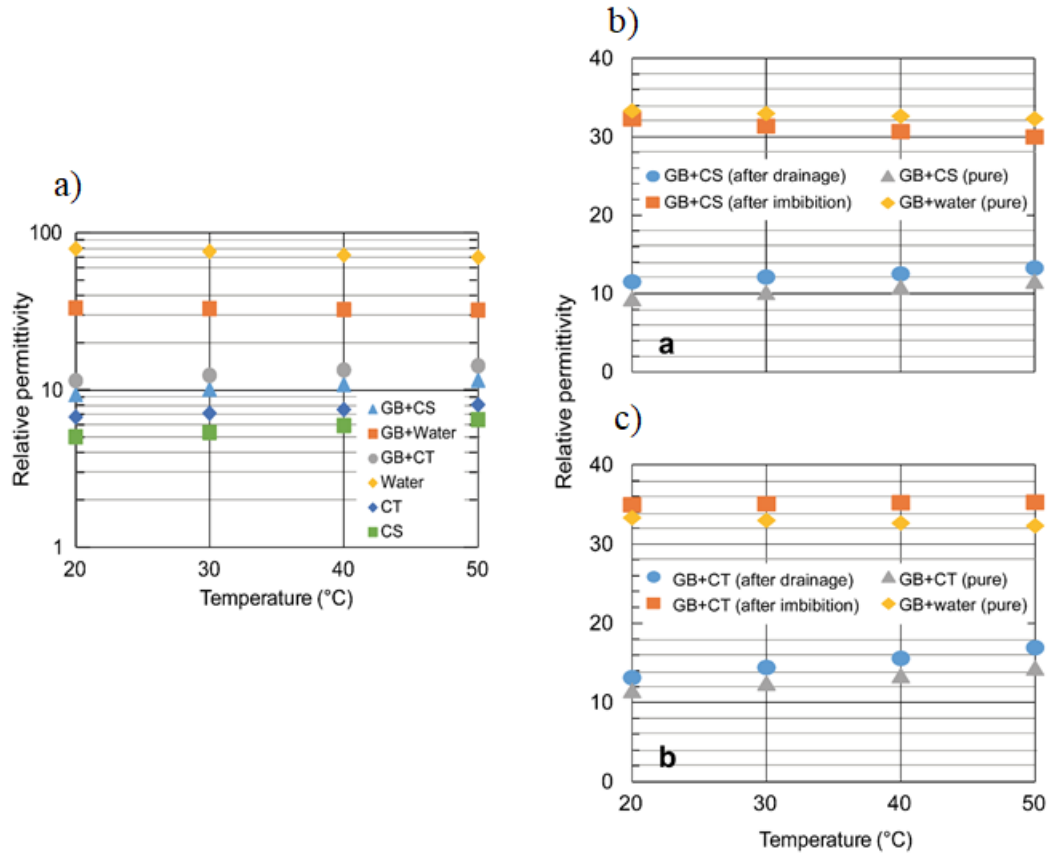


Fig. II : Variations de la permittivité diélectrique relative en fonction de la température a) pour des produits purs : solvants chlorés (CS), goudron de houille (CT), eau (water), billes de verres (GB)+CS, GB+CT et GB+eau, et pour des mélanges : b) CS et c) CT après drainage (80% de DNAPL et 20% d'eau) et imbibition (92% d'eau et 8% de DNAPL)

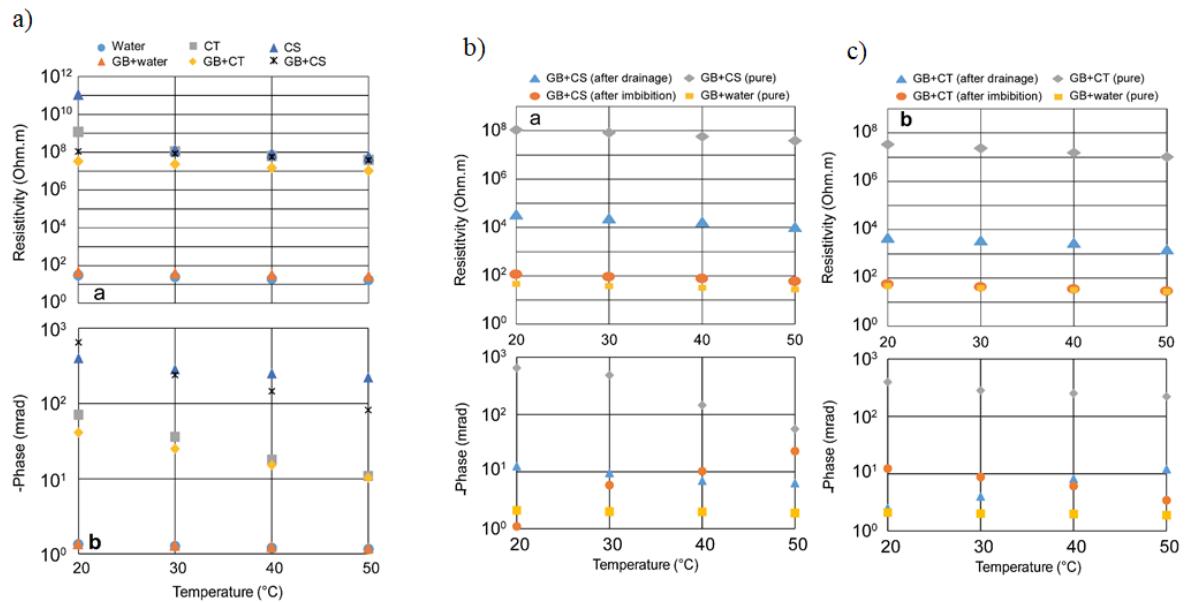


Fig. III : Variation de la résistivité et de la phase en fonction de la température à 1,46 Hz a) pour les produits purs : CS, CT, eau, GB+CS, GB+CT et GB+eau, et pour des mélanges : b) CS et c) CT après drainage (DNAPL à 80% et 20% d'eau) et imbibition (92% d'eau et 8% de DNAPL)

courbes de corrélation obtenues pourront être utilisées dans des futures études de laboratoire sur un réservoir 2D (petit modèle des conditions réelles sur le terrain).

Après l'étude de l'effet de la température, des expérimentations à une température fixe (20°C) ont été menées avec des couples polluants DNAPL/fluide (CT+eau, et CO+SE) au cours de deux cycles de drainage et d'imbibition, afin d'étudier les effets des changements de saturation sur les paramètres électromagnétiques. L'augmentation des saturations en eau et en SE entraîne une augmentation de la permittivité relative, confirmant ainsi la relation directe entre la saturation en fluide (eau ou SE) et la permittivité relative d'un milieu poreux multi-phasique. Selon ces résultats, la permittivité relative diminue (respectivement augmente) linéairement pendant le drainage (respectivement l'imbibition) en raison de la permittivité relative élevée du fluide comparée à celle du polluant DNAPL. La figure IV montre que la permittivité relative mesurée est conforme au modèle CRIM ('Complete Refractive Index Method' en anglais) qui est un modèle empirique bien connu pour étudier la relation entre la saturation et la permittivité relative dans un milieu poreux multi-phasique.

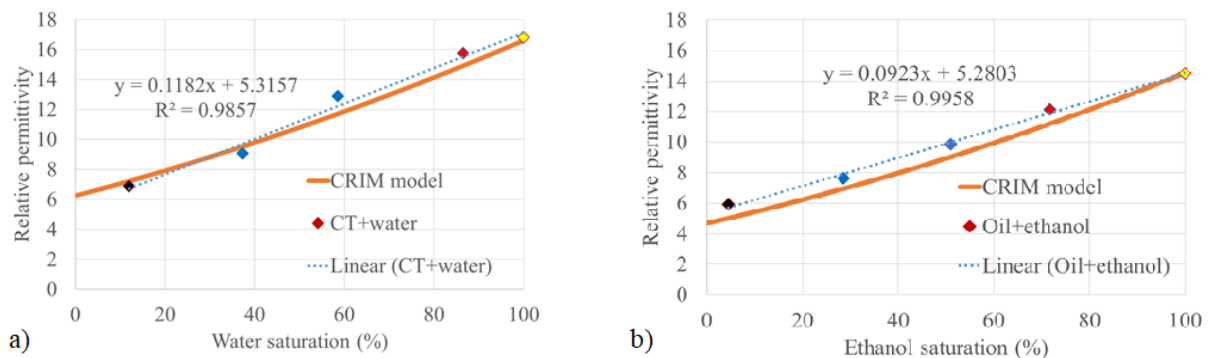


Fig. IV : Courbes de corrélation de la permittivité relative et de la saturation en eau (a) et en SE (b) ajustées par le modèle CRIM. Point jaune : début de l'expérience (début du premier drainage), point rouge : saturation résiduelle et point noir : saturation irréductible

La variation de la résistivité complexe et de la permittivité relative dans deux séries d'expériences dans une colonne garnie de GB saturée de mélanges CT/eau et CO+SE a été étudiée. Les observations montrent que la résistivité augmente à mesure que les saturations en fluide (eau ou SE) diminuent. L'évolution de la résistivité complexe avec la saturation obéit à la loi d'Archie généralisée (Fig. V).

Les mesures en laboratoire de la résistivité complexe ont montré que le premier cycle de drainage et d'imbibition donnait de meilleurs résultats, en particulier pour la phase, par rapport au deuxième cycle. Comme les courbes de pression capillaire et de saturation pour chaque drainage et imbibition des deux cycles sont différentes et comme les données expérimentales montrent des courbes différentes pour chaque cycle en raison de phénomènes

d'hystérésis, cela peut justifier ces données inappropriées pour le second cycle. Nous pensons que la précision et l'exactitude de nos mesures sont directement liées à l'existence d'eau (en tant que fluide conducteur) dans le milieu poreux. Lors du drainage, la totalité de DNAPL ne peut pas être extraite du milieu poreux, ce qui peut entraîner ces mesures géophysiques désordonnées du deuxième cycle. Au cours du premier cycle, la phase ne montre de tendance claire pour les expériences avec CO+SE. En revanche, une corrélation linéaire est observable pour la phase dans la cellule de CT/eau. Pour ce mélange CT/eau, la phase et la saturation en eau présentent un comportement inverse : diminution de la saturation en eau entraîne une augmentation de la phase. À une fréquence plus élevée, la partie maximale du spectre de phase s'est déplacée vers une fréquence plus basse en raison d'une augmentation de la saturation en CT.

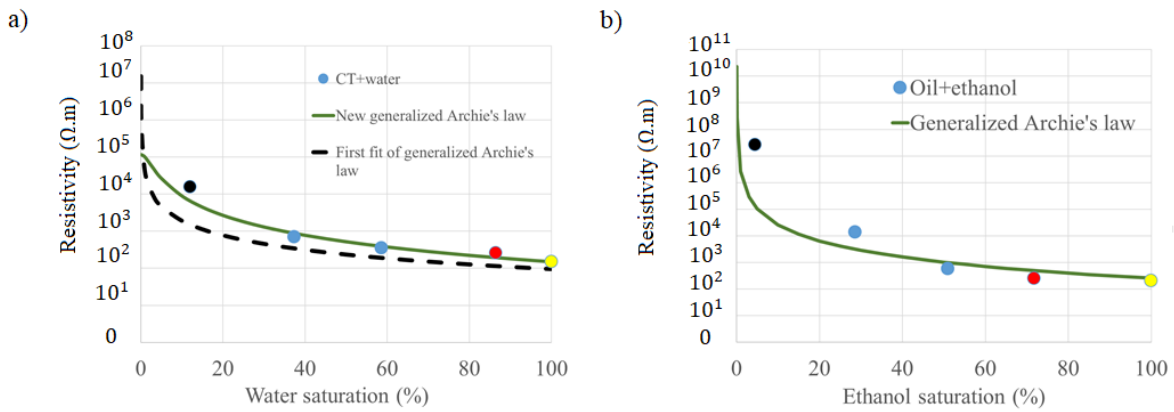


Fig. 5 : Courbes de corrélation de la résistivité et (a) de la saturation en eau, (b) de la saturation en SE ajustées par la loi d'Archie généralisée. Point jaune : début de l'expérience (début du premier drainage), point rouge : saturation résiduelle et point noir : saturation irréductible

Nous concluons que les méthodes SIP et TDR sont bien des pistes pour suivre les variations de résistivité électrique et de permittivité diélectrique lors de surveillance à long terme de processus de dépollution. Le diamètre des GB en laboratoire a été choisi pour simuler au mieux les caractéristiques physiques du milieu poreux réel du terrain ciblé (porosité en laboratoire de $38\% \pm 2\%$, et porosité sur le terrain de 36 à 42%). L'utilisation des GB au lieu d'échantillons de sol prélevés sur le site réel a été aussi motivée par : (i) la transparence des GB qui permet de mieux surveiller et consigner les niveaux des différents liquides afin de calculer les saturations, (ii) l'empêchement de l'apparition de phénomènes comme l'adsorption. Nous avons également utilisé le même couple polluant/fluide (CT/eau). Les résultats validés avec des modèles empiriques doivent être maintenant testés sur de futurs travaux sur le terrain. Au final

les résultats obtenus donnent des perspectives sur la surveillance des techniques de dépollution type récupération thermique de DNAPL.

Sur le terrain, le milieu poreux est constitué de sols ayant une résistivité inférieure et une permittivité relative supérieure à celle des GB. Néanmoins ces résultats devraient s'appliquer à des sols sableux et à des grès perméables de porosité et de résistivité proches aux GB, mais pas forcément à d'autres sols de texture différente, car la résistivité électrique des sols est liée à la composition des sols et aux propriétés physiques des différents constituants. Ces résultats ne s'appliquent donc qu'au milieu considéré et à des milieux ayant des caractéristiques et propriétés physiques proches.

Quelques perspectives de ce travail sont :

- L'auteur recommande d'étendre les mesures et d'utiliser les courbes de corrélation obtenues dans les futures études de laboratoire sur un réservoir 2D ou cuve (petit modèle des conditions réelles de terrain). Le champ de saturation dans le réservoir 2D sera déterminé en fonction des mesures électromagnétiques. L'objectif principal de l'expérimentation sur le réservoir 2D, *i.e.* avec un écoulement 2D, sera la validation du modèle de mélange et des courbes d'étalonnage obtenues avec les cellules et les colonnes 1D. Des expériences isothermes seront effectuées à 20 et 35°C avec de l'eau chaude à une température donnée circulant autour du réservoir 2D pour maintenir la température constante dans le réservoir 2D. Pour simuler les conditions de terrain, où la température n'est pas constante, une expérience en conditions non isothermes sera également réalisée. Dans des conditions non isothermes, un appareil de chauffage chauffera un côté du réservoir. La perte de chaleur se produit ensuite dans le réservoir 2D. En condition non isotherme, il est possible d'étudier les paramètres électromagnétiques dans différentes zones du réservoir en fonction de la variation de la température et de la variation de la saturation lors du pompage de DNAPL à partir du bas au centre du réservoir. Alors que les expériences sur la cellule (respectivement la colonne) ont été réalisées avec 1 (respectivement 3) sonde TDR et 1 (respectivement 6) mesure SIP, l'expérience avec le réservoir 2D utilisera 15 TDR et 47 mesures SIP. Les saturations en polluant estimées par l'analyse des données TDR et SIP seront ensuite comparées aux celles obtenues directement par une technique d'imagerie (basée sur les différences de densité optique).
- Les hydrocarbures légers (LNAPL) constituent une autre source importante de contamination du proche sous-sol. Des études futures avec un scénario imbibition

et drainage de LNAPL, permettrait de décrire les relations de la résistivité complexe et de la permittivité relative avec la saturation et la température dans un milieu de fluide tri-phasique (air, LNAPL et eau). A noter que dans des petits pores, les LNAPL peuvent se comporter comme des films à la surface de l'eau. Le principal défi consistera à distinguer les saturations en air et en LNAPL dans la zone de pompage, les résistivités de l'air et du LNAPL pur étant proches.

- Effectuer les mêmes expériences avec des sols prélevés sur un site pollué et comparer les nouveaux résultats aux études avec des GB pour clarifier l'effet de l'utilisation de ces GB.

This page has been intentionally left blank

Acknowledgements

First, I would like to express my acknowledgements to my supervisor, Professor Roger GUERIN and my co-supervisors Dr. Alexis MAINEULT, Dr. Jacques DEPARIS, Dr. Hossein DAVARZANI. Thank you for all of your knowledge, encouragement and confidence in me. I have really appreciated your dedicated and positive energy at all of our meetings through the years, and your willingness to help when needed. You are all supportive, knowledgeable and very kindhearted persons.

There are also other persons, without whom this work would not become what it is. A special acknowledgement to the project manager of Bioxyval, Dr. Stéfan COLOMBANO as an unofficial assistant supervisor, for all the time, support and energy you have put into my works. I wish to thank the members of my dissertation jury: Prof. Myriam SCHMUTZ, Prof. Frédéric NGUYEN, Prof. Loïc LABROUSSE and Dr. Vincent ALLEGRE for generously offering their time, guidance and good will throughout the review of the thesis manuscript and dissertation defense. Also special thanks to my colleagues and friends Mohammad GHASEMI HAMED, Fakhraddin SEYFADDINI, Pooya NADERI, Nicolas PHILLIPE, Benjamin DOUCHE, Benjamin FRANCOIS, Benjarese ONIANGUE and Sabrina BEN RHOUMA. Without your help and accompany, being successful in this PhD thesis would not be possible. I would especially like to acknowledge my uncle, Dr. Said IRAVANI for his positive attitude and all the energy and time spent with me during these three years.

There are so many people who have influenced my work and life in different ways during this time. It is not possible to mention them all here. In the everyday world, thank you all colleagues and friends at French Geological Survey (BRGM). BRGM with you feels like a home in the friendly, open minded and entertaining environment.

I would also like to thank my parents, grandma and brothers for all their support and interest in what I do. I love you.

Above all, I would like to thank my wife Setareh for her love and constant support, for all the late nights and early mornings, and for keeping me sane over the past few months. Thank you for being my AutoCAD supporter, editor, proofreader, and sounding board. Nevertheless, most of all, thank you for being my best friend. I owe you everything my love.

This study was performed in the framework of the BIOXYVAL project. I would like to thank ADEME for funding part of the project under the “Investissements d'Avenir” program, BRGM, “Hegmatan-Mahar Ab” the Iranian consulting engineers, for providing the PhD thesis

scholarship for me, we gratefully acknowledge the financial support provided to the PIVOTS project by the “Région Centre – Val de Loire” and the European Regional Development Fund.

Mohammad Ali IRAVANI

30th of January 2020

Abstract

During the past two decades, the remediating and monitoring of polluted sites have become an important issue. Health and ecological regulations in developed and progressing countries are more restrictive concerning the abandoned polluted sites. Classical well monitoring techniques are not enough to monitor soil characteristic change in subsurface. Among all geophysical techniques, electrical methods showed their ability to monitor clean-up programs in these sites.

Spectral induced polarization (SIP) technique (also called complex resistivity) is a method in near surface geophysics to measure complex electrical resistivity of a medium in the frequency domain. Many geophysical techniques help us to discover organic contamination, the bedrock position, mineral ores, ancient buildings and many other valuable stuffs on the subsurface. The other geophysical method was used is time domain reflectometry (TDR) that has been developed to measure relative dielectric permittivity, water content and temperature in homogeneous or heterogeneous porous media. This thesis is a challenge to evaluate efficiency and potential of SIP and TDR for a long-term monitoring of dense non-aqueous phase liquids (DNAPLs) recovery in contaminated porous media in the laboratory. Different sets of experiments designed to study the impacts of temperature and saturation changes on electrical complex resistivity and relative permittivity of saturated porous media on isothermal and non-isothermal conditions were examined in different 1D columns. The measurements were made with different couples of pollutants and fluids (i.e. coal tar/water, chlorinated solvent/water and canola oil/salty ethanol) in porous media simulated with glass beads of 1 mm diameter.

Our findings concerning to temperature change show that experimental data of relative permittivity and complex resistivity of pure water obey empirical models validating our experimental setup and protocol. Results demonstrated that the real parts of relative permittivity and electrical resistivity are functions of temperature. While the imaginary part of relative Permittivity has not been studied, but our observations in the samples of DNAPLs indicated that the temperature increase leads to decrease in imaginary parts of complex electrical resistivity of DNAPLs. Two sets of experiments examined impacts of saturation changes in these two geophysical parameters. Our findings show that due to high resistivity of oil and coal tar, increase in water/oil saturations led to decrease in resistivity and phase. Interpreting experimental data showed that resistivity and relative permittivity measurements were compatible with Generalized Archie's law and complex refractive index method (CRIM)

model, respectively. Moreover, the effects of temperature and saturation on complex resistivity have a secondary effect on frequency domain and Cole-Cole parameters.

The results from the laboratory measurements will be used in the real conditions in field measurements in a remediation program.

Table of contents

1	Introduction	1
1.1	General introduction.....	1
1.2	Different remediation techniques	4
1.2.1	Soil Vacuum Extraction (SVE)	4
1.2.2	Bioremediation	6
1.2.3	Enhanced thermal soil remediation	7
1.3	Interest of geophysical methods	10
1.4	Polluted site	14
1.5	Objectives	16
1.6	Outline	18
2	Geophysical backgrounds.....	19
2.1	Porous media	19
2.1.1	Topology and Porosity	19
2.1.2	Multiphase media	21
2.1.3	Saturation	22
2.1.4	Wettability and non-wettability	24
2.1.5	Permeability and Darcy's law	26
2.2	Electromagnetic properties.....	27
2.2.1	Complex resistivity	29
2.2.2	Relative permittivity.....	32
2.2.3	Chargeability	34
2.2.3.1	Membrane or electrolytic polarization	35
2.2.3.2	Electrode Polarization with mineral particles (overvoltage)	36
2.2.4	Mixing models	37
2.2.4.1	Mixing models of electrical resistivity	37
2.2.4.2	Mixing models of dielectric permittivity.....	46
2.3	Geophysical techniques	49
2.3.1	DC resistivity	49
2.3.2	TDIP and SIP	51
2.3.3	TDR.....	57
3	Material and methods	59
3.1	Non-polarizable electrodes	59
3.2	Cells and columns	63
3.2.1	White test (with water) before performing experiments	68

3.3	Principle of drainage and imbibition	68
3.4	TDR application	69
4	The effects of temperature on geophysical parameters	75
4.1	General introduction.....	75
4.2	Abstract	78
4.3	Introduction	79
4.3.1	Influence of temperature on relative permittivity: a review	80
4.3.2	Effect of temperature on complex resistivity: a review.....	82
4.3.3	Objectives.....	85
4.4	Experimental setups and data acquisition.....	85
4.5	Results	89
4.5.1	Effects of temperature on the relative permittivity.....	89
4.5.2	Effects of temperature on the relative permittivity of pure products	89
4.5.3	Effects of temperature on relative permittivity after drainage (irreducible wetting phase saturation) and imbibition (residual non-wetting phase saturation)	90
4.5.4	Effects of temperature on the electrical resistivity	92
4.5.5	Effects of temperature on the electrical resistivity of pure products	92
4.5.6	Effects of temperature on the electrical resistivity after drainage (irreducible wetting phase saturation) and after imbibition (residual non-wetting phase saturation).....	96
4.5.7	Frequency domain of electrical resistivity and phase	97
4.6	Discussion	98
4.6.1	Empirical models for relative permittivity	98
4.6.2	Temperature coefficient of resistivity (α).....	101
4.6.3	Effect of temperature on Cole-Cole parameters.....	103
4.7	Conclusions	104
4.8	General conclusions	105
4.9	Appendix: Detailed figures of chapter 4	106
4.9.1	The detail figures of TDR measurements (Relative permittivity).....	106
4.9.2	The detailed figures of SIP measurements (Complex resistivity)	109
5	The effects of saturation on geophysical parameters.....	113
5.1	General introduction.....	113
5.2	Abstract	116
5.3	Introduction	117
5.4	Experimental setups	119
5.5	Results	122
5.5.1	Effect of saturation on the complex resistivity.....	122
5.5.2	Effect of saturation on relative permittivity	126

5.6	Discussions	127
5.6.1	Empirical models for the amplitude of the resistivity	127
5.6.2	Empirical models of relative permittivity	130
5.6.3	Effects of saturation on Cole-Cole parameters.....	131
5.6.4	About the second cycle	132
5.7	Conclusion.....	133
5.8	Appendix C: Detailed figures of chapter 5.....	134
6	General conclusions and perspective.....	136
6.1	Conclusions	137
6.2	Perspective.....	139
7	References	145
8	Appendix A: Experimental protocol	171
8.1	Procedure to switch the column to the tank.....	171
8.2	Procedure to switch the tank to the columns	174
8.3	TDRs' Numbers	177
8.4	Connecting the tank to SIP-lab IV.....	178
8.5	Some important points:	180

This page has been intentionally left blank

1 Introduction

1.1 General introduction

The soils is contaminated due to human activity and existence of human-made chemicals. The different chemicals like petroleum hydrocarbons, polynuclear aromatic hydrocarbons such as naphthalene, solvents, pesticides and lead are spreaded in the soil because of industrial activity, agriculture chemical and unusable wastes normally cause it.

Among all pollutions in soil, most of them are classified in a group (Zehnder, 1995), which referred as non-aqueous phase liquids (NAPLs). NAPL are hazardous organic liquids such as dry cleaning chemicals, fuel oil and gasoline that do not dissolve in water. They are always associated with human activity, cause severe environmental and health hazards, and are difficult to remove from the water supply once it has been compromised. In non-polar molecule, NAPLs are hydrophobic, it means that these liquid solution contaminants do not dissolve in or easily mix with water (e.g. oil, gasoline and petroleum products). NAPLs includes in two different groups. The first group, light non-aqueous phase liquids (LNAPLs) are referred to the liquids that are lighter than water and non-soluble in water (e.g. gasoline, benzene, toluene and xylene). LNAPLs are less dense than water, therefore, after mixing they remain on top of the water. The second group, dense non-aqueous phase liquids (DNAPLs) are denser than water and like LNAPL they do not dissolve in water (chlorinated solvents, coal tar, creosote and heavy crude oil). Unlike LNAPLs, after spilling DNAPLs in water, they sink below the water. Fig. 1 shows the migration of NAPLs and DNAPLs against ground water after spilling in the soil (Whelan et al., 1994).

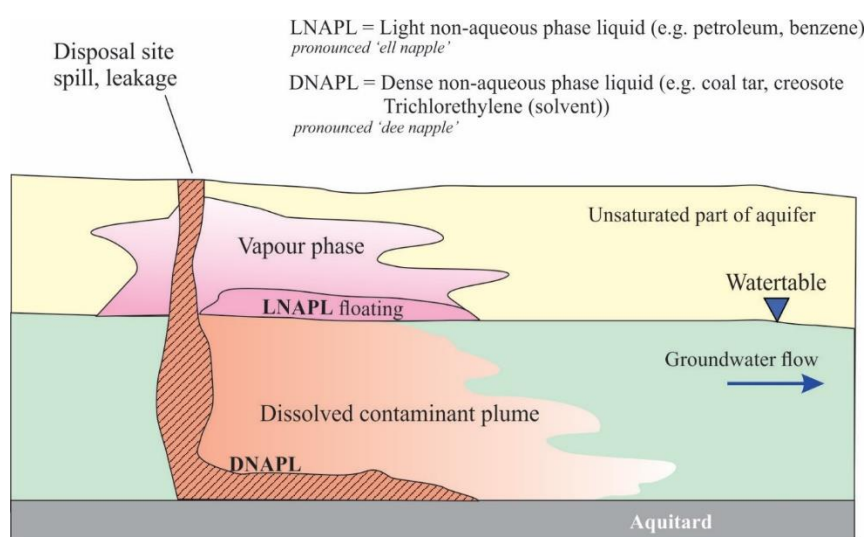


Fig. 1. Organic contaminants, like petroleum fuels and solvents may be present as a free liquid, dissolved liquid (in water) and as vapor (ref: <https://www.heroninstruments.com/news/dnapl-and-lnapl/>).

After many years of research soil cleanup, the contamination of soil due to DNAPLs is still one of the main environmental challenges of the environmental and geophysical communities (Kavanaugh et al., 2003).

Geo-environmental problems in sites contaminated by dense non-aqueous phase liquids (DNAPLs) residing below the water table, become more serious in last decade (Power et al., 2014). DNAPLs including especially coal-tar (CT) and chlorinated solvents (CS) are widely contaminating soils and water when release in the subsurface. DNAPLs penetrate inside the saturated zone from the migration pathways as an immiscible material due to gravity and capillary forces (Power et al., 2014). Their complex behavior in the subsurface is related to the specifications of the site and the nature of the hydrogeological environment, properties of the DNAPL, and subsequent mass transfer and transformation processes (Lerner et al., 2003). As a result, contaminated zones can be in form of a laterally extensive pool or a complex distribution at depth (Gerhard et al., 2007). DNAPL zones can be a reason of the groundwater contamination posing high risk to humans and ecosystems (Power et al., 2014). ADEME, Ernest and Young (2014) (The French Environmental Protection Agency) has recently published a report indicating the cost and implementation frequency of various remediation techniques (ADEME, Ernest and Young, 2014). This report is based on a questionnaire sent to soil remediation professionals (research and operations consultancies). Fig. 2 displays the type of pollutants treated in groundwater remediation sites in France in 2012. It also shows that organic compounds, which can be present as LNAPL or DNAPL, represent the majority of the pollution encountered in these sites (53%).

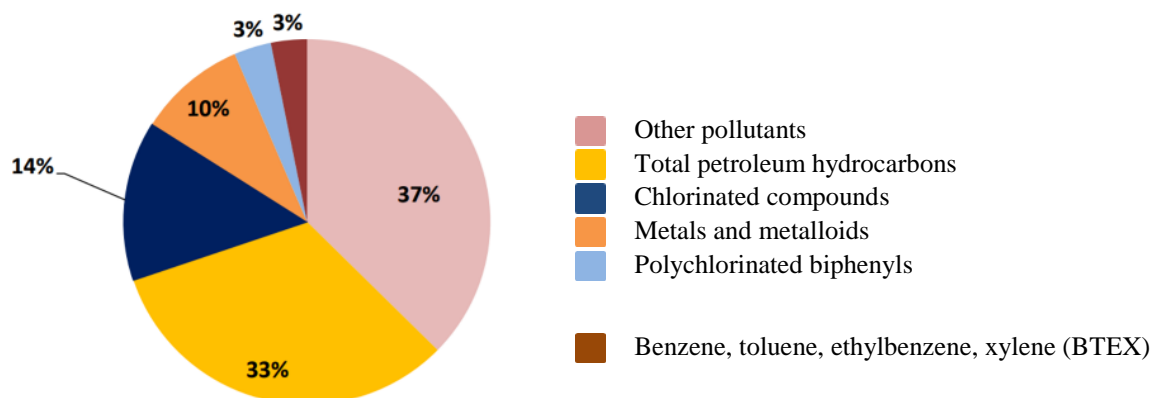


Fig. 2. Pollutants treated in 2012 on groundwater remediation sites located in France (ADEME, Ernest and Young, 2014)

Different remediation techniques can be used in these sites in order to depollute them like pump and treat, thermal and chemical methods. These methods have for consequence to modify the physical properties of the soil. Usually, cleanup is controlled by geochemical analysis of water prelevement inside borehole, but physical properties variation could be

monitoring by sensor inside borehole and/or geophysical methods. So monitoring these variation method is an essential in this way.

In many developing and developed countries, for instances in industrial parks and cities, large quantities of waste were released in soils due to industrial activities for years. Such pollutions can cause many ecological and health issues. The toxicity of pollutants to aquatic organisms is affected by metabolism and photo-oxidation (Abdel-Shafy and Mansour, 2016). Pollutants in soil are likely to exert toxic effects on terrestrial field. In area close to urban and industrial activities, high level of toxicity were reported in raw foods (Abdel-Shafy and Mansour, 2016). Such area need to be remediated either because they present a health risk to nearby communities. IARC (2013) reported that the pollutions a leading environmental cause of cancer deaths are classified in four groups:

Group 1: The agent is carcinogenic to humans.

Group 2: This category includes agents for which, at one extreme, the degree of evidence of carcinogenicity in humans is almost sufficient, as well as those for which, at the other extreme, there are no human data but for which there is evidence of carcinogenicity in experimental animals.

Group 3: The agent is not classifiable as to its carcinogenicity to humans. This category is used most commonly for agents for which the evidence of carcinogenicity is inadequate in humans and inadequate or limited in experimental animals.

Group 4: The agent is probably not carcinogenic to humans. This category is used for agents for which there is evidence suggesting lack of carcinogenicity in humans and in experimental animals. In some instances, agents for which there is inadequate evidence of carcinogenicity in humans but evidence suggesting lack of carcinogenicity in experimental animals, consistently and strongly supported by a broad range of mechanistic and other relevant data, may be classified in this group.

It may also be needed to reuse some of the abandoned industrial sites because of limited available property for industrial use or because of strategic location. Such activity may be due to strategic planning for future economic growth or due to cost benefits. With a rising rate of human population, demands are increasing on this non-renewable resource (earth). Land pressure is becoming a challenge due to change in land-use patterns driven by technological and economic interests. Land pressure causes emergence to remediate the polluted sites.

Remediation methods have significantly advanced and play a leading role in environmental cleanup (Rew, 2007; Vidonish et al., 2016). Cleaning up of these sites often encounters technical and financial obstacles. In the areas where land value is low, financial

incentive to justify cleanup cost is extensively limited. Therefore, it is required to develop new techniques that are both more effective and more economical in order to promote redevelopment of such areas, which were designated by the government for cleanup purpose.

1.2 Different remediation techniques

The seepage and spill of toxic fluids and materials can lead to contamination in the soil. Not only pollution concentration but also mobility of contamination plumes can cause serious health and environmental issues. The random distribution of DNAPLs (depending on soil heterogeneities and associated variations in the required threshold pressure intake) makes free products migrate downward by fingering until they are blocked at the impermeable substratum (if the volume of DNAPL is high enough). Several remediation techniques are developed in order to clean the soils. Like many research domain, depollution of contaminated soils use multidisciplinary approach. Many physical, chemical, biological, thermal, fixation and encapsulation methods, classified as in-situ, prepared bed, and/or in tank reactors, are used to remove contaminants from soil. Nowadays, monitoring of soil clean up in contaminated sites is mainly done by analyzing samples taken from boreholes to find the degree of contamination in soil and groundwater. The number of boreholes and the level of the accuracy of the measurements are primarily decided by economic restraints. Therefore, the results should be use based on the scale and accuracy of the study.

Among many remediation methods, we can describe the following technics:

1.2.1 Soil Vacuum Extraction (SVE)

Soil Vacuum Extraction (SVE) is an in-situ technique that is also referred to as soil vapor extraction (SVE) that is based on the coating of the soil grains. SVE consists of vacuum extraction wells (Fig. 3), air inlet wells, and vapor-monitoring wells distributed across a contaminated site, and a blower(s) to control airflow.

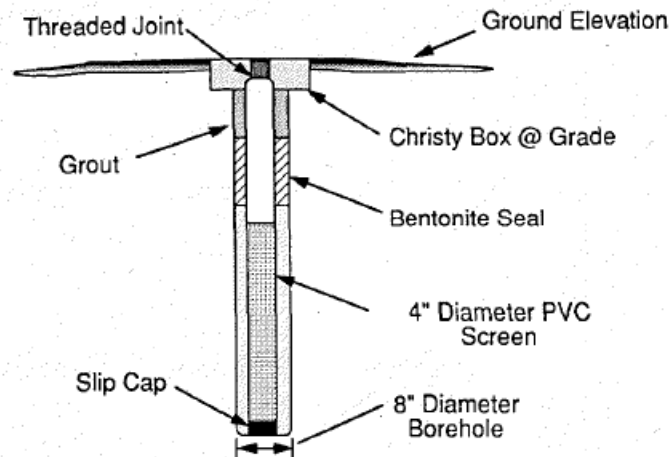


Fig. 3. Schematic of a gas extraction well (Sims, 1990)

The chemicals (e.g. vapor pressure) and site properties (e.g. soil moisture content and soil texture) affect performance of SVE. Vapor pressure of chemical becomes important where it exist in most pure form (Sims, 1990).

When chemical elements / compounds are in the water, Henry's Law constant will be important. Generally, movement of volatile organic chemicals (VOCs) is 10,000 times faster in gas compared to water. Soil moisture has a direct relationship with VOC removal. However, when soil is very dry, due to entering dry air in the soil, VOCs may adsorb on mineral surfaces. In this situation the magnitude of sorption is normally increases as volatilization decreases (Fig. 4). When removal plan is in soil-air two-phase medium, Henry's Law constant is not suitable under these conditions (Sims, 1990).

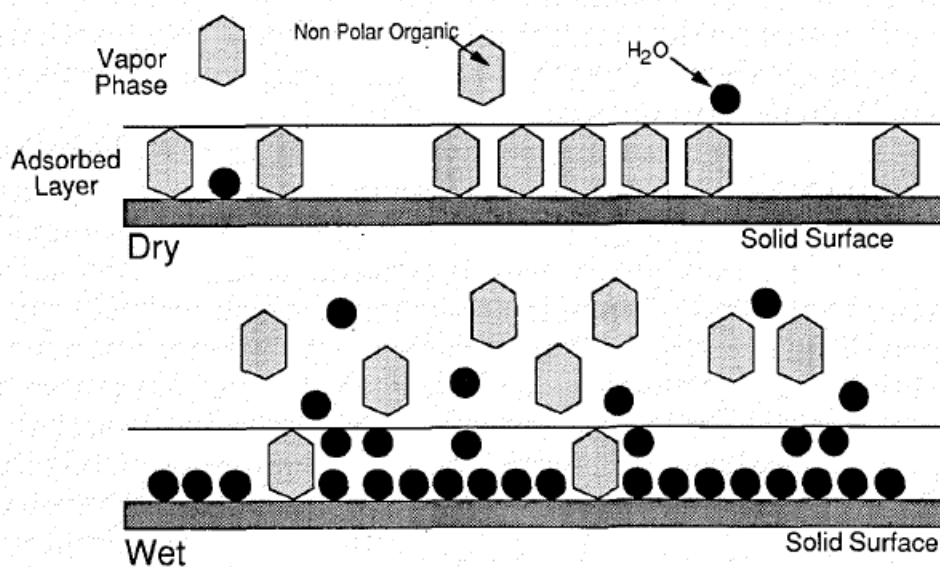


Fig. 4. Effect of moisture on VOC adsorption and desorption in soil
—VOC adsorption with two moisture regimes (Sims, 1990)

1.2.2 Bioremediation

Another in-situ technique is bioremediation or biodegradation. It is based on the degradation of organic contaminants by microorganisms (microbial degradation). It can be part of the clean-up process especially in the vadose zone. Using biological process can efficiently reduce ground water pollution. This method is based on biological mechanisms instead of using mechanical tools and techniques. In this method, contaminated soil is remediated by applying different bacterium that feed on the specific type of contaminant. The role of bacterium is consuming and breaking down the hydrocarbons and other contaminants in the soil. *Geobacter sulfurreducens* can form electrically conductive biofilms. The biofilms grow from a wastewater sludge inoculum was highly conductive with low charge transfer resistance even though microorganisms other than *Geobacteraceae* accounted for nearly half the microbial community (Malvankar et al., 2012). The optimal soil temperature to perform bioremediation is 20°C (70°F). In colder climates, soil surface must be covered in order have any gains from bioremediation. It may take longer time to achieve positive results. A schematic picture of In-situ bioremediation is illustrated in Fig. 5.

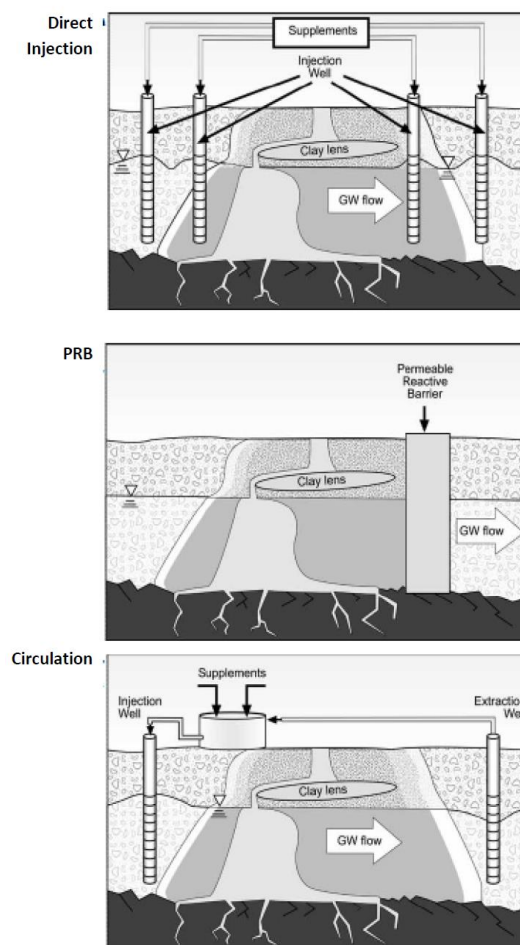


Fig. 5. In situ Bioremediation System Configurations (<https://sempub.epa.gov/work/11/171054.pdf>)

For the first time, Wilson (1983) introduced biological processes (e.g. microbial Degradation), as an important mechanism to reduce contaminants throughout vadose zone and groundwater. Soil remedial measurements using biological processes significantly reduced potential groundwater contamination. This method can be an alternative clean-up technology for achieving a permanent remediation at hazardous waste sites (Sims, 1990). In situ bioremediation of polluted sites impacted by petroleum and DNAPL release can take years, particularly in presence of recalcitrant species such as heavy hydrocarbons (Vidonish et al., 2016).

1.2.3 Enhanced thermal soil remediation

Applying high temperature to a contaminated soil is another method for removing some specific types of pollutions. This technique is typically used for soils that has been contaminated by hydrocarbon compounds such as oil, DNAPLs or other petroleum products. Essentially, high temperature leads to evaporating pollution or decreasing its viscosity to facilitate pumping. If contamination evaporates, it is necessary to capture extracted materials. A conveyor system normally used to cool treated soil for future use and recycling. Unlike bioremediation method, thermal method can depollute a site very fast in a matter of hours to months. It can remove almost 99% of DNAPLs and contaminations (Stegemeier and Vinegar, 2001; and Valenti, 1994). Fig. 6 illustrates in situ thermal desorption for shallow (0-3 feet) and deep contamination (>3 feet).

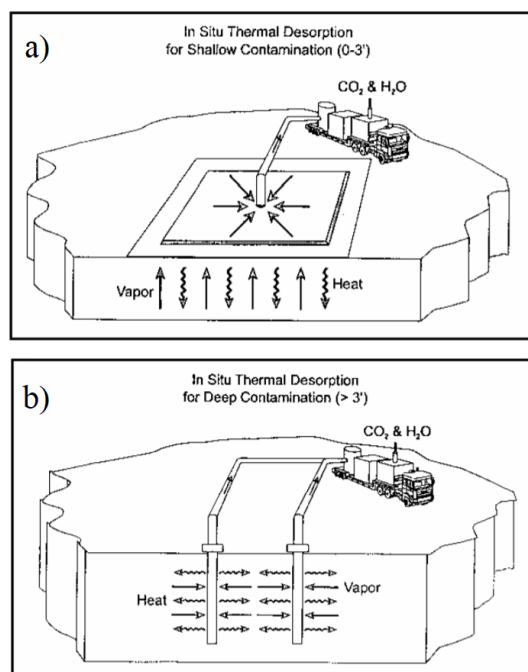


Fig. 6. Thermal enhanced technique for a) shallow contamination (0-3') with thermal blankets and b) deep contamination with thermal wells (>3')

Several points are important to know before proceeding with thermal technique (Vidonish et al., 2016):

1. This method is relatively costly
2. High temperature can destroy soil minerals and organic matters (OM) and change some physical properties of the soil.
3. Thermal remediation techniques can have an impact on ecosystems such as plant growth and revegetation.

Two different thermal techniques are shortly explained below:

A) Thermal desorption (TD)

The development of thermal remediation should not incur environmental damages. After thermal desorption (TD), destroyed hydrocarbons should be carried away by a sweep gas or vacuum. TD is done in two different temperature categories: low temperature (LT TD, 100-300°C) or high temperature (HT TD, 300-550°C).

In situ and Ex situ TD are both effective but in situ technique is more expensive. In Ex situ TD, excavated soil is heated in TD units (e.g. thermal screws or rotary drums) (Fig. 7).

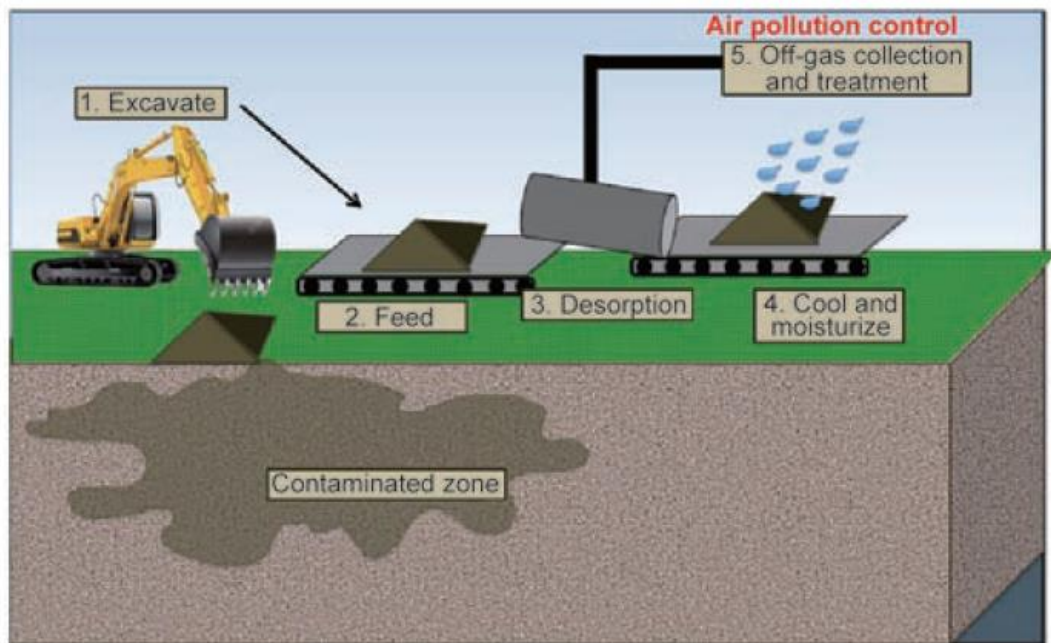


Fig. 7. Ex situ TD includes the excavation of contaminated soils, which are heat-treated in a desorption unit (gas flow conditions may vary). Off-gases are collected for reuse or disposal (Vidonish et al., 2016).

However, In situ TD is performed by using dual heater or vacuum wells to remove pollutants via vapor extraction (Fig. 8). Thermal conduction heaters are used to heat the contaminated zone, and due to low heat capacity of soil, heating contaminated region takes long time before desorption starts (Vidonish et al., 2016).

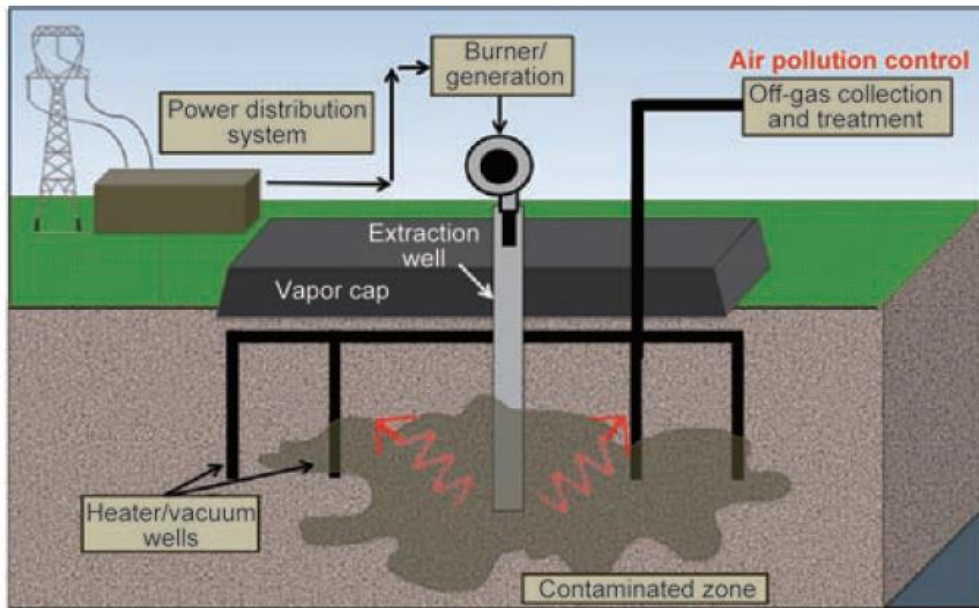


Fig. 8. In situ TD utilizes dual heater/vacuum wells to heat soils and remove contaminants. Off-gases are collected for reuse or disposal (Vidonish et al., 2016).

B) Smoldering

Smoldering is used in oil/DNAPL recovery. This technique lowers the viscosity of oil and DNAPL to facilitate movement of these fluids to extraction wells. Smoldering is also a flameless combustion process (Fig. 9). Combustion transforms pollution to heat, carbon dioxide, and water. The average temperature needed for this method is 600-1100°C.

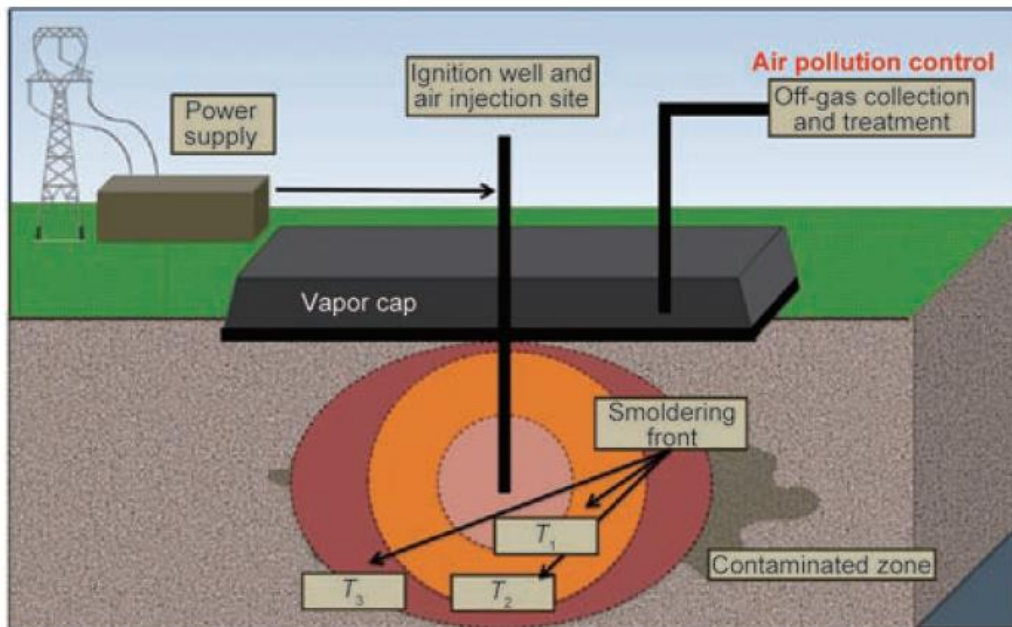


Fig. 9. In situ smoldering utilizes a self-sustaining smoldering wave to destroy hydrocarbons without excavation. The smoldering reactions are started at a central ignition well. Off-gases are collected for reuse or disposal (Vidonish et al., 2016).

Primary application of smoldering remediation is for the remediation of coal tar DNAPLs. This technique is used to treat contaminated soils with heavy hydrocarbon due to high temperatures reachable in this method. Previous studies proved that Smoldering can extract almost 98.5% coal tar in shallow and deep polluted layers but in the lab total take away hydrocarbon is more than 99% (Vidonish et al., 2016).

The other thermal methods such as Incineration, Pyrolysis, In situ vitrification, Radio frequency heating/microwave heating, Hot air injection and Steam injection also used for remediation of contaminated soils. Discussing these methods is beyond the scope of this study.

1.3 Interest of geophysical methods

Geophysics is one application of physics in earth, atmosphere and marine sciences. Exploration geophysics is carried out to get information of physical parameters from subsurface of earth due to inaccessibility of needed data from surface geological surveys. Application of geophysics is defined in different scales from pore scale to planetary scale (Nabighian, 1991). Among all methods, electromagnetic methods and especially electric methods are useful to study process involved during clean up and degradation of pollutant (Mao et al., 2016). The electro-geophysical methods, especially direct current (DC) resistivity, induced polarization (IP) techniques and spectral induced polarization, SIP (<10 kHz) have potential in many domain. We can cite oil, gas and mining industries (e.g., Friedrichs et al., 1999); soil remediation (e.g., Pearce and Zuluaga, 2004; Rojo et al., 2014); waste management (e.g., Lesparre et al., 2013); civil engineering (e.g., Susanto et al., 2013; Weiss et al., 2012); natural hazards characterisation (e.g., Jackson et al., 2002); study of earthquakes and volcanic activity (e.g., Di Maio and Patella, 1991; Revil et al., 2002), understanding the continental crust (e.g., Glover, 1996) and oceanic crust (e.g., Baba, 2005); understanding of the triggering of natural and human induced earthquakes (e.g., Chelidze et al., 2002); volcanic activity monitoring (e.g., Revil et al., 2010); the properties of lunar soils and rocks (e.g., Dihui et al., 2005), and soil science (e.g., Robinson et al., 2003). In the context of electrical method in geophysical study, Conrad Schlumberger in 1920 was the first person that studied electrical polarization effects in soils and rocks (Collett, 1990). In the field with direct current, he found that after switching off injecting current, a transient voltage happened. He called it electrical polarization of the earth. He used this electrical property of the ground to find a deposit of ores. In 1930s and 1940s, USA and Soviet Union were the first two countries that used IP for their oil explorations (Vanhala, 1997b). The first uses of IP method in environment go back to 1950s when Vacquier et al. (1957), Wait, (1959) and Marshall and Madden, (1959) classified different rocks and soils

by this method (Vanhala, 1997b). Bleil (1953) used IP method to study two mining regions. Sumner (1976) stated that IP could be used in low-grade disseminated mineralization. IP was one of the most successful method to study in-situ exploring of porphyry copper deposits (Seigel et al., 2007) because it is based on an interface electrochemical phenomenon, rather than on a purely physical property of rocks or minerals. (Seigel et al., 2007). Pelton et al., (1978) were presented first study that used Cole Cole model for electrical resistivity and proved that SIP can be widely use in mineral prospecting. Vacquier et al. (1957) studied the application of IP method in ground water studies. They found that IP spectra is related to cation exchange on the clay minerals contaminating the aquafer. They demonstrated that this effect is due to electro-dialysis of the clay in the aquifer that work as a distributed electronegative membrane. IP, either in the time domain (TDIP) or frequency domain (SIP) is a promising method for addressing different geophysical challenges. Two researchers who have key roles to develop SIP methods were Kenneth Zonge and W.H. Pelton. Zonge advanced the SIP measurement apparatuses and a general method to deal with EM coupling. Many IP studies were done until end of 1970s but after decreasing copper price due to declining oil price in 1879, IP research activities immediately collapsed (Mathews and Zonge, 2003). The petroleum industry revived SIP and IP methods for shaly sand formation characterization of well logs and many studies have been developed in this subject (e.g. Bussian, 1983; Vinegar and Waxman, 1984). Recently, Revil and Florsch (2010) were demonstrate that in low frequency (<100 Hz), electrical double layer has the main role in IP response.

During the 1980s, SIP was increasingly used for environmental application, called environmental geophysics (Ghorbani, 2007). Olhoeft (1984, 1985) are one of the first studied on the liquid organic pollutions in different clay samples. He compared SIP response for different clean and contaminated sample from a same region. He got to the conclusion that it is not easy to distinguish oxidation-reduction, cation exchange and clay organic reaction by complex resistivity spectra. Sadowski (1988) was performed a first laboratory study on different clay sample with different pollutants and different concentrations. He found that SIP method can be used to identify organic contaminants in clay mineral soils for different concentrations. In different study, Börner et al. (1993) attributed to a laboratory research on the effects of organic liquid contaminations on different clay and sandstones. They demonstrated that both real and imaginary parts of complex resistivity affected by properties of the pore-filling contaminant on shape and frequency domain. They noted that imaginary part in some cases allows a differentiation of the various contaminants. They emphasized on the effect of interactions of pore fluid properties and internal surface structure.

The existence of organic contamination can affect ohmic and capacitive conduction in the IP response due to surface reaction between contamination and soil grains (Vaudelet et al., 2011). IP responses in these contaminated soils is related to the saturation (Breede et al., 2012), distribution, concentration, and types of contaminants present in contaminated soil (Kemna et al., 2012). Previous studies demonstrate that presence of contamination in the soil increases the resistivity (Benson et al., 1997; Sauck, 2000). Martinho et al. (2006) reported an increase in chargeability due to presence of organic contamination in the soil. Many studies based on SIP method have shown increase in amplitude and phase shift due to existence of hydrocarbon oil (Börner et al., 1993; Schmutz et al., 2010; Vanhala et al., 1992). These results are not conclusive results of all studies in this field, other SIP studies presented a decrease in amplitude and phase shift in hydrocarbon media (Revil et al., 2011; Vanhala, 1997b; Weller and Börner, 1996).

Most recently, Blondel et al. (2014) quantified an increase in resistivity, normalized chargeability and with oil content when DNAPLs are not degraded, and a decrease in resistivity, no modification of the phase-lag and chargeability parameters when DNPLs are partially degraded (Blondel et al., 2014). Gourry et al. (2001) also showed that under certain conditions, this type of pollution (DNAPL) can generate an increase in chargeability because of their high resistivity but this statement was not confirmed by Blondel et al. (2014). An augmentation of chargeability was also observed by Gazoty et al. (2012) on other types of pollutants in a study conducted on municipal wastes. Previous studies (e.g., Hallof and Pelton, 1980; Horton et al., 1985; Smith et al., 1983) have shown that the laboratory measurements might not characterized different parameters, similar to the field data (Razafindratsima et al., 2014). Different laboratory and field studies are needed to characterize geophysical properties in contaminated sites.

The methods based on the electromagnetic waves is also used to characterize contaminated soils and groundwater. The dielectric response of a heterogeneous multiphase porous media reflects the combined polarization effects of water, the solid-water interface, and pollutant (Kraszewski, 1996). The variation of relative permittivity of soil samples as a function of moisture content and soil texture has been investigate by a number of previous studies (e.g. Wang and Schmugge, 1980). Experimental studies conducted by Raythatha and Sen, (1986), and Santamarina and Fam, (1997) have examined the dielectric behaviour of several clay minerals and soils mixed with organic and inorganic fluids. These investigations indicate that the relative permittivity of soil-fluid mixtures is affected by water content, density, mineralogy, and the chemical composition of the pore fluid, as well as by temperature. Changes in the characteristics of the pore fluid may also change the soil fabric, the fraction of bound water and free water, the double-layer formation, and the conductivity of the pore fluid, all of which can

influence the dielectric polarization. Ajo-Franklin et al. (2004) performed five sets of experiments (two synthetic and three natural aquifer samples saturated with water with vertical solvent injection) to develop the dielectric properties of different granular materials. They found that their results were in accord with empirical Complex Refractive Index Method (CRIM) model. Comegna et al. (2013) investigated the dielectric response of different saturated soil contaminated by non-aqueous phase liquids (NAPLs) with TDRs. Their results demonstrate that, the amount of pollution in soil can be guessed if the total volume of pore fluid and the dielectric permittivity of the contaminated soil will be measured. In the other study on NAPLs, Carcione et al. (2003) investigated the acoustic and electromagnetic characteristics of soils saturated with coupled fluids of salty water and NAPL. They found that LNAPL and DNAPL saturated porous media have same electromagnetic properties at radar frequency. The electromagnetic characteristic at the radar frequency range were obtained by using the Hanai–Bruggeman equation for sand and clay grains and LNAPL or DNAPL in water or air.

Using electromagnetic soil water sensors like TDRs significantly facilitate measurements of relative permittivity in high spatial resolution. TDRs showed large sensitivity to bulk EC. Schwartz et al. (2013) found that bulk electrical conductivity can control the low frequency dielectric loss spectrum in soils. They used TDR 5TE and two other sensors to study the relationship apparent permittivity on soil conductivity in different soils. They used sand and clay loam soil for their study and installed sensors in columns. By using TDR, they found that apparent permittivity has a direct dependency with conductivity. The slope of the curves for sandy soil was higher than clay loam. For TDR model 5TE, Rosenbaum et al. (2011) proposed an empirical correction function for the temperature effect between 5 and 40°C, tested on eight different liquids. They noticed underestimated values of relative permittivity for temperatures over the range 5 to 25°C (-2.7 for EC-5 and -3.9 for 5TE) and overestimated values for 25 to 40°C (+3.6 for both TDRs). They identified strong correlation between permittivity and electrical conductivity with increasing electrical conductivity with adding salt content. Persson and Berndtsson (2002) tried to find a relation between relative permittivity (measured by TDR), NAPL saturation and electrical conductivity. By further validating the results using a mixing model, they demonstrated that TDR measures relative permittivity values very well.

During the progress of the remediation program, it is important to be able to verify and validate the method and the progress made. This validation process requires tools to evaluate the performance and efficiency of the pollution control / reduction processes. The geophysical methods can be a useful tool in this process to validate remediation programs. In addition, the geophysics can be used to adjust and optimize the clean-up process during the implementation

work. We need reliable tools to study and have an understanding of the long-term monitoring of electro-geophysical parameters and process. Existence and removal of DNAPLs in polluted soil directly affect the electro-geophysical parameters of contaminated medium. A reliable method is needed to monitor this procedure.

In this decade, different geophysical field measurement methods have been used to monitor the depollution in soil and water. The effectiveness of the methods used varies based on the characteristics of the contaminated fields. The geophysical methods tend to monitor various resistivity and permittivity indicators of the environment. This study is based on the spectral induced polarization (SIP) and time domain reflectometry (TDR) with laboratory measurements. In a brief statement, charges go through a porous medium with the help of electrons and ions. Electrons act as charge carriers in metals and semiconductors while and ions act as charge carriers in fluids in multiphase porous media. Electrical double layer (EDL) is the main origin of induced polarization that coats the surface of insulating grains with special emphasis on silica and alumino-silicate. Ions cause conduction in EDL of pore fluid's interface.

The objective of this work is to monitor evolution of electrical complex resistivity and relative permittivity on remediation process. One of the main challenges on monitoring the subsurface with geophysical methods is that there is few methods (e.g. borehole) for verifying the recorded geophysical response of the medium to validate depollution process. Geophysical properties are functions of several parameters like temperature (Sen and Goode, 1992) and saturation (Denicol and Jing, 1998). In other words, in a multiphase porous media, various combination of different parameters such as temperature, saturation, level of compaction, pore fluid properties etc. can have the similar measurement output. Therefore, study of the effect of each parameter to determine their role and its effect on geophysical parameters is necessary. A systematic set of laboratory measurements was designed to study these parameters.

The porosity of the contaminated soil is the other effective physical property of the soil that has a notable effect on the soil remediation progress.

1.4 Polluted site

This study was done in the framework of Bioxyval project. The focus of this study is laboratory work to model the close condition to the field. The study site is Bioxyval brownfield (Fig. 10), it is a contaminated polluted site in France. The site is located on the left bank of the Orne, south of Moyeuvre-Grande. Its western area is located within the municipality of Moyeuvre-Grande and its eastern side in the town of Rosselange. It is located at the heart of the Orne, which borders on the south. The D9 departmental road runs along the site to the North.

The closest residences are located on the other side of the D9 road, about fifty meters from the northern boundary of the site. The exact address of the site is: rue de l'Avenir, ZA Orne Valley, 57780 Rosselange. The site is 2.9 ha. Diagnosis reports the presence of embankments composed of slag on a large part of the site. The rest on the alluvium of the Orne (silty alluvions then coarse in depth). The ground water table in the alluvial soil layer (accompanying layer of the Orne) is approximately 3 m deep. The substratum is 7-8 m thick. The overall flow direction is along from southwest to northeast. Various diagnoses made by the AMREF Company have revealed a significant residual pollution, mainly consisting of PAH but also cyanide (ARTELIA, 2013).

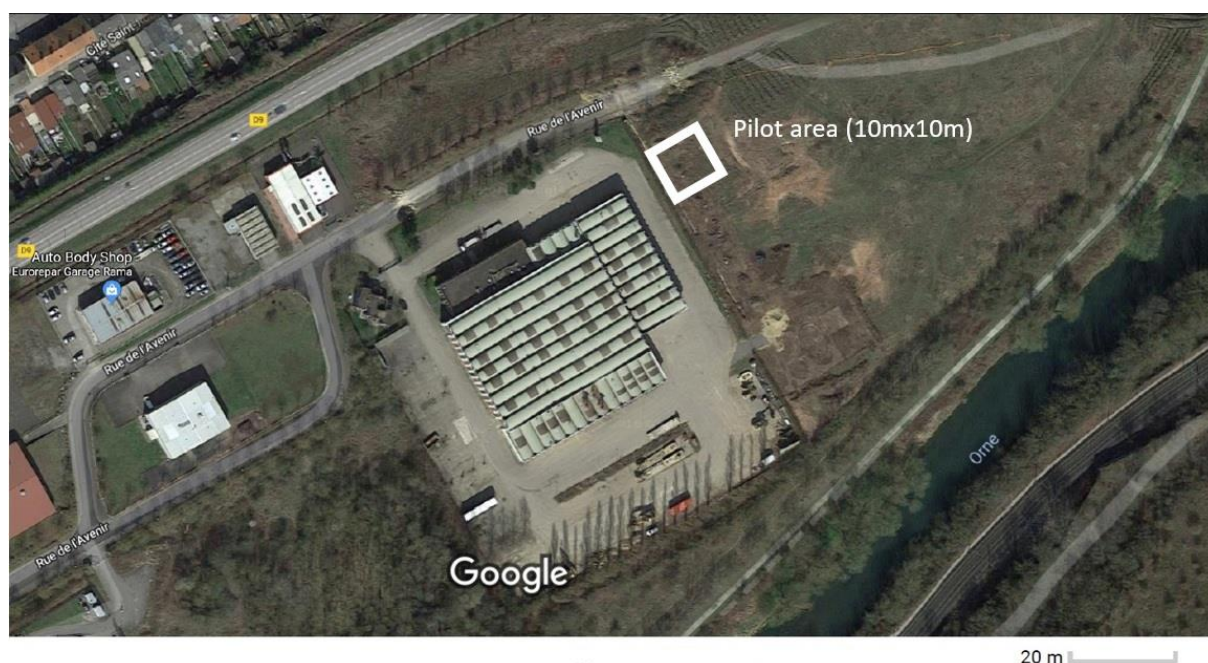


Fig. 10. Aerial view of the polluted site

The Bioxyval is a program with the aim of developing remediation program for pollution in about 16% of polluted sites that are identified and monitored by French public authorities.

The objective of the Bioxyval program is to build a sector to bring integrated management solutions to depollute the industrial wastelands with complex pollutions dominated by organic compounds. The project develops processes for applicable treatment to sites polluted by DNAPLs especially coal tar. Coal tar is a product resulted from the carbonization of coal to produce coke and natural gas. The composition of coal tar is not constant. It is a mixture of phenols, polycyclic aromatic hydrocarbons (PAHs), and heterocyclic compounds. Physical and chemical characteristic of coal tar depend on the temperature of the carbonization and on the type of the carbon-containing material (Li and Suzuki, 2010).

The combination of treatment techniques, characterization tools and approaches to validation / verification make it possible to optimize the integrated management of pollutions on these sites. The project will thus promote the emergence management of a complex pollution management system dominated by coal tar.

The emergence of the work will make it possible to propose techniques in which costs will be competitive compared to currently available approaches. All these techniques and costs must result in effective reconversion of degraded spaces.

This emergence can also facilitate treating the wastelands and preserving other land resources. Decontamination helps to improve the environment and "On-site" clean-up land reduces nuisance and GHG (greenhouse gases) emissions by avoiding their transport to waste storage facilities.

The aim of the Bioxyval project was to bring out an integrated work of complex depollution management dominated by DNAPLs on sites and polluted wasteland. This will be based on the following actions:

- ✓ Development and combinations of technologies to optimize the diagnostic phase;
- ✓ Development and combination of proven treatments to improve and optimize groundwater and soil pollution control;
- ✓ Destructive material recovery to re-functionalize polluted soils (ARTELIA, 2013).

A comprehensive knowledge of remediation techniques is key to address the optimum economic, environmental and technical aspects for each condition.

1.5 Objectives

Objectives of this study are discussed in this section. The main objective is to find answers to these four questions:

- **Q1:** Can electro-geophysical methods help to monitor DNAPLs recovery?
- **Q2:** What are the impacts of temperature on electrical complex resistivity and relative permittivity of saturated porous media on a multiphase non-isothermal flow? Answer to this question can evaluate efficiency of electro-geophysical measurements to follow up remediation of a contaminated soil with thermal enhanced recovery technique.
- **Q3:** How do electrical complex resistivity and dielectric permittivity of a porous media change as the saturation changes in an isothermal system? While soil remediation happens, removing of DNAPLs due to their high electrical resistivity and low relative permittivity causes variation in these two electro-geophysical parameters in the medium. Answering to this question demonstrates accuracy of this assertion.

To accomplish the objectives of this study, understanding of the main concerns and all environmental and theoretical aspects and limitations of the work is important. Generally, soil remediation has some difficulties. Remediation study included many thematics, and especially geophysics, especially geophysics, in order to increase the accuracy of the remediation process and decrease the depollution cost. In many previous works (e.g. Conrad et al., 2002) interaction between DNAPLs and different fluids were studied. The goal of this study is to characterize the effect of electrical complex resistivity and permittivity relation versus variation of water and DNAPLs contents on isothermal and non-isothermal situations will be discussed. Temperature variations in the contaminated soil can change the complex conductivity and permittivity value of the soil due to the effects on the chemistry and moisture of the soil (Hayley et al., 2007; Ajo-Franklin et al., 2004). In addition, temperature changes impacts the viscosity of the pollution in the soil. Taking into account, the variations and effects of these parameters can improve the accuracy of method in addressing above mentioned questions.

There are some observation points in the field. Imaging between these boreholes is the final goal of the Bioxyval project. The effects of pollutant on geophysical signals will be evaluated and will be used in order to locate and monitor the clean-up process. Later, by using a mixing model, geophysical signals will be used to estimate the residual content.

The main question that this thesis intends to answer is how geophysics can assist with what is happening in between these monitoring / recovery wells. Specifically, we try to make empirical models in order to estimate the DNAPL content in function of saturation and temperature. Working on the quantitative of pollution before and after the remediation process is not enough. We need the qualitative idea to monitor the progress of the soil remediation to validate the process in a long term monitoring. Geophysics may help to monitor the remediation of soil and groundwater, first by following the short-term injection of remediation agents, which could be chemical, biological or physical, then by monitoring the long-term response of the site provided that the latter can be fully understood from a petrophysical point of view. The latter point remains challenging.

Saturation vs. complex electrical resistivity and relative permittivity will be correlated to interpolate between the wells and to find the value of residual saturation. This leads to finding more polluted areas in the field which lead to installing more wells in those areas and extracting more DNAPL.

1.6 Outline

This manuscript consists of six chapters. The first chapter is an introduction to this study. In this chapter, objectives of this study, description of the polluted site and a summary of previous works that were done in order to highlight the effects of remediation and physical processes on the geophysical parameters. The second chapter is the geophysical background information required for this study with the focus on the concept and characteristics of geophysical parameters, porous media, electromagnetic properties, geophysical techniques and mixing models. The third chapter contains the methodology, materials used in the laboratory work. It is dedicated to the description of the experimental methods used in the laboratory. It is a question of describing the measuring devices and the protocols used for the experiments in columns. Chapter 4 present the results on the effects of temperature increase on multiple geophysical parameters like complex resistivity and relative permittivity of porous media contaminated by two DNAPLs (coal tar and chlorinated solvent). This chapter is based on a paper accepted with moderate revision to be published in the Journal of Applied Geophysics. Chapter 5 is an experimental study of electro-geophysical properties in multiphase saturated porous media under DNAPL recovery. In this chapter effects of saturation changes on electro-geophysical parameters during clean-up programs is studied. Final chapter is the conclusions and perspectives of this study.

2 Geophysical backgrounds

This chapter is divided in three main subchapters to deal with theories and the geophysical background related to this study. The first part is about the hydraulic concepts in porous media dealt with in this study. The second part is a summary of the electromagnetic properties to develop theoretical concepts of electrical complex resistivity, relative permittivity and chargeability, and their corresponding empirical models that are largely used in recent studies. In the third part, electro-geophysical methods with the focus on the methods used to study the geophysical parameters mentioned in second part will be discussed. The focus of this chapter is on the concepts, parameters and methods using in the laboratory.

2.1 Porous media

Dullien (2012) defined porous medium with two properties:

1. The material that is ubiquitous in nature and includes relatively small spaces, called pores or voids, fixed in the solid or semisolid surrounding substance. The pores contain air or fluids and are interconnected, or in some materials, pores are not connected (e.g. vuggy porosity in certain volcanic and carbonated rocks)
2. The body matrix can allow passing fluids and air through itself. This works like a septum made from materials that permit penetration from one face and emerge on the other, this kind of medium also called permeable.

Generally, in a porous medium, that is a network of different size pores, large pores connected by smaller pores. The human skin, lungs, bones and hair are some examples of porous media in our body. We use the other porous media like textiles, paper towels, tissues, soil and sandstone every day. Study about porous media are important in hydrogeology, petroleum science and soil depollution studies. Porous media properties can be defined at microscopic and macroscopic scales. Porosity, permeability, formation resistivity factor and breakthrough capillary pressure are microscale characteristic of a porous media that reflect average behavior of them, on the other hand microscale characteristics are related to the distribution of the pore and their matrix body and interconnectedness of pores.

2.1.1 Topology and Porosity

The porosity (Φ) is the ratio of pore volume (V_p) to the total (bulk) volume (V_t) and is expressed as:

$$\Phi = \frac{V_p}{V_t} \quad \text{Equation 2-1}$$

The porosity values can be between 0 and 1. There are two kinds of porosity:

1. Effective (interconnected) porosity that is the fraction of bulk volume occupied by interconnected pores, which has the main role in fluid flow due to advection, named conductive pores.
2. Isolated (non-interconnected) porosity that is also called dead-end pores. The mechanism of fluid flow in dead-end pores is based on diffusion. System of this pore network is interconnected to the continuum of void space only in separate passage, therefore, it cannot contribute in fluid flow with advection.

Besides these properties, the topology of the medium is highly crucial for any kind of fluid transport in pore spaces; topology is defined as the way the structural units are interconnected in space. A topological description of a three dimensional medium needs comprehensive information at the scale of corresponding structural units, e.g. pores, in all three dimensions. But there are no stereological methods to infer 3D topological characteristics from two-dimensional sections (Vogel, 2002).

In contaminated soils, higher interconnected porosity may facilitate pumping rate of DNAPL components from polluted regions. After decontamination, the replacing and release of these components is expected to be very slow for medium with lower porosity. This is because little or no water flushes through dead-end pores segments. Therefore, in low-porosity rocks clean-up potential is estimated to be less than that expected for sand and gravel medium.

The porosity in hydrogeological point of view could be described in three different groups that illustrated in Fig. 11 (e.g., Vouillamoz, 2003).

1. Total porosity that is the total voids volume.
2. Specific yield that is the ratio of the volume of gravity water to the total volume. The specific yield represents the volume of water that can be drained by the action of the gravitational force until reaching the saturation equilibrium.
3. Effective porosity that is the ratio of the connected pore volume to the total volume. The effective porosity quantifies the volume of mobile water in a saturated zone under the action of a load gradient.

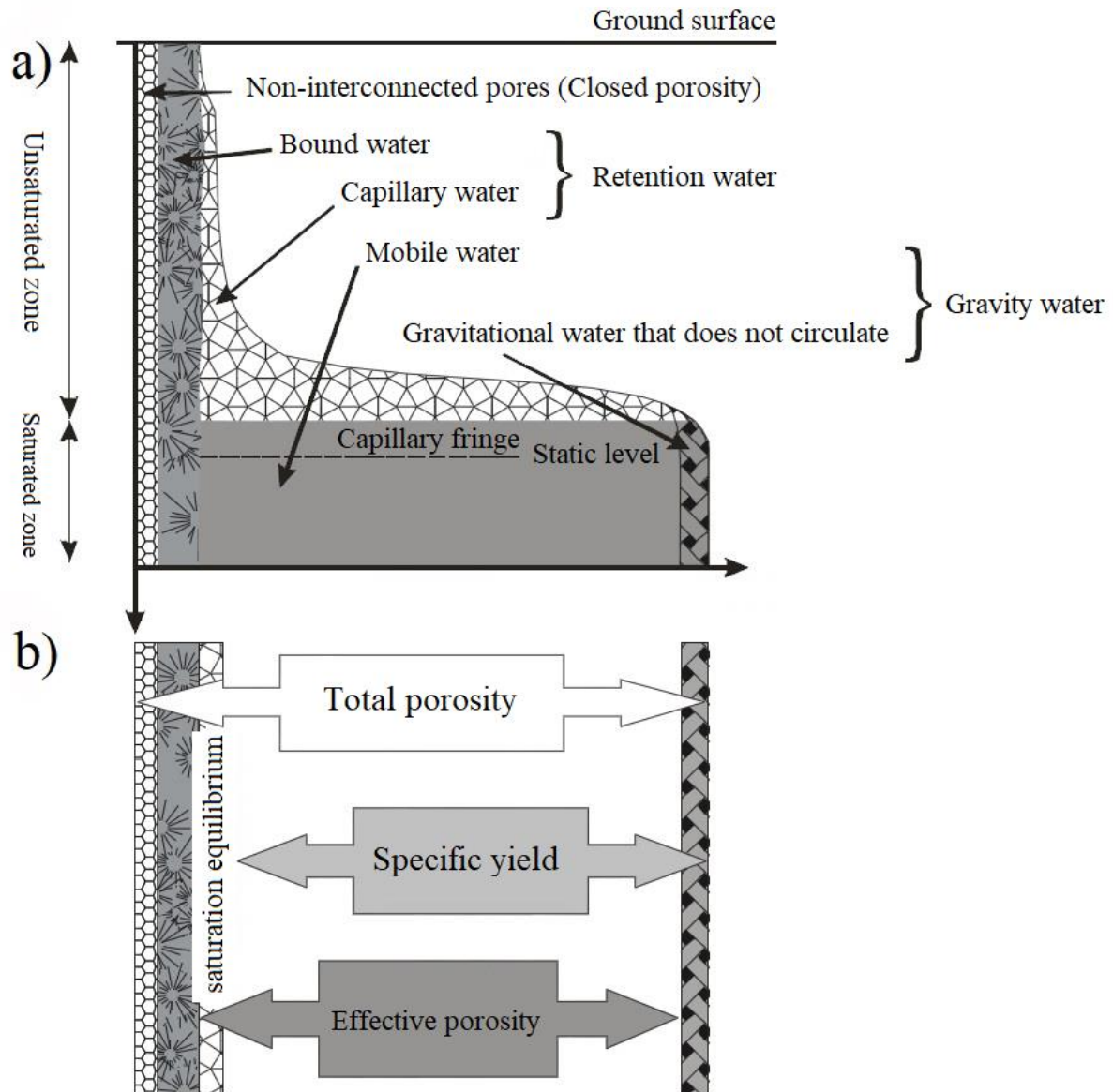


Fig. 11. Hydrogeological porosity. a) Representation of the saturation profile and b) Comparison of the hydrogeological porosities (Vouillamoz, 2003).

2.1.2 Multiphase media

Multiphase flow in porous media concerns engineering problems in geophysics, geology, hydrogeology, petroleum engineering and biological engineering. All these fields need to have a comprehensive understanding of multiphase flow in porous media, like air-water interaction in the vadoze zone, gas-oil-brine in fractured rocks, blood flowing into tissue and a drop of ink dipping on a paper. All phenomena linked to fluids flow against gravity in porous media is governed by capillary effect on the interface between two immiscible fluids.

In geophysical view, three major cases are important:

1. Air-water motion in unsaturated soil. In this case, air is non-wetting and water is wetting phase. The interface between air and water in this region is governed by multiphase flow and effects soil stiffness and deformability.
2. The second case is a system consisting of oil and brine. Oil-gas and brine system happens in the oil/gas reservoir. For oil and gas reservoir, a large amount of natural gas are deposited in natural formations, definitely under high pressure.
3. The third case is contamination mostly classified as DNAPLs and water appears in contaminated sites. In this case, air consists as the third fluid in some conditions. For polluted sites, depollution engineers often use gas injection, water injection and thermal method to enhance DNAPL extraction. Due to complexity of the multiphase fluid leakage measurements in these sites, the theory of multiphase flow in porous media offers researchers solutions to predict the DNAPL recovery.

In large-scale porous media, looking at any minor multiphase physics of complex immiscible fluids in details is impossible. Understanding of the fundamental relationships that govern the properties of multiphase media behavior is very important. The constitutive relationships that include the influence of subscale phenomena have to be defined in every micro/macroscale model. The key point for solving the complex multiphase flow in porous media is to explore and establish a simple and effective relationship.

Fatt (1956) was the first to study pore networks to characterize multiphase flow in porous media. Percolation theory was used to describe multiphase motion in porous media in 1980s (Helba et al., 1992). In addition, the pore-scale displacement mechanisms for both imbibition and drainage were observed directly in micro model experiments (Lenormand et al., 1983).

Most of the studies are focused on the water-wet porous media. In 1990s, pore-scale modeling of multiphase porous media became popular due to moving away from fundamental studies and shifting to predictive models to describe the multiphase flow in porous media.

2.1.3 Saturation

At the Darcy scale (that is the scale between pore and core scales that is governed by the Darcy's law), a relevant physical property of a point in a multiphase porous media define as an average of a pore scale representative elementary volume (REV) related to that given point. At the Darcy scale, this point can fill with all phases in a same time that is defined by the volume fractions and saturations. The volume fraction of phase α is the ratio of volume of the REV part filled by phase α to the total volume of REV given as:

$$\theta_{\alpha} = \frac{|U_{\alpha}|}{|U|} \quad \text{Equation 2-2}$$

According to the volume fraction definition, porosity could be define as volume fraction of pores fluids (fluid a $|U_a|$ and water $|U_w|$) that can be given by

$$\Phi = \frac{|U_w| + |U_a|}{|U|} = \theta_a + \theta_w \quad \text{Equation 2-3}$$

where θ_a and θ_w are named fluid a and water contents. Furthermore, saturation of phase “a” (S_a) can be defined as ratio of fluid “a” content to its porosity so

$$S_a = \frac{\theta_a}{\Phi} \quad \text{Equation 2-4}$$

In a two-phase porous medium of water and air, sum of air and water saturations should be equal to one

$$S_a + S_{fluid} = 1 \quad \text{Equation 2-5}$$

Where S_{fluid} is the saturation of fluid. Note that the saturation is between 0 and 1. In other case, a saturated contaminated soil with DNAPL, Equation 2-5 must be written as:

$$S_{air} + S_{DNAPL} + S_w = 1 \quad \text{Equation 2-6}$$

Where S_{air} is the air saturation that can be zero in a saturated medium. The range of variability is normally smaller than one. For example after drainage of a saturated medium with water, at some points liquid flow is not possible because of breaking continuity of pore water the corresponding volume of this water after drainage an after imbibition are named as irreducible (S_{iw}) and residual saturations (S_{rw}). Captured air bubbles occupy some pores during imbibition; therefore, it is impossible to get the full water saturation (in a dry and natural condition). If the saturation of these isolated air bubbles is named S_{ra} , water saturation will be $1-S_{ra}$.

In practical works, the fluid saturations should be normalized according to the range of values occurring in the problem under consideration. The normalized (effective) saturations can be obtained from:

$$S_{e\alpha} = \frac{S_{\alpha} - S_{\alpha}^{min}}{S_{\alpha}^{max} - S_{\alpha}^{min}} \quad \text{Equation 2-7}$$

where S_{α}^{max} and S_{α}^{min} are the maximum and minimum saturation for a problem. Indeed, in our studies we should count the irreducible and residual saturations as problem-specific parameters, not material parameters (Helmig, 1997).

In soil physics, volume fractions (θ_{α}) is normally used to compute the relative quantity of fluid phases. In field conditions, residual water content can be define as:

$$\theta_{rw} = \Phi S_{rw} \quad \text{Equation 2-8}$$

Then, saturated water content will be:

$$\theta_{sw} = \Phi(1 - S_{ra}) \quad \text{Equation 2-9}$$

The saturated water content refers to the state of maximum attainable water saturation.

2.1.4 Wettability and non-wettability

Fluids inside pores in a multiphase porous media can be classified according to their wettability due to their tendency to be attracted by soil particles. Two different phases describe in a multiphase system, wetting phase that presents great tendency to contact with soil particles and non-wetting phase that normally refers to fluids that have least tendency to contact with soil particles. Fig. 12 shows the idealized interface between different phases (solid phase and two immiscible liquid phases) in a multiphase system.

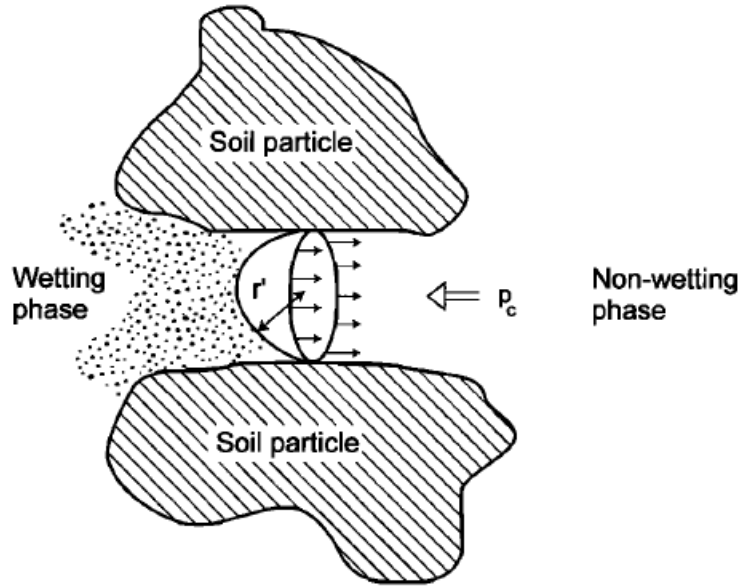


Fig. 12. Cross section of interface between soil particles, wetting phase and non-wetting phase (Mayer, 2005)

Wetting phase saturation expressed as:

$$S_w = \frac{\theta_w}{\Phi} \quad \text{Equation 2-10}$$

where θ_w is wetting phase content and Φ is the porosity of the medium. Then non-wetting phase saturation is expressed as:

$$S_{nw} = 1 - S_w \quad \text{Equation 2-11}$$

The non-wetting phase saturation (S_{nw}) is the ratio of non-wetting fluid volume over pore volume.

Wettability is related to interfacial tensions and contact angle. The contact angle is defined in Fig. 13 in three different modes:

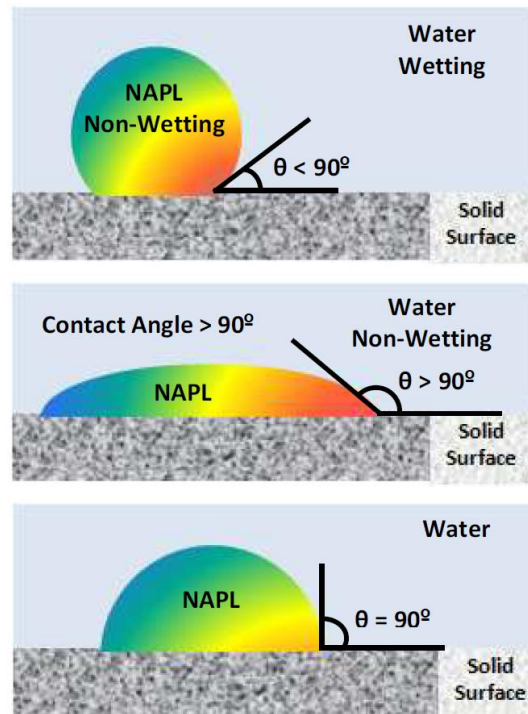


Fig. 13. Contact angle and typical fluid relationship (Cohen and Mercer, 1993)

1. $\theta < 90^\circ$: Compared to water, NAPLs consider as non-wetting phases due to more affinity of water for the surface.
2. $\theta > 90^\circ$: This mode is rare but in some cases the contact angle is more than 90° due to less affinity of water compared to NAPL for the solid surface.
3. $\theta = 90^\circ$: In this mode that is theoretically possible, NAPL phase is neutrally wetting (Cohen and Mercer, 1993).

Anderson (1986) called the wettability mode when $0^\circ < \theta < 65^\circ$ - 70° , water-wet and when 105° - $120^\circ < \theta < 180^\circ$, oil-wet. When θ is between 70° to 105° in intermediate range, the system is define as neutrally or intermediately-wet.

Interfacial tension represents the force parallel to the interface of one fluid with another fluid, which leads to the formation of a meniscus and the development of capillary forces and a pressure difference between different fluids in the subsurface (Wischkaemper et al., 2013). The interfacial tension of chlorinated solvent DNAPLs and coal tar in the subsurface are generally much lower than that of pure solvent compounds due to the admixture of surface-active agents from soil humus and other waste materials (Wischkaemper et al., 2013).

For a system that DNAPL infiltrates into the saturated sandy aquifer, the first state ($\theta < 90^\circ$) is established. It demonstrates that water is wetting and DNAPL will be non-wetting phase (Power et al., 1996). As the non-wetting fluid DNAPLs should replace water in pore spaces, the lower

contact angle and higher interfacial tension between the two phases lead more resistance of water to infiltrate into the aquifer.

For small DNAPL spills, DNAPL distributes until being the disconnected droplets or blobs at the residual non-wetting saturation. On the other hand, for large spills, DNAPL can pool on low permeability formations (Bear, 1972, Kueper et al., 1993)

We reviewed that wettability is related to the contact angle but contact angle is hysteretic it means that for the same couple of fluid contact angle will be different for advancing (moves out over a solid surface) or receding (moves off over a formerly occupied surface) (Adamsom and Gast, 1997). Receding contact angle is normally smaller than advancing one. The surface heterogeneity and surface roughness could be the reasons for this difference (Adamsom and Gast, 1997).

2.1.5 Permeability and Darcy's law

Permeability is an indication of the capacity of a porous medium to let fluids flow through it. The higher the permeability, the easier the fluid flow in a porous medium. Darcy (D) is the unit of permeability. One Darcy is defined as the permeability that will conduct a fluid of 1 mPa.s viscosity at a flow rate of 1 cm³/s through a cross-sectional area of 1 cm² when the pressure gradient is 1 atm/cm. 1 Darcy is approximately equal to 10⁻¹² m².

The equation that defines permeability in terms of measurable parameters is called Darcy's law. When the fluid flow is, unidirectional and laminar, under steady-state conditions, Darcy's law is expressed as:

$$Q = \left(\frac{kA}{\mu}\right)\left(\frac{\Delta P}{L}\right) \quad \text{Equation 2-12}$$

where Q is the volumetric flow rate, $\Delta P = P_1 - P_2$ is the pressure drop, μ is the viscosity, k is the permeability of the porous medium, A and L are the normal cross sectional area and length of the sample, respectively.

In the study of the fluid flow through porous media in the Darcy scale under drainage and imbibition, we deal with a hydraulic phenomenon. Fig. 14 shows the capillary pressure-saturation relationship after a drainage-imbibition. In this figure, two graphs of drainage and imbibition do not overlap on each other because the ways that pores inside porous media are drained and imbibed are not same. This phenomenon is known as hysteresis. By repeating another drainage and imbibition after finishing first imbibition, new curves of drainage and imbibition would be obtained and hysteresis will happen again. It is worth mentioning that there is no limitation on repeating drainage-imbibition cycle and hysteresis will occur depending on

drainage-imbibition curves. Precise reporting of volume change inside sample is very important.

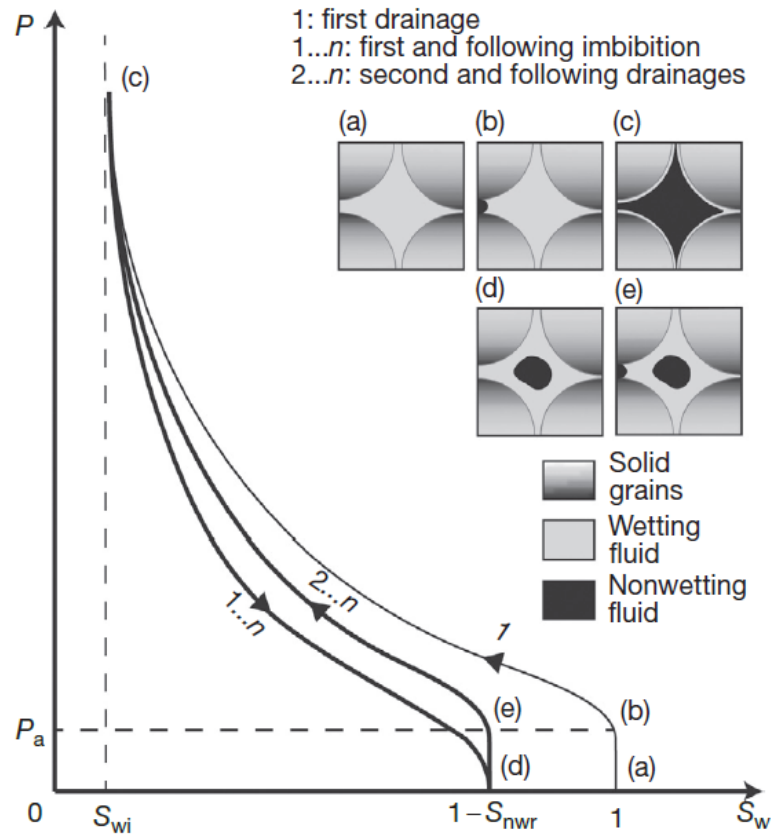


Fig. 14. A generic example of capillary pressure curves (i.e., nonwetting fluid pressure plotted against wetting fluid saturation). During the first drainage, a nonwetting fluid (represented as black in the insets) is gradually injected into a porous body initially saturated with a wetting fluid (light gray). This stage is followed by imbibition–drainage cycles that all follow the same curves. The insets illustrate the pore-scale distribution of the phases at various stages during the drainage–imbibition cycles. (a) In the initial state, only the wetting fluid is present. (b) A small nonwetting fluid meniscus appears on the left side, indicating the onset of penetration by the nonwetting fluid. (c) The irreducible wetting fluid saturation is shown as a film of wetting fluid along the pore walls (implying that γ is zero). (d) At the residual nonwetting fluid saturation, some amount of nonwetting fluid is trapped in the pore space. (e) A small nonwetting fluid meniscus appears on the left side, indicating the onset of penetration by the nonwetting fluid at the beginning of a new drainage cycle (Bernabé and Mainault, 2015).

2.2 Electromagnetic properties

A brief summary of the geophysical parameters used in this study is presented here. Complex electrical resistivity and relative permittivity have been used in our study as parameters characterizing the geophysical characteristics of solid and aqueous phases. An understanding of the theory and fundamentals behind them is necessary understanding and interpreting the data.

James Clerk Maxwell (1831-1879) presented the governing equations of electric and electromagnetics in four partial differential equations which can also be expressed in integral form:

- Faraday's law: $\nabla \times E = -\frac{\partial B}{\partial t}$ Equation 2-13

- Ampere's law: $\nabla \times B = \mu_0 J + \frac{1}{c^2} \frac{\partial E}{\partial t}$ Equation 2-14

- Electric form of Gauss's law (Field diverges from electric charges):
 $\nabla \cdot E = \frac{\rho}{\epsilon_0}$ Equation 2-15

- Gauss's law for magnetism (No magnetic monopoles): $\nabla \cdot B = 0$ Equation 2-16

where E is electric field intensity, B is magnetic field intensity, ρ is the total electric charge density, J is the total electric current density, ϵ_0 is permittivity of free space and equals to 8.854×10^{-12} F/m, μ_0 is permeability of free space equals to $4\pi \times 10^{-7}$ H/m, $\epsilon_0 \mu_0 = 1/c^2$ and c is speed of light equals to 2.998×10^8 m/s ≈ 300000 km/s.

In macroscopic scale, the exact boundary conditions are major preconditions for solving Maxwell equations. Kirchhoff's circuit laws, which are driven from Maxwell equations, are the principal equations used in electrical circuit interface. In these equations, study platforms can be in frequency or time domains. Particularly, solving Maxwell equations can conduct conventional AC circuit for the situation that electric field varies sinusoidally (with equation of $I = I_0 \sin(\omega t)$ where ω is the angular frequency and t the time) in time domain and consequently, Oscillation equations for electric field vectors are driven from Maxwell equations.

By considering all four Maxwell equations and correction of Ampere's law, Maxwell can demonstrate that electromagnetic can spread as traveling waves. In the simplest case, we supposed that in some part of space electric field $E(x)$ and magnetic field $B(x)$ are non-zero along z and y axes, respectively. In this simple case, both fields are function of x . Then the Faraday's law converts to (Purcell and Morin, 2013):

$$\frac{\partial E}{\partial x} = -\frac{\partial B}{\partial t}$$
 Equation 2-17

and when $J=0$, Amperes law gives:

$$\frac{\partial B}{\partial x} = -\frac{1}{c^2} \frac{\partial E}{\partial t}$$
 Equation 2-18

Solving partial derivative of Equation 2-17 and Equation 2-18 with respect to x and t gives (Purcell and Morin, 2013):

$$\frac{\partial^2 E}{\partial x^2} = -\frac{\partial^2 B}{\partial x \partial t}$$
 Equation 2-19

$$\frac{\partial^2 B}{\partial t \partial x} = -\frac{1}{c^2} \frac{\partial^2 E}{\partial t^2} \quad \text{Equation 2-20}$$

By assembling Equation 2-19 and Equation 2-20:

$$\frac{\partial^2 E}{\partial x^2} = \frac{1}{c^2} \frac{\partial^2 E}{\partial t^2} \quad \text{Equation 2-21}$$

This equation is in a similar format like wave equation in x direction. As a result, both electric and magnetism laws demonstrate traveling of electric and magnetic fields as waves. The general solution consists of linear combinations of sinusoidal components as shown below.

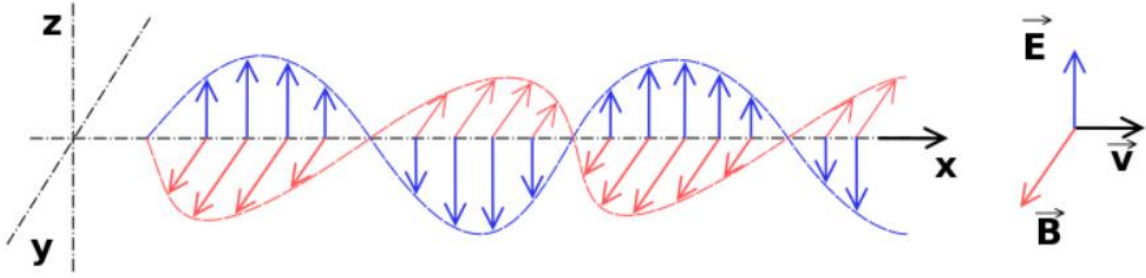


Fig. 15. The general solution consists of linear combinations of sinusoidal components (Purcell and Morin, 2013)

2.2.1 Complex resistivity

Ohm's law is a physical relationship between current through a medium or material and the potential response difference across it (Glover, 2015).

Ohm's law expresses the current injected through a conductive medium (I, in A) between two points is directly related to electric potential response (V, in V) between two other points in an electrical field. Fig. 16 shows a simple schematic presentation of the parameters in Ohm's law. It is inversely proportional with resistance of the medium (R, in Ω).

$$I = \frac{V}{R} \quad \text{Equation 2-22}$$

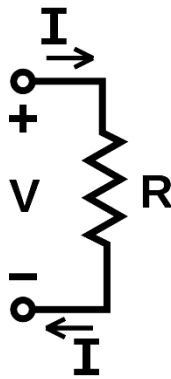


Fig. 16. V, I, and R, the parameters of Ohm's law

The potential difference between two points after introducing current shows the electric force that leads to a flow of charge which carries the current (Glover, 2015). The property of material that resist against flow of charge carriers is referred to as resistance.

At the local scale, Ohm's law can be expressed as:

$$\vec{j} = \sigma \vec{E} \quad \text{Equation 2-23}$$

where \vec{j} is the current density (A.m^{-2}), σ is the electrical conductivity of medium (S.m^{-1}) and \vec{E} is electric field (V.m^{-1}).

The conductivity is frequency dependent and can vary as a nonlinear tensor due to temperature, saturation and pressure changes. In a case where the material has the velocity of \vec{v} in a magnetic field \vec{B} , the magnetic field is contributing in to the amount of current density. Equation 2-23 will be:

$$\vec{j} = \sigma(\vec{E} + \vec{v} \times \vec{B}) \quad \text{Equation 2-24}$$

This equation is used in many electromagnetic methods (e.g magnetotellurics).

Resistance is the capability of a material to resist against passing electric current through it. The SI unit for resistance is ohms (Ω). In porous media, the resistance is related to the size and shape of the body of porous media and physio-chemical characteristics of pore fluids. Resistance has a direct correlation with the distance which current flows through and an inverse relationship with cross-sectional area of the material. In a homogeneous and isotropic medium that current passes through it, the value of resistivity (ρ) is proportional to the measured resistance, length (L) and cross-sectional area (A). The electrical resistivity is:

$$\rho = R \frac{A}{L} \quad \text{Equation 2-25}$$

The other ways of describing resistivity are:

$$\rho = \frac{\vec{E}}{\vec{j}} \quad \text{Equation 2-26}$$

and

$$\rho = Rk \quad \text{Equation 2-27}$$

where k is the geometric factor. Resistivity is related to the temperature. In metals, the resistivity increases with temperature and in semiconductors decreases with temperature.

The resistivity is related to the ionic content of the fluid inside the porous media. In near surface geophysics, the resistivity of aqueous phase, which is the dominant conductive component, decreases as temperature increases about 4%, 2% and 1% per 1°C at low temperature (about 5°C), room temperature and about 100°C , respectively (Sen and Goode, 1992). This demonstrates that the stability of temperature during electrical measurements is

important and crucial for having a successful experimental program. This sensitivity of measurements has been shown in different studies. When results are compared with different studies, experiments should be conducted at similar temperature conditions in porous media or permeable rocks. Inversely, in geothermal field applications or ground water studies, resistivity of the subsurface materials is used to estimate the temperature. Guéguen and Palciauskas (1994), Schon (2004) and Keller (1989) presented the resistivity of some materials that are shown in Fig. 17. Pierson (1993) expressed that resistivity varies between $10^{-7} \Omega.m$ (copper) and $10^{18} \Omega.m$ (diamond). With proper accurate laboratory measurements of resistivity, various geo-materials can be differentiated. It can be achieved by application of probes that are adequately sensitive to the structure, composition, and fabric of the porous media. High degree of heterogeneity of geo-materials can make application of electrical characteristics for distinguishing various geo-materials.

Conductance (G_c) (in Siemens (S)) has an inverse relationship with resistance (R), therefore:

$$G_c = \frac{1}{R} \quad \text{Equation 2-28}$$

Therefore, it represents the ability of a material to pass the electric current (charge flow).

Conductivity (σ) in ($S.m^{-1}$) can be expressed in term of resistivity (ρ):

$$\sigma = \frac{1}{\rho} = \frac{\vec{J}}{\vec{E}} \quad \text{Equation 2-29}$$

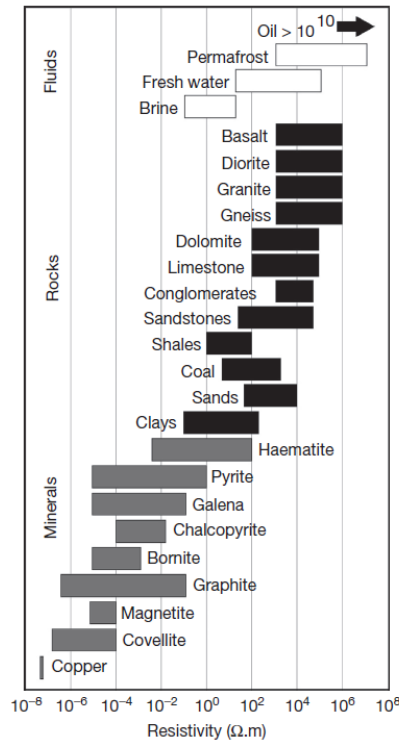


Fig. 17. Electrical resistivity of several geomaterials (Glover, 2015).

The conductivity can be expressed as a complex value as stated below:

$$\sigma^* = \sigma' + i\sigma'' \quad \text{Equation 2-30}$$

Superscripted asterisks are used to indicate the complex form of a parameter. In this equation σ' is a real part and σ'' is the imaginary part. As electrical resistivity is the inverse of electrical conductivity, then (Guéguen and Palciauskas, 1994):

$$\rho^* = \rho' - i\rho'' \quad \text{Equation 2-31}$$

These electrical conductivity and electrical resistivity composed of two main parts, the real parts (in-phase component) that is describing energy transport and the imaginary parts (out-phase component or quadrature component) that is related to energy loss (energy dispersion). These two complex parameters are frequency dependent and can be expressed as an amplitude and a phase. In polar form, Equation 2-31 can be written as (Ghorbani, 2007):

$$\rho^* = \rho' - i\rho'' = |\rho^*| \exp(i\varphi) \quad \text{Equation 2-32}$$

Where $|\rho^*|$ and φ are the amplitude (resistivity) and the phase of complex resistivity that can typically be expressed as:

$$\varphi = \tan^{-1} \left(\frac{\rho''}{\rho'} \right) \approx \frac{\rho''}{\rho'} \quad (\text{classically when } |\varphi| < 100\text{mrad}) \quad \text{Equation 2-33}$$

or

$$\varphi = -\tan^{-1} \left(\frac{\sigma''}{\sigma'} \right) \approx -\frac{\sigma''}{\sigma'} \quad (\text{classically when } |\varphi| < 100\text{mrad}) \quad \text{Equation 2-34}$$

Phase can be defined as a function of real (ϵ') and imaginary (ϵ'') components of relative permittivity (Ghorbani, 2007):

$$\varphi = -\tan^{-1} \left(\frac{\epsilon''}{\epsilon'} \right) \quad \text{Equation 2-35}$$

Associated results of complex resistivity can be shown in “amplitude-phase” or “real-imaginary parts”.

2.2.2 Relative permittivity

In addition to the electrical conduction, electrical fields also interact with materials by electric displacement of charge, D (C.m⁻²). The material property describing the electric displacement field is the dielectric permittivity ($D=\epsilon E$). Dielectric relative permittivity, ϵ^* , is a physical property which characterizes the degree of electrical polarization of a material under the influence of an external electric field. The complex dielectric permittivity consists of two parts, a real (ϵ') and an imaginary part (ϵ'') (Ledieu et al., 1986):

$$\varepsilon^* = \varepsilon' + i(\varepsilon'' + \frac{\sigma_c''}{\omega_{cf}\varepsilon_0}) \quad \text{Equation 2-36}$$

where σ_c'' is the dissipation due to the finite rate of displacement that charge carries and also due to the various losses from dispersion ($S.m^{-1}$) and ω_{cf} is the circular frequency.

At high frequencies (3 MHz to 300 MHz), for measurement tools such as TDR probes used in this work (70 MHz), ε^* is considered to be equal to real part (ε') and imaginary part is negligible (Glover, 2015; Heimovaara et al., 1994). At much high frequencies, there is not enough time for polarization mechanism; therefore, real and imaginary parts do not have any contribution on the permittivity.

The relative permittivity, ε , is defined as the ratio of the real effective dielectric permittivity, ε_{eff}' , and the free space permittivity, ε_0 .

$$\varepsilon = \frac{\varepsilon_{eff}'}{\varepsilon_0} \quad \text{Equation 2-37}$$

The relative permittivity is the ability of a material to obtain intrinsic polarization. The relative permittivity of materials with polar molecules like water is high (almost 80) due to electric polarization and dipolar polarization. In most oils and DNAPLs, the dielectric constant is about 2 due to lack of polar substances. Therefore, permittivity is due to electrical polarization (Glover, 2015).

The relative permittivity of a rock or a porous media made from geomaterials, saturated by water or any other fluid, is expressed as a two-component mixture of the matrix relative permittivity (ε_{rs}) a fluid relative permittivity (ε_{rf}). Both components are frequency dependent. In frequencies less than 100 GHz, we can consider relative permittivity of all components as real and independent from frequency except water that is still expressed as:

$$\varepsilon_{rw}(\omega) = \varepsilon_{rw}'(\omega) + i\varepsilon_{rw}''(\omega) \quad \text{Equation 2-38}$$

Imaginary part of relative permittivity of water is also negligible for the critical frequency for dipolar relaxation (10^{10} Hz). In this condition, imaginary part of the dielectric constant is assumed to be almost 0. Then for water

$$\varepsilon_{rw} = \varepsilon_{rw}'(1 - i\tan\delta_w) \cong \varepsilon_{rw}' - i\frac{\sigma_w}{\varepsilon_0\omega} \quad \text{Equation 2-39}$$

Therefore in a saturated porous media or rock, three parameters of ε_{rs}' , ε_{rw}' and σ_w have the roles of defining the dielectric response. Relative permittivity in a saturated rocks can also expressed as:

$$\varepsilon_{rr}^* \equiv \varepsilon_{rr}' - i\frac{\sigma_w}{\varepsilon_0\omega} \quad \text{Equation 2-40}$$

where ϵ_{rr}' and σ_w are the effective dielectric constant and effective electrical conductivity of the composite medium, respectively. Both Equation 2-39 and Equation 2-40 must be applicable for the same composite.

The electrical resistivity and dielectric permittivity are normally used at low and high frequency surveys (Kessouri, 2012).

2.2.3 Chargeability

Three different methods are used in IP surveys. These methods are different according the measuring parameters and their instrumentations that they use to study geological characteristics of the study sites. The measuring parameters of polarization are chargeability (M), percentage frequency effect (PFE), and the phase angle (ϕ). In IP studies, chargeability is in time domain when the other two parameter are in frequency domain.

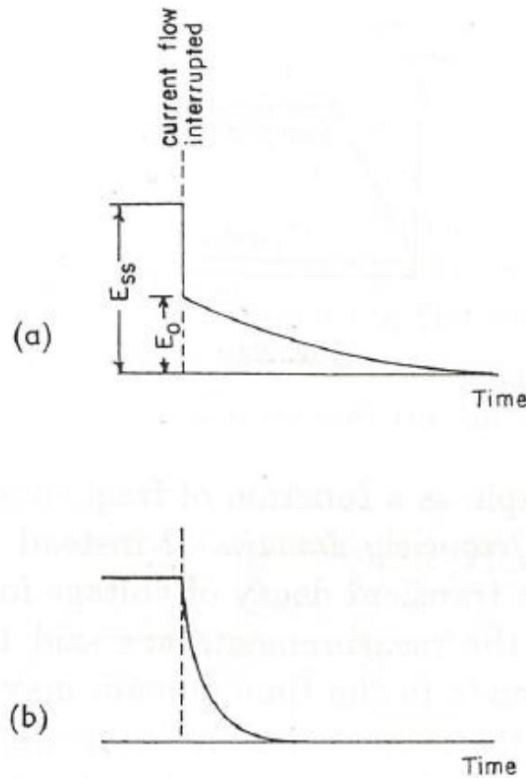


Fig. 18. Transient decay of electric field strength in a rock sample. (b) Transient decay of voltage in an RC circuit (Keller and Frischknecht, 1966).

Chargeability is a physical concept related to conductivity (resistivity) of the medium. Electric field, made of electric currents in a saturated porous media, causes movement of ionic charges through pore fluid. In this procedure, some ions gather at some boundaries. This collection of ionic charges is called IP. Chargeability characterizes the power and formation of

IP in porous media, affected by electric field. Physical description of chargeability is not easy but two mechanisms have the main influence on it: membrane polarization and electrode polarization

2.2.3.1 Membrane or electrolytic polarization

Membrane polarization normally happens because of three reasons: 1. narrowing of pore throat, 2. Existence of clay inside the pore channels, and 3. superposition of diffuse layer.

Mineral surfaces have strong leaning to make a negative charge because of their anions. For instance, clays are negative because they are composed of layered silicates and this derives a negative charge. When an electric field is applied to porous media, ionic charges cannot pass through the narrowed pore spaces and accumulation of positive charges happens in one side of the pore throat (Fig. 19). The collection of ionic charges can make a layer up to 100 μm and blocking of pore space when an electric field is applied. Subsequently, negative and positive charges make a blockage as shown in Fig. 19 in two sides of the pore's throat. As soon as voltage is cut off, ionic charges come back to their steady situation by diffusion that develops the measured IP response (Reynolds, 2011).

The electric dipoles made by accumulation of negative and positive ionic charges in each sides of pore throat are responsible (or source of) measured voltage in IP measurements.

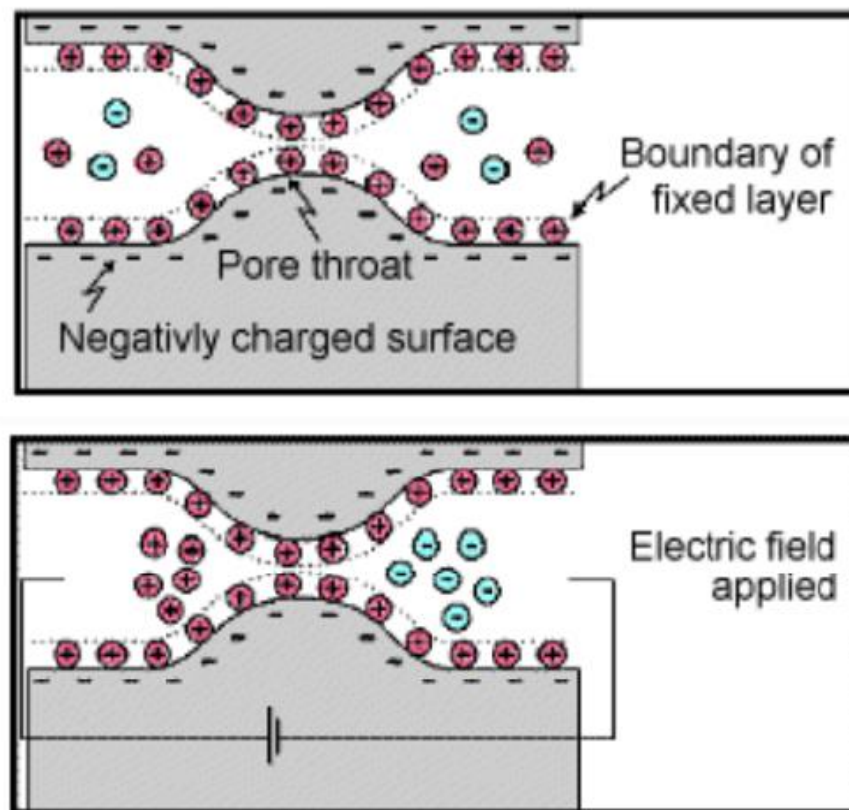


Fig. 19. Schematic form of membrane polarization (ref: <https://bit.ly/2mdLFVy>)

The existence of clay can lead to gathering of negative charges that can attract positive ionic charges. When an electric field is applied, ionic concentration changes.

2.2.3.2 Electrode Polarization with mineral particles (overvoltage)

In the interface of a metallic bar that is sank in an electrolyte, separation of charges happens as shown in Fig. 20.

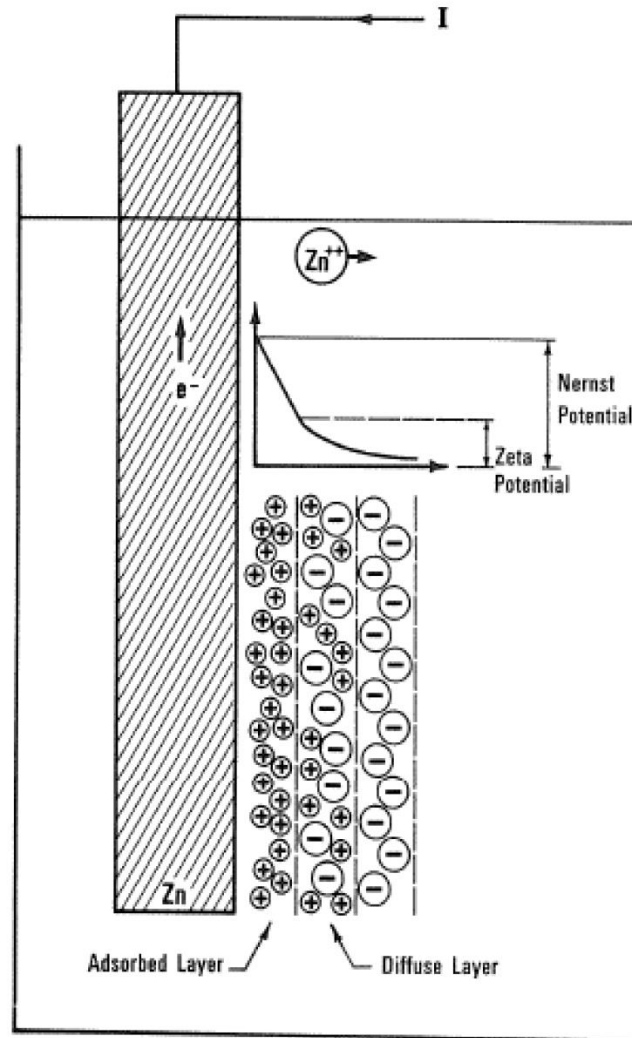


Fig. 20. Illustration of elements of electrode polarization (Beck, 1981).

Mechanisms of electrode polarization are due to the flow of inactive ions in the mobile part of EDL normal to the metal surface and accumulation of inactive charges in excess close to the metal bar (Wong, 1979).

Absorbed layer and diffuse layer close to the metal bar are making an EDL that is due to different potential between metal and electrolyte. The Nernst and zeta potentials are potential difference between electrolyte and solution plus contribution from absorbed layer. An external voltage can disturb these charged layers and as soon as voltage is switched off, both charged

layers will come back to the initial state due to ions diffusion (Beck, 1981). In this situation overvoltage is disappeared by a slow ion diffusion mechanism in a time domain IP measurement. The restoring ionic balance is related to the shape and size of pore(s), permeability, electrical resistivity of fluid and gains, and concentration of ions (Reynolds, 2011). EDL electrochemical theory assumes that the EDL thickness is much less than grain radius (Slater et al., 2005).

2.2.4 Mixing models

2.2.4.1 *Mixing models of electrical resistivity*

Interpretation of a multiphase medium has the strong connection to the understanding of the mixing models theories, which prepare methodology for multiphase systems. Many studies in mixing models were done which are applicable to the other situations with the same properties.

In multiphase porous media, media under study are the combination of different phases. Study about these phases and the standard method to study the relationship between the conductivity of the sedimentary rocks and its porosity expressed in Archie's law. Archie (1942) expressed one of the most basic but important model for electrical conductivity and resistivity. It was an extension of the LR model proposed by Lichtenecker and Rother (1931). The following information on Archie's model and its generalized form is based on Glover (2010). It is important to have a better understanding of the characteristics of the Archie's law. Archie's law was developed using experimental data for limited number of soil and rock samples. It was derived for a limited selection of porosities and fluid conductivities (Archie, 1942). It was mentioned that Archie's law should not be used for the other soils and outside of this range. However, it has been in many studies with material and properties outside of those limits. Regardless, it has shown some of the best results available in the literature. Generalized Archie's law is not the only mixing model presented. Some of the other most common mixing models for electrical conductivity in porous media are shown in Table 1.

The classical Archie's law is usually used if the matrix is a sedimentary material without clays and if the matrix is nonconductive (Glover, 2009).

$$\sigma = \sigma_f \Phi^m = \frac{\sigma_f}{F} \quad \text{Equation 2-41}$$

then,

$$F = \frac{\sigma_f}{\sigma} = \frac{\rho_f}{\rho} \quad \text{Equation 2-42}$$

where σ is the bulk effective conductivity of the rock, σ_f is the conductivity of the pore fluid in [$\mu\text{S/cm}$], Φ is the porosity, m is the cementation exponent and F is the formation factor. Archie

(1942) defined that “the ratio of the conductivity of the pore fluid to that of the rock (or of the resistivity of the rock to that of the pore fluid) is called the formation factor”. Glover (2010) was published the modified version of the Archie’s law to cover the conductive soil matrixes (Equation 2-44). A phase conductivity, a phase volume fraction and phase exponent are the three parts of the generalized Archie’s law. The classical and modified Archie’s law are used for one and two phases, respectively (Glover, 2010).

$$\sigma = \frac{1}{F^*} (\sigma_f + B Q_v) \quad \text{Equation 2-43}$$

where F^* is the shaly sand formation factor, B is the average mobility of the counterions close to the grain surface ($S \text{ m}^2/\text{meq}$) and Q_v is the ionic per unit pore volume (meq/m^3). A saturation exponent for each phase is made with the comparison of the classical second Archie’s law and the generalized form of the Archie’s law that can help us to find the proper relationship between the phase exponents and saturation exponents of each phase. The generalized law provides results that are more detailed for two and three phases but it can be used for media with numerous phases. The three dimensional numerical modeling can prove this behavior but it is hard to carry out it experimentally (Glover, 2010).

In the Archie’s law equation, the cementation exponent, as a variable and exchangeable parameter, is an advantage because it provides flexibility in accommodating diverse set of variables. Rocks with cementation exponent value of one are rare. Typical values are less than one. Cementation exponent value for most common porous media is between 1.5 and 2.5. Generally, the value of the cementation exponent increases when the degree of connectivity of pores decreases (Glover, 2010).

No empirical models like Waxman and Smits, 1968, Equation 2-43, and Dual water model (Clavier et al., 1984) consider the surface conduction. The modified versions of these models are applicable for the nonconductive matrix and if the conducting phase is liquid, it should fill all the pores, i.e. no gas phase.

The second Archie’s law expresses the relationship between rock resistivity with degree of saturation

Glover et al. (2000), Equation 2-44 , proposed a modified version of Archie’s law for the clean rock with the two conductive phases. This model, in a special case that the matrix is nonconductive or the porosity is 100%, can turn to the classical Archie’s law.

$$\sigma = \sigma_1 \Phi_1^p + \sigma_2 \Phi_2^m \quad \text{Equation 2-44}$$

where σ is the bulk effective conductivity of the rock, σ_1 and σ_2 are the conductivities of the two conductive phases (matrix and fluid), Φ_1 and Φ_2 are the volume fraction of the two

conductive phases, and p and m are the exponents of each phase. p exponent can be calculated as below

$$p = \frac{\ln(1-\Phi_2^m)}{\ln(1-\Phi_2)} \quad \text{Equation 2-45}$$

The lower the value of p is the higher is the value of connectivity.

In the porous medium the connectedness is expressed as (Glover, 2009):

$$G \equiv \frac{\sigma}{\sigma_f} = \frac{1}{F} = \Phi^m \quad \text{Equation 2-46}$$

While the connectedness of a given phase is an indication of the physical measure of the availability of pathways for conduction through a phase, the connectivity is an indicator of the configuration of the pore space. The connectivity (χ) is defined as:

$$\chi = \sigma^{m-1} \quad \text{Equation 2-47}$$

Combining Equation 2-46 and Equation 2-47, the connectedness can be expressed as:

$$G = \Phi\chi \quad \text{Equation 2-48}$$

It is clear that the connectivity is related to the porosity and the cementation exponent but the connectedness is dependent on porosity (total volume of pore space) and the connectivity (pore space configuration) (Glover, 2009).

The porosity of a porous media is the ratio of pore volume to total volume of the porous medium. The sum of volume of phases present in a porous medium or rock should be equal to one,

$$\sum_{i=1}^n \Phi_i = 1, \quad \text{Equation 2-49}$$

For porous medium with n-phases, Archie's law can be expressed as (Glover et al., 2000):

$$\sigma = \sigma_1 \Phi_1^{m_1} + \sigma_2 \Phi_2^{m_2} + \sigma_3 \Phi_3^{m_3} + \dots + g(\sigma_i, \theta_k) \quad \text{Equation 2-50}$$

where $g(\sigma_i, \theta_k)$ is the function that represents the relationship between the phases. It resonances density functions between each pair of phases. If $g(\sigma_i, \theta_k) = 0$, the Equation 2-50 reduces to:

$$\sigma = \sum_i^n \sigma_i \Phi_i^{m_i} \quad \text{Equation 2-51}$$

This equation is called the Stieltjes integral. For each phase, the values of σ_i, G, χ and Φ_i are unique because the distribution of the phases are different. The value of phase exponents can vary from zero to infinity. A value less than 1 is for the mediums with high connectedness such as rocks. In other words, the phase exponent and the connectedness have an inverse relationship, i.e. if the phase exponent decreases; the connectedness increases (Glover et al., 2000).

It is easy to understand that exponents of both classical and generalized Archie's law modify the volume component of the phase relative to total rock volume. Glover (2010) found that the classical Archie's law and the generalized Archie's law could be obtained from each other (Equation 2-50 and Equation 2-51).

In a three phase media consists of solid, liquid, and gas phases. By assuming the mineral solid phase as a nonconductive material and assuming pores are full of fluid (i.e. no air or gas inside), it becomes a two phase medium and Equation 2-50 and Equation 2-51 change to:

$$\sigma = \sigma_{fluid} \Phi_{fluid}^{m_{fluid}} \quad \text{Equation 2-52}$$

As $\Phi = \Phi_{gas} + \Phi_{fluid}$ and because there is no gas, $\sigma = \sigma_f \Phi^m$ which is the classical Archie's law. This direct and inverse relationship show that Classical Archie law can be driven from generalized Archie's law and each phase and component of generalized Archie's law define a phase in classical Archie's law because combining n phases is possible assuming a conductive phase and n-1 nonconductive phases with conductivity equal to zero.

If there is just one phase, the connectedness is equal to one and if it is a multiphase system, then the sum of the volumes and connectedness of all phases should be equal to one (Glover, 2010), therefore:

$$\sum_i^n \Phi_i^{m_i} = \sum_i^n G_i = 1 \quad \text{Equation 2-53}$$

Equation 2-51 is symmetric. After rewriting the equation, in Glover et al. (2000), the phase exponent of the jth phase in an ensemble of n phases:

$$m_j = \log(1 - \sum_{i \neq j} \Phi_i^{m_i}) / \log(1 - \sum_{i \neq j} \Phi_i) \quad \text{Equation 2-54}$$

The value of the phase exponent of a given phase is equal to the connectednesses of remaining phases divided by the connectedness of that phase

Assuming solid and gas phases being nonconductive ($\sigma_m = 0$ and $\sigma_g = 0$), Equation 2-50 can be written as:

$$\sigma = \sigma_f \sigma_f^{m_f} \quad \text{Equation 2-55}$$

In this situation, because of $\Phi_g \neq 0$, the pores are saturated with water and gas, it can be expressed as:

$$\Phi_f = \Phi S_w \text{ and } \Phi_g = \Phi(1 - S_w) \quad \text{Equation 2-56}$$

where $S_w = \frac{\phi_f}{\phi}$

Therefore, the Equation 2-55 can be written as

$$\sigma = \sigma_f \sigma_f^{m_f} = \sigma_f (\Phi S_w)^{m_f} = \sigma_f \Phi^{m_f} S_w^{m_f} \quad \text{Equation 2-57}$$

This equation is similar to the second Archie's law equation (Glover, 2010). Therefore, Tiab and Donaldson, 2004 showed that:

$$\sigma = \sigma_f \Phi^m S_w^n, \quad \text{Equation 2-58}$$

The important difference between Equation 2-57 and the second Archie's law is that this equation is related to the volume fraction of fluid but in the second Archie's law, it is related to the porosity. From the combination of Equation 2-57, Equation 2-58 and Equation 2-46, the following equations can be obtained

$$\varphi^m = \Phi^{mf} S_w^{(m_f - n_f)} \quad \text{Equation 2-59}$$

$$G_{pore} = G_f S_w^{-n_f} \quad \text{Equation 2-60}$$

$$G_f = G_{pore} S_w^{n_f} \quad \text{Equation 2-61}$$

$$G_g = G_{pore} S_g^{n_g} \quad \text{Equation 2-62}$$

and

$$G_i = G_{pore} S_i^{n_i} \quad \text{Equation 2-63}$$

Where n_f is the exponent of the saturation with water. Because of the symmetry of the system, these equations can be rewritten for the gas and other phases. Moreover, Equation 2-63 can be used for a n-phase system. If the exponent of the gas saturation is n_g and the gas saturation is S_g , then:

$$\Phi_g = \Phi S_g \quad \text{Equation 2-64}$$

$$\Phi_f = \Phi(1 - S_g) \quad \text{where}$$

$$S_g = \frac{\Phi_g}{\Phi}$$

In these equations $S_w + S_g = 1$, or $\Phi_f + \Phi_g = \Phi$ and $G_f + G_g = G_{pore}$.

From Equation 2-53, it was obtained

$$\sum_{i=2}^n S_i^{n_i} = 1 \quad \text{Equation 2-65}$$

Then a generalized form of the saturation of each n-1 phases of the multiphase system can be written as:

$$S_i = \frac{\Phi_i}{\sum_{i=1}^{n-1} \Phi_i} \quad \text{Equation 2-66}$$

The classical Archie's law is used for 100% water saturation and the second classical Archie's law for the partially saturated medium.

Mixing models listed in table 1 are classified into two groups of models for with and without variable exponents. Some models are consonant to situation with three phases that is the basis of this work. Generalized Archie's law is used in this study.

Name	Conducting phase		Equation	References
	(min)	(max)		
Models without variable exponents				
Parallel model	1	Many	$\sigma_{\text{eff}} = \sum_{i=1}^n \phi_i \sigma_i$	Guéguen and Palciauskas (1994), Luo et al. (1994), Somerton (1992)
Perpendicular model	1	Many	$\frac{1}{\sigma_{\text{eff}}} = \sum_{i=1}^n \frac{\phi_i}{\sigma_i}$	Guéguen and Palciauskas (1994), Luo et al. (1994), Somerton (1992)
Random model	1	Many	$\sigma_{\text{eff}} = \prod_{i=1}^n \sigma_i^{\phi_i}$	Guéguen and Palciauskas (1994), Luo et al. (1994), Somerton (1992)
Hashin-Shtrikman upper bound	2	2	$\sigma_{\text{eff}}^+ = \sigma_2 \left(1 - \frac{3(1 - \phi_2)(\sigma_2 - \sigma_1)}{3\sigma_2 - \phi_2(\sigma_2 - \sigma_1)} \right)$	Hashin and Shtrikman (1962)
Hashin-Shtrikman lower bound	2	2	$\sigma_{\text{eff}}^- = \sigma_1 \left(1 + \frac{3\phi_2(\sigma_2 - \sigma_1)}{3\sigma_1 + (1 - \phi_2)(\sigma_2 - \sigma_1)} \right)$	Hashin and Shtrikman (1962)
Waff model	2	2	$\sigma_{\text{eff}} = \frac{\sigma_2 + (\sigma_1 - \sigma_2)(1 - (2\phi_2/3))}{1 + (\phi_2/3)(\sigma_1/\sigma_2 - 1)}$	Waff (1974)
Brick-layer model	2	2	-	Beekmans and Heyne (1976)
Modified Brick-layer model	2	2	$\sigma_{\text{eff}} = \frac{\sigma_2 \left(\sigma_2 \left(\phi_1^{2/3} - 1 \right) - \sigma_1 \phi_1^{2/3} \right)}{\sigma_1 \left(\phi_1 - \phi_1^{2/3} \right) + \sigma_2 \left(\phi_1^{2/3} - \phi_1 - 1 \right)}$	Schilling et al. (1997)
Models with variable exponents				

Lichtenecker–Rother equation	1	2	$\sigma_{\text{eff}} = (\sigma_1^{1/m}(1 - \phi_2) + \sigma_2^{1/m}\phi_2)^m$	Lichtenecker and Rother (1936); Korvin (1982)
Bussian's equation	2	2	$\sigma_{\text{eff}} = \sigma_2 \phi_2^m \left(\frac{1 - \sigma_1/\sigma_2}{1 - \sigma_1/\sigma_{\text{eff}}} \right)^m$	Bussian (1983)
Conventional Archie's law	1	1	$\sigma_{\text{eff}} = \sigma_2 \phi_2^m$	Archie (1942)
Extended and generalized models with variable exponents				
Lichtenecker–Rother equation (generalized)	1	Many	$\sigma_{\text{eff}} = \left(\sum_{i=1}^n \sigma_i^{1/m} \phi_i \right)^m$	Lichtenecker and Rother (1936); Korvin (1982)
Modified Archie's law	1	2	$\sigma_{\text{eff}} = \sigma_1(1 - \phi_2)^p + \sigma_2 \phi_2^m$ Where $p = \frac{\log(1 - \phi_2^m)}{\log(1 - \phi_2)}$	Glover et al. (2000)
Generalized Archie's law	1	Many	$\sigma = \sum_i^n \sigma_i \phi_i^{m_i}$ where exact solution $m_j = \log \left(1 - \sum_{i \neq j} \phi_i^{m_i} \right) / \log \left(1 - \sum_{i \neq j} \phi_i \right)$ First order approximation $m_j = \sum_{i \neq j} \phi_i^{m_i} / \sum_{i \neq j} \phi_i$	Glover (2010)

Table 1: Some of the most common mixing models for electrical conductivity in porous media (Glover, 2015).

Three models (parallel model, perpendicular model and random model) have been presented for instance in Guéguen and Palciauskas, 1994; Luo et al., 1994 and Somerton, 1992 to calculate the conductivity of a reservoir rock according to the porosity, fluid characters and temperature values. They are used fabric theory and validated their work with the experimental data. The dependencies of thermal conductivity were discussed with them and they found that the conductivity is related to the volume fraction of components, the temperature and the mineral components' aggregation style. Between geometric mean model and fabric model, the second one has the better results because it has the minimum mean errors and its parameters can change with respect to the different lithology (Guéguen and Palciauskas, 1994; Luo et al., 1994 and Somerton, 1992).

Hashin and Shtrikman (1962) have developed a model for a two-phase system. They tried to find a solution to determine the effective magnetic permeability of macroscopically homogeneous and isotropic multiphase materials, in terms of the volume fractions and permeability of the constituting phases. Their results are applicable for multiphase materials, the dielectric constant, electric conductivity, heat conductivity and diffusivity of such materials. If there are just two phases in the multiphase system, the most contrary bound derived that is directly related to the phase permeability and volume fractions. They validate their model with experimental data (Hashin and Shtrikman, 1962).

Waff (1974) has derived a model for one or two phases. This model has been developed in a partially melted material to find the relationship between bulk effective electrical conductivity, melt fraction, and liquid path connectivity. With the calculation of Hashin-Shtrikman bounds for the conductivity and comparing the results with these two geometrical models, i.e. (1) a system with an infinite number of composite spherical particles and (2) a 3D cube with the unique phase that is covered with the other phase. He found that the melt fraction and liquid path connectivity are the main factors for electrical conductivity.

Modified-Brick-Layer (MBL) model has developed by Schilling et al. (1997) for a two-phase medium. They consider a high conductivity zone (HCZ) in Chile. They observed the conductivities about one S/m in this area because of the active volcanoes. High conductivities are observed from 20 to 60 km because of the partial melting. Some other geophysical observations are also considered in this study. The model results were examined with the experimental data. The calculated and experimental observations correlated with each other (Schilling et al., 1997).

Lichtenecker (1931) and Korvin (1982) have developed an equation between porosities and conductivities of each phase to obtain the overall conductivity. This model has been derived

from the functional equations theory under the proper boundary conditions. In a particular situation if the porosity of the first term is equal to zero this model will be same as Archie's law (Lichtenecker, 1931 and Korvin, 1982). Then they derived a generalized form of their equation applicable for many phases.

Bussian (1983) has developed a two-component model for a rock, immersed in water, this model based on the finding of the electrical properties of a rock matrix at any frequency. From the experimental results, they found that their model has the best results to fit the data.

2.2.4.2 *Mixing models of dielectric permittivity*

The classical model for relative permittivity developed by Debye (1929). He defined the model for dipolar liquids and with one polarization mechanism with a well-defined timescale. He expressed that relative permittivity, ϵ^* , as:

$$\epsilon^* = \epsilon_{\infty} + \frac{\epsilon_0 - \epsilon_{\infty}}{1 + i\omega\tau} \quad \text{Equation 2-67}$$

where ω is the angular frequency that equals to $2\pi f$ (rad.s⁻¹), τ is the relaxation time (s), and ϵ_0 and ϵ_{∞} are permittivity values at low and high frequency. The critical frequency (τ_{crit}) to distinguish high and low frequency is τ^{-1} . Equation 2-67 can be divided to real and imaginary parts as below (Guéguén and Palciauskas, 1994):

$$\epsilon'_{(\omega)} = \epsilon_{\infty} + \frac{\epsilon_0 - \epsilon_{\infty}}{1 + \omega^2\tau^2} \quad \text{Equation 2-68}$$

and

$$\epsilon''_{(\omega)} = \frac{(\epsilon_0 - \epsilon_{\infty})\omega\tau}{1 + \omega^2\tau^2} \quad \text{Equation 2-69}$$

Both real and imaginary parts of relative permittivity are shown in Fig. 21.

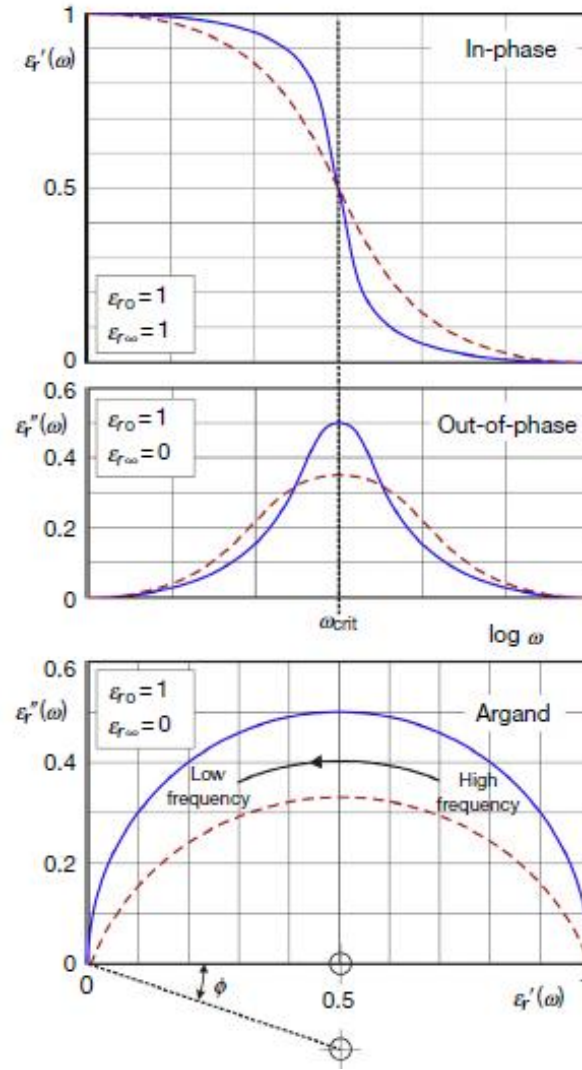


Fig. 21. The behavior of the Debye (solid blue) and Cole and Cole (dashed red) dispersion models shown as a function of frequency for each of the in-phase (upper) and out-of-phase (middle) components and as an are Argand diagram (bottom).

An arbitrary value of $\alpha = 0.22$ has been used for the Cole and Cole model (Glover, 2015).

At the upper part of this figure, blue solid line is the way in which the phase relative permittivity is changing between 0 and 1. Out of phase is shown in middle figure by soil blow line that describes energy loss. As it is clear, it is a frequency dependent parameter and peak point of energy loss happened at critical frequency that is equal to $1/\tau$. The bottom part is the Argand diagram of real part of relative permittivity versus imaginary part. The blue line is presenting Debye model.

There is a broad frequency dependence in Debye model (Chelidze and Guéguen, 1999; Chelidze et al., 1999), however, this model applied to interfacial polarization. Cole-Cole (1941) with taking an ensemble of relaxation times and using Debye model:

$$\varepsilon^*_{(\omega)} = \varepsilon_{\infty} + \frac{\varepsilon_0 - \varepsilon_{\infty}}{1 + (i\omega\tau)^{1-\alpha}} \quad \text{Equation 2-70}$$

where α is equal to 1 this equation will be same as classical Debye model but α can be in the range of 0 and 1. In Fig. 21, red dashes lines are presenting Cole Cole model. Glover et al. (1994) found the relationship between α and ϕ (in radian). These two parameters are related by the equation $\alpha = 2\phi/\pi$. They claimed that four exponent of Cole Cole model are related to fractal dimension of the surface of the grains of the porous media and rocks. It is noteworthy that there are not that many experimental studies in support this theory.

Some models according to the Dissado and Hill (1984) approach developed to find the relationship between Cole-Cole parameter and fractal dimension of the grain and fluid interface (Le Méhauté and Crepy, 1983; Ruffet et al., 1991a,b; Wong, 1987).

The other model developed by Davidson and Cole (1951):

$$\varepsilon_{(\omega)}^* = \varepsilon_{\infty} + \frac{\varepsilon_0 - \varepsilon_{\infty}}{1 + (i\omega\tau)^{\beta}} \quad \text{Equation 2-71}$$

In Cole-Davidson model, β is between 0 and 1 like α in Cole Cole model. Lockner and Byerlee (1985) claimed that this model hardly fit with the complex electrical data due to asymmetry of out-phase component.

Guéguen and Palciauskas (1994) have expressed that:

$$\frac{\varepsilon_{rr}^*}{\varepsilon_{rs}^*} = f\left(\frac{\varepsilon_{rw}^*}{\varepsilon_{rs}^*}, \Phi\right) \quad \text{Equation 2-72}$$

where the f function is determined by porous media's microstructure. In a high frequency (more than 100 MHz), f function describe a form named CRIM that is expressed as:

$$\varepsilon_r^{*1/2} = \varepsilon_{rw}^{*1/2}\Phi + \varepsilon_{rs}^{*1/2}(1 - \Phi) \quad \text{Equation 2-73}$$

In this equation at high frequency, square root of phase velocity and dielectric constant have an inverse relationship. Equation 2-73 describes the transmission of an electromagnetic wave in a layered composite medium of matrix $(1-\Phi)L$, pore fluid ΦL with a total length of L and porosity of Φ . CRIM model can be converted to Archie's law with the cementation of exponent of 2 when $\omega \rightarrow 0$ and $\delta_w \rightarrow \pi/2$.

The Lichtenecker-Rother model is an equation to characterize permittivity behavior in a medium in a more general form that is given as (Glover 2015):

$$\varepsilon_r^* = \left(\sum_{i=1}^n \varepsilon_{ri}^{*1/m} \Phi_i\right)^m \quad \text{Equation 2-74}$$

where $-1 < 1/m < 1$ and like CRIM model each phase affects the overall relative permittivity by relative permittivity ε_{ri}^* , and volume fraction Φ_i . This equation for $m=2$ ($1/m=0.5$) can be reduced to the CRIM model. M value changes as frequency changes. In dielectric logging, for water phase polarization factor (ρ) will engage to the equation. For solid and hydrocarbon phases $1/m$ remains unchanged.

2.3 Geophysical techniques

Geophysical methods have proved their wide potential for detailed characterization of earth, atmosphere and marine properties in the most cost-effective way. A variety of techniques, such as electromagnetic, electric, magnetic, seismic, georadar, etc. There are some techniques, available using electrical methods. Electrical prospecting indicates detection of subsurface geophysical properties produced by injecting electrical current inside the ground or a laboratory sample. Moreover, for each method, the measurements can be made in different ways, places and scales. In the following, most used electro-geophysical methods is described.

2.3.1 DC resistivity

DC resistivity method is a surface electro-geophysical technique that electrical current is injected into the ground through two current electrodes and voltage response on the surface is measured revealing the direction and amount of current flow in the subsurface. DC resistivity characterizes special distribution of resistive properties of the subsurface soils (Binley and Kemna, 2005). The observed data is used to produce the imaging of the subsurface resistivity. This method is a technique used to search for mineral deposits, metallic ores, DNAPLs, salts and water. Hydrogeologists used this method to study underground water reservoirs. Use of DC resistivity goes back to 1883. Two famous scientists have key roles in the introduction and characterization of this method, Conrad Schlumberger and Frank Wenner who expanded this method in the early 1900.

The measured current and voltage are used to obtain apparent resistivity that is the weighted average of ground resistance to the current flow. The fluid properties like saturation, mineral concentrations and resistivity inside the soil pores have the main role in the observed resistance. Soil type, porosity and permeability also have a direct effect on measured values.

This method is applicable in both field and laboratory. Instruments and data analyzing tools are easily available. Field measurements are usually done at the soil surface or inside boreholes. In the lab, based on the geometry of casing, electrodes are implanted inside the body of the sample. A proper field test setup is needed for this method because an actual contact with ground called galvanic contact (ohmic contact) is necessary in this method against georadar and electromagnetic methods.

Most DC resistivity methods are based on 4 electrodes (Fig. 22) (two electrodes for injecting current and two electrodes for measuring potential (voltage) difference) with different layout arrangements. Different layouts are shortly explained in the following section because it is the same as DC resistivity method.

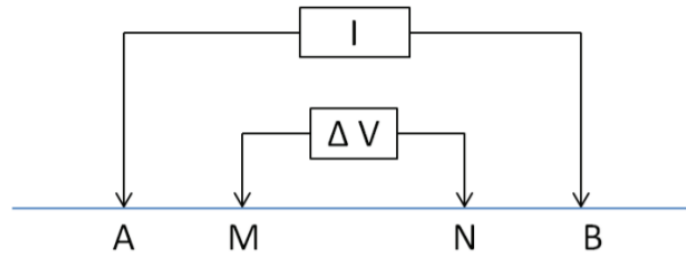


Fig. 22. Example of configuration of an electrical device. *a* and *b* are the electrodes injection (current) and *m* and *n* are measuring electrodes (potential) (Noel, 2014).

Generally, DC resistivity is used in identifying mining targets, potential deposits in mining, measuring earth resistivity for estimation of bedrock depth and water table and geologic features mapping.

Electrical resistivity tomography (ERT) or subsurface imaging (SSI) is a high-resolution imaging and interpretation of DC resistivity survey with contemporary and modern imaging geophysical tools. The measured data is used to solve complicated inverse computer models of the resistivity/conductivity of the subsurface. The resistivity and the term of electrical impedance tomography (EIT) is obtained from the resulting data of injected current and measured voltage. EIT is the geophysics methods when transmitters and receivers are down-hole.

The depth of investigation are different for different arrays, hence, it is related to the electrodes spacing. More distance between electrodes leads to increase in the penetration in depth and decrease in resolution. Most common acquisition arrays are presented in Fig. 23.

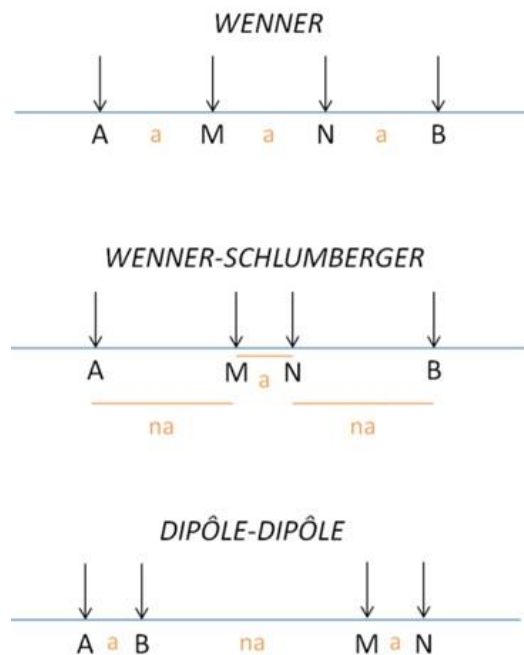


Fig. 23. Most common electrical acquisition arrays (Noel, 2014).

2.3.2 TDIP and SIP

IP is an electro-geophysical method that electric field is generated by low frequency current (0.1 to 10 Hz). Like DC resistivity method, in this method current was injected from two grounded current electrodes and the potential response is measured in two grounded potential electrodes (Fig. 22). IP examines the capacitive potential of a medium. In geophysics studies, capability of ground to store electrical field is measured by IP method. Soils and rocks have electrode polarization (IP response of metallic ore). A weak background IP, membrane polarization, and soil particles have negative electric surface charge (Vanhala, 1997a).

SIP is an advanced version of IP method, developed in 1970s. SIP measures amplitude and phase of the ground or other heterogeneous porous media in the range of 10^{-2} Hz to 20 kHz. In this method, current in alternating with time (AC current) is injected. The resistivity is obtained from impedance of the medium. When an AC current is applied to a medium, measured voltage and injected current at each frequency has a phase shift (Fig. 24). The output voltage is the vector summation of in phase and out phase components that are referred to as the real and the imaginary parts, respectively. The value of these components are directly related to the electrical properties of the medium. The phase shift and amplitude are dependent on the excitation frequency. SIP is measured in time and frequency domains (Fig. 24).

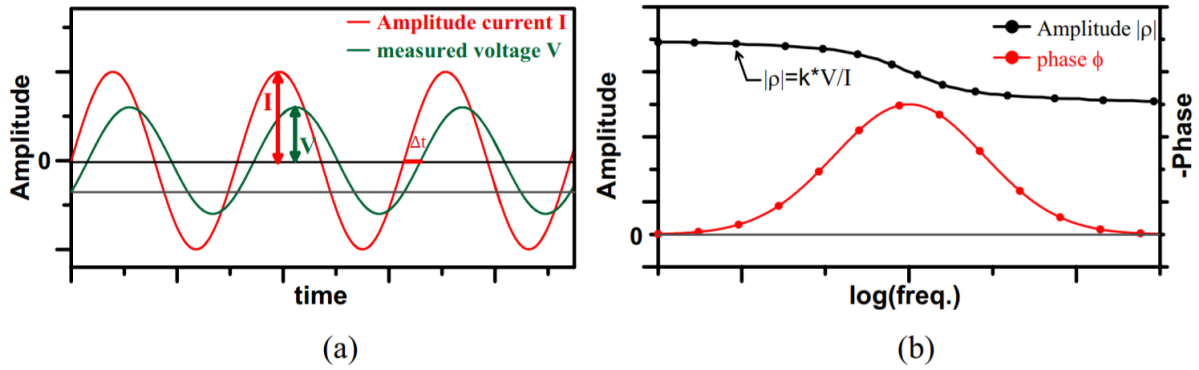


Fig. 24. Data acquisition in spectral-induced polarization. (a) A sinusoidal electric current I of period T in a single frequency is imposed on a medium and the resulting voltage V is measured. The measured voltage is characterized by a phase lag in time relative to the excitation current. (b) Resistivity and phase spectrum. The ratio of voltage $|V|$ to current $|I|$ multiplied by the geometric factor, K , expresses the magnitude (amplitude) of the complex resistivity of the medium, where both its magnitude and the phase depend on the specific electrical properties of the sample (Ghorbani, 2007).

In TDIP method, the study of the potential decay curve after excitation by an electrical current, the ratio of voltage after shutting off the current (V_p) to maximum potential difference (V_0) is called chargeability (M). Integral of chargeability (M_a) is the area under decay curve between two times (t_1 and t_2). This principle of polarization measurement in time domain is illustrated in Fig. 25.

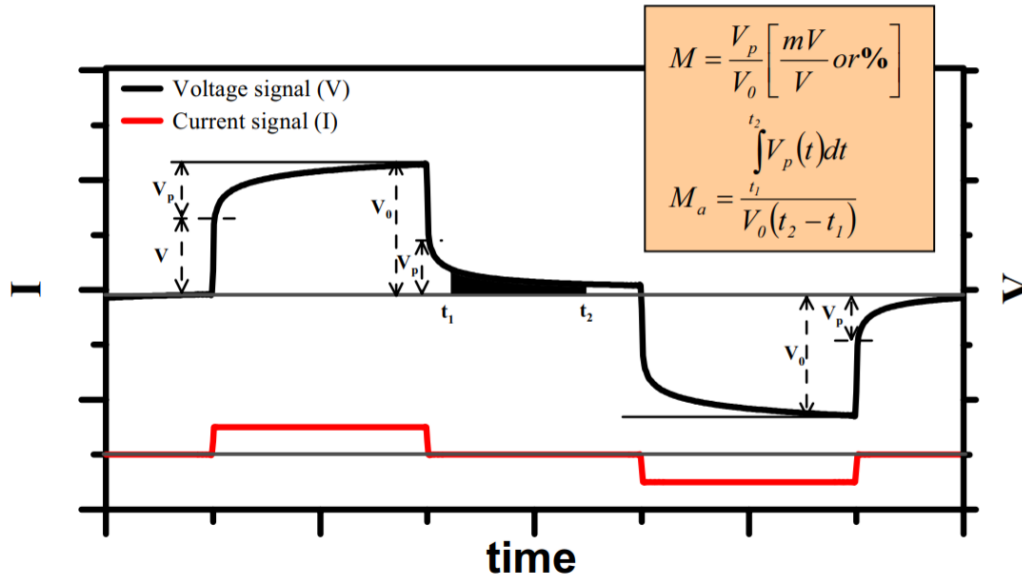


Fig. 25. Data acquisition in the time domain induced polarization (TDIP) method. The voltage decay after excitation by a current pulse is measured (Ghorbani, 2007).

Different origins of IP explained below:

Electrical double layer (EDL) is the main origin of IP. EDL that coats the surface of insulating grains with special emphasis on silica and alumino-silicate. When different minerals are contacted with water, a surface charge developed at surface sites of materials that are different in the case of silica and clay. This charge is in balance with the charge in the Stern layer. In Fig. 26, the position of Stern layer is presented that is placed between o-Plane and d-plane. O-plane is referred to the true mineral surface, and p-plane is the inner surface of electrical diffuse layer (Revil and Florsch, 2010).

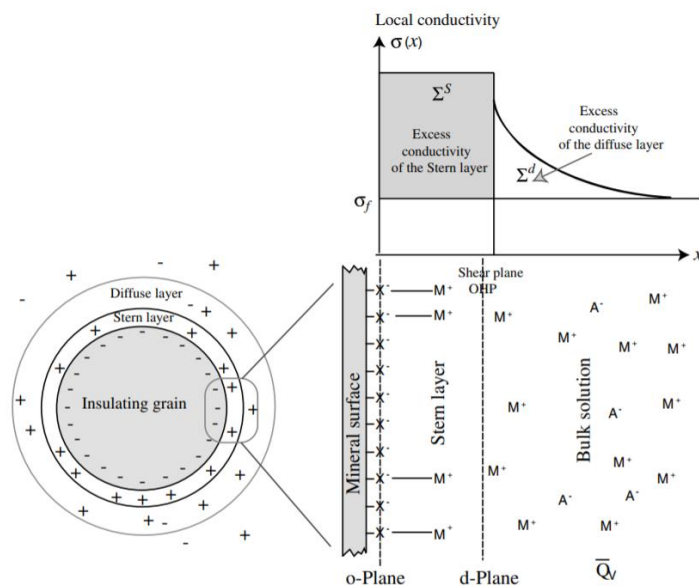


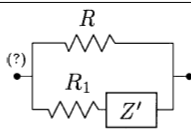
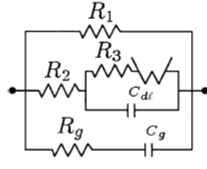
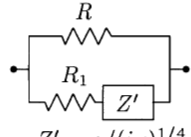
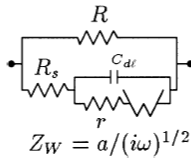
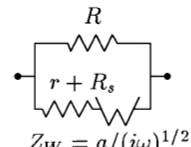
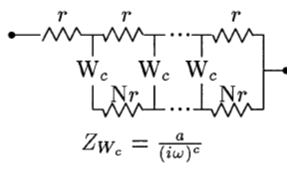
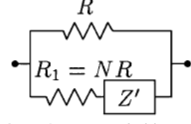
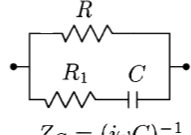
Fig. 26. Sketch of the distribution of the ionic species in the pore space of a charged porous medium at equilibrium (Revil and Florsch, 2010).

In order to affect surface conductivity, Helmholtz or Stern layer is expressed in two different parts: inner Helmholtz plane (IHP) and the outer Helmholtz plane (OHP). In the IHP, water and salt are limited to the mineral structure but in the OHP, solvated salt has a weak limitation to the mineral structures and charges propagate perpendicular to the surface of the minerals in a mixture. It is worth noting that there is no way to measure charge corresponding to the IHP or OHP (Ishido and Mizutani, 1981; Lesmes and Morgan, 2001).

Geometrical and interfacial characteristics of the ground is the second mechanism that has the most effect on induced polarization. Charges store on interface of components of heterogeneous porous media due to conductivity differences. It is the source of special polarization. Maxwell (1891) present the interfacial polarization on layered materials. In the other study, Wagner (1924) demonstrated complex permittivity of a dilute suspension of conductive spheres. In honor of the works of these two researchers, interfacial polarization is called the Maxwell-Wagner effect (Ghorbani, 2007). Sum of surface and Stern layer charges are in a balance with electrical diffuse layer charge.

Generally, in the interface of a multiphase medium, Maxwell-Wagner effect is the result of the discontinuity of displacement currents with discontinuities of dielectric permittivity or electrical conductivity. Kemna et al. (2012) stated that Maxwell-Wagner effect is based on the tortuosity of the different phases, their volume fractions and the conductivity and permittivity of the different phases.

SIP has five main mechanisms including electrode polarization, membrane polarization, Maxwell-Wagner Polarization, polarization of the diffuse layer (electrical double layer, EDL), and polarization of the Stern layer (Kemna et al., 2012). The behaviors of SIP spectra might be interpreted with different phenomenological models. Table 2 is a list of common empirical models (Dias, 2000).

Item	Model/reference	Circuit	Complex resistivity
1	Wait (1959a)	 <p style="text-align: center;">$Z' = Z'(i\omega)$</p>	$\rho = \rho_s \left(1 - \frac{A}{1+2A/3}\right)$ <p>A = average polarizability per unit volume of an infinite heterogeneous medium ρ_s = resistivity of the host medium</p>
2	Ward and Fraser (1967)	 <p style="text-align: center;">$Z_W = a/(i\omega)^{1/2}$</p>	$\rho = \rho_D \left[1 - \frac{1}{1+(\rho_g + \gamma/i\omega)/\rho_D}\right]$ <p>ρ_D = resistivity function associated with Dias model</p>
3	Madden and Cantwell (1967)	 <p style="text-align: center;">$Z' = a/(i\omega)^{1/4}$</p>	$\rho = \rho_0 \left[1 - m \left(1 - \frac{1}{1+(i\omega\tau)^{1/4}}\right)\right]$ <p>$m = (\rho_0 - \rho_\infty)/\rho_0 = \frac{R}{R+R_1}$ $\tau = ((R + R_1)/a)^4$</p>
4	Dias (1968, 1972)	 <p style="text-align: center;">$Z_W = a/(i\omega)^{1/2}$</p>	$\rho = \rho_0 \left[1 - m \left(1 - \frac{1}{1+i\omega\tau'(1+\mu^{-1})}\right)\right]$ <p>$m = (\rho_0 - \rho_\infty)/\rho_0 = \frac{R}{R+R_s}$ $\mu = i\omega\tau + (i\omega\tau'')^{1/2}$ $\tau = rC_{dl}$; $\tau' = (R + R_s)C_{dl}$ $\tau'' = (aC_{dl})^2$</p>
5	Warburg Dias (1968, 1972) Pelton (1977)	 <p style="text-align: center;">$Z_W = a/(i\omega)^{1/2}$</p>	$\rho = \rho_0 \left[1 - m \left(1 - \frac{1}{1+(i\omega\tau)^{1/2}}\right)\right]$ <p>$m = (\rho_0 - \rho_\infty)/\rho_0 = \frac{R}{(r+R_s)+R}$ $\tau = \left(\frac{r+R_s+R}{a}\right)^2$</p>
6	Zonge (1972) Pelton (1977)	 <p style="text-align: center;">$Z_{Wc} = \frac{a}{(i\omega)^c}$</p> <p>also</p>  <p style="text-align: center;">$Z' = (R + R_1)/(\theta \mathcal{L}(\theta))$</p>	$\rho = \rho_0 \left[1 - m \left(1 - \frac{1}{1+\theta \mathcal{L}(\theta)}\right)\right]$ <p>$\theta = (i\omega\tau)^{c/2}$ $\mathcal{L}(\theta) = \coth \theta - \frac{1}{\theta}$ $m = (\rho_0 - \rho_\infty)/\rho_0 = \frac{R}{R+R_1}$ $\tau = \left(\frac{R+R_1}{a}\right)^{1/c}$; $0 \leq c \leq 1$ $0 < N \leq 1$</p>
7	Debye Pelton (1977)	 <p style="text-align: center;">$Z_C = (i\omega C)^{-1}$</p>	$\rho = \rho_0 \left[1 - m \left(1 - \frac{1}{1+i\omega\tau}\right)\right]$ <p>$m = (\rho_0 - \rho_\infty)/\rho_0 = \frac{R}{R+R_1}$ $\tau = C(R + R_1)$</p>

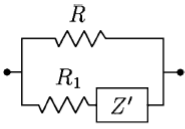
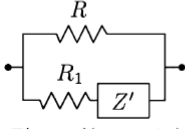
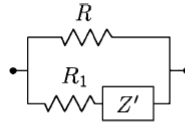
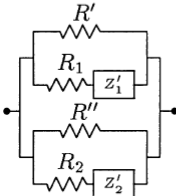
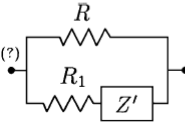
Item	Model/reference	Circuit	Complex resistivity
8	Cole-Cole Pelton (1977)	 $Z' = a/(i\omega)^c$	$\rho = \rho_0 \left[1 - m \left(1 - \frac{1}{1+(i\omega\tau)^c} \right) \right]$ $m = \frac{R}{R+R_1}; 0 \leq c \leq 1$ $\tau = \left(\frac{R+R_1}{a} \right)^{1/c}$
9	Davidson-Cole Pelton (1977)	 $Z' = a/(\omega_L + i\omega)^c$ <p>with $(R + R_1)/(a/\omega_L^c) \gg 1$</p>	$\rho = \rho_0 \left[1 - m \left(1 - \frac{1}{(1+i\omega\tau)^c} \right) \right]$ $m = \frac{R}{R+R_1} \frac{a/\omega_L^c}{R_1 + a/\omega_L^c}; 0 \leq c \leq 1$ $\tau = 1/\omega_L$
10	Generalized Cole-Cole Pelton (1977)	 $Z' = a/(\omega_L^c + (i\omega)^c)^k$ <p>with $(R + R_1)/(a/\omega_L^{ck}) \gg 1$</p>	$\rho = \rho_0 \left[1 - m \left(1 - \frac{1}{[1+(i\omega\tau)^c]^k} \right) \right]$ $m = \frac{R}{R+R_1} \frac{a/\omega_L^{ck}}{R_1 + a/\omega_L^{ck}}$ $0 \leq (c; k) \leq 1$ $\tau = 1/\omega_L$
11	Multi-Cole-Cole Pelton et al. (1978)	 $Z'_j = a_j/(i\omega)^{c_j}; j=1,2$ <p>at least one of the following conditions satisfied:</p> <ol style="list-style-type: none"> 1) $R_1 \gg R' \gg R''$ 2) $R_2 \gg R'' \gg R'$ 3) $R_1 \gg R'; R_2 \gg R''$ 	$\rho = \rho_0 \left[1 - m_1 \left(1 - \frac{1}{1+(i\omega\tau_1)^{c_1}} \right) \right] \cdot \left[1 - m_2 \left(1 - \frac{1}{1+(i\omega\tau_2)^{c_2}} \right) \right]$ $m_1 = \frac{R'}{R_1+R'}; 0 \leq (c_1; c_2) \leq 1$ $\tau_1 = \left(\frac{R_1+R'}{a_1} \right)^{1/c_1}$ $m_2 = \frac{R''}{R_2+R''}$ $\tau_2 = \left(\frac{R_2+R''}{a_2} \right)^{1/c_2}$
12	Wong (1979)	 $Z' = Z'(i\omega)$	$\rho = \rho_s \left(1 - \frac{3 \sum_j N_j f_j}{1 + 2 \sum_j N_j f_j} \right)$ <p>N_j = number of spherical particles j per unit volume f_j = reflection coefficient at the interface between a homogeneous infinite ionic solution and the medium j ρ_s = resistivity of the homogeneous solution</p>

Table 2. Models, equivalent circuits and complex resistivity proposed for SIP (in chronological order) (Dias, 2000).

Variety of models in this list show that each model defined for a particular condition of fluids and porous media. A model can be a fit for one experiments but fails for another situation with different experimental elements. Some of the most common empirical models that were recently used in SIP studies are explained in the following.

Nordsiek and Weller (2008) developed a method base on the superposition of some Debye models known as the Debye Decomposition. Unlike the other methods, the Debye Decomposition is not limited on one relaxation peak and it can cause flexibility of spectral shape and trend of variation.

There is no limitation for IP spectra to have one or several relaxation peaks. It can be a linear relationship between spectra and frequency. The Drake model as a Constant Phase Angle (CPA) model developed by Van Voorhis et al. (1973) can be used for interpreting this kind of data.

Fitting experimental data with a phenomenological model is a common way to validate and to interpret any experimental data. Cole-Cole (1941) investigated the dielectric permittivity dispersion of polar liquids by a model, which became known by his name hereafter. Pelton et al. (1978) adapted the Cole-Cole model as a relaxation model to study resistivity behavior of geological materials as:

$$\rho(\omega) = \rho_0 \left[1 - m \left(1 - \frac{1}{1+(i\omega\tau)^c} \right) \right] \quad \text{Equation 2-75}$$

where ρ_0 is low frequency resistivity, m is intrinsic chargeability, c is Cole Cole exponent and τ is mean relaxation time. This equation is expressed as below for complex conductivity dispersion:

$$\sigma(\omega) = \sigma_0 \left[1 + m \left(\frac{(i\omega\tau)^c}{1+(i\omega\tau)^c(1-m)} \right) \right] \quad \text{Equation 2-76}$$

$$\sigma^* = \sigma_0 \left(1 + \frac{m}{1-m} \left(1 - \frac{1}{1+(i\omega\tau)^c} \right) \right)$$

where σ_0 is the DC conductivity. Cole-Cole model is a modification of Debye model to get a better description of dielectric polarization.

$$m = \frac{(\rho_0 - \rho_\infty)}{\rho_0} \quad \text{Equation 2-77}$$

where ρ_0 and ρ_∞ are the low frequency and high frequency values of electrical resistivity. Equation 2-76 and Equation 2-77 are used in studies to describe electrical resistivity and electrical conductivity but these two equations are not equivalent (Tarasov and Titov, 2013).

Pelton et al. (1978) used a model derived from Cole-Cole model to express dispersion of resistivity and similarity of its nature with dispersive concept of dielectric permittivity. This study is the first application of Cole-Cole model with replacing relative permittivity with resistivity (or conductivity). Tarasov and Titov (2013) showed that Pelton's model in resistivity and conductivity have a slight deviation from model proposed by Cole-Cole (1941).

Some other less common models like Cole-Davidson model (generalized Cole-Cole model) were also proposed to study the evolution of SIP spectra. Davidson and Cole (1951) were developed a model for the situation with a remarkable dispersion at lower and higher frequencies when Cole-Cole model fail to fit data. They found that their model fitted well with

the resistivity spectra of parts that original Cole-Cole model failed to predict. This model assumes and allows asymmetric spectra (Nordsiek and Weller, 2008). Cole-Davidson model is described as:

$$\rho(\omega) = \rho_0 \left[1 - m \left(1 - \frac{1}{(1 + (i\omega\tau)^c)^a} \right) \right] \quad \text{Equation 2-78}$$

In Equation 2-75, when $a=1$, it becomes Cole-Cole model. When $a=1$ and $c=1$, it becomes the Debye model.

2.3.3 TDR

An elegant method to study water content of a medium is based on measuring soil dielectric permittivity. A variety of commercial probes is using to estimate volumetric water content (VWC). In order to compare the relative permittivity results reported in different previous literature, it is essential to know what device measures and its measurement limitations. The advantages of using time domain reflectometers (TDRs) are that they are automated and can be used in very close and very deep to the soil surface and contain no radioactive source. Their application is in irrigation and drainage, hydrology, soil depollution and in commercial use in horticulture where it is necessary to understand the water content and relative permittivity of porous media (Robinson et al., 1999). TDRs are presenting the best technique to measure relative permittivity in a porous media (Topp et al., 1980) but there are other tools like the surface capacitance insertion probe (SCIP), which is low-priced compared to TDR and more adaptable and recently popular Theta probes that are cheap and work with a fixed frequency (Robinson et al., 1999).

Direct TDR measurements are sensitive to the effect of the temperature. For instance, Malmberg and Maryott (1956) established a relationship between the relative permittivity of water and temperature (in the range 0 to 100°C) as below, using experimental methods:

$$\varepsilon' = 87.740 - 0.40008T + 9.398(10^{-4})T^2 - 1.410(10^{-6})T^3 \quad \text{Equation 2-79}$$

where T is the temperature (°C). They stated that the proposed equation has a maximum error of 1%. They also stated that the dielectric constant of water decreases with temperature, but for air, the temperature change does not have a significant effect on relative permittivity. Chen and Or (2006) used TDR to obtain dielectric permittivity and found that even for frequencies lower than 100 MHz, TDR probes clearly showed effects of temperature (5-55°C) and electrical conductivity (due to Maxwell-Wagner (M-W) effect that is the charge at the interface of two materials due to difference of their charge relaxation times) on dielectric permittivity. They expressed that the effective range of the TDRs used is greater than 100 MHz and at low frequency (<100 MHz) this influence (M-W effect) is not noticeable compared to the higher

frequencies. For each 1°C increase in temperature, they reported a 0.3% decrease in the relative permittivity of water. For TDR model 5TE, Rosenbaum et al. (2011) proposed an empirical correction function for the temperature effect between 5 and 40°C, tested on eight different liquids. They noticed underestimated values of relative permittivity for temperatures over the range 5 to 25°C (-2.7 for EC-5 and -3.9 for 5TE) and overestimated values for 25 to 40°C (+3.6 for both TDRs). They identified strong correlation between permittivity and electrical conductivity with increasing electrical conductivity with adding salt content. Persson and Berndtsson (2002) tried to find a relation between relative permittivity (measured by TDR), NAPL saturation and electrical conductivity. By further validating the results using a mixing model, they demonstrated that TDR measures relative permittivity values very well.

3 Material and methods

Two different series of Darcy scale laboratory experiments were carried out to develop a better understanding of temperature and saturation effects on complex electrical resistivity and relative dielectric permittivity during drainage and imbibition. All experiments were done in saturated porous media with two different couples of immiscible liquids. In this chapter, we describe the essential points for performing and preparing experimental setups and apparatuses to perform experiments.

3.1 Non-polarizable electrodes

Non-polarizable electrodes are used in SIP studies to measure voltage response of an injected current in a medium (e.g., Abdulsamad et al., 2016). In non-polarizable electrodes, current can freely pass without polarization. Indeed, polarizable electrodes are not adequate for SIP measurement due to polarization effect. Unlike polarizable electrode, potential in non-polarizable electrodes does not change due to passage of current. It is due to almost infinite exchange current density that causes very fast electrode reaction (Bagotsky, 2005). A series of test were performed to find the best solution for non-polarizable electrodes (Fig. 27). These tests were performed in order to measure the electric potential differences (EPDs) in response to AC current injection using two ring electrodes and to characterize phase shift at high frequency. The non-polarizable electrodes usually used in telluric prospecting (Petiau and Dupis, 1980; Petiau, 2000) where too large for our purpose, so we constructed small laboratory electrodes (as done for instance by Mainault et al., 2004).

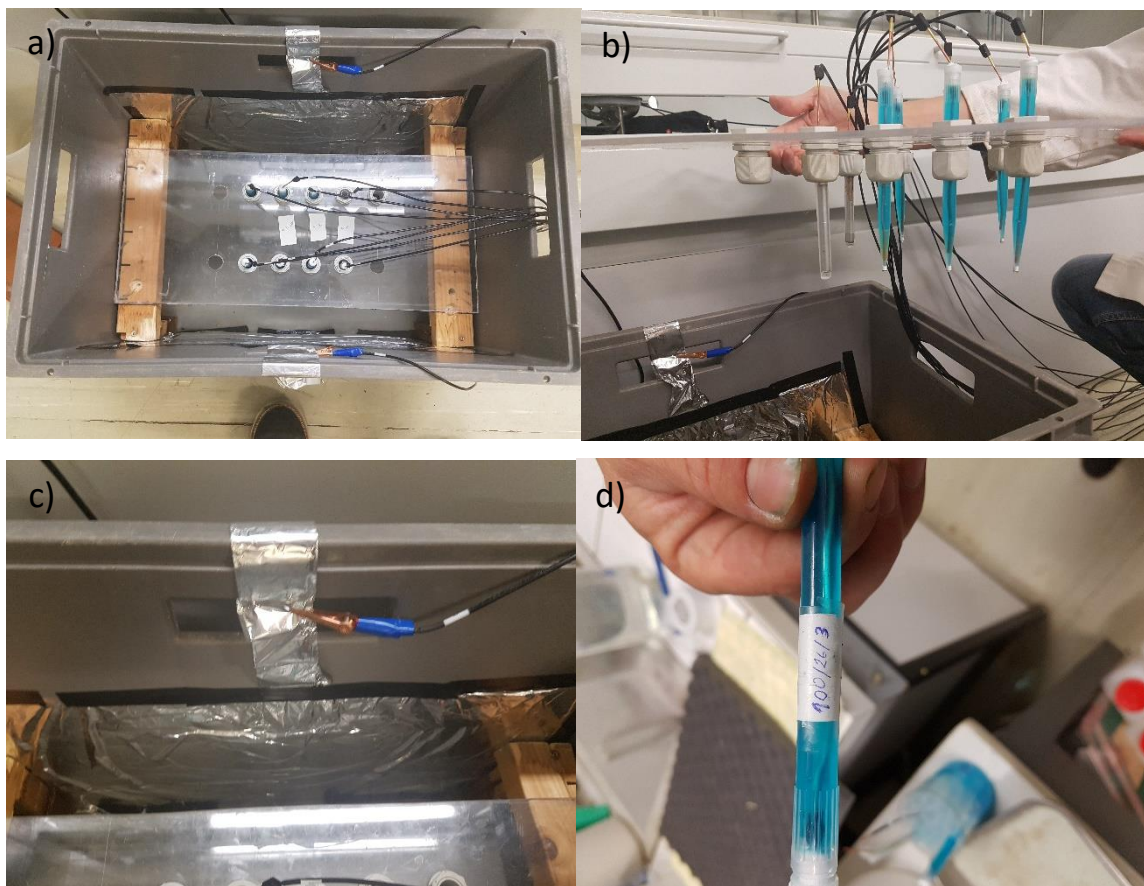


Fig. 27. Preliminary tests to find the best solution portions for non-polarizable electrodes, a) top view of the test box, b) position of different non-polarizable electrodes in a glass tray, c) one of the injection points and d) electrodes portions written in an electrode

Among common electrodes solution, Cu/CuSO_4 was chosen based on the method proposed by Mainault et al. (2004). These electrodes were made using a mixture of 72.75 g of milli-Q water (ultrapure water), 26 g of CuSO_4 and 1.25 g of Gelatin in 100 g of solution. A heating shaker was used to mix the solution for an hour at 80°C .

The non-polarizable electrodes were placed outside the samples in order to avoid in flow interference that in turn can interfere with electrical current signals (Mainault et al., 2004). Different steps to make non-polarizable (Cu/CuSO_4) electrodes are shown in Fig. 30. The different steps to make Cu/CuSO_4 electrodes.

Making these non-polarizable electrodes can be challenging and requires precision, attention to details, and understanding. After preparing the solution, the next step is making the electrode's pipette. In order to make the pipettes,

1. Cutting copper wires (coated with plastic) to a length of at least 18 cm. Stripping the wires but leaving approximately 3 cm coated in order to help with waterproofing the top part (Fig. 28).

2. Polishing copper wires with the sandpaper is the next step. Washing all the wires with ethanol and water prior to use.

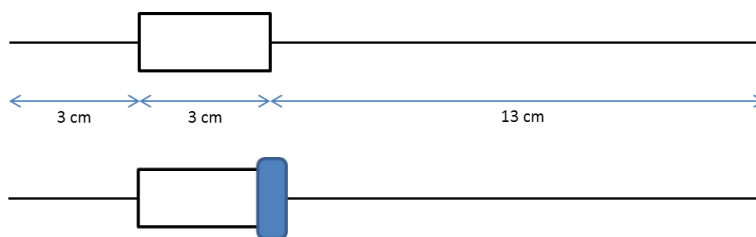


Fig. 28. Length of copper wire and cap position

After preparing wires, the next steps are

3. Cutting 3.5 mm of the narrow end of the pipette cones (Fig. 29). Choice of 3.5 mm is suitable for this experiment. It may be different for other experimental setups. For the experiment, it was found that cutting more or less than 3.5 mm can lead to problems related to being in the same level of non-polarizable electrodes and body of samples holders.

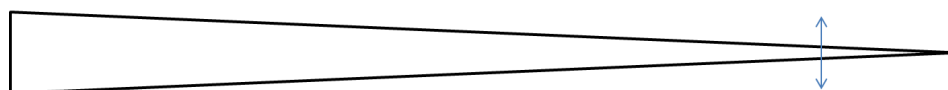


Fig. 29. Position of cutting of the narrow part of the pipette cone

4. Washing all pipette cones with ethanol and water.
5. Fixing heat-shrinkable tube and porous ceramic at the end of the pipette cone with the heat gun and a little amount of glue. Adding too much glue can block the connection point of the pipette cone and the porous ceramic. The other way to help porous ceramic to be well attached is coarsening of the common surface of the pipette cone and heat-shrinkable tube by sandpapers.
6. Filling the pipette cones with the solution of CuSO_4 almost 8 to 10 ml per electrode. Generally, the amount of solution that should be prepared is the multiplication of the required volume for each electrode and the number of electrodes with an additional 20% solution as contingency.
7. After injecting solution inside the pipette cone, removing the air bubbles with shaking the cone is important.
8. Making some holes (with copper wires or other thin and sharp tools) on the cap. One hole is for passing the wire through it and the other holes for allowing excess solution overflow. A cap with no hole, may lead to separation of the porous ceramic.

9. Putting silicon inside the caps of electrodes and make them waterproof to avoid leakage of solution. Electrodes will be prepared for use after silicon dry out.

While, it is hard to prepare identical electrodes, efforts should be made to minimize the differences. The porous ceramic of the electrodes must not be exposed to the air, so we can put them in a solution of CuSO_4 . Steps are shown in Fig. 30.

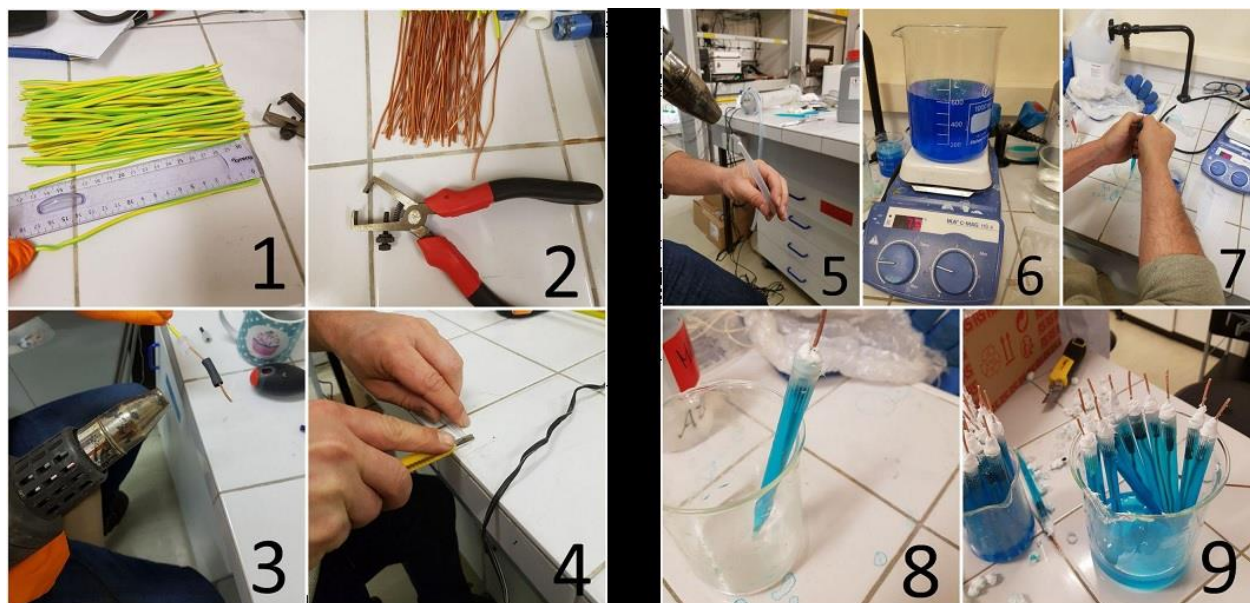


Fig. 30. The different steps to make Cu/CuSO_4 electrodes (see text for details)

The stability and reliability of the non-polarizable electrodes are checked before running the SIP-lab software and if some of them had problems, replacements were made. The stability checks of potential electrodes were performed before and after each experiment with tap water. Fig. 31 shows a monitoring graph of these electrodes before and after an experiment in a cell. The difference of $\pm 10\%$ in resistivity was counted as the reliability limitation for validating the accuracy of non-polarizable electrodes.

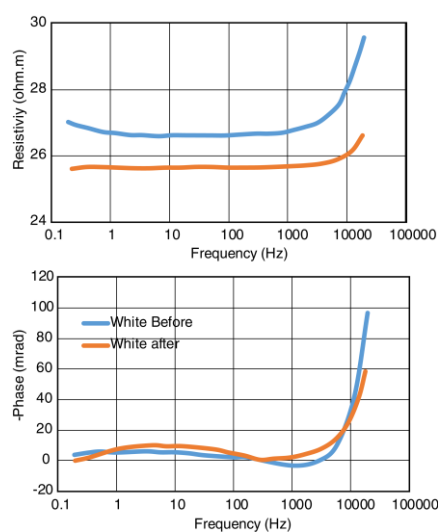


Fig. 31. The frequency series of resistivity before and after an experiment in a cell

Each non-polarizable electrode was connected to the SIP-lab with a shielded cable. The SIPlab IV with wiring is presented in (Fig. 32).

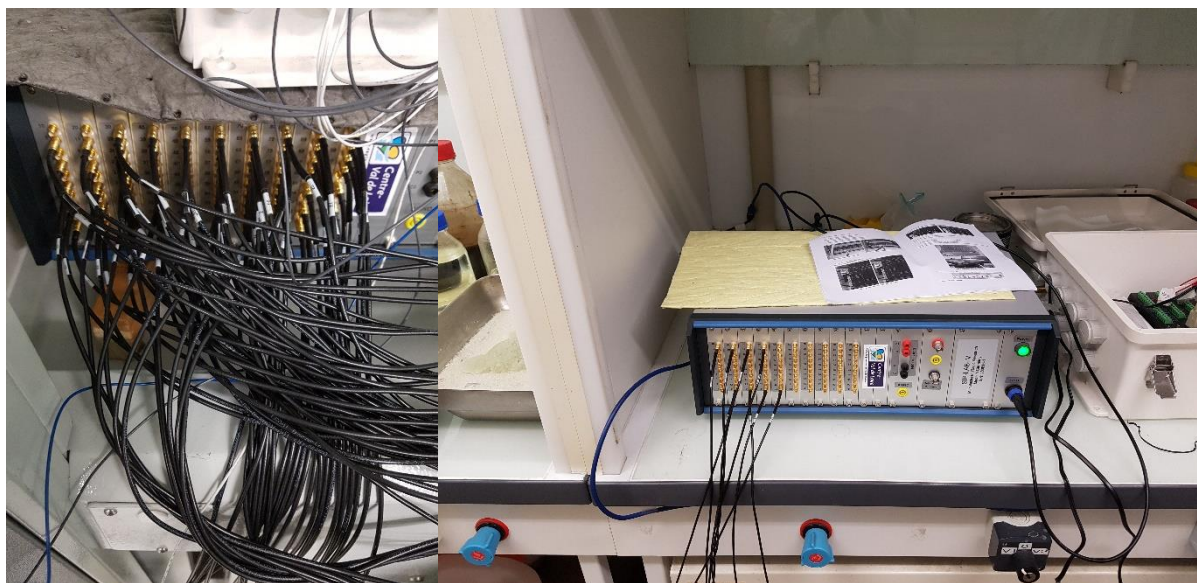


Fig. 32. SIP lab IV and connected cables

3.2 Cells and columns

The experiments consisted of conducting drainage and imbibition for two non-miscible fluids in different sample holder geometries. First series of sample holders were 1D, and consist of two different sizes referred to as cells and columns (Fig. 33). The cells and columns are 5.56 and 25 cm long with 5.8 cm internal diameter. It is supposed that fluids flow in the porous medium contained in them is in 1D. In the closest perspective of this work, results of different columns will be used in a 2D tank. All samples were made of polyvinylidene fluoride (PVDF), a highly non-reactive, thermoplastic polymer that is very resistive for chemical and abrasion resistance compared to other thermoplastic materials especially when in contact with halogens (chlorine and bromine) and powerful acids such as organic solvents and oils. PVDF works well in the wide temperature range of -40 to +120 C. PVDF is very tough against mechanical stress and pressure. The other important characteristics of PVDF that makes it suitable for making cells and columns include low gas and air permeability you already said this above Main samples are connected to the water and DNAPL reservoir by two thermo-scientific Nalgene (180) clear polyvinyl chloride (PVC) tube with 1 cm inside diameter. These tubes were made from the finest specialty resins and plasticizers.

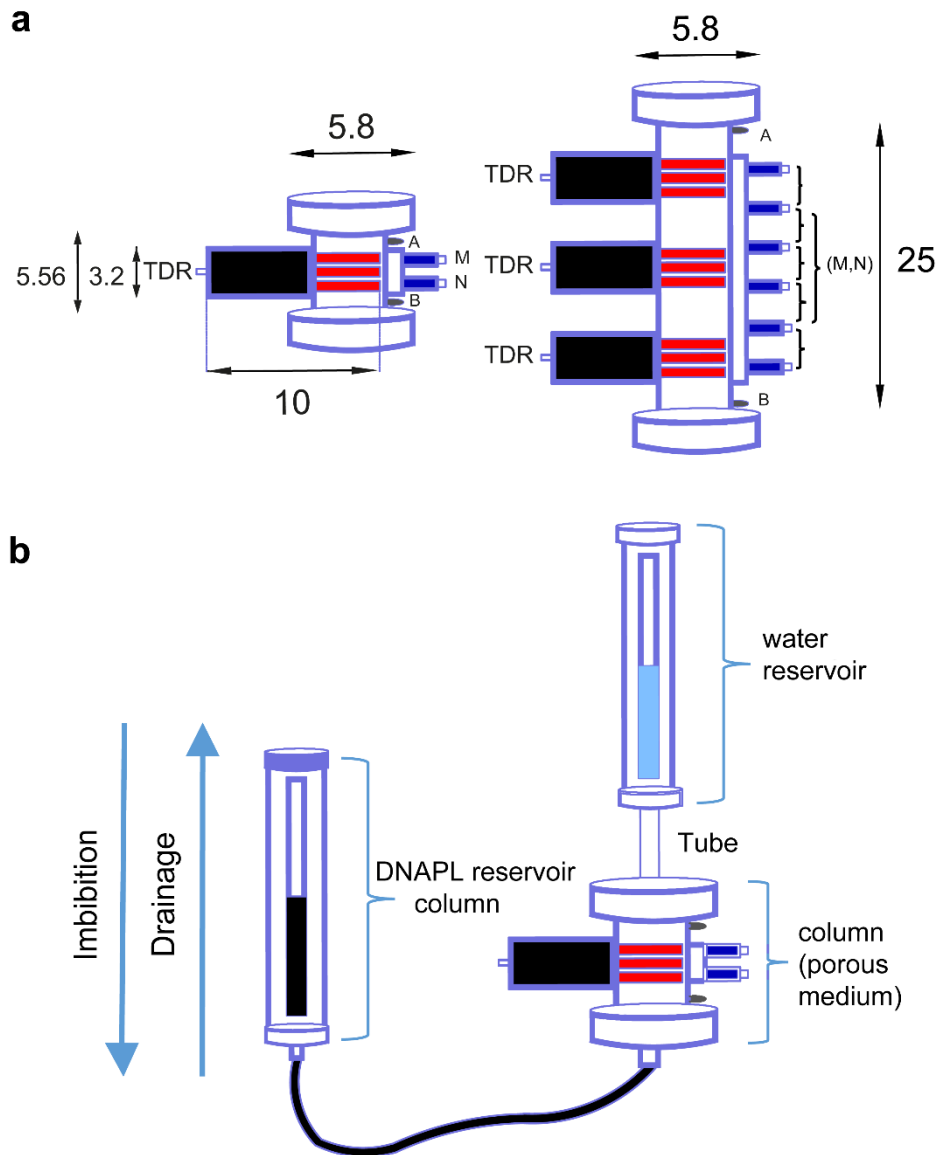


Fig. 33. Schematic of experimental setup (lengths are in cm). a) Geometry of a cell and a column with the position of TDRs, current (A and B) and potential (M and N) electrodes. Each bracket indicates a measurement in a sample. b) Experimental setup including water and DNAPL reservoirs and sample.

Two stainless and PVDF filters are used at the top and the bottom of samples in order to keep the glass beads in place

Fig. 34a shown a cross section of a cell with more detail and Fig. 34b is a photo from inside a cell. The body of the TDR (that is placed outside of the cell) is almost $\frac{3}{4}$ of the porous medium (not whole cell) because there are two caps and filters at the top and bottom of the porous media to fix it. The volume of the cell is 146.9 cm^3 and there are three prongs (each prong has the volume of 2.5 cm^3) of TDR inside it. Therefore, the volume of the cell without probes will be around $146.9 - (3 \times 2.5) = 139.4 \text{ cm}^3$. Volume of three prongs of TDR is almost 0.051 of the whole cell's volume.

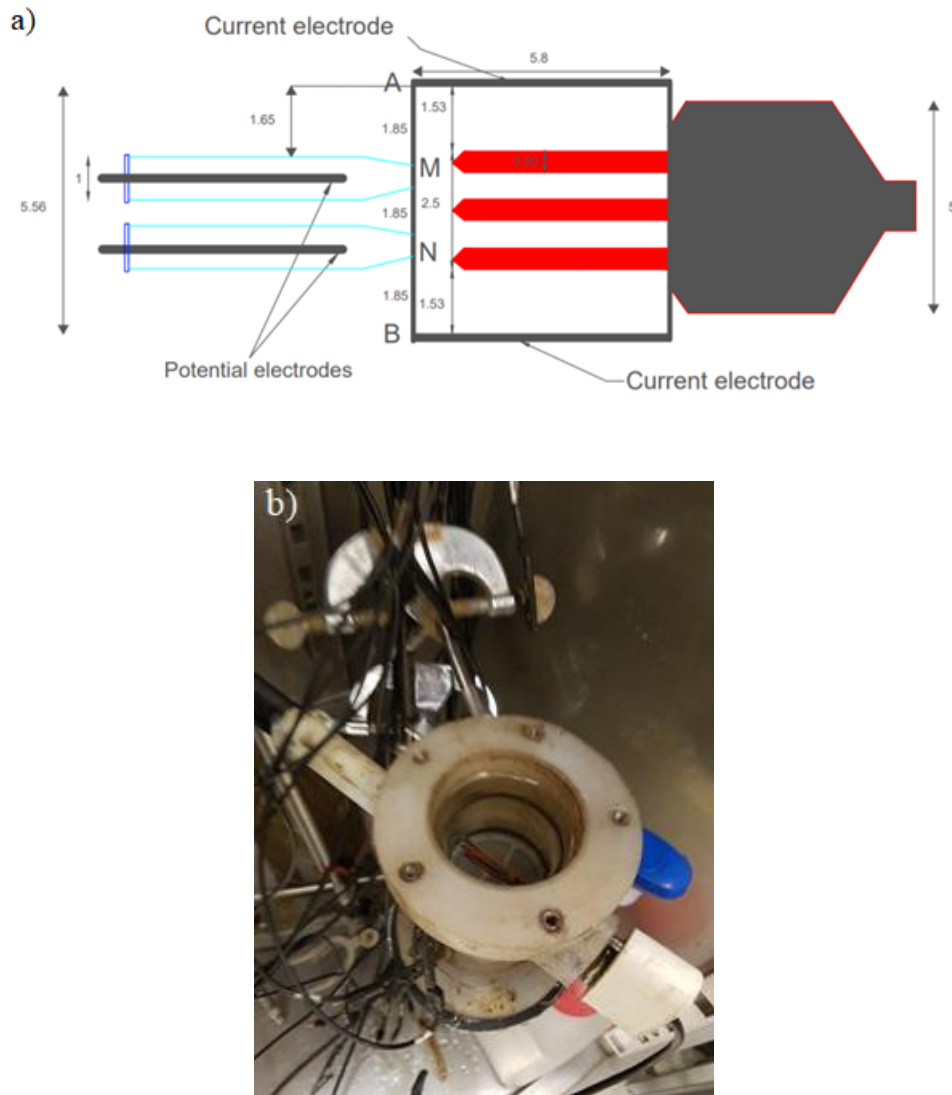


Fig. 34. a) Schematic of a cross section of a cell with exact positioning of TDR and the other elements and
b) a photo from inside a cell

A valve is placed at the bottom of samples to slowly inject water inside the samples. Slow speed is important to prevent trapping air inside the pores and making air bubbles. Air inside the porous media not only changes the two-phase medium to three-phase but also causes numerous measurement errors because of high resistivity of air. After pouring GBs inside the samples and weighting it to find the porosity, next step is fixing the porous media inside the samples with two filters, two plastics O-rings and adding grease to make it waterproof. These filters and O-rings are fixed on top and bottom of the samples. DNAPL or oil are slowly added to the setup from top of the DNAPL reservoir. Each experimental setup has three main parts: water reservoir, DNAPL reservoir and main sample (porous medium). All samples and reservoirs were fixed on metallic supports. During attaching the reservoirs on the supports, we

should be sure there are enough length and space for displacement during drainage and imbibition.

. Each of the main samples were connected to a DNAPL reservoir outlet valve and a water reservoir inlet vale using 36 cm and 8 cm long plastic tubes with an internal diameters of 1 cm, respectively (Fig. 35). One of the most important point in measuring the volume of each fluid, the saturation and the fluid contents is considering the dead volumes. The dead volumes consist of the volumes of two pipes and the fluids inside the filters. It is important to take note of all injected or withdrawn quantities of fluids. The columns and reservoirs should be vertical after installation. We can verify it by using a spirit level. We placed it on the upper flat part and the graduated front of each column to check that the column is vertical or not. Both DNAPLs and salty ethanol that will be used in our experiments were respectively filtered with 2.7 and 0.7 mm paper filter with the help of a suction pump to make them homogenized.



Fig. 35. Sets of test cells and columns

After saturating the main samples, water goes to the water reservoir through the small pipe at the top of the samples, then the water starts to fill the water reservoir until the water could be readable (almost 1 cm in this reservoir) then we stopped injecting water to the sample.

In the next step, we should block the tube between sample and DNAPL reservoir and then fill the left reservoir with DNAPL. At first the tube should be filled otherwise air trapping will be probable. The amount of pollutant is precisely determined in order to reach equilibrium with the water at the bottom entrance of the main column. The height in DNAPL reservoir is calculated according to the equation below,

$$\rho_{water} h_{water} = \rho_{DNAPL} h_{DNAPL} \quad \text{Equation 3-1}$$

It should be known that the DNAPL is injected from the bottom part of the sample in order to avoid any gravity-driven flow instability (fingering) because DNAPLs are denser than water. At the initial moment, the respective heights of the water and DNAPL in both reservoir columns are noted. Then, the experiments had begun. The initial level of DNAPL inside the samples is 0.8 cm from the top end of the metal grid support to the bottom end of the PVDF grid.

Geophysical equipment such as SIPlab IV, Campbell CR-1000, TDRs and electrodes were used for monitoring porous medium properties during experiments. The two ring current electrodes made of nickel-cobalt alloy (MP35N) (this alloy is non-magnetic and possesses an ultra-high tensile strength, and provides for good ductility. This alloy has a maximum 400°C temperature capability and in addition, it has excellent corrosion resistance) inject AC current from top and bottom of cells and columns. The cells have two potential electrodes and columns have six of them. Accordingly, in experimental setups, one and six measurements were done in the cells and the columns, respectively. Electrodes spacing and choosing proper arrays are important in cells and columns. The Wenner alpha and Schlumberger arrays were chosen for cells and columns, respectively. In these arrays, all the electrodes were embedded on the same orientation and the electrodes for measuring M and N were laid out between the current electrodes A and B (as illustrated in Fig. 33). According to the principles of these configurations, for Wenner alpha distances between two electrodes next to each other are same, but for Schlumberger the distance MN is small compared to AB (e.g., Clément et al., 2009).

Glass beads (GB) made of silica with a diameter of 1 mm and porosity of $40\% \pm 2\%$ were used as porous medium. This GB size was chosen to simulate porous medium in the lab with close physical property to the soil with porosity of 40%. In different experiments, two DNAPLs (cola-tar (CT) and chlorinated solvent (CS)) with water and canola oil and salty ethanol were used to study different sets of two-phase-fluid systems. In all experiments, tap water was used as the reference liquid. In the first study that was related to the temperature effects, all samples were placed in an oven. In the second study that focused on the saturation effects, these

experimental setups were placed under a protection hood to prevent spreading pollution and to reduce the risk related to product evaporation inside the laboratory.

3.2.1 White test (with water) before performing experiments

It is worth mentioning that before and after starting each experiment, the measurements with tap water were carried out to examine the performance and accuracy of electrodes and finding the geometric factors. To validate the experimental device, the measured geometric factors of each array should be close to each other; otherwise, there are some problems. These problems could be related to the electrodes or their environments. For instance as mentioned before, air bubbles close to potential electrodes can totally change the potential values. The white test (with water) was done for at least 24 hours to have enough data to increase measurement accuracy.

3.3 Principle of drainage and imbibition

In the following, different steps and principles of performing drainage and imbibition are described. First, sample holder should be filled with the wetting phase liquid that is water in the laboratory setups. In Fig. 36, water was drained from inside sample's pores by incrementally increasing level (2 cm) of DNAPL reservoir. Subsequently, capillary pressure was increased, resulting in replacement of non-wetting phase fluid (DNAPL) with wetting phase fluid (water). For each incremental step, water and DNAPL levels in their reservoir were precisely noted for determining the volume of wetting fluid remaining inside the sample and volume of DNAPL entered to the sample. After finishing drainage, any more increase in DNAPL reservoir level does not change saturation balance inside samples, this remaining DNAPL saturation is known as irreducible saturation. This phenomenon happened due to strong tendency of wetting phase to stick to GBs. After finishing draining and getting irreducible saturation, rewetting of samples and porous media can happen by doing all the steps of the drainage in reverse. Imbibition of samples has done by gradually decreasing DNAPL reservoir (2 cm for each step) to displacement of non-wetting phase (DNAPL) with wetting phase (water) liquid. After imbibing sample, whole wetting phase cannot remove from the sample and full water saturation (100%) cannot be obtained after imbibition. During imbibition, a portion of DNAPL is captured inside the pores and removing of them with this pressure looks impossible. This DNAPL saturation value is called residual saturation or trapped non-wetting phase saturation.

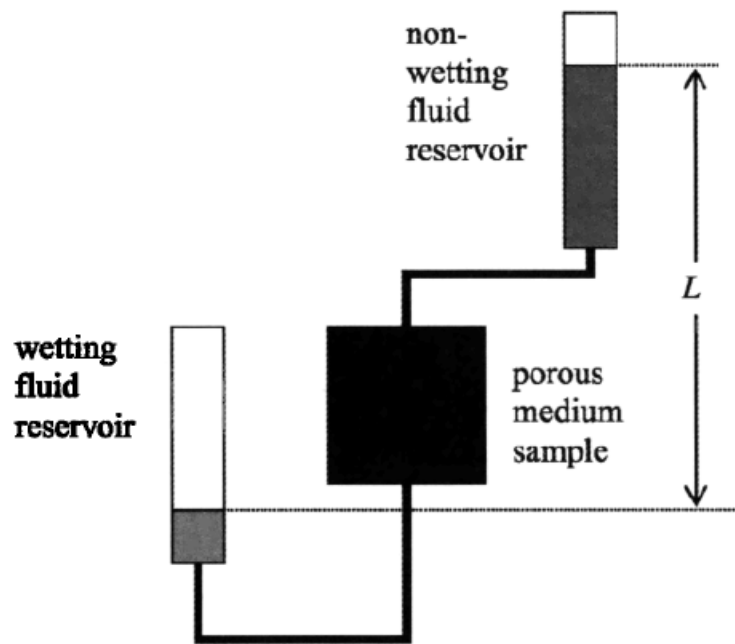


Fig. 36. Experimental setup for determining water and DNAPL saturation and geophysical parameters inside the samples (cells or columns) (Mayer, 2005)

In a cell that is filled with GB and is fully saturated with water, drainage only happens at times that the capillary pressure exceeds the displacement pressure before entering DNAPL inside the saturated pores and layers. From the principle of drainage and imbibition, the smaller the GBs size the smaller the pore size and the higher the capillary retention ability. In fine-grained porous media, for a capillary pressure, wetting phase saturation will be higher compared to the medium with coarse grained porous media with larger pores.

3.4 TDR application

The 5TE (TDR) sensors are volumetric water content (VWC), temperature, and electrical conductivity (EC) probes that used in the field and laboratory works. 5TE works at 70 MHz frequency to provide relative permittivity of soil. Subsequently, water content will obtain from relative permittivity of the medium. Fig. 37 shows the 5TE main components. In this figure, a thermal sensor (thermistor) is placed on the body of TDR to measure temperature around the sensor in °C. Two screws on prongs of 5TE make a two sensors AC electrical array for measuring resistance and then obtaining conductance (inverse of resistance). The factor (ratio of distance between electrodes and their area) multiplied by conductance provides EC value. Recorded EC is normalized at 25°C. The body of 5TE is made of polyurethane to protect sensors from damages and contact with water. This plastic cover protects TDR from possible risks in soils.

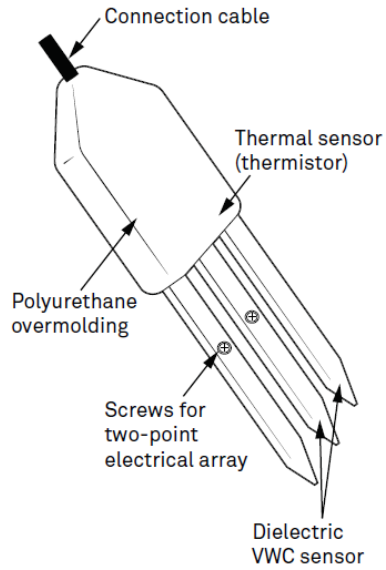


Fig. 37. 5TE components (5TE manual "METER group")

Table 3 is the physical characteristics of 5TE:

Dimension	
Length	10.9 cm (4.3 in)
Width	3.4 cm (1.3 in)
Height	1.0 cm (0.4 in)
Prong length	5.0 cm (1.9 in)

Table 3. Dimensions of 5TE

Because we are using these probes in the lab, before installation, attention should be given to neighboring soils or GBs regarding to noticeable effects on probe's readings. Being close to big metal objects, air capturing and any soil compaction (normally it does not happened in the experiments were performed in the lab because of using GB instead of soil); being close to TDR prongs can affect the measurements. Testing all TDRs is an imperative work before starting any experiments. A simple test can prevent false measurements or error. In the field, because of the space among TDR prongs, many foreign objects such as tree roots can penetrate inside them and affect the measurements but in experiments in the lab due to using GBs under controlled conditions, we do not face with these problems. The advantage of working in the field is placing whole TDRs body in the soil but in the laboratory setups (cells, columns and 2D tank) the black part of the TDR bodies were implanted in the samples body not in porous media. It can affect the data significantly on temperature measurements because the temperature sensors are in the back part of TDRs. One of the advantage of lab measurements is the position

of each TDR that is fixed contradictory to the field that we always have problem of moving TDRs due to instability of soil and landslides.

According to the manual of 5TE, the distance between TDR probes can affect measurements. When they are placed close to each other (less than 20 cm); it is possible that injected currents pass through other close TDRs. In the experimental setups, in cells, columns and 2D tank, considering a multiplexing option could be helpful. Secondly, when the vertical distance is less than 20 cm, sensors can be implanted horizontally, then setup in this case follow the distance.

In the current work, TDRs were connected to the data logger with a 5 m cable. We used a Campbell data logger Scientific. Inc. CR-1000. This TDR needs an excitation voltage in the range of 3.6 to 15 VDC. 5TE should be used with SDI-12 protocol when we use a Campbell CR-1000. There are two types of data loggers, one that TDRs are connected to the data logger with a 3.5 mm stereo plug connector and the second type that are connected to a screw terminal and then the Campbell CR-1000. In this study, we used second one. Screw Terminals help us to classify and to use maximum TDR numbers (10 TDRs for each SDI12 port) for each sensor port in the . Using screw terminals also help to avoid turmoil and twisting of wires inside the box of the Campbell. Using associated software adapted to be used with data logger is important to configure the TDR with appropriate sensor port in Campbell and proper measurement interval to have adequate readings according as needed. 5TE probes are configured using loggernet software.

Sampling interval for measurement in all experiments is 30 s. If the interval is more than one minute, 5TE measures every one minute and uses the minute-average for the selected measurement interval but it can be different for different measurement and which parameters are going to measure.

Fig. 38 shows the internal wires and wiring diagram of a TDR. The power supply wire should connect to the excitation current, the digital out wire to a digital input, the ground wire (bare) to the ground.

In Campbell Scientific data loggers, the TDR probes are powered from a switched 12 V port. For instance, power for TDR were from switched 12 V port and power for thermocouples in 2D tank were from the 12 V port with using a multiplexer.

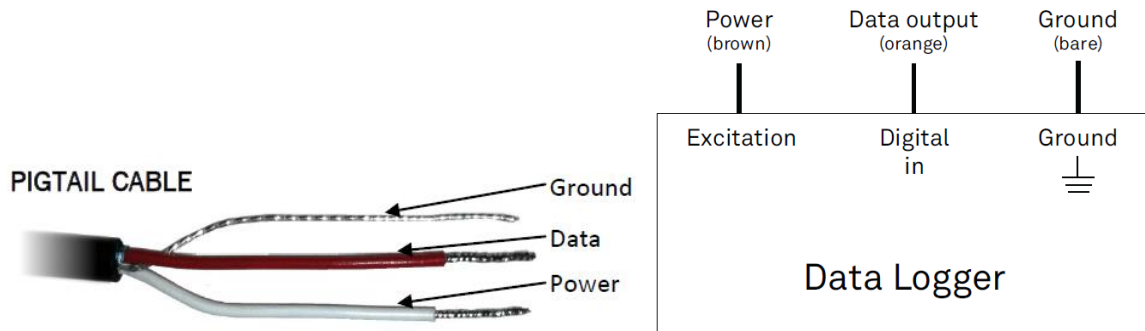


Fig. 38. Pigtail wiring and wiring diagram of a TDR 5TE (5TE manual “METER group”)

Connection of TDRs and Campbell is a sensitive digital connection, so it needs precision and concentration to avoid any disconnecting. If wiring and connections with screw terminal or the Campbell are not done right, there will be a possibility of sensor unplugging and, subsequently, losing experimental data for a period of experiment.

The TDR makes a measurement when excitation voltage is applied to the medium. According to the manual of TDR 5TE, in 120 ms of current excitation, three measurement for different parameters are transmitted to the Campbell as a serial stream of ASCII characters. The serial out is 1200 baud asynchronous with 8 data bits, no parity, and 1 stop bit. The voltage levels are 0 to 3.6 V and the logic levels are TTL (active low). The power must be removed and reapplied for a new set of values to be transmitted because of that we connect power wire of TDR to the switched 12 V port in Campbell. The ASCII stream contains three numbers separated by spaces. These numbers are raw dielectric output, EC, and temperature.

The range of raw dielectric value (ϵ_{Raw}) is 1 to 4094 but the dielectric permittivity values are between 1 and 81.88. 5TE uses 4094 for permittivity when TDR does not work properly, so as soon as the value of 4094 is detected for relative permittivity it means that this TDR has problem and it doesn't work properly anymore. The raw temperature data (T_{Raw}) is between 0 and 1022 but 5TE uses an algorithm to present it in °C. The working temperature range of TDR (5TE) is between -40 and +50°C. For the higher temperatures (+50.5 to +111°C), 5TE report temperature with lower resolution. Similar to what was stated about maximum relative permittivity, 5TE reports its maximum raw temperature value (i.e. 1022) when it does not work properly.

The range of each parameter and the corresponding resolution is shown in Table 4:

Parameters	Range	Resolution
Relative permittivity	1 (air) and 80 (water)	0.0008 m ³ /m ³
Temperature	-40 to 50°C	0.1°C
Electrical Conductivity	0 to 23 μS/m	0.01 μS/m from 0–7 μS/m 0.05 μS/m from 7–23 μS/m
Volumetric Water Content (VWC)	0.0–1.0 m ³ /m ³	0.0008 m ³ /m ³ from 0%–50% VWC

Table 4. Range of variations and resolutions of measuring parameters

Many studies were done about the relationship between relative permittivity and VWC. TDR 5TE uses the equation proposed by Topp et al. (1980) to derive VMC from relative permittivity.

Calibration of 5TE TDRs used in this study are based on the specified relative permittivity of water and air, which are reported 81 and 1, respectively. The range of relative permittivity of water and air in different cells was between 35 to 39.96 for water and 1.1 to 1.2 for air. Fig. 39 presents a calibration curve and the obtained equation (Equation 3-2) to regulate the measured relative permittivity.

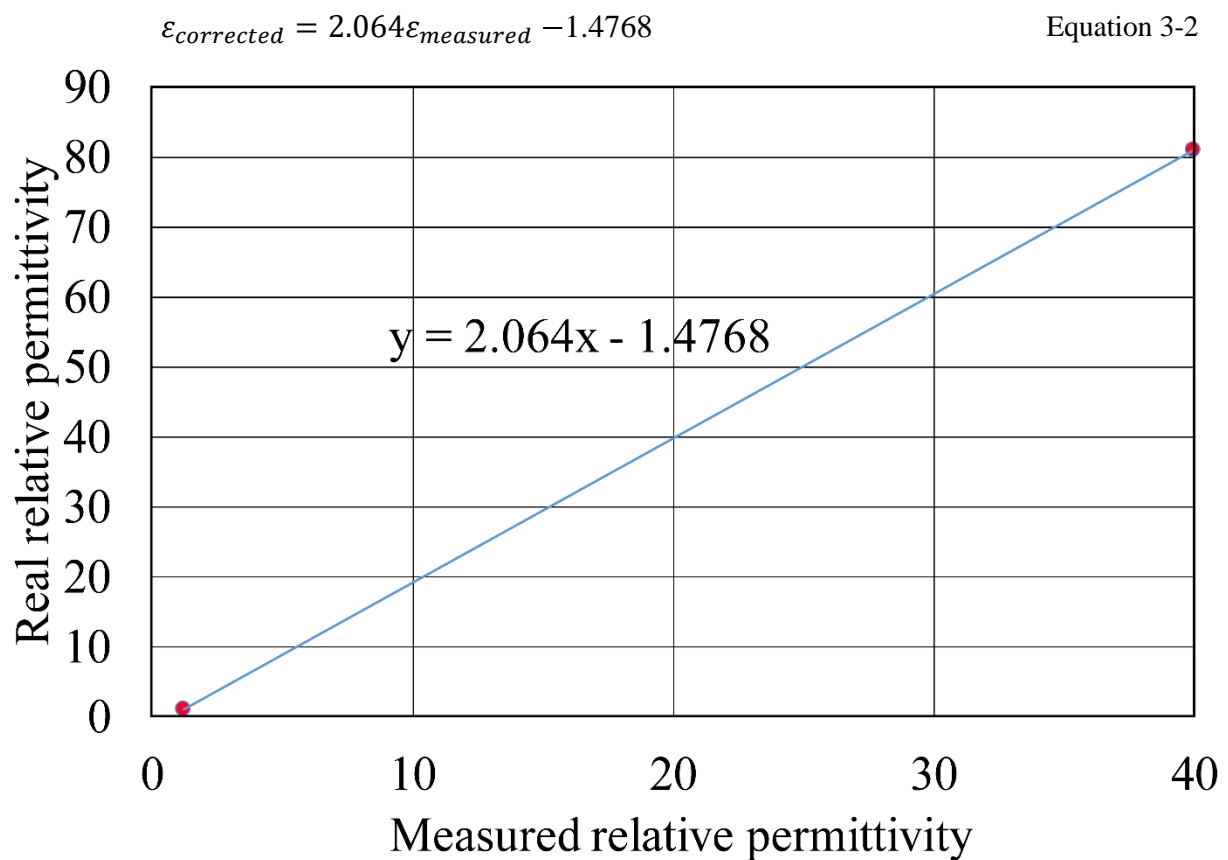


Fig. 39. The TDR calibration curve according to the air and water relative permittivity

At the end, it is worth noting, washing and keeping TDRs clean are the most important maintenance requirements for obtaining accurate measurements.

The fifty-five preliminary test and experiments were performed on cells/columns prior to experiments, which are discussed here (Table 5). The results of those preliminary experiments are not included in this manuscript.

Samples	Preliminary tests	Main series of experiments	pollutants
Cells and columns	55	2 (temperature and saturation effects)	Coal-tar/water, Chlorinated Solvent/water, Canola oil/ Salty ethanol

Table 5. All experiments were done for this study

The preliminary experiments were undertaken to reduce the number of unsupported assumptions and design deficits, and to test the possibility of expansion of results for other fluids. In this stage, applying of conclusions of certain previous studies was examined.

Most of the initial tests were performed on the effects of saturation changes but some tests also did on the impact of temperature change and how we must deal with temperature variations.

4 The effects of temperature on geophysical parameters

4.1 General introduction

Cumulating of dense non-aqueous phase liquids (DNAPLs) in the subsurface at a large number of industrial cities compel authorities to remediate these sites. Remediation of these sites is a long process that needs a reliable technique to follow up and validate the clean-up process.

As explained in the introduction, geophysical approaches are increasingly developed for monitoring of decontamination of the polluted sites. In recent decades, using of electro-geophysical techniques like self-potential (SP) helped researchers to characterize the location of contaminated plumes (Naudet et al., 2003) and follow up in-situ remediation programs (Atekwana and Slater, 2009).

Several studies also have used relative dielectric permittivity measured by time domain reflectometry (TDR) to characterize the dielectric properties of different fluids in porous media (e.g. Persson and Berndtsson, 2002).

Variation in temperature and saturation are the main external parameters that have effects on electro geophysical parameters in contaminated soils. The relationship between temperature and soil dielectric permittivity is studied (Wraith and Or, 1999), but it can be complicated and depends on the soil and liquid properties. Some previous studies were investigated effects of temperature on these parameters for different fluids in porous media and rocks, but there is no study on DNAPLs specially coal tar and chlorinated solvent.

Some depollution methods consist to perform a thermal enhancement in order to reduce the viscosity of the pollutant (Colombano, 2019). We can cite for example Thermal Conduction Heating (TCH), also called In Situ Thermal Desorption (ISTD), Steam-Enhanced Extraction (SEE) or RadioFrequency Heating (RFH). Significant reductions in water and NAPL viscosities have been reported when temperature increases (e.g., Edmondson, 1965; Sleep and Ma, 1997; Villaume et al., 1983).

In polluted site, it is important to know the relationship between relative permittivity, electrical complex resistivity and when thermal enhanced auxiliary method applied to the field for facilitating pumping of DNAPLs from the subsurface. In order to characterize and modelling these effects, we performed a systematic laboratory investigation using SIP and TDR to study temperature effect on these two geophysical parameters. Our findings will be used to correct the measured values due to temperature changes. It is important to separately determine the effect of temperature and saturation in remediation of polluted site in a non-isothermal system.

The multiphase porous media were made by coupling of polar fluid (water) and non-polar fluids (CT and CS) in a logical range of temperature variation (20 to 50°C). Unlike polar liquids, nonpolar substances are made up of molecules that do not have positive at one end and negative charges at the other end. Tap water, ultra-pure water and degassed tap water were used for calibration of electrodes before and after the experiment, manufacturing of potential electrodes and experiments, respectively. This range of temperature variation in the laboratory is normally used in the enhanced thermal technique in the field. Two sizes of sample holders referred as cells and columns were used to investigate the impacts of temperature on these geophysical parameters in different porous media.

The analysis of the evolution of the Cole–Cole parameters of the SIP spectra in function of the saturation will be presented. The Cole-Cole model was chosen due to variety of usage and high potential of this model to characterize different conditions in the field and laboratory work. Besides that this model is the most common used model in this subject. We tried to find the relationship between saturation state and the amplitude and phase shift of the SIP spectra, in order to have a calibration relationship for the further uses in the 2D tank and even thereafter in the field studies.

We will compare our experimental measurements with empirical models. Before explaining the methodology, presenting the results and conclusion of this study, we will first give a more complete description of the previous works and the concepts of the work in more detail.

In the following, the revised version of a paper that has been accepted with moderate revision in the journal of applied geophysics will be presented. We developed the effects of temperature on complex resistivity and relative permittivity on porous media saturated with CS and CT).

The influence of temperature on the dielectric permittivity and complex electrical resistivity of porous media saturated with DNAPLs: a laboratory study

Mohammad Ali Iravani^{1,2}, Jacques Deparis¹, Hossein Davarzani¹, Stefan Colombano¹, Roger Guérin², Alexis Maineult²

1) BRGM, French Geological Survey, 45060 Orléans, France

2) Sorbonne Université, CNRS, EPHE, UMR 7619 METIS, 75005 Paris, France

4.2 Abstract

While some recent studies have discussed various effects of temperature on the electric and electromagnetic properties of multiphase porous media, the effect of temperature changes in multiphase porous media polluted by dense non-aqueous phase liquids (DNAPLs) has rarely been documented. We attempted to characterize how relative permittivity and electrical resistivity vary with temperature in multiphase porous media. The measurements were carried out using two different column sizes. Glass beads with a 1 mm diameter were used to simulate porous media. Spectral induced polarization (SIP) and time domain reflectometry (TDR) were used to measure complex electrical resistivity and relative permittivity, respectively. We investigated the geophysical characteristics of two DNAPLs, coal tar (CT) and chlorinated solvent (CS), from 20 to 50°C; ultra-pure water was used as the reference fluid. Experimental data on the relative permittivity and complex resistivity of pure water obey empirical models, validating our experimental setup and protocol. Results demonstrated that the real parts of relative permittivity and electrical resistivity are functions of temperature in the medium with the presence or absence of a solid phase. While we did not study the imaginary part of relative permittivity, our observations in the DNAPL samples indicated that temperature increases decreased the imaginary parts of the complex electrical resistivity of DNAPLs tested, whether in the presence or absence of the solid phase. Temperature dependency of relative permittivity and complex resistivity were also studied in multiphase porous media, after drainage (80% DNAPL and 20% water) and after imbibition (8% DNAPL and 92% water). The effect of temperature increases on complex resistivity has a secondary effect on frequency domain and Cole-Cole parameters. It was found that the relationship between temperature and resistivity is linear; therefore, resistivity temperature coefficients were obtained for water and both DNAPLs with the presence and absence of solid phase.

Keywords: Spectral induced polarization, dense non-aqueous phase liquids, time domain reflectometry, temperature, complex resistivity, relative dielectric permittivity.

4.3 Introduction

Interpreting the geophysical parameters acquired during monitoring of subsurface soil strata is an important component of soil remediation programs. These parameters play a key role in validating the accuracy and efficiency of remediation methods in soils contaminated with organic and industrial chemicals commonly referred to as DNAPLs (Dense non-aqueous phase liquids). All over the world in the last decade, many sites polluted by industrial activities were abandoned. Study of the factors contributing to the pollution and of the remediation itself has significant environmental and health benefits. There is a consensus about the fact that geophysical techniques are among effective methods for long term monitoring of clean-up processes in soils (e.g., Cardarelli and Di Filippo, 2009; Hwang et al., 2008; Snieder et al., 2007; Sogade et al., 2006; Brewster and Annan, 1994). The majority of the study cases are scientific and this claim remains to be demonstrated for field applications. Among geophysical techniques that can be used to monitor physical properties on contaminated sites, electrical and electromagnetic methods are now proved to be reliable monitoring techniques that provide multiple geophysical parameters such as electrical resistivity and relative dielectric permittivity (e.g., Seyfried and Grant, 2007; Binley et al., 2005). Electro-geophysical methods have been used in many studies, such as estimation of the shallow subsurface conditions (e.g., Romig, 2000), environmental and engineering applications (e.g., Grimm and Olhoeft, 2004; Briggs et al., 2004), and detection of light non-aqueous phase liquids (LNAPL) (e.g., Atekwana et al., 2000). In these applications, the purpose of geophysical testing is to identify technical challenges and assist with implementing solutions during the clean-up process. So studying and monitoring two geophysical parameters, relative permittivity and complex resistivity, can be useful geophysical tools to achieve this.

The remediation method that we consider here is the thermally enhanced (using conduction heating) recovery of coal tar (CT) by means of the “pump and treat” technique to extract and remove CT from polluted soil. According to rheological principles, when temperature increases, viscosity decreases and the pumping rate consequently increases (Ajo-Franklin et al., 2006). Among all auxiliary treatment methods, the thermally enhanced technique is one of the most helpful techniques compared to biological methods (Nathanail et al., 2011; Colombano et al., 2010). Thermally enhanced treatment is the effective remediation technique on deep and shallow soil clean-up processes. Soil digging, excavation, transport and heating make this a costly yet affordable technique in many remediation projects. The results from our laboratory

measurements were used to model the temperature dependence of complex resistivity and relative permittivity to interpret geophysical field measurements. While we know that the application of this work is in a similar range of temperature variations, two important points are worth mentioning in what follows. First, in the corresponding ongoing field survey, the maximum heating temperature was 50°C; therefore, we chose 50°C as the maximum temperature to have the closest simulation of the field work in the lab. Second, choosing a lower temperature limitation compared to feasible field studies can be recognized as a challenge, but if that high temperature limitation in the field will be less than this study, it may give other researchers the option to use these results according to their temperature limitations. Changes in water and DNAPL saturations might have much greater impact on permittivity and resistivity compared to temperature, but after pumping DNAPLs in the contaminated soils, we face change in resistivity and relative permittivity of the soil. These variations are due to temperature and saturation changes. Independent study on the impact of each of these two factors to determine how effective each factor is a must. Recently, the authors have investigated effects of saturation changes on these two parameters with more details in a separate study.

4.3.1 Influence of temperature on relative permittivity: a review

One of the important parameters for understanding the electric and electromagnetic characteristics of a fluid is the relative dielectric permittivity, or dielectric constant. Relative permittivity $\varepsilon = \varepsilon' + i\varepsilon''$ is a complex frequency dependent parameter, where $\varepsilon'(f)$ is the real part and $\varepsilon''(f)$ is the imaginary part, f is the frequency of the excitation current, and i is the pure imaginary unit ($i^2 = -1$). In this study, we only worked with relative permittivity, equal to $\varepsilon_r = \varepsilon / \varepsilon_0$, where ε_0 is vacuum permittivity and has a value of approximately 8.85×10^{-12} F/m. In the controlled experimental laboratory setups described below, in which time domain reflectometry (TDR) probes model 5TE were used (See below for description), the results only related to the real part of the relative permittivity.

Direct TDR measurements are sensitive to the effect of the temperature. For instance, Malmberg and Maryott (1956) established a relationship between the relative permittivity of water and temperature (in the range 0 to 100°C) as below, using experimental methods:

$$\varepsilon' = 87.740 - 0.40008T + 9.398(10^{-4})T^2 - 1.410(10^{-6})T^3 \quad \text{Equation 4-1}$$

where T is the temperature (°C). They stated that the proposed equation has a maximum error of 1%. They also stated that the dielectric constant of water decreases with temperature, but for air, the temperature change does not have a significant effect on relative permittivity. Nath and Dubey (1980) and Nath (1995) have investigated that common error of dielectric constant

measurements is $\pm 5\%$. They carried out their experiments on binary liquid mixtures like trichloroethene ($\text{CHCl}_2\text{CCl}_2$) at 1.8 MHz with a dielectrometer (Dekameter DK₀₃). They used the equation that was proposed by Malmberg and Maryott (1956) to calculate relative permittivity and a relationship for electrical conductivity of soil water as a function of temperature:

$$\sigma_{dc}(T) = \sigma_{dc(25^\circ\text{C})} \exp[-\Delta(2.033 \times 10^{-2} + 1.266 \times 10^{-4}\Delta + 2.464 \times 10^{-6}\Delta^2)] \quad \text{Equation 4-2}$$

in which $\Delta = 25 - T$ and σ_{dc} is the electrical conductivity of soil water. Chen and Or (2006) used TDR to obtain dielectric permittivity and found that even for frequencies lower than 100 MHz, TDR probes clearly showed effects of temperature (5-55°C) and electrical conductivity (due to Maxwell-Wagner (M-W) effect that is the charge at the interface of two materials due to difference of their charge relaxation times) on dielectric permittivity. They expressed that the effective range of the TDRs used is greater than 100 MHz and at low frequency (<100 MHz) this influence (M-W effect) is not noticeable compared to the higher frequencies. For each 1°C increase in temperature, they reported a 0.3% decrease in the relative permittivity of water. For TDR model 5TE, Rosenbaum et al. (2011) proposed an empirical correction function for the temperature effect between 5 and 40°C, tested on eight different liquids. They noticed underestimated values of relative permittivity for temperatures over the range 5 to 25°C (-2.7 for EC-5 and -3.9 for 5TE) and overestimated values for 25 to 40°C (+3.6 for both TDRs). They identified strong correlation between permittivity and electrical conductivity with increasing electrical conductivity with adding salt content.

The influence of temperature on relative permittivity has also been discussed for different fluids. Shah and Tahir (2011) investigated the dielectric properties of oils such as corn oil, cottonseed oil, and polychlorinated biphenyl (PCB) over a temperature range of 25 to 70°C. The effect of temperature on relative permittivity of a soil polluted by oil (petroleum) as a NAPL have also discussed by Iordache et al. (2010) on microwave at frequency 2450 MHz. They have presented that the relative permittivity of the oils increase with temperature increase over the range of 10 to 90°C. There, the increase in dielectric permittivity was related to the humidity values that relative permittivity varied from almost 20% to 70% for humidity 5% to 30%, respectively. Persson and Berndtsson (2002) tried to find a relation between relative permittivity (measured by TDR), NAPL saturation and electrical conductivity. By further validating the results using a mixing model, they demonstrated that TDR measures relative permittivity values very well. Finally, in a study about two kinds of chlorinated solvent (CS), Ajo-Franklin et al. (2006) performed experiments to study the effects of temperature, acoustic velocity and frequency on trichloroethylene (TCE) and tetrachloroethylene (PCE). They fitted

experimental data of temperature with a simple linear equation. They stated that the dielectric permittivity of all solvents decreased due to increasing temperature.

In porous media, Keller and Frischknecht (1966) found that the relative permittivity of dry rock depends on temperature especially at audio- and subaudio-frequency (<10 kHz). They have stated the relative permittivity of dry rock increased as a function of temperature but they reported an inverse relationship between dielectric permittivity and frequency. The ratio of variation in frequency domain is greater in low temperature (100°K) compared to high temperature (850°K). Seyfried and Grant (2007) have characterized the real and imaginary parts of complex relative permittivity for 19 different soils from different areas of the USA at frequency 50 MHz. They found 2% °C⁻¹ change in the imaginary part of the dielectric constant similar to what was proposed by Campbell et al. (1949) for soil's electrical conductivity. This effect is six times less for the real part of the relative permittivity as a function of temperature.

4.3.2 Effect of temperature on complex resistivity: a review

According to Ohm's law, electrical resistivity is the ratio of the electrical current over the applied electric field. The applied electric field is closely related to the current behavior (e.g., Wightman et al., 2004). Electrical resistivity is a complex value described by $\rho = \rho' + i\rho''$ in which $\rho'(f)$ and $\rho''(f)$ are the real and imaginary parts of the complex resistivity, respectively $i^2 = -1$. Note that electrical resistivity (ρ) is the inverse of electrical conductivity σ ($\sigma = \rho^{-1}$).

Many studies have found that temperature has a strong effect on the electrical resistivity of subsurface strata (e.g., Sen and Goode, 1992; Waxman and Thomas, 1974). Electrical resistivity decreases as temperature increases in water (Chen and Or, 2006; Hayashi, 2004; Weast, 1986; Stogryn, 1971), vegetable oil (Lakrari et al., 2013), semiconductors (Keller and Frischknecht, 1966), ionic fluids (Noritomi, 1958), permeable water-saturated rocks (Binley et al., 2010; Llera et al., 1990; Coster, 1948), sodium chloride solutions (Arps, 1953), different soil types (Nouveau et al., 2016) and soil zones (Sherrod et al., 2012).

To find a relationship between temperature and conductivity (or resistivity), Campbell et al. (1949) provided the effect of temperature change on electrical conductivity of 30 different saturated soil samples from different regions of the USA and India. They found that electrical conductivity changed by approximately 2.02% and 1.79% per degree of temperature change over the range of 15 to 35°C and 0 to 15°C, respectively. Before this research, for many years, a table issued by Whitney and Briggs (1897) was a guide for researchers to adjust soil resistance at a given temperature; Richards (1954) published another table to correct temperature for multiple soil samples. The results of Chen and Or (2006) supported further those by Campbell

et al. (1949), i.e. an approximately 2% increase in electrical conductivity for each degree centigrade change in temperature. They also reported that increasing concentration of suspended material decreases how electrical conductivity depends on temperature. Hayashi (2004) evaluated electrical conductivity during mixing of water and saline water with different compositions and its dependency on temperature. They tested the arbitrary constant of a 2% increase in electrical conductivity per 1°C, which was proposed by Campbell et al. (1949). They discovered that the relationship is non-linear when temperature is between 0 and 30°C but a linear relationship could also estimate the variation reasonably. Above 30°C, it appeared that a viscosity-based relation estimated the electrical conductivity better than the temperature-based relation. Hayley et al. (2007) modified a petrophysical model over a temperature range of 0-25°C. Between the exponential Arrhenius equation and the linear equation proposed by Campbell et al. (1949), linear approximation has properly predicted the results at low temperatures. Arps (1953) has discussed the relationship between electrical resistivity, temperature, and sodium chloride concentration (SCC). Sen and Goode (1992) have published an equation showing the relationship between temperature and electrical conductivity. They compared the results of their model with Arps (1953) formula and found that their relation could better predict the conductivity variations. Finally, Grellier et al. (2006) investigated the effect of temperature on the electrical conductivity of leachate. They showed the electrical conductivity of leachate alone and granular media saturated with leachate as a function of temperature. They separately demonstrated their results for pure leachate and a granular sample saturated with leachate.

Many materials and compounds are semiconductors, including those based on the periodic table's carbon group, like silicon, and binary compounds between different group elements like silicon carbide and organic semiconductors, oxides and alloys. For semiconductors, Keller and Frischknecht (1966) have stated that temperature increase has a direct impact on the amplitude of ion movement and vibration. It also has an exponential effect on how frequently ions jump into the vacancies after temperature increases. All semiconductors have negative temperature coefficients of resistivity. Noritomi (1958) published the curve of an ionic fluid for conductivity as a function of temperature. It showed the inverse relation between conductivity and temperature.

Keller and Frischknecht (1966) have also published the effect of temperature on the resistivity of water-bearing rocks. They found that at normal temperatures (moderate temperature around 18 to 25°C), electrical resistivity (conductivity) is related to the resistivity (conductivity) of the electrolyte in rocks. Moreover, they found that the resistivity of water

decreased as its viscosity decreased (because of temperature increase). They identified that for the same rock, resistivity at 12°C is 10 to 100 times higher than resistivity at 18°C. Focusing on water-bearing rocks, Binley et al. (2010) worked on the effects of temperature on the real and imaginary parts of electrical conductivity and the spectra of three permeable sandstones (Berea, Cottaer and Sherwood with porosity of 19, 21 and 32%, respectively) at 1.5 Hz. For simplicity, they developed a simple model to study the relaxation time related to the peak of the imaginary part of electrical conductivity rather than theoretical and phenomenological models like Cole-Cole model, successfully for the experimental data. Llera et al. (1990) proposed a quasi-exponential relation between temperature and resistivity of water-saturated rocks. This relation also confirmed the decrease in resistivity with temperature increases above 200°C induced by high pressure. Coster (1948) found that at high temperature (up to 1000°C), conductivity of rocks increased exponentially with temperature for seven rocks tested. They used DC current to measure the resistance and then calculate conductivity. They published a table demonstrating the dependency of conductivity, temperature, and depth. Not only for different soil types (Nouveau et al., 2016), but also Sherrod et al. (2012) have provided the data for apparent resistivity and temperature monitoring for 3 years in different soil zones in a moderately heterogeneous shallow field subsurface. They have published equations for the relationship between temperature and resistivity in the vadose zone (to the depth of almost 1 m) and saturated zone (at depth among 1 to 2 m). Due to seasonal variations in precipitation during the measurement period, they clearly monitored the effects of drainage and imbibition in the shallow subsurface. Finally, Zhu et al. (2018) have described the electrical properties of five coal samples. At low and high temperatures (30 to 200°C), they prepared two complex resistivity-temperature and complex relative permittivity-temperature models by separately measuring electrical impedance in samples. Subsequently, complex resistivity and relative permittivity were obtained by calculation. They found that at low frequencies (less than 100 kHz), volume resistivity rapidly decreased, but the rate of decrease at medium (100 kHz to 10 MHz) to high frequencies (10 to 30 MHz) was much slower. At a fixed frequency (100 kHz), with temperature increase, volume resistivity initially increased, but it conversely decreased at the end. They reported that both the real and imaginary parts of relative permittivity had the inverse behavior than temperature increases.

Some studies reported inverse behavior for how resistivity changed with temperature. For instance, Quist and Marshall (1968) found that for water in some specific conditions, dielectric permittivity decreased but electrical resistivity increased for temperatures above

300°C. In a study on lateritic soil, Bai et al. (2013) found that the electrical resistivity decreased non-linearly with increasing temperature.

4.3.3 Objectives

Studies on DNAPLs, which are non-polar insulators, are harder than studies on polar water due to heterogeneity in DNAPLs resulting from weathering and biodegradation (Ajo-Franklin et al., 2006). It is interesting from the geophysical standpoint to study how these two fluids with different polarity and dielectric properties interact after drainage and after imbibition of water on soil and comparing the results with results obtained from pure products. Some studies have reported effects of soil heating on different liquids and materials like NAPLs but little attention has been paid to effects of temperature change on soils polluted by DNAPLs and their electro-geophysical characteristics. A lack of study and data regarding how to clean up pollution in these contaminated soils and porous media from the geophysical perspective in the literature. After years of geophysical study, debate continues to swirl around this subject.

The aim of this experimental study was to assess the effects of temperature changes on the complex electrical resistivity, relative permittivity, and temperature coefficient for the conductivity, for two different types of DNAPLs (i.e., CT and CS) and water in porous media. This study examined the application of spectral induced polarization (SIP) and TDR as electro-geophysical methods for estimating the efficiency of soil heating methods used as remediation processes for sites polluted by DNAPLs.

This research provides a better understanding of how effective thermal enhancement is, highlights the dependency of geophysical parameters on temperature change for DNAPL remediation, and could be useful for accelerating the remediation process by choosing the optimum temperature in soil heating techniques. Choosing the optimal temperature can be a critical issue. Firstly, this temperature should be less than heat of vaporization of the DNAPLs because smelling DNAPL vapor can be very hazardous. Secondly, as far as increasing temperature caused decreases and increases in electrical resistivity and dielectric permittivity (measured by TDR) respectively, the higher temperature heating leads to the faster DNAPL recovery. In the following part, we express the experimental setups to obtain these goals.

4.4 Experimental setups and data acquisition

The methodology used in this study is based on the laboratory experiments carried out to estimate electrical resistivity and relative permittivity of multiphase porous media developed recently by Colombano et al. (2017). The complex resistivity data were collected using SIP. Resistivity measurements were taken at 20 frequencies ranging from 0.183 Hz to 20 kHz.

Relative permittivity values were obtained from 5TE TDR probes (METER Group), at 70 MHz (to diminish salinity and textural effects to obtain data that are more comprehensive (Kizito et al., 2008)).

Laboratory tests were carried out on cells and columns. All cells and columns were made of PVDF, a highly non-reactive, thermoplastic polymer normally used when strong solvent-resistance is needed (Schweitzer, 2004). Coarse glass beads (GB) with a diameter of 1 mm were used to simulate a porous medium. Water saturations, DNAPL saturations, and temperature variation were used as the variables in the experimental program. CT and CS with water were used to model a two-phase fluid system. In our experiments, water was treated as the reference liquid to compare the results of contaminations and to monitor the effects of pollution removal in porous media. Table 6 shows both DNAPL's (CT and CS) properties at 20°C. In all experimental setups, one measurement and six measurements were done in the small cell and the columns, respectively (Fig. 40).

	Density (kg/m³)	Viscosity (Pa.s)	Interfacial tension (mN/m)	Contact angle/glass (°)
Coal tar (CT)	1099	0.054	2.5	128
Chlorinated solvent (CS)	1660	0.0045	11.15	60.67

Table 6. Physical characteristics of the DNAPL (CT and CS) used in experiments at 20°C

Fig. 40 shows a schematic layout of the cell and the column used in this study. Each experimental setup has three main parts: water reservoir, DNAPL reservoir and main column (porous medium). The cells were 5.56 cm long with the internal diameter of 5.8 cm, but the columns were 25 cm long with the same internal diameter. Each of the main samples was connected to a DNAPL reservoir and a water reservoir with plastic tubes with internal diameters of 3.5 cm, and 36 cm and 8 cm long, respectively.

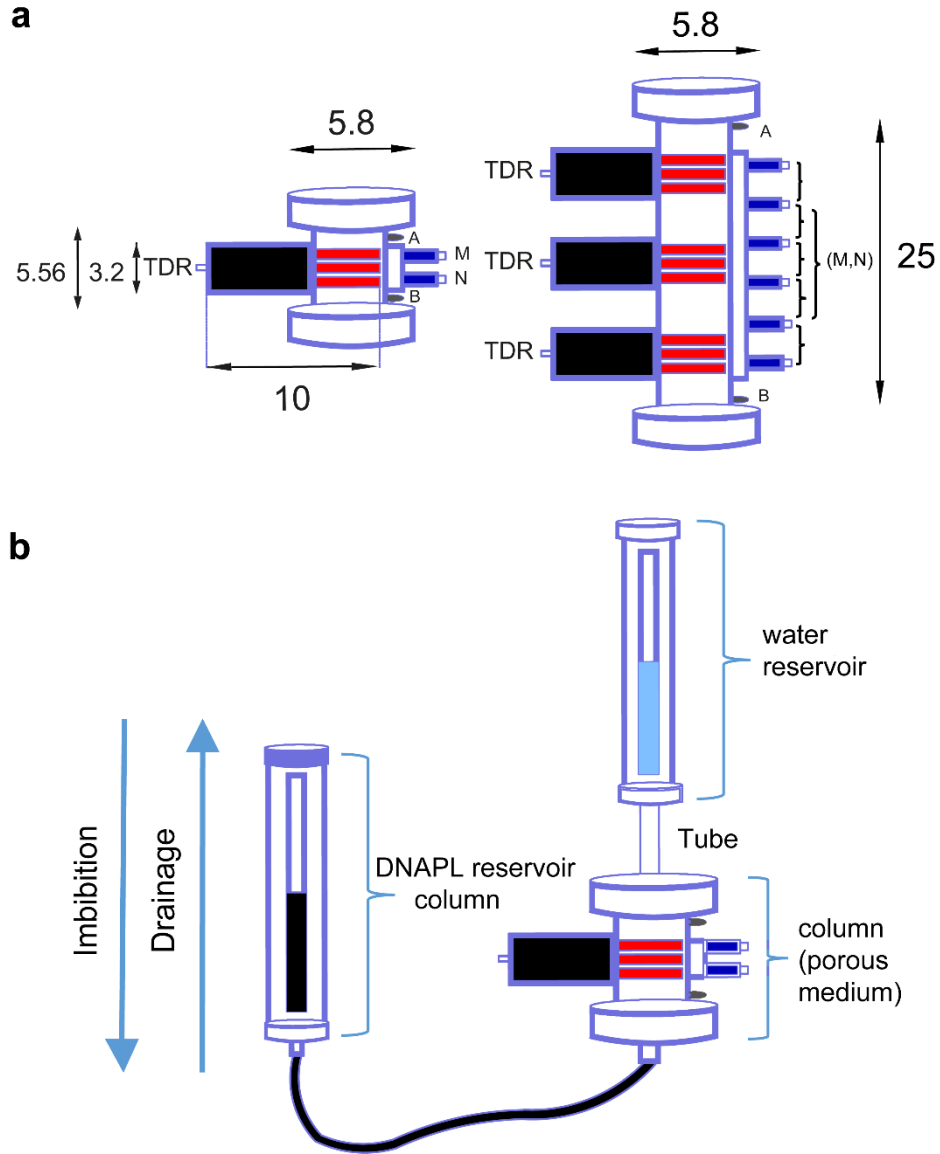


Fig. 40. Schematic of experimental setup (lengths are in cm). a) Geometry of a cell and a column with the position of TDRs, current (A and B) and potential (M and N) electrodes. Each bracket indicates a measurement in a sample. b) Experimental setup including water and DNAPL reservoirs and sample.

The distribution of the electrical potential in porous media around two current-carrying electrodes depends on the electrical resistivity and distribution of the surrounding media. In the laboratory measurements with the configurations of Wenner α and Schlumberger for cells and columns, respectively, an AC current was applied between two ring-current electrodes implanted in the columns and two potential electrodes used to collect the potential difference. In these configurations, all the electrodes were embedded on the same orientation and the electrodes for measuring M and N were laid out between the current electrodes A and B. As illustrated in Fig. 40, according to the principles of these configurations, for Wenner α distances between two electrodes next to each other are same, but for Schlumberger the distance MN is small compared to AB.

For the small cells and columns, two and six non-polarizable hand-made Cu/CuSO₄ potential electrodes (Maineult et al., 2004) were installed between the two current electrodes, respectively. The two metallic ring current electrodes that are made of nickel-cobalt alloy (MP35N) were placed on the top and bottom of cells and columns. These current electrodes had the same diameters as the internal diameter of the columns. For the potential electrodes, the saturating solution was made of milli-Q water (ultrapure water) 72.75%, CuSO₄ 26% and gelatin 1.25% that were mixed and heated ($\approx 80^{\circ}\text{C}$) for 45 minutes using a shaking heating plate. The stability and reliability of these potential electrodes was checked by performing resistivity measurements of tap water 12 hours before running and ending experiments. These measurements with the water also helped us to find the geometric factors of each sample for calculating the resistivity values from measured impedance. The conductivity and temperature of water also measured with a portable conductivity meter, model pH/Cond 340i (WTW Measurement System Inc.) before starting experiments to obtain the geometric factor of each sample. Finally, the SIP measurements were done using the SIP-lab-IV instrument (Radic Research).

Relative permittivities of each cell and column were measured with 10 cm (l) \times 3.2 cm (w) model 5TE TDR sensors and cable length of 5 m located at the middle of the cells and columns (Fig. 40). The effective zones of the TDRs were examined in a complex multiphase sample before designing the cells and columns; the radius of influence of these TDRs is 2.5 cm in all directions. There were one TDR in cells and three TDRs in columns. All TDRs were connected to a CR-1000 data logger (Campbell Scientific Inc.), in order to independently monitor the relative permittivity and temperature in our porous medium.

The temperature variations were applied first on pure products with and without GB, second in glass beads packed after drainage and third after imbibition. During the first stage (experiments on pure products), the geophysical characteristics of water, CT and CS were obtained to facilitate comparing and understanding the effects of saturation of each phase besides temperature in the next stages.

The second and the third experimental setups, i.e., after drainage (wetting phase irreducible saturation) and after imbibition (non-wetting phase residual saturation), were designed to obtain measurements in different contaminant saturations over time and frequency. In our experimental setups, the DNAPL saturation after drainage was $80\% \pm 1\%$ and water saturation was $20\% \pm 1\%$. The ratios of water and pollution were 92% and $8\% \pm 1\%$, respectively. With these experimental setups, we planned to evaluate the effect of temperature

change in different saturations to estimate correctly the DNAPL saturations during the remediation processes.

Before starting drainage, degassed-tap water obtained from an ultrasound tank (VWR Ultrasonic Cleaner - USC500D) was injected into the cells/columns from the valve placed at the bottom by a peristaltic pump (Watson Marlow 530U). Drainage and imbibition were simulated by increasing and decreasing level of the DNAPL column at the left side of the cell and water reservoir. The methodological approach taken in this study is based on the variation of electrical resistivity and relative permittivity due to temperature increase throughout the different experimental setups. In all setups, experiments were launched at 20°C then the temperature was increased to 30°C, 40°C, and 50°C after 24 hours or in some cases after a shorter period of time but never less than 12 hours. The oven used for this study was isolated and had a temperature sensor inside it. All measurements were recorded as soon as the same temperatures were obtained inside the samples (recorded by TDRs) and the oven. In our experiments, all these geophysical parameters were measured in a regular time schedule of two hours for complex resistivity and thirty seconds for relative permittivity.

4.5 Results

4.5.1 Effects of temperature on the relative permittivity

TDRs separately collected relative permittivity data during simultaneous experiments on cells and columns. As we mentioned in section 2, all the TDR probes were placed inside the columns. When the temperature was increased, one hour of delay was observed in the reported temperature from TDRs. Because 70 MHz was the applying frequency of the TDRs used in this study, the real part of the complex permittivity was much more than the imaginary part (e.g., for water it is ≈ 81 versus ≈ 2) (Raju, 2003), therefore, only the real part of the complex frequency dependent absolute permittivity of water and DNAPLs were considered to obtain the relative (dielectric) permittivity.

4.5.2 Effects of temperature on the relative permittivity of pure products

The first sets of analyses examined the impact of temperature increases on the pure products. The results of the analysis of relative permittivity data for pure product with and without GB for different temperatures are presented in Fig. 41. It is apparent that temperature increase decreases the relative permittivity of water with and without GB. On the contrary, in the columns saturated with CT or CS, temperature increases increased relative permittivity. This could be because both DNAPLs are non-ionic fluids whereas water is an ionic fluid (Riley,

1988). The relative permittivity of the columns saturated with CT, with and without GB, was higher than the relative permittivity of columns saturated with CS. These results also evidence the effect of adding GB to the medium. In three columns with GB, adding GB led to a 2.37 to 2.15 times decrease in the relative permittivity of water over the range of 20 to 50°C, but in the DNAPL columns, it increased the relative permittivity of almost 1.7 to 1.77 and of 1.85 to 1.77, respectively. This inverse behavior of CT and CS compared to water is because the relative permittivity of GB is higher than the relative permittivity of CT and CS, but lower than the relative permittivity of water.

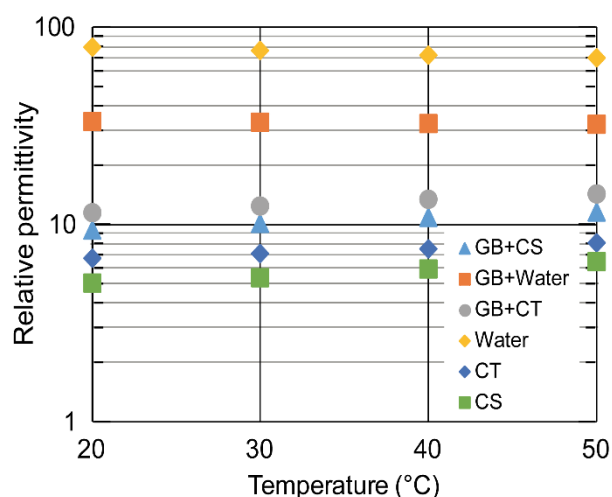


Fig. 41. Variations of relative permittivity as a function of temperature for pure products: CS, CT, water, GB+CS, GB+CT and GB+water.

From the data concerning water, we can see that the temperature change from 20 to 30°C had a lower slope than the next temperature increase. Temperature increases led to 29.04%, 19.91%, 23.59% and 24.80% increases in the relative permittivity of CS, CT, GB+CS and GB+CT over the range of 20 to 50°C.

4.5.3 Effects of temperature on relative permittivity after drainage (irreducible wetting phase saturation) and imbibition (residual non-wetting phase saturation)

DNAPLs as a non-wetting fluid and water as a wetting fluid were used as two different liquid phases. Experiments on the columns were performed with gradual draining of main samples by increasing the DNAPL reservoir column with incremental steps. After replacing the non-wetting phase by the wetting phase, the experiments were stopped and the temperature increased, as we did for pure products. How relative permittivity (real part) changed for both DNAPLs after drainage and imbibition over the temperature range of 20 to 50°C is presented in Fig. 42. The DNAPLs and water saturations were about 80% and 20% after the drainage stage, respectively, but these proportions were respectively 8% and 92% after imbibition. Analyzing

these two stages needs the reference data of pure DNAPLs and water with GB (100% DNAPLs and 100% water) that are also presented in Fig. 42.

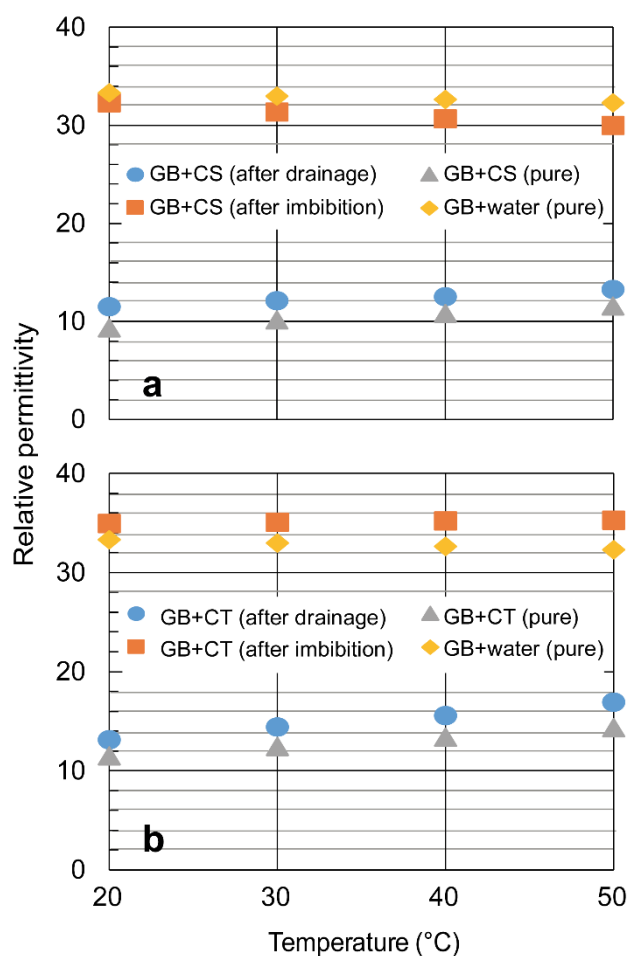


Fig. 42. Change in relative permittivity as a function of temperature for a) CS and b) CT after drainage (80% DNAPLs and 20% water) and imbibition (92% water and 8% DNAPLs) compared to the pure products.

From this data, after drainage, because of DNAPL saturation dominating compared to water, it was apparent that the relative permittivity of both DNAPLs increased with increasing temperature. During the experiments, sometimes a slight difference between the permittivity of the different columns with the same DNAPL was observed. It could be because of the difference in geometry and the amount and distribution of DNAPL saturations of cell and column. Heterogeneity in the distribution of pollutants may explain these discrepancies between the different columns saturated with the same pollutant. After drainage, for both GB+CS and GB+CT, the trends of the results agreed with the results for pure products (see Fig. 41).

After rewetting the sample by replacing water with DNAPLs (by decreasing the DNAPL reservoir column), the residual DNAPL saturation could not be removed from the sample. In this stage, the measured relative permittivity was used, in order to assess the temperature increase after imbibition with the residual non-wetting saturations. Because water saturation (92%) was

much higher than DNAPL saturation (8%), temperature increases should normally cause a permittivity decrease. As shown in Fig. 42, the variation of relative permittivity as a function of temperature after imbibition for CS follows the water trend precisely but for the CT column, this variation was constant with a slight increase. It seems possible that these results were due to DNAPL saturation of more than 8% after imbibition in this column. It is helpful to note that after finishing the experiment and while the columns were being cleaned, it was obvious that CT saturation was higher than CS saturation in these columns. It seems that the higher adhesion of CT compared to CS tends to make it stick to the glass beads and increase the residual saturation.

4.5.4 Effects of temperature on the electrical resistivity

The electrical resistivity of a porous medium contaminated by DNAPLs depends on many geological, geophysical and environmental factors but the most important parameters are proportionality of water and DNAPL saturations, porosity of the porous media, salinity and temperature. The dominant conductor between water and DNAPL and the degree of saturation of each fluid in the porous media have important effects on electrical complex resistivity. In the following sections, we focus on the effects of how varying water and DNAPL saturations and temperature change affect the real and imaginary parts of the complex electrical resistivity.

4.5.5 Effects of temperature on the electrical resistivity of pure products

To have a better understanding of how temperature changes regulate and affect resistivity values, Fig. 43 summarizes all measurements to show how resistivity and phase spectra of complex resistivity of pure products change as a function of temperature at 1.46 Hz. Temperature increases decreased resistivity values for water and two DNAPLs with and without GB. Adding GB to the samples increased resistivity for water and decreased resistivity for both DNAPLs.

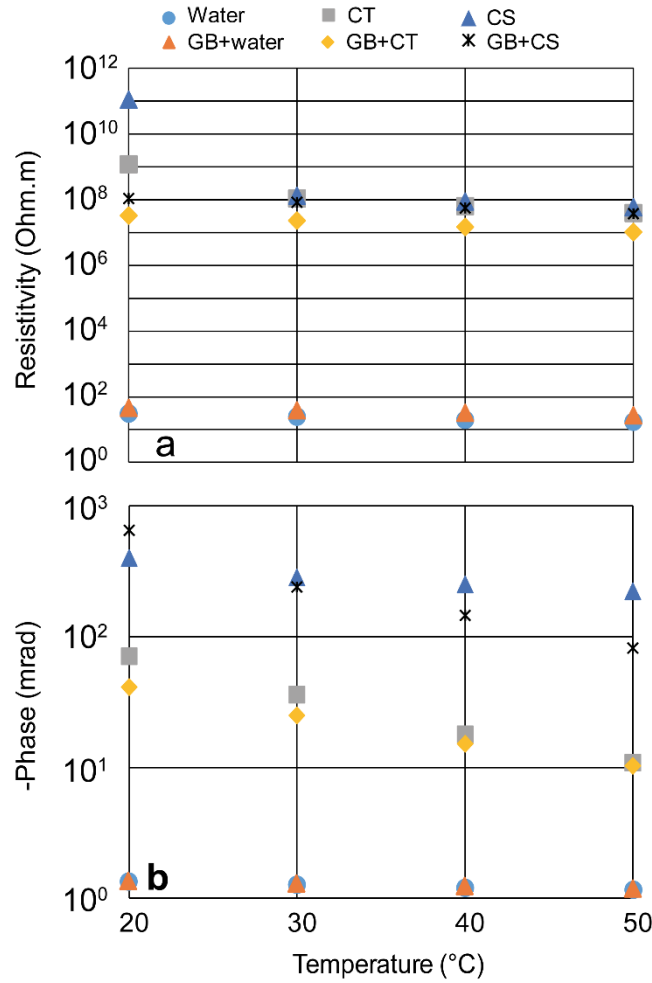


Fig. 43. Variation of (a) resistivity and (b) phase as a function of temperature at 1.46 Hz for pure products: CS, CT, water, GB+CS, GB+CT and GB+water.

Resistivity was higher for CS than for CT. This difference is more significant at 20°C and from 30 to 50°C the resistivity values were close to each other. Higher decreases in resistivity for columns of CT and CS were observed from 20 to 30°C compared to the other temperature changes. From this data, resistivity of water and GB+water also decreased with temperature increases, with the same slope. In a cell resistivity of the sample and intensity of the current has an inverse relationship. In high resistivity samples mostly higher than $10^{+5} \Omega.m$, the intensity of the current became less. Table 7 is an example of SIP data of CT. After current and potential injection SIP port numbers, the resistance (Ω), phase ($^\circ$), resistance error (%) and phase error ($^\circ$) are presented in “txt” file of SIP outputs. The K factor that had been calculated from the test with water before experiment was used to obtain resistivity ($\Omega.m$). The K factor for this cell is 0.15466. For unit conversion of phase and error phase that is in degree, these parameters can be multiplied by “ $-1000*\pi/180$ ” for converting to $-\text{phase}$ in mrad.

Resistance (Ω)	Phase ($^{\circ}$)	Error resistance (%)	Error phase ($^{\circ}$)
6136465419.869480	-3.270664	1.367537	0.783565
6415808743.744370	-3.106138	1.108034	0.634870
6568094317.755410	-3.544381	1.650114	0.945489
6606842577.242600	-4.054735	1.330152	0.762143
6589726614.944500	-3.868323	0.832968	0.477261
6575438918.188540	-3.619194	1.035904	0.593540
6552023027.539510	-3.937480	0.890984	0.510503
6530347149.623130	-3.841423	1.215952	0.696706
6506564043.489960	-4.312883	1.737290	0.995444
6479803644.676120	-3.992971	0.892748	0.511514
6506128907.198990	-4.001023	1.250736	0.716638
6509917494.026190	-3.801757	1.371661	0.785928
6465915265.493240	-4.061723	1.186159	0.679635
3982448342.054900	-2.483216	0.692454	0.396750
1725031688.612990	-1.786293	0.867063	0.496797
1362670992.693150	-1.793787	0.657213	0.376558
1358091572.537880	-1.562359	0.864760	0.495477
1367721031.207020	-1.756417	0.943832	0.540784
1373109025.596330	-2.033820	0.531672	0.304627
1374769262.018250	-1.779814	0.678346	0.388667
1382569601.288540	-1.715938	0.909032	0.520844
1379151023.493670	-1.568110	0.883767	0.506368
1383232014.224310	-1.989650	0.962014	0.551202
1387891982.463830	-1.689818	0.703489	0.403073
1396887565.329010	-1.908861	0.643796	0.368870
1394409797.713160	-1.963486	0.537402	0.307910
1399638833.474180	-1.660298	0.539596	0.309167
1399359192.700890	-1.886332	0.656286	0.376027
1401594952.415850	-1.523809	0.741053	0.424596
1401513503.735310	-1.793045	0.890856	0.510429
1410984540.376720	-1.880876	0.640566	0.367020
1408745222.995050	-1.905574	0.703072	0.402834
1423239119.976370	-1.775655	0.588397	0.337129
1421750026.374730	-1.824072	0.858601	0.491948
1423505359.441630	-1.652678	0.565180	0.323826
1419648037.491100	-1.594946	0.821362	0.470611
1420239999.937270	-2.070749	0.669541	0.383621
1430146890.850220	-1.914330	0.934815	0.535617
1439924579.251450	-1.952319	0.659311	0.377760
1437567463.146170	-1.947622	0.648359	0.371485
1433493832.112650	-2.050121	0.625029	0.358118
1443723555.716980	-2.065156	0.908054	0.520284
1437540468.033040	-1.945049	0.700409	0.401308
1442799772.115330	-1.894759	0.721055	0.413137
1393370641.464510	-1.859595	0.862125	0.493967

913878229.841830	-1.168113	0.562577	0.322334
433391575.569027	-1.155040	0.348590	0.199728
432136028.482802	-0.946279	0.433833	0.248569
430196027.464305	-0.972087	0.409292	0.234507
428327295.699222	-1.180998	0.291498	0.167016
426948896.497440	-0.915337	0.514233	0.294635
424985888.914015	-0.985460	0.477992	0.273870
427940907.030370	-1.022364	0.324698	0.186039
430425444.887078	-0.969801	0.495480	0.283890
429815910.550302	-0.875610	0.351985	0.201673
430830450.072847	-1.004244	0.514512	0.294795
420034476.475919	-1.028067	0.428883	0.245733
288837047.316809	-0.614040	0.327178	0.187459
282716929.582045	-0.663477	0.355236	0.203536
261632068.480256	-0.527192	0.438132	0.251032
257773177.705870	-0.505189	0.275710	0.157970
259971034.997188	-0.577503	0.224092	0.128395
258380555.163487	-0.539954	0.221486	0.126902
258400951.102938	-0.651710	0.248674	0.142480
256598332.636527	-0.539125	0.311064	0.178227
256875382.133602	-0.583654	0.279436	0.160105
258467114.708294	-0.597616	0.370387	0.212217
258329045.612153	-0.620992	0.395165	0.226414
257658473.276820	-3.894524	0.274780	0.157438

Table 7. SIP spectra elements of resistance (Ω), phase ($^\circ$), error resistance (%) and error phase ($^\circ$) for CT

Phase shift spectra in water samples with and without GB were constant between 0 to 2 mrad but temperature increases decreased phase spectra for both pollutants with and without GB. Compared to the amplitude of complex resistivity, phase shift was not significantly affected by adding GB for CT but for CS, a significant change in phase was observed, especially at 40 and 50°C. Generally, in all samples with DNAPLs, temperature increases decreased both the real and imaginary parts of complex resistivity (electrical resistivity and phase). Table 8 shows the number of measurements/samples. For this study, the number of samples and measurements are shown in Table 8.

Sample type	Number of samples	Number of measurements
After drainage		
GB+CT	2 cells, 1 column	2 measurements (cells) 6 measurement (column)
GB+CS	1 cell, 2 columns	1 measurement (cell) 12 measurements (columns)
After imbibition		
GB+CT	2 cells, 1 column	2 measurements (cells) 6 measurement (column)
GB+CS	1 cell, 2 columns	1 measurement (cell) 12 measurements (columns)
Pure product		
Water	3 cells	3 measurements
GB+water	3 cells	3 measurements
CS	1 cell	1 measurements
GB+CS	2 cells	2 measurements
CT	1 cell	1 measurement
GB+CT	2 cells	2 measurements

Table 8. The number of samples and measurements for each stage

4.5.6 Effects of temperature on the electrical resistivity after drainage (irreducible wetting phase saturation) and after imbibition (residual non-wetting phase saturation)

As investigated in section 3.2.1, after performing measurements on pure products, all the experiments were done after drainage and after imbibition, respectively, to see the effects of temperature for different phase saturations in a multiphase system. Fig. 44 shows how resistivity and phase carried as a function of temperature for all columns, after drainage, after imbibition and for pure products. After drainage and imbibition, resistivity linearly decreased due to temperature increases for both DNAPLs. The influence of 20% water after drainage compare to the pure products is clearly evidenced in Fig. 44. As we expected, resistivity was higher in pure products than after drainage but the downward trends were almost the same.

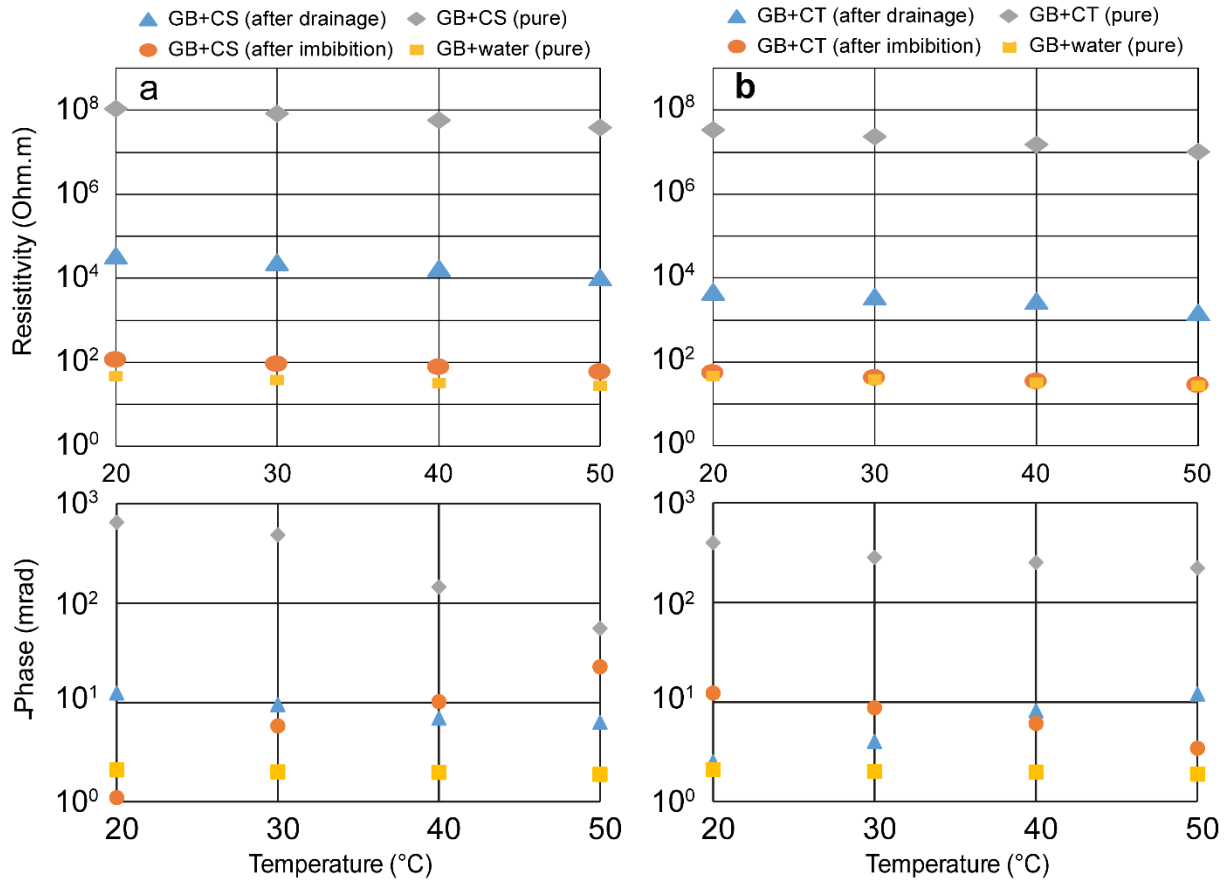


Fig. 44. Changes in electrical resistivity (a and b) and phase (c and d) as a function of temperature at 1.46 Hz for CS and CT after drainage (80% DNAPLs and 20% water) and after imbibition (92% water and 8% DNAPLs) compared to the pure products.

The difference between the resistivity of both DNAPLs after imbibition with water were very low. After imbibition, the domination of water saturation versus DNAPLs saturation in these columns could be the reason for this similarity and low differences (because of regular behavior of water compared to DNAPLs).

For CS, temperature increases decreased the phase spectra after drainage and after imbibition like pure products but for CT, after drainage and after imbibition the phase spectra decreased and increased as a function of temperature, respectively.

4.5.7 Frequency domain of electrical resistivity and phase

Amplitude and phase spectra obtained from SIP response of the samples of CT with and without GB at all frequencies are shown in Fig. 45. The results of laboratory spectra show that temperature increases decreased resistivity for both cases. The difference in resistivity was more significant in low frequencies than for high frequencies.

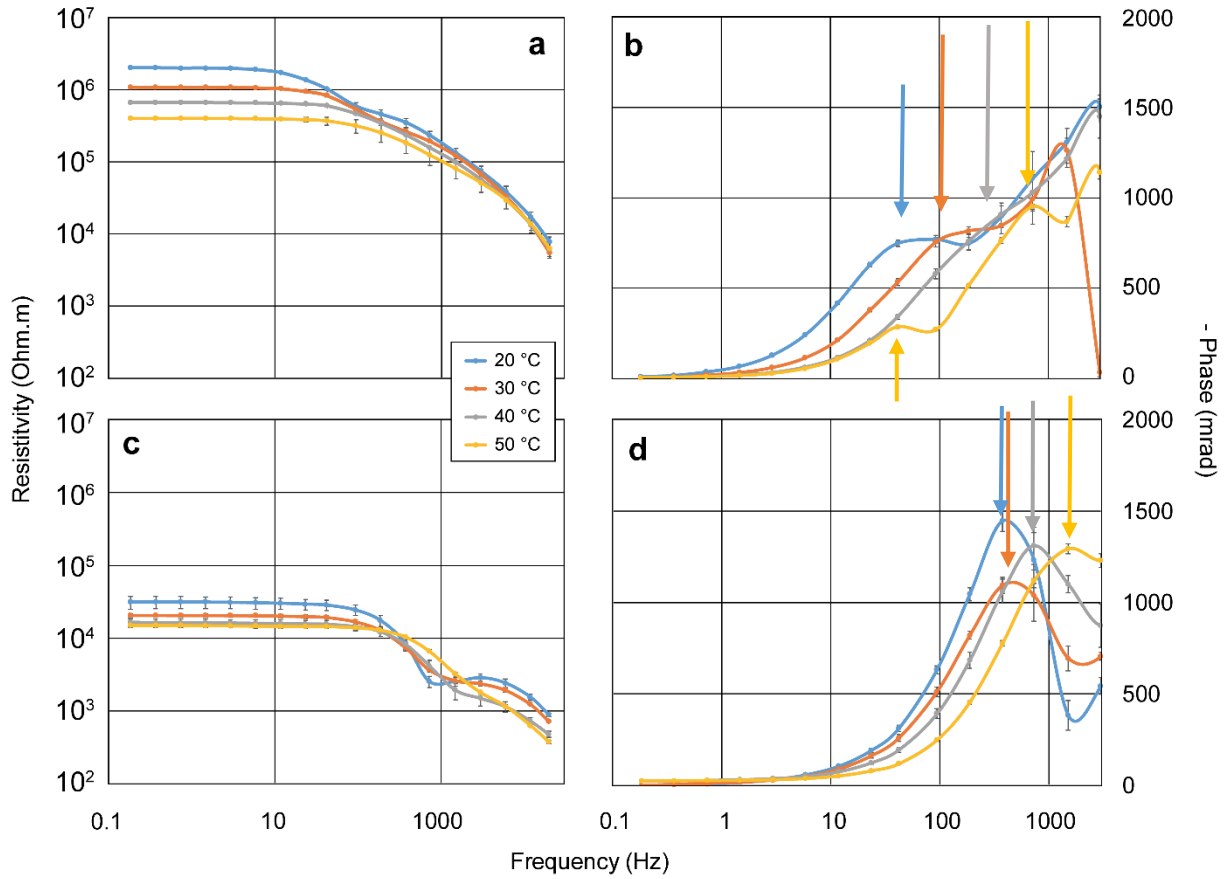


Fig. 45. SIP response and comparison between resistivity and phase spectra of samples with (a) CT and (b) GB+CT as a function of temperature.

Phase spectra of both CT and GB+CT show that increasing temperature shifts the bell curve (peak) to the higher frequency. This finding is consistent with those of Binley et al. (2010) about the effect of temperature change on phase spectra at the frequency range of 0.002 to 100 Hz. As they explained, this expected phenomenon is because of lower relaxation time for the diffusive process. In Fig. 45b, the first peak happened in low frequency and multiple peaks were observed. We believe that electromagnetic coupling of electrodes are the main reason of presenting multiple phase peaks. The experiments on the other DNAPL (CS) with and without GB followed the same trend for both the real and imaginary parts of complex resistivity but the peak of the bell shape curve was at a lower frequency than for CT.

4.6 Discussion

4.6.1 Empirical models for relative permittivity

Our experimental data for the relative permittivity of pure water (Fig. 46) corroborated previous research (Lide, 2008; Weast, 1986; Malmberg and Maryott, 1956 (see Equation 2-79)).

Weast (1986) proposed an equation to study the real part of relative permittivity of pure water as a function of temperature:

$$\varepsilon' = 78.54[1 - 4.58 \times 10^{-3}(T - 25) + 1.19 \times 10^{-5}(T - 25)^2 - 2.8 \times 10^{-8}(T - 25)^3] \quad \text{Equation 4-3,}$$

whereas Lide (2008) gave the following relation:

$$\varepsilon' = 0.24921 \times 10^3 - 0.79069T + 0.72997 \times 10^{-3}T^2 \quad \text{Equation 4-4,}$$

where in this equation T is the absolute temperature in °K. In Fig. 46, there is a similarity between the trend of measured relative permittivity of water in this study and past studies. Our experimental data fell within the area between the curves obtained by Malmberg and Maryott (1956), Weast (1986) and Lide (2008). In Fig. 46, the curves of Lide (2008) and Malmberg and Maryott (1956) are completely superimposed. The fact that our results are in agreement with the expected behavior of pure water makes us confident of the validity of the measurements for other compounds and multiphase media.

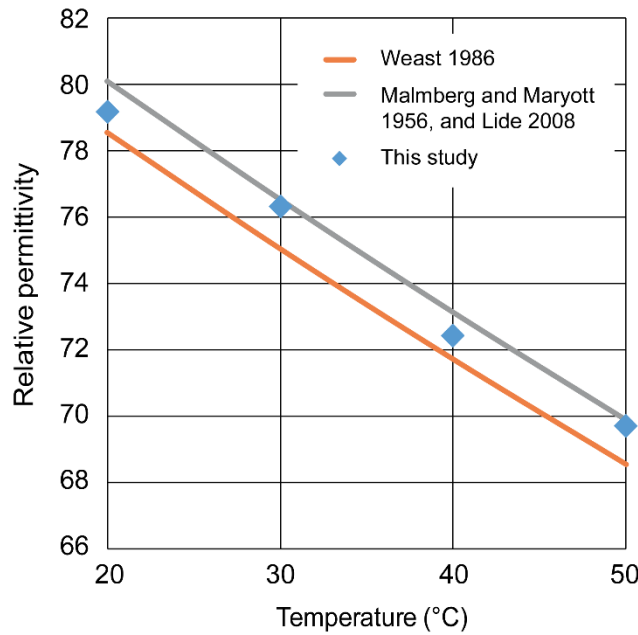


Fig. 46. Fitting of experimental data of relative permittivity with three empirical models (Lide, 2008; Weast, 1986; Malmberg and Maryott, 1956)

Two different experimental setups, a cell with one TDR and a column with three TDRs, recorded values every 30 s after increasing temperature for each step, therefore, hundreds of data points were obtained for each TDR for a given temperature. Since changes in recorded relative permittivity were very low, mean values with standard deviation less than 0.05 (for all compounds) were used to show the permittivity for each temperature in Fig. 41. For other compounds, we fit the permittivity change with temperature using the following equation:

$$\varepsilon' = \varepsilon'_{20} + a(T - 20) + b(T - 20)^2 \quad \text{Equation 4-5}$$

where T is temperature in °C. After fitting the experimental data, the obtained coefficients ε'_{20} , a and b , adjustment coefficient (R^2) and p -value are reported for our different multiphase systems in Table 9. In terms of statistical changes, our calculated R^2 and p -value for all three compounds were significantly fitted; therefore, the proposed models have reasonable predictions of experimental data.

	ε'_{20}	a	b	R^2	P -value
GB+water	33.337	-0.0393	0.0001	0.9997	0.0117
GB+CT	11.476	0.0971	-5.00×10^{-5}	0.9996	0.0177
GB+CS	9.3644	0.0779	-0.0002	0.999831	0.0172

Table 9. Relative permittivity at 20°C (ε'_{20}) and coefficients of a , b and (R^2) (Equation 4-5) for different multiphase media used in this study

One of the empirical mixing models for relative permittivity in multiphase porous media at high frequency (more than 100 GHz) is the complex refractive index method (CRIM) model (Glover, 2015), which for our experimental setups can be expressed as:

$$\varepsilon_{mixed} = (\Phi \sqrt{\varepsilon_{water,CT \text{ or } CS}} + (1 - \Phi) \sqrt{\varepsilon_{GB}})^2 \quad \text{Equation 4-6}$$

where ε is the relative permittivity and Φ is the porosity of the medium. CRIM model is a derivative (when $m = 2$) of a general empirical mixing model for relative permittivity that is called the Lichtenecker–Rother equation (Glover, 2015):

$$\varepsilon_{mixed} = (\sum_{i=1}^n \varepsilon_i^{1/m} \Phi^i)^m \quad \text{Equation 4-7}$$

In this equation m is a frequency-dependent coefficient that can vary for different frequencies in both high and low frequency but in high frequency, the polarization factor will affect the relative permittivity of water (Glover, 2015). From our experimental data, the porosity is $38 \pm 2\%$, and we assume that the relative permittivity of glass beads is 13.8. In Fig. 47, the CRIM model properly fit the experimental data for water and CT at 20 and 30°C but there are small underestimations at 40 and 50°C. For CS, the CRIM model has an underestimation over the temperature range of 20 to 50°C but the trend of predicted relative permittivity matches the experimental data for this DNAPL. As Fig. 47 shows, the CRIM model is a relationship between a material's permittivity and its volume fractions in a multiphase system. Correction of this equation by adding temperature effects can avoid inaccurate data estimations for high temperatures.

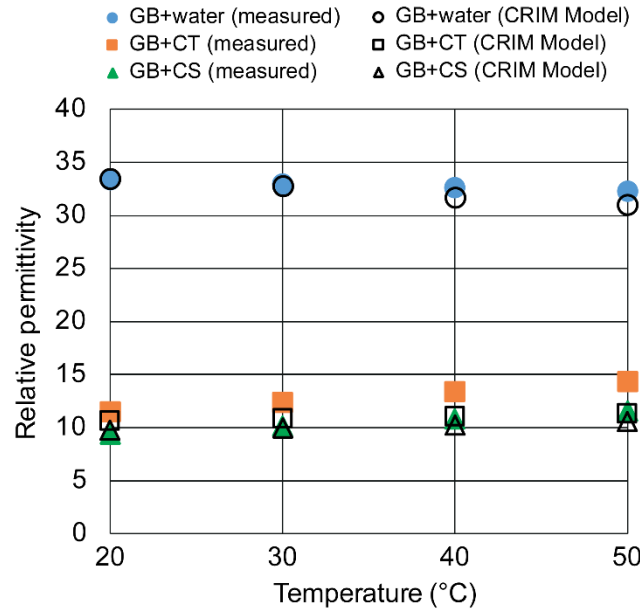


Fig. 47. Mixing model of experimental data of relative permittivity for different multiphase systems

For CS, temperature increases led to a greater difference between experimental and predicted data.

4.6.2 Temperature coefficient of resistivity (α)

How the electrical resistivity of water and other materials varies has been widely studied. For instance, the resistivity of metals and semiconductors respectively increase and decrease with temperature increase, but alloys' resistivities do not have very strong temperature dependency (Keller and Frischknecht, 1966).

Dakhnov (1962) and Keller and Frischknecht (1966) have presented a relation to describe the temperature dependency of resistivity for an aqueous liquid over the temperature range of 0-200°C:

$$\rho_w = \frac{\rho_{w0}}{1 + \alpha(T - T_0)} \quad \text{Equation 4-8}$$

where ρ_{w0} is the resistivity of the aqueous fluid at temperature T_0 and α is the temperature coefficient of resistivity. From our result, the calculated α for water is 0.027°C^{-1} . This finding is in agreement with Keller and Frischknecht (1966) and Campbell et al. (1949), who showed that α is about 0.025 and 0.02°C^{-1} , respectively. Hayley et al. (2007) and Scott and Kay (1988) have reported a range of temperature coefficient between 0.018 - 0.022 for water. Heimovaara et al. (1995) and Amente et al. (2000) also published 0.019 for water. For unsaturated soil in a field scale, Nouveau et al. (2016) found α value of 3 - 3.5% . They stated that the main reason for this difference with the past work could be because of using resistivity data after inversion.

This equation for an ionic salty aqueous solution showed that resistivity and temperature have are inversely connected. For water, increasing mobility of ions because of temperature increase decreased viscosity. One of the main challenges in this study was verifying this relation for two different DNAPLs as non-ionic fluids. According to an intuitive hypothesis, after monitoring the trend in resistivity variation with temperature in our experimental data and accuracy and precision of fitting, temperature coefficients for resistivity were obtained for all measurements in all cells and columns. In some cases, the parabolic equation had the better fitting with adjustment coefficient (R^2) almost equal to one, but with the parabolic fitting the final equation is more complicated. The results of linear fitting of DNAPL data properly demonstrated the accuracy of the equation proposed by Dakhnov (1962) for both DNAPLs.

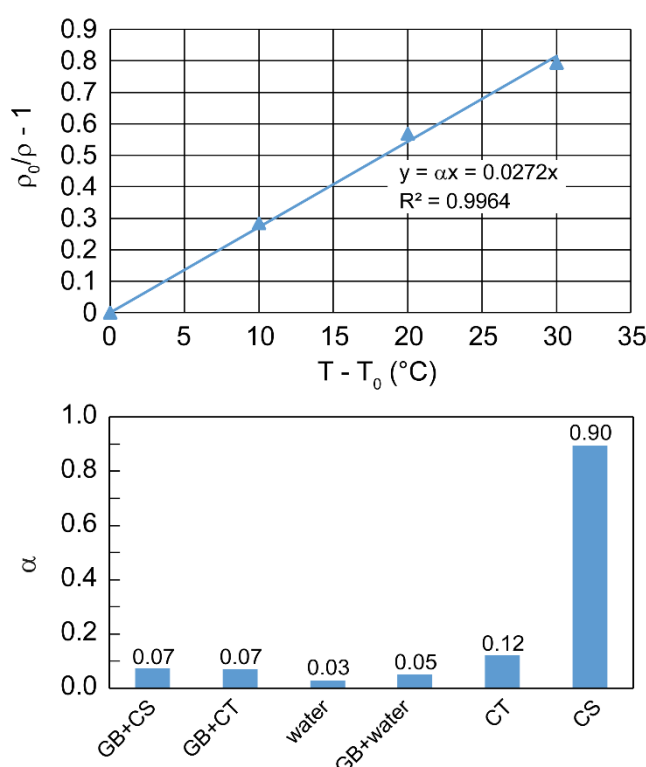


Fig. 48. (a) An example of using linear regression to obtain α value for water (b) comparison between α values obtained for water ($R^2=0.9964$), GB+water ($R^2=0.9937$), CT ($R^2=0.9522$), GB+CT ($R^2=0.9538$), CS ($R^2=0.9824$) and GB+CS ($R^2=0.9734$) for $f=1.46$ Hz.

Fig. 48 shows the linear method that was used to obtain the α coefficient and α value for all cells and columns. The CS α value is much higher than the α values for CT and water, but we saw less variation in α values when they are with GB. By contrast with both DNAPLs, adding GB increased α value of water from 2.7 to 5%.

4.6.3 Effect of temperature on Cole-Cole parameters

Pelton et al. (1978) discussed the relevance of induced polarization and the Cole-Cole model. The Cole-Cole presents the resistivity of a porous medium as:

$$\rho(\omega) = \rho_0 \left[1 - m \left(1 - \frac{1}{1 + (i\omega\tau)^c} \right) \right] \quad \text{Equation 4-9}$$

How the four major parameters in the Cole-Cole model (with the code developed by Mainault et al., 2017), low frequency resistivity ρ_0 , intrinsic chargeability m , Cole Cole exponent c and mean relaxation time τ that characterizes the decay (Pelton and Smith, 1976) change as a function of temperature for CT, with and without GB, is shown in Fig. 49. Increasing temperature increases ρ_0 , m , $\log(\tau)$ but parameter c fell after a change from 40 to 50°C for CT. Temperature increases decreased ρ and $\log(\tau)$ and increased m but after 40°C this parameter became constant. c was also constant and equal to 1, that is conform with the Debye model (Kalmykov et al., 2004). The Cole-Cole parameters are studied for the first peak of phase, because the higher frequency peaks are not related to the porous medium studied but rather to the measurement system and the sample holder.

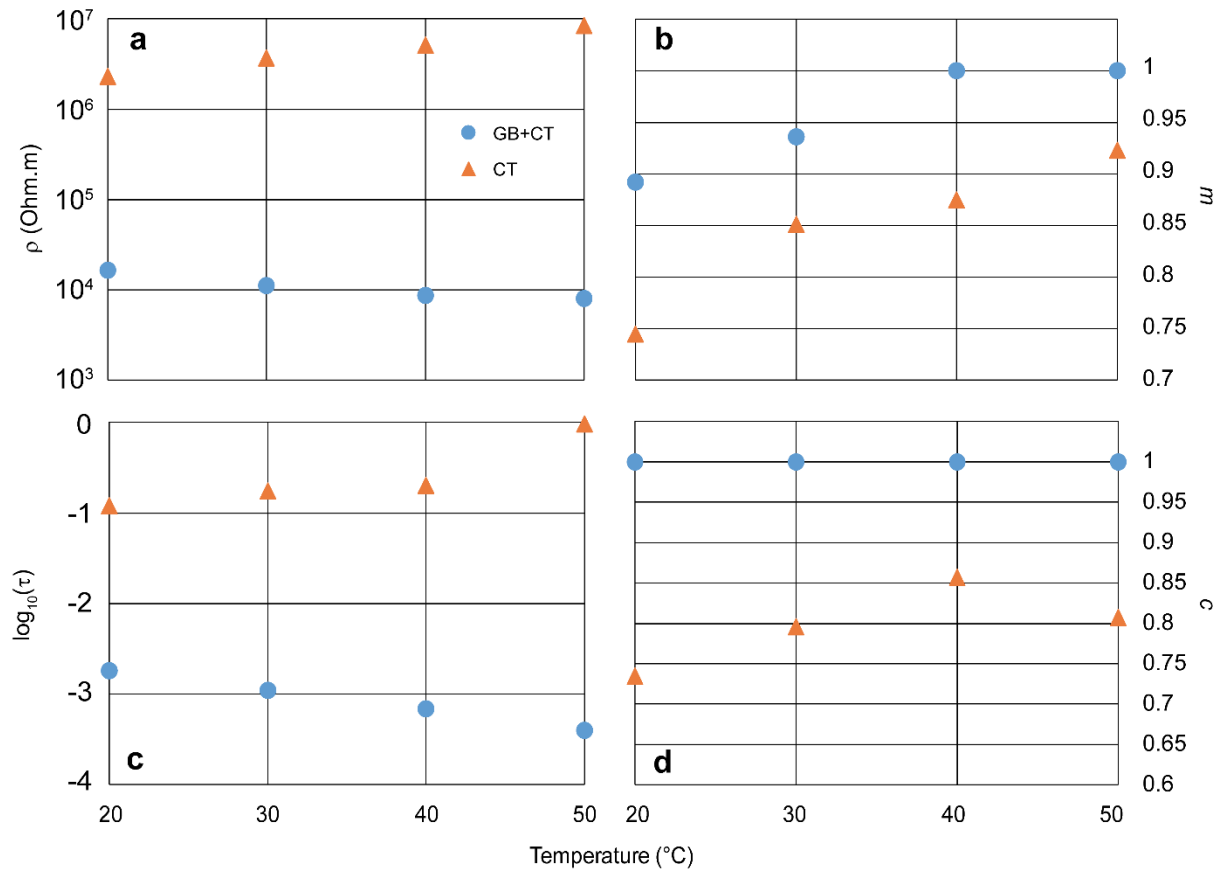


Fig. 49. Cole-Cole parameters as a function of temperature for CT, with and without GB.

4.7 Conclusions

This study attempted to extend our understanding of how temperature changes affect relative permittivity and complex electrical resistivity in multiphase porous media saturated with coal tar or chlorinated solvent. Our findings enhance knowledge on auxiliary techniques (e.g., thermally enhanced DNAPL remediation techniques), which accelerates clean-up processes (pump and treat) for sites polluted by DNAPLs. Whether a solid phase was present or absent in the experiment, results showed that as temperature increased, the real component of the relative permittivity of water and DNAPLs decreased and increased, respectively. Adding solid phase to pure samples increased and decreased the relative permittivity of DNAPLs and water, respectively. The effect of temperature change on relative permittivity of both DNAPLs was the same as for pure DNAPLs but after imbibition (8% DNAPL and 92% water), unlike CT, the relative permittivity of CS samples did not conform to the relative permittivity of pure CS.

Temperature increased decreased both the amplitude and phase shift component of the electrical resistivity of water and both DNAPLs tested in the presence or absence of the solid phase. How Cole-Cole parameters change as a function of temperature were also discussed in this study. The laboratory spectra showed temperature increases decreased resistivity on the frequency domain for CT in the presence or absence of the solid phase. It was found that the difference in resistivity was more significant for low frequencies than for higher frequencies. Laboratory phase spectra of both CT and GB+CT showed that increasing temperature shifted the bell curve of the spectrum to higher frequency. Our experimental data of electrical complex resistivity and relative permittivity conform to the empirical models on these subjects.

These current results demonstrated that SIP and TDRs follow variations in electrical resistivity and relative permittivity during the long-term monitoring of soil remediation processes. Despite soil not only depend on porosity and texture, we tried to model site soil in the closest textural characteristics. The GB diameter was purposefully selected to simulate the same physical characteristics in laboratory setups and our targeted fieldwork (e.g., same porosity in the lab ($38\% \pm 2\%$) and the field (36% to 42%)). Results compared with empirical models and can be extended to field work. In general, we believe that these results might be applied to sandy soils and permeable sandstones with close porosity and resistivity but we cannot claim that these findings would be suited to other soils with different porosities and resistivity because the electrical resistivity of soils is related to their composition and corresponding physical indexes like the plasticity index, coarse fraction and more (Abu-Hassanein et al., 1996).

In the field, the body of porous media are soils with lower resistivity and higher relative permittivity compared to GB. We believe that along with its benefits, using GB may influence the temperature dependency of a medium but this difference should not be significant unless particularly fine-grained soil with high electrical conductivity will be used.

Finally, we found that changes due to temperature are not really significant on relative permittivity but that combining resistivity and TDR data could be a key point. Further research on the effects of temperature change on the imaginary component of relative permittivity is needed. Additional research on geophysical characteristics of other DNAPLs will expand the application of this study.

Acknowledgements

This study was performed as part of the BIOXYVAL project. The authors would like to thank ADEME for funding part of the project under the “Investissements d'Avenir” program, BRGM, Iranian consulting engineers “Hegmatan-Mahar Ab” for providing the PhD thesis scholarship of Mohammad Ali Iravani, and Nicolas Philippe, Benjamin Douche from BRGM and Setareh Behjatamin for valuable experimental assistance. Finally, we gratefully acknowledge the financial support provided to the PIVOTS project by the “Région Centre – Val de Loire” and the European Regional Development Fund.

4.8 General conclusions

In this chapter, we present the impacts of temperature on electrical complex resistivity and relative permittivity in contaminated saturated porous media. Indeed, the goal of soil heating is to increase the temperature of pollutant in order to decrease his viscosity (Martín-Alfonso et al., 2007). So these phenome as for consequence to increase the mobility of pollutant and so during depollution, increase the pumping rate of contamination in saturated soil (Colombano, 2019). Heating of the soil have also for consequence a modification of geo electrical and permittivity parameters.

These results are based on the laboratory studies with limitations and different from field. The characteristics of the used GBs are far from soil properties in the field, for instance despite GBs, significant interactions to be expected with natural soils. On the other hand, the products considered here are pure and not subject to microbial activity, which strongly modifies the physio-chemical properties of the system.

The study of geophysical parameters during this operation is influenced by two environmental parameters: temperature due to soil heating and saturation change due to contamination pumping. The relationships between these geophysical parameters and

temperature were clarified through laboratory tests on two different column sizes with different fluid couples. Then saturation field in 2D tank will be determined according to the electro-geophysical measurements. We found that separate studies on the effects of temperature and saturation changes on geophysical parameters are needed. In the first step with the finding in chapter 4, the geophysical parameters will be corrected according to temperature effects. The next step will be finding the relationship between these geophysical parameters and saturation. The obtained correlation curves will be used in the future laboratory studies on a 2D tank (a small model of actual field conditions). Fig. 50 is a schematic of decontamination of soil in fields, carries out under enhanced thermal technique.

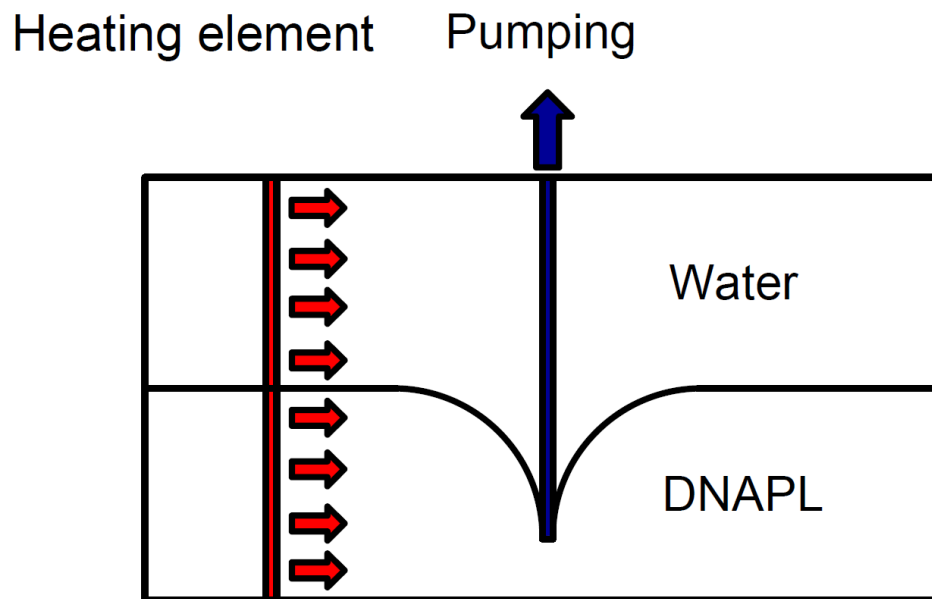


Fig. 50. Schematic cross-section of a site polluted by DNAPL during DNAPL pumping

In the following chapter, the effects of saturation changes on electrical complex resistivity and dielectric relative permittivity will be discussed.

4.9 Appendix: Detailed figures of chapter 4

In this annex, there are detail figures of SIP (resistivity and phase) and relative permittivity (obtained from TDR) of all measurements. The SIP and TDR measurements were classified in two subchapters to present time series of data for pure products, after drainage and after imbibition. The merged forms of these figures were shown in chapter 4.

4.9.1 The detail figures of TDR measurements (Relative permittivity)

In chapter 4, the relative permittivity measurements were performed to assess the dielectric behavior of different porous media saturated with CS/CT and water. In the Fig. 51 to Fig. 53, the evolution of relative permittivity in time domain were presented based on the raw

TDR measurements of pure products, after drainage and after imbibition, respectively. All TDR data were corrected (in chapter 4) based on the relative permittivity of water and air (that are specified in many references). The relative permittivity of water must be between 80 and 81, and relative permittivity of air must be 1 at 20°C, but the TDR measurements of water and air were presented 39.48 and 1.2 at 20°C. An equation of $\varepsilon = 2.068 \times \varepsilon_{\text{raw}} - 1.4768$ was proposed to correct the dielectric constant measured by TDR. Where ε is the corrected relative permittivity and ε_{raw} is the raw relative permittivity recorded by TDR probes. We conclude that this difference between measured and expected relative permittivity is due to geometries of the sample holders. Using same TDR in the same water without placing inside the sample holders showed a value between 80 and 81 that prove our hypothesis.

The interval of TDR measurements was every 30 s and we continue measurements for at least 12 hours to reach the exact relative permittivity of each temperature.

We found that there are a series of different recording (indentations) of relative permittivity frequently in all experiments. The time difference between these indentations was 2 hours. As SIP currents were injected every two hours and these indentations were in the same time with these current injections, we found that it is the effect of SIP on TDR data (For instance, see Fig. 51a).

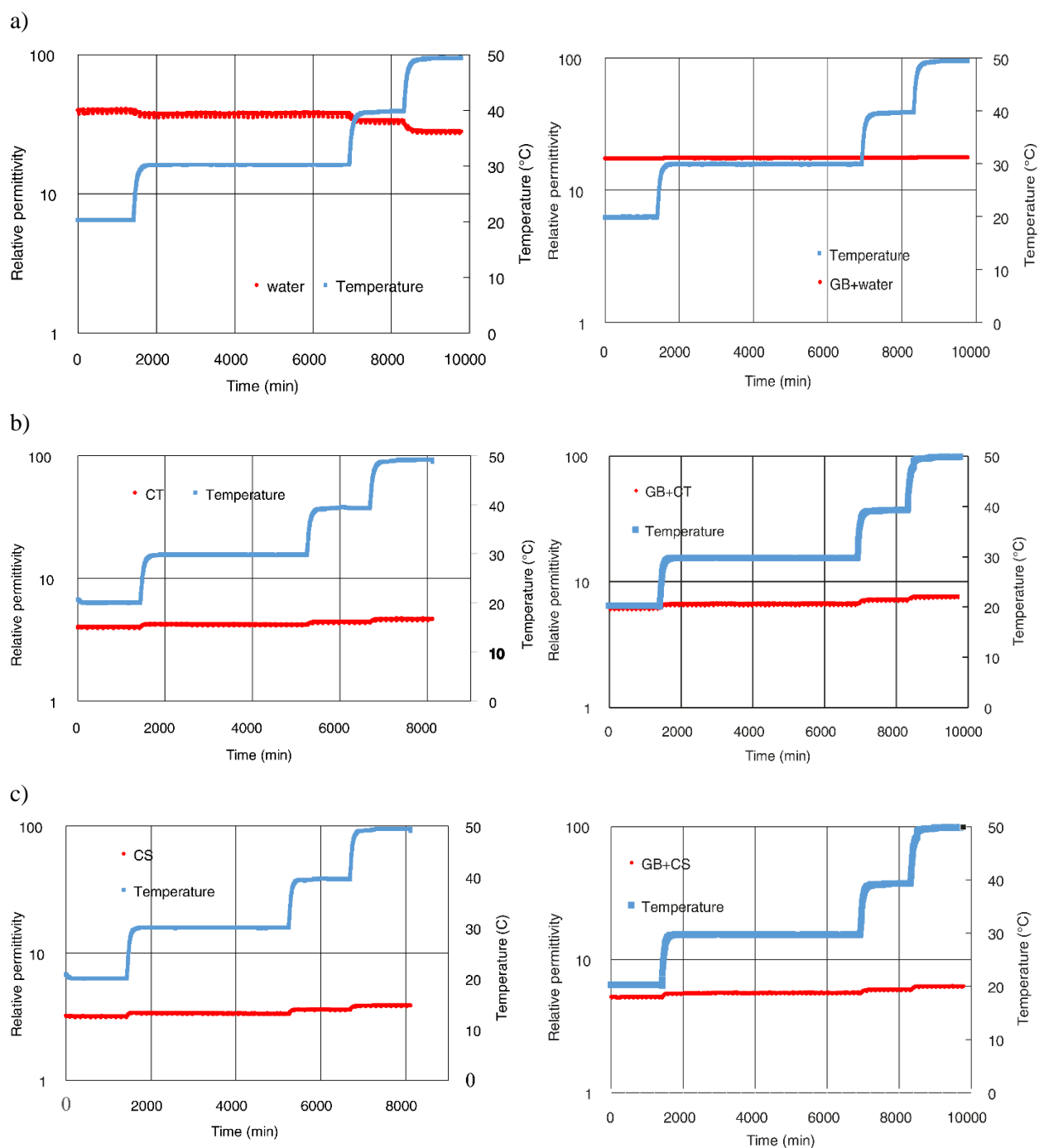


Fig. 51. Time domain of relative permittivity and temperature for pure products for a) water and GB+water, b) CT and GB+CT and c) CS and GB+CS.

Unlike Fig. 51a that shows decreasing in relative permittivity of water with and without GB, Fig. 51b and Fig. 51c are presenting increase in relative permittivity of both DNAPLs (CT and CS) with and without GB. The change in relative permittivity due to temperature variation is more visible for water compared to GB+water (See Fig. 51a), but it is not that obvious for DNAPLs.

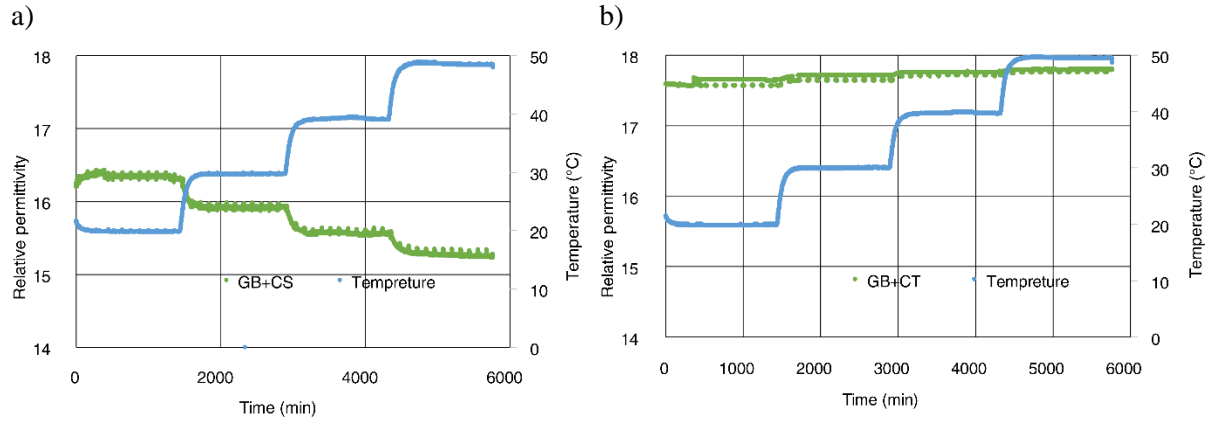


Fig. 52. Time domain of relative permittivity and temperature after imbibition for a) GB+CS and b) GB+CT.

In Fig. 52a and b, after imbibition majority of fluid inside the pores is water and as we expected from the results of pure product, the relative permittivity decreased for GB+CS (Fig. 52a) but it is almost constant with a slight increase for GB+CT.

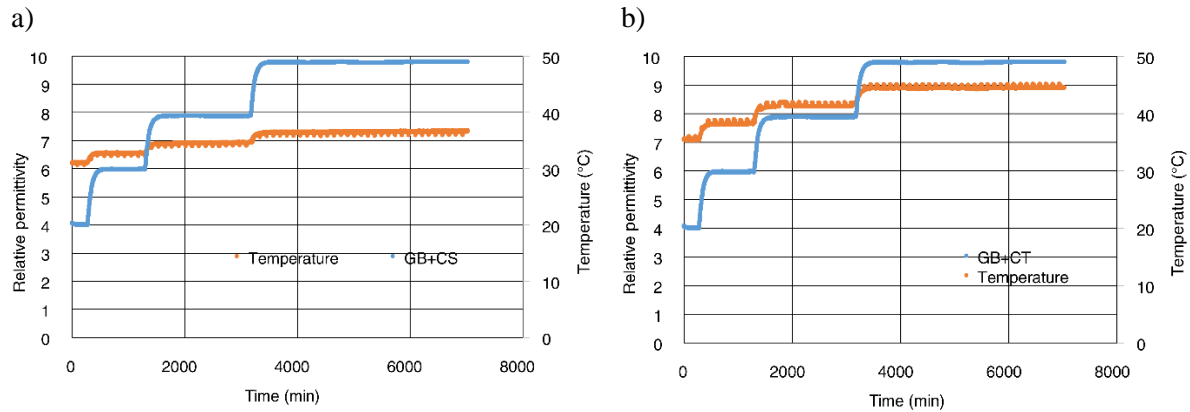


Fig. 53. Time domain of relative permittivity and temperature after drainage for a) GB+CS and b) GB+CT.

In Fig. 53, after drainage the majority of pores filled by DNAPLs, according to what we found for pure products, temperature increase should cause increase in relative permittivity. Again, this result approved what we found in Fig. 51.

4.9.2 The detailed figures of SIP measurements (Complex resistivity)

IP measurements operated both in time and frequency domains are effective on monitoring of the depollution of the soil. Time series of complex resistivity changes show the evolution of resistivity and phase during the remediation process. In the laboratory, SIP lab 4 was recorded the complex resistivity data every two hours (120 min).

Unlike permittivity measurements, complex resistivity shows a complex and unstable evolution. We had different ways to specify a value for each temperature when it did not become constant at the time of temperature changing. 1) Choosing the last value before changing the

temperature and 2) getting an average value of last 3-5 measurements. I found that the values obtained from both ways are very close to each other, so I chose the first method!

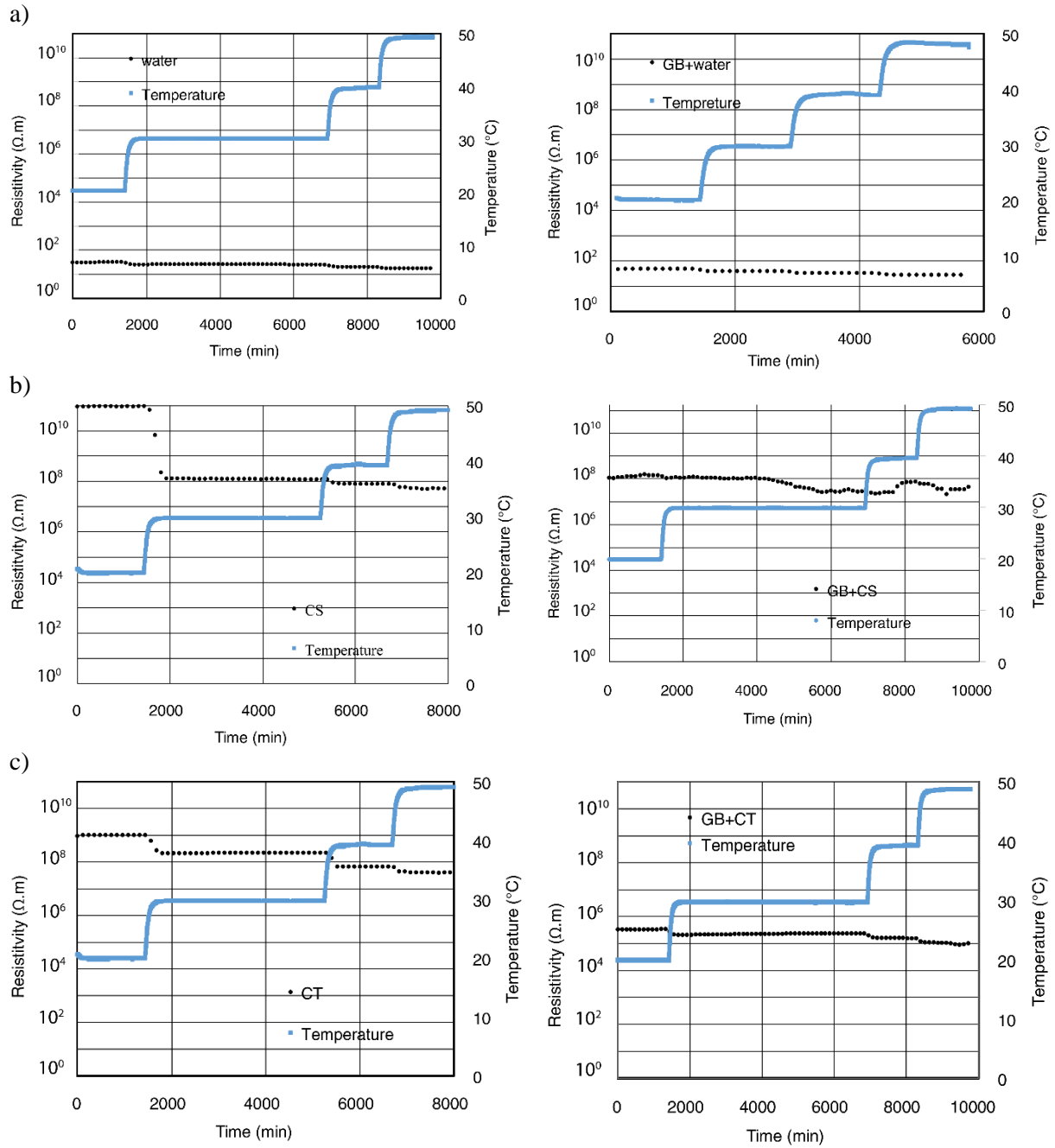


Fig. 54. Evolution of resistivity with time for pure products, a) water and GB+water, b) CS and GB+CS and

c) GB+CT at 1.46 Hz

It is worth noting that if fluid injection did not perform well, existence of air bubbles captured in the pores can make serious challenges. According to what we see during our white test experiments with only water (especially on 2D tank that was clearer because of the glass front), the existence of a small bubble close to potential electrodes could completely change the resistivity values (due to high resistivity of air). The different distributions of the DNAPLs and

water could also make anomaly in our measurements. In Fig. 54, evolution of water (Fig. 54a) is different from both DNAPLs with and without GB (Fig. 54b,c). For pure products, temperature increase led to decrease in water resistivity and increase in CS and CT resistivity with and without solid phase.

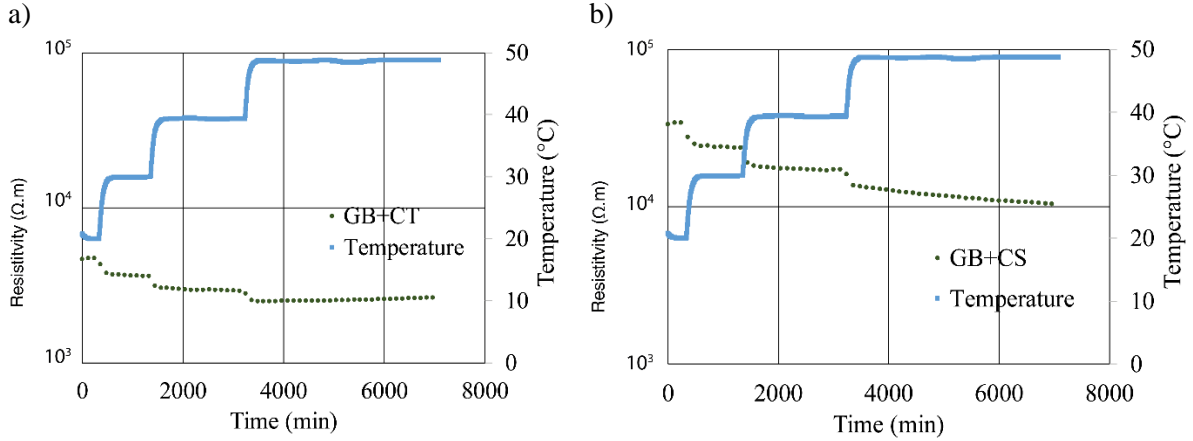


Fig. 55. Evolution of resistivity with time after drainage for a) GB+CT and b) GB+CS at 1.46 Hz

We performed experiments in different cells and columns and chose the best data according to the quality of SIP spectra. The second challenge on SIP measurements was choosing a certain value of resistivity for each temperature. In some cases (especially after drainage in Fig. 55) even after two days, the value of resistivity did not become constant. Sometime we see slight increasing when we expect decreasing (e.g. GB+CT, after drainage for 50°C). In Fig. 55b, an anomalous behavior was observed in the last change of temperature to 50°C. By considering the sample behavior of GB+CS for pure product (Fig. 54b), heating the sample for a long time, in this cell after around 4000 min from the beginning of the experiment the resistivity data became unstable without changing in temperature. Since in the cell of GB+CT such an anomaly did not observed it can reported as a specific characteristic of GB+CS. Monitoring the same behavior with pure product ignores any relationship between this phenomenon and remaining water in the sample after drainage.

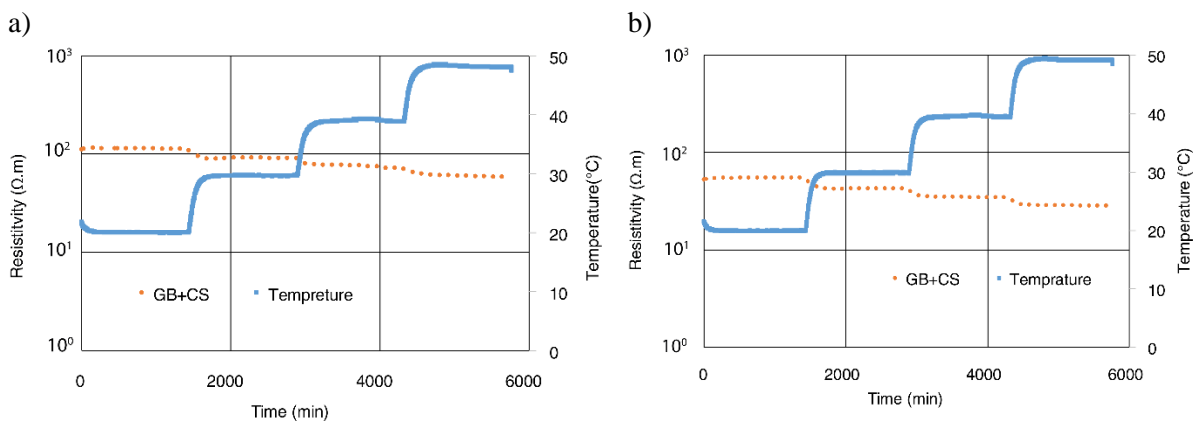


Fig. 56. Evolution of resistivity with time after imbibition for a) GB+CS and b) GB+CT at 1.46 Hz

After imbibition as shown in Fig. 56, increase in temperature caused decrease in resistivity due to replacing of water inside the pores (See Fig. 54a) for both cells (GB+CS and GB+CT).

5 The effects of saturation on geophysical parameters

5.1 General introduction

As explained in the introduction, geophysical methods are now usually used in environmental studies. In the last decade, some studies have shown for instance the variation of induced polarization response of porous media with saturation (Schmutz et al., 2010).

We carried out systematic experiments to simulate drainage and imbibition in saturated porous media, in the 1D cells (see chapter 3). Different couples of liquids (i.e. coal tar (CT)/water and canola oil (CO)/salty ethanol (SE)) were used in a porous medium made of glass beads (GBs) (silica beads, 1 mm in diameter). The final goal of laboratory measurements in this thesis is finding correlation between hydraulic and geophysical parameters in a contaminated site polluted by DNAPLs especially coal tar. The first couple of fluids, coal tar/water was chosen to simulate field condition in an under remediation polluted site in France. There is no field geophysical interest in using the fluids couple of canola oil and salty ethanol, but we wanted to carry out another series of experiments with a fluid, not too complex like coal tar but with similar hydraulic and geophysical properties. The other reason for choosing canola oil was to facilitate distinguishing the interface between two fluids from the front part of a 2D tank (that is made by glass) in future studies. In the 2D tank study, obtained saturations from geophysical measurements will be compared with imaging techniques.

The variation of the electrical complex resistivity and the dielectric relative permittivity respectively were measured by spectral induced polarization (SIP) and time domain reflectometry (TDR). The evolution with saturation of these geophysical responses were studied during drainage and imbibition process.

The analysis of the evolution of the Cole–Cole parameters of the SIP spectra in function of the saturation will be presented.

In the following, the preliminary draft of a paper that has been planned to be submitted in the journal of geophysical prospecting will be presented. In this work, we tried to find the relationship between saturation state and the amplitude and phase shift of the SIP spectra, in order to have a calibration relationship for the further uses in the 2D tank and even thereafter in the field studies.

This page has been intentionally left blank

Complex electrical resistivity and dielectric permittivity responses to study DNAPL imbibition and drainage in porous media: a laboratory study

Mohammad Ali Iravani^{1,2}, Jacques Deparis¹, Hossein Davarzani¹, Stefan Colombano¹, Roger Guérin², Alexis Maineult²

1) BRGM, French Geological Survey, 45060 Orléans, France

2) Sorbonne Université, CNRS, EPHE, UMR 7619 METIS, 75005 Paris, France

5.2 Abstract

Effective techniques for remediation of sites polluted with dense non-aqueous phase liquids (DNAPLs) remains a challenge. Among the various technical monitoring methods, there is a increasing interest in studying the geophysical characteristics of contaminated soils, as indicators of the progress in clean-up programs. This work sought to investigate the variation of the electrical complex resistivity and the relative permittivity by analyzing the results obtained from spectral induced polarization (SIP) and time domain reflectometry (TDR) measurements to validate clean-up process on sites polluted by DNAPLs. Indeed, there were only limited previous studies investigating these geophysical properties with saturation in soils contaminated with DNAPLs. Therefore, a methodology based on laboratory work was designed and carried out to study the electrical complex resistivity (both in magnitude and phase) in the frequency range 0.183 Hz to 20 kHz, and the relative dielectric permittivity (but only thereal part) at 70 MHz. The experiments were done on small 1D cells. In these cells, glass beads were used as porous medium. Two different fluid couples, i.e. Coal Tar (CT)/water and Canola Oil (CO)/Salty Ethanol (SE), were used to produce two-phase flow.

The set of experiments examined the impact of saturation change on the complex resistivity. Our findings evidenced that due to high resistivity of CO and CT, increase in water saturation led to decrease in amplitude and phase. Saturation change of SE had the same effect on resistivity but no relationship was found for phase and saturation for the mixture CO+SE. It is also showed that the complex resistivity and relative permittivity measurements were compatible with Generalized Archie's law and complex refractive index method (CRIM) model as two empirical laws for defining correlation between the electrical resistivity, relative permittivity and saturation of each phase in multiphase porous medium. Moreover, we also discussed the variation of the Cole-Cole parameters as a function of saturation. Finally, we demonstrated that SIP and TDR are promising techniques for the monitoring and tracking of the progress in remediation process.

Key words: complex resistivity, dielectric properties, hydrogeophysics, induced polarization, pollution

5.3 Introduction

The delineation and remediation of sites polluted with Dense Non-Aqueous Phase Liquids (DNAPLs) are generally believed to be one of the most challenging concerns for the environmental science and engineering communities. DNAPLs are the largest source of soil pollutions in the world (Pankow and Cherry, 1996). While it is primarily the responsibility of polluting industries or governments to clean up polluted sites, it is also up to environmental researchers to come up with practical and effective remediation measures. As a part of the remediation indications, various geophysical methods can be used to detect DNAPLs and monitor the effectiveness of remedial actions (Romig, 2000).

. Optimal usage of geophysical tools and technology based on the economic considerations is a key point for all practical works. To follow field remediation by geophysics, the behavior of geophysical parameters should be understood, and therefore empirical laws known to transform geophysical parameters to saturation will be used to obtain the saturation field concerning to magnitude of each parameter. Compared to field works, laboratory measurements have more precision, but the accuracy of these measurements should be validated in the field study. In the field, saturation of the coal tar in the contaminated soil was decreased by DNAPL recovery with the method of pump and treat. Validating the clean-up process is the main responsibility of the geophysics in remediation programs. Quantifying of spatial characteristics of physical properties (e.g electrical resistivity and relative permittivity) of the polluted soil needs precise measurements in both laboratory and field. In this study, suitability of one electro-geophysical methods, spectral induced polarization (SIP), for evaluating the resolution and the accuracy of resistivity data and time domain reflectometry (TDR) for obtaining relative permittivity and their potentials for cleanup monitoring were investigated.

SIP and time domain induced polarization (TDIP) might have enough resolution and precision to be suitable for DNAPL detection and validating depollution processes in contaminated soils, but it needs to be proven by further electro-geophysical studies in laboratory and field. Recently, induced polarization (IP) method was used to investigate the geophysical characteristics of soils (e.g., Revil et al., 2015; Slater et al., 2014; Attwa and Gunther, 2013; Weller et al., 2010). Many laboratory studies discussed effects of saturation changes on IP responses (e.g., Schmutz et al., 2012; Breede et al., 2011; Jougnot et al., 2010; Cosenza et al., 2007; Titov et al., 2004) and dielectric relative permittivity (e.g., Carcione et al., 2003). They

found that there is a significant relationship between the saturation variation and the IP response.

Several previous studies have documented the vast potential of using geophysical methods to monitor cleanup in both field and laboratory scales (e.g., Cardarelli and Di Filippo, 2009; Hwang et al., 2008; Snieder et al., 2007; Sogade et al., 2006; Brewster and Annan, 1994). Between various geophysical approaches, electrical methods have proven their potentials to characterize subsurface changes (e.g., Binley et al., 2005). They have been used to investigate geophysical properties of soils in a wide range of environmental applications (e.g., Grimm and Olhoeft, 2004; Briggs et al., 2004), especially within shallow soils (e.g., Romig, 2000). Some previous studies focused on Light Non-Aqueous Phase Liquids (LNAPL) detection (e.g., Atekwana et al., 2000). In this study, we focus specifically on DNAPL. Spherical glass beads (GB), were used as porous medium and various conductive fluids (Canola Oil (CO)/Salty Ethanol (SE)/water (W) and CT) were used as liquid phases.

Electrical charge transport and separation in a porous medium are referred to electrical conduction and polarization, respectively. A saturated porous medium is made of two components, a solid phase (porous matrix) and pores that are filled with fluids. The electrical conductivity of the solution inside the pores generally represent the in-phase conduction of the medium. Nevertheless, interfacial conduction (in the case of high specific surface, i.e. clay) on grain surfaces can leads to polarization phenomena and out-phasing components in the conductivity (Kemna et al., 2000). Due to nonappearance of electrode polarization (Tsonos, 2019), the complex resistivity consists of two terms, described by $\rho = \rho' + i\rho''$ where $\rho'(f)$ and $\rho''(f)$ are respectively the real and imaginary parts as a function of frequency (f) and $i^2 = -1$. The magnitude $|\rho|$ and phase φ of the complex resistivity can be obtained from the following equations:

$$|\rho| = \sqrt{(\rho'^2 + \rho''^2)} \quad \text{Equation 5-1}$$

$$\varphi = \tan^{-1}\left(\frac{\rho''}{\rho'}\right) \quad \text{Equation 5-2}$$

The unit of phase and magnitude of complex resistivity is radian (is practically using milli-radian) and $\Omega.m$, respectively. The frequency of mixture phase shift is related to the grain size, the specific surface (Borner and Schon, 1991) and pore space shape. For instance, the larger the grain size, the smaller the phase shift. It means that phase lag in sandy medium is less than the lag in silty and loamy media (Kemna et al., 2000).

The relative permittivity (ϵ_r), also named dielectric constant, is a fundamental geophysical parameter that is for quantitative description of electrostatic characteristics of

particles of a medium under immersed charge (current) and resulting electric field (Archer and Wang, 1990). Relative permittivity is the ratio of substance permittivity (ϵ) and permittivity of vacuum (ϵ_0) expressed by:

$$\epsilon_r = \frac{\epsilon}{\epsilon_0} \quad \text{Equation 5-3}$$

The relative permittivity is a frequency dependent complex value, $\epsilon(f) = \epsilon'(f) + i\epsilon''(f)$ which $\epsilon'(f)$ is the real part and $\epsilon''(f)$ is the imaginary part. As it was illustrated in a previous study (Iravani et al., 2019), for two-phase fluid in a porous medium made of GB, relative permittivity is a frequency and temperature dependent parameter.

In this paper, effects of two-phase flow (DNAPL saturation change) on the complex resistivity and dielectric permittivity are studied. A series of laboratory experiments were performed to characterize various effects of saturation changes. Small 1D cells were initially filled with water or SE and GB, and were subjected to a vertical CT or CO injection to apply imbibition and drainage tests. Similarity in hydraulic and geophysical properties of CO with CT encourage us to carry out another experiment with CO in parallel. Before starting experiments, water was used as the reference liquid to evaluate the electrodes which measured the electrical potential. In fact, originally, the experiments were performed using CT and water. Due to specific physical and chemical characteristics of CT, it was decided to use a less complex fluid compare to CT with hydraulic and geophysical characteristics close to this DNAPL to perform another set of experiments. CO, which has hydraulic and electrical properties similar to CT, might have been the best option but it is lighter than water. The challenge was finding a fluid lighter than CO but with similar characteristics to water. The optimum option was ethanol which is considered a non-conductor fluid with null electrical conductivity (Rocha and Simões-Moreira, 2005), but similar to water. As long as there is no ions in a fluid, the current cannot pass through it. Consequently, ethanol requires adding some other chemicals electrical conductor like salt (NaCl) to increase its electrical conductivity. We then applied mixing laws to explain the observed responses.

5.4 Experimental setups

The laboratory program was designed and carried out in line with methods and procedures defined in previous studies by Colombano et al. (2017) and Iravani et al. (2019) in order to be able to monitor effects of saturation changes on the electrical complex resistivity and the relative permittivity. In order to achieve this, two cylindrical cells, designed at BRGM and manufactured by Scodip in France, were used (Figure 51). Both cells have an internal diameter of 5.8 cm and they are 5.56 cm long, respectively.

Cells were manufactured using a thermoplastic non-reactive polymer called PVDF to prevent potential reaction between strong resistant liquids like CT and the test setup (Schweitzer 2004). In addition, PVDF is a nontoxic material with no impact on liquid or solid phases of the sample. PVDF also has a high temperature refractory (-40 to 120°C). Low air and gas permeability and high electrical isolation and dielectric constant of PVDF made this polymer suitable to be used in the setup (Schweitzer, 2004).

The cells were filled with a non-consolidated, highly permeable porous medium with 40% porosity, namely 1 mm diameter coarse-grained glass beads. There were some reasoning behind application of GB instead of soil samples. The first reason is taking advantage of transparency of GB to better monitor and report CT and CO levels in the samples to calculate water/SE and CT/CO saturations. The use of GB also prevents occurrence of unexpected phenomena such as adsorption during the experiment. The relative permittivity of a GB pack is 5.9 (Orlando and Palladini, 2019). The complex resistivity of the medium was measured with SIP method using SIP-lab IV manufactured by Radic research in Germany. The resistivity was measured in a broad frequency range (0.183 Hz to 20 kHz) with incremental coefficient of 2, according to SIP-lab IV apparatus properties that was proposed by manufacturing company. The relative permittivity was measured with TDRs probes (model 5TE (METER Group)) with dimensions of 10 cm×3.2 cm (with 2.5 cm space between the first and the third branch). TDRs were connected to a Campbell CR-1000 data logger. For these probes, the measurement frequency is 70 MHz, this frequency has been chosen in order to reduce salinity and textural effects of medium compare to low frequencies (Kizito et al., 2008). For the SE solution, taking into account the solubility of salt in ethanol at 25°C, 0.65 g of salt were mixed with 1 kg of ethanol (Burgess, 1978). The resulting conductivity was 0.0251 S/m at 20°C which is less than conductivity of tap water (0.0345 S/m) at the same temperature but sufficient to be used in the experiments. Liquids (CT+water and CO+SE) saturations were supposed to be variable parameters in our experiments.

Each cell and column was equipped with a small tap at the bottom to slightly introduce water/SE to samples by a peristaltic pump (Watson Marlow 530U). Degassed tap water, prepared in an ultrasound tank (VWR Ultrasonic Cleaner - USC500D), was used in this experiment. Degassed water was used to prevent air bubbles forming in samples. There were two holes at the top and the bottom of the main sample for introducing and draining fluids (water/SE and CT/CO). The sample was connected to two graded reservoirs with internal diameter of 3.5 cm and height of 36 cm. Two PVDF filters were used at the top and the bottom of each sample to keep GB (porous media) inside cells/columns. In Fig. 33, the right and the left

reservoirs are for water/SE and CT/CO, respectively. Both reservoirs were connected to samples using two flexible plastic tubes. The water/SE reservoir placed at the top of the sample and it is fixed while CT/CO reservoir can move vertically.

AC current was injected using two ring metallic electrodes A and B (, made of nickel-cobalt alloy (MP35N)), exactly at the top and the bottom of the sample. Voltage response of the medium was measured using non-polarizable potential electrodes, which were inserted in a row with spacing of 1.85 cm in pre-drilled holes. These hand-made Cu/CuSO₄ potential electrodes (after Mainault et al., 2004) were made of 72.75% of milli-Q water (ultrapure water), 26% of CuSO₄ and 1.25% of Gelatin. A heating shaker was used to mix the solution at 80°C for approximately an hour. Wenner-alpha array was chosen with distance of AB=MN=AM=AN=1.85 cm.

Before starting the experiments, in order to examine the stability of the copper sulfate electrodes, resistivity of tap water was measured and compared with conductivity data obtained from a conductivity meter model pH/Cond 340i (WTW Measurement System Inc.). These measurements were used to compute geometric factors for samples in order to obtain the resistivity from the measured impedance of the medium. Two potential electrodes were used to measure the response.

Samples were drained and imbibed by gradually raising or lowering the DNAPL (or CO) reservoir, at the rate of 2 cm per 3 hours to prevent air trapping in the medium in two series of drainage-imbibition cycles. Two cycles of experiments in a given cell was usually performed in two weeks. There were two cells, one for CT+water and the other for CO+SE. Experiments were performed in an oven at a temperature of 20°C. The dielectric relative permittivity and the electrical complex resistivity were recorded at a rate of one measurement every 30 s and 2 hours, respectively. After balancing the level of CT/CO in the left reservoir with the water/SE level in the reservoir at the top of the sample to reach equilibrium and to prevent CT/CO from entering the bottom of the sample, experiments were started. Volume and height of CT/CO and water/SE added to the system should be documented precisely. Each time before changing CT/CO reservoir level (2 cm), the water/SE and CT/CO levels were carefully monitored to calculate the drained or injected volume. The volume and the porosity of the samples were determined before starting the experiments. Therefore, the saturation could be determined simply by measuring the volume changes. Drainage was finished when the CT/CO was observed in water/SE reservoir and imbibition was finished when CT/CO was observed in the linking tube between sample and CT/CO reservoir.

This laboratory setup was designed to assess the effects of saturation changes in saturated multiphase media. The high reliability of three saturation points are very important to obtain for each cycle:

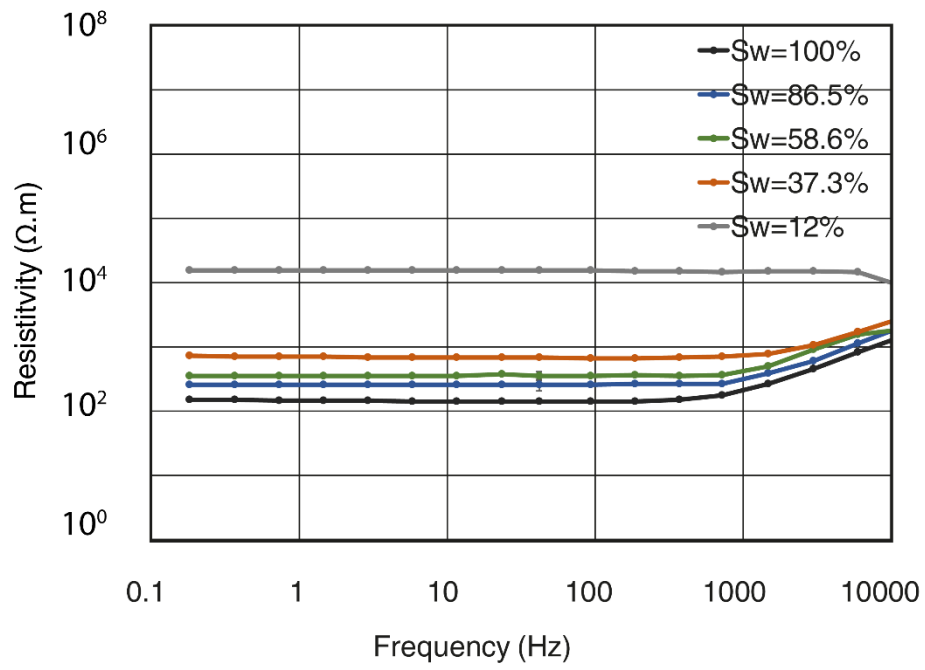
- The starting point of the experiment, i.e. when the first cycle of drainage and imbibition is going to start. At this point water/SE saturation is 100%;
- Irreducible saturation (wetting phase) which is the stage after finishing drainage and resistivity and relative permittivity of porous media have become stable at their maximum and minimum values, respectively; and
- Residual saturation (non-wetting phase) after imbibition and replacement of CT/CO with water in a multiphase porous media, the capillary forces, which act in the opposite direction from buoyancy, and viscous forces might result in some entrapment of fluids with porous media. The residual saturation is the remaining volume of fluid, which could not be discharged from samples. In other words, at residual saturation point, water/SE saturation would be less than 100%.

5.5 Results

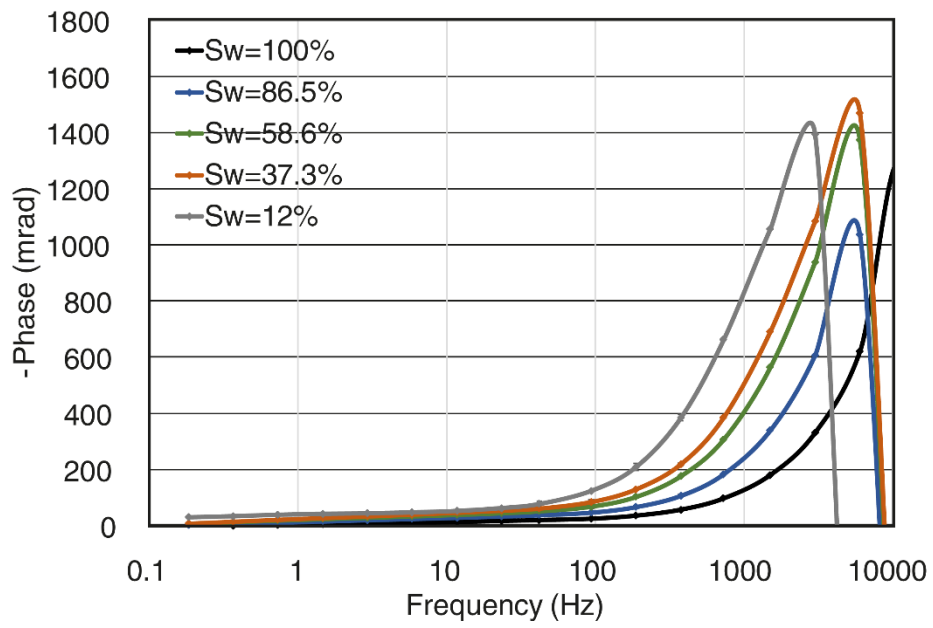
5.5.1 Effect of saturation on the complex resistivity

The electrical complex resistivity was measured in a wide range of frequencies (0.183 Hz to 20 kHz) but due to electromagnetic coupling, measurements at frequencies larger than 10 kHz are not considered. The results are shown in Fig. 57. As mentioned in the experimental setup description, two cycles of drainage and imbibition were performed. The variations of the phase during the second drainage-imbibition cycles varied widely for both cells and are difficult to interpret. Consequently, we chose to show only the first cycles. As expected, an increase in water or SE saturation led to a decrease in amplitude of the resistivity. This occurred because CT and CO are significantly more resistive compared to water and SE. Resistivity at frequencies between 0.183 to 1000 Hz was almost constant and at higher frequency (more than 187.5 Hz) increasing. On the other hand, for CO and SE, the amplitude of the resistivity decreased at higher frequencies (more than 5.859 Hz). For CT and water, the variation of the phase spectrum at low frequencies was less compared to higher frequencies. In addition, the bell shape part of the phase spectrum was shifted to higher frequencies. The evolution of the amplitude and phase variations are in agreement with the behaviors reported by Mainault et al. (2017) from numerical simulation of drainage and imbibition in pore networks.

a



b



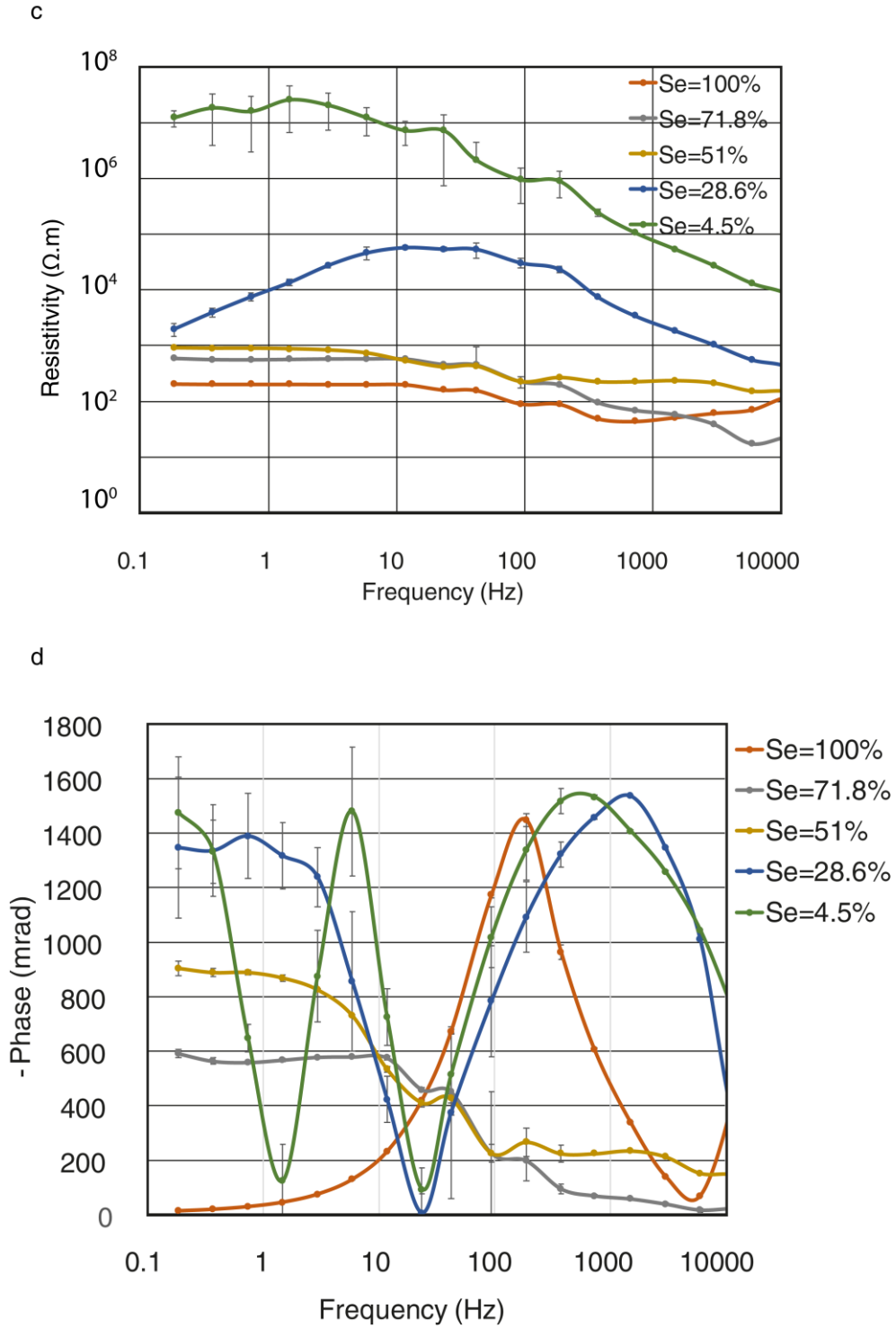


Fig. 57. SIP response of resistivity and phase spectra of samples with (a and b) CT+water and (c and d) CO+SE as a function of saturation change, for the first cycle of drainage and imbibition.

There was no systematic relationship between the measurement errors and the frequency, but the measurement errors for the phase were larger for the CO+SE case compared to CT+water one. For the measurement with SE saturation (S_e) equal to 4.5%, error bars were larger compared to other measurements, because of the decreasing volume of conductive SE in the cell. All resistivity measurements in frequency domain of CO+SE are selected from the first

drainage of SE except for $S_e=28.6\%$ that came from the first imbibition stage. This might clarify the different trend of variation in this saturation compared to the other measurements. Time series for the amplitude of the resistivity and the phase at the frequency of 1.46 Hz are shown in Fig. 58. Note that the phase in the second cycle of CT+water experiment is negative, but we have no explanations. The time series of spectra in the other cell of CT+water are presented in the annex 2.

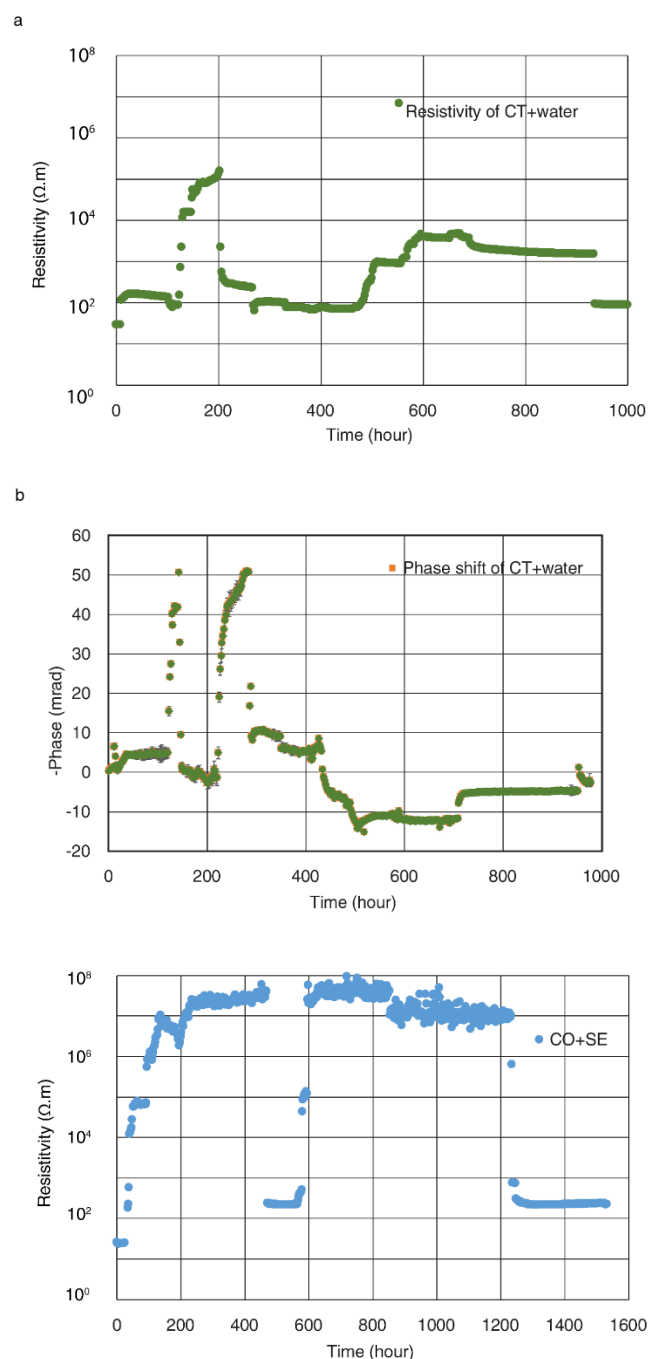


Fig. 58. Time series of SIP responses of cells with a and b) for resistivity and phase of CT+water and c) resistivity of CO+SE at $f=1.46$ Hz

5.5.2 Effect of saturation on relative permittivity

The variation of the relative permittivity with water and SE saturation are shown in Fig. 59a and Fig. 59b, respectively. The variation of the relative permittivity was measured for five different saturation stage. The results showed that water and SE saturation triggers a decrease in the relative permittivity in both cases. According to our last study (Iravani et al., 2019), at higher water saturation, due to higher relative permittivity of water compared to CT, increase in relative permittivity was expected. Results during imbibition supports the idea that increasing in water/SE saturation increase measured relative permittivity.

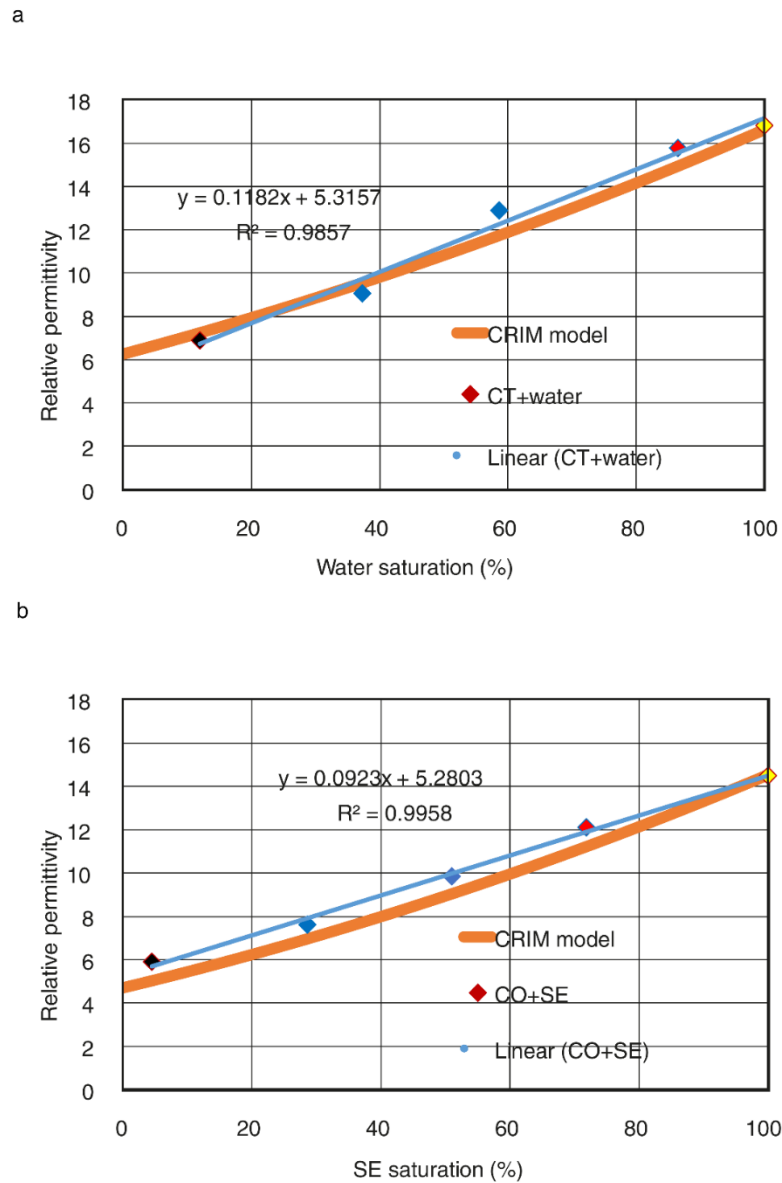


Fig. 59. Correlation curves of relative permittivity and (a) water saturation and (b) SE saturation fitted by CRIM model.

Yellow point: beginning of experiment (beginning of the first drainage), red point: residual saturation and black point: irreducible saturation

5.6 Discussions

5.6.1 Empirical models for the amplitude of the resistivity

Since the electrical conductivity σ ($\rho=1/\sigma$) depends on the geometry and topology of the porous medium, many studies (Glover, 2010; Glover et al., 2000; Schilling et al., 1997; Guéguen and Palciauskas, 1994; Luo et al., 1994; Somerton, 1992; Bussian, 1983; Korvin, 1982; Hashin and Shtrikman, 1962; Archie, 1942; Lichtenecker and Rother, 1936) were carried out to investigate the relationship between the bulk electric conductivity of the medium and fluid saturation. Some models are working with a maximum of two conductive phases (e.g., Schilling et al., 1997; Waff, 1974; Hashin and Shtrikman, 1962) while some have the option of applying multiple phases (e.g., Parallel model used by Guéguen and Palciauskas, 1994; Luo, et al., 1994; Somerton, 1992). The very classical and often used Archie's law was defined for only one phase. Some proposed models are with (e.g., Generalized Archie's law and Bussian equation) and some without (e.g., Random model by Guéguen and Palciauskas, 1994) variable exponents. For instance, m_i in generalized Archie's law is the variable exponent that we found it for each phase by least mean square (LMS) method.

In the last decade, Generalized Archie's law was used in many studies (e.g., Glover, 2010; Tiab and Donaldson, 2004; Mendelson and Cohen, 1982; Sen et al., 1981) to investigate the relationship between the bulk conductivity of the porous medium, its porosity and the conductivity of the liquids in pores.

The most investigated simple model to study relationship between the bulk conductivity, its porosity and fluid conductivity, when the porous media is nonconductive (Glover 2010), is the classical Archie's law (Archie, 1942):

$$\sigma = \sigma_{fluid} \Phi^m \quad \text{Equation 5-4}$$

where, σ_{fluid} (S/m) is the conductivity of the liquid inside the pores, Φ (-) is the porosity and m is the cementation exponent. One of the advantages of Archie's law compared to many mixing models is that it has a variable component (m_i) that make this model applicable in many cases. A more recent model, called Generalized Archie's law was a derivative of traditional Archie's law (e.g., Glover, 2010). The Generalized Archie's law for n phases is given by

$$\sigma = \sum_{i=1}^n \sigma_i \Phi_i^{m_i} \quad \text{Equation 5-5}$$

where

$$m_j = \frac{\log(1 - \sum \Phi_i^{m_i})}{\log(1 - \sum \Phi_i)} \quad i \neq j \quad \text{Equation 5-6}$$

In this equation the summation of all fractions should equal to one (for n phases, $\sum_{i=1}^n \Phi_i = 1$).

In a saturated porous media $\Phi_1 + \Phi_2 + \dots + \Phi_{(n-1)} = \Phi^*$ that Φ^* is the porosity and $\Phi_{(\text{soild phase})} = 1 - \Phi^*$. In interpretation of saturation exponents of Generalized Archie's law, water/fluids contents should be used instead of water/fluids saturations. For instance if the fluid is water, the relationship between water content (θ_w) and water saturation (S_w) is $\theta_w = S_w \times \Phi$.

The Generalized Archie's law (Equation 5-5) for our experimental setups can be expanded as :

$$\sigma_{mixed} = \sigma_{fluid1} \theta_{fluid1}^{m_1} + \sigma_{fluid2} (\Phi - \theta_{fluid1})^{m_2} + \sigma_{GB} (1 - \Phi)^{m_3} \quad \text{Equation 5-7}$$

The conductivity values of water, SE, CT and CO are 0.0345, 0.251, 10^{-9} (reported by Iravani et al. 2019) and 10^{-11} , respectively. Electrical conductivity of GB was determined between 10^{-11} to 10^{-15} by Griffiths (1999) and we chose 10^{-14} . Due to the low conductivity of CT and GB, the second and third parts of the Equation 5-7 are almost negligible. Coefficients m_1 , m_2 and m_3 were calculated by the least squares method. As mentioned before, the porosity is 40%, therefore, the solid fraction will be 60%. According to these characteristics, Generalized Archie's law equations for both cells are:

$$\text{CT+water: } \sigma_{mixed} = 0.0345 \theta_w^{1.3} + 10^{-9} (0.4 - \theta_w)^{1.64} + 10^{-14} (0.6)^{2.34} \quad \text{Equation 5-8}$$

$$\text{CO+SE: } \sigma_{mixed} = 0.0251 \theta_e^{2.01} + 10^{-11} (0.4 - \theta_e)^{0.36} + 10^{-14} (0.6)^{1.23} \quad \text{Equation 5-9}$$

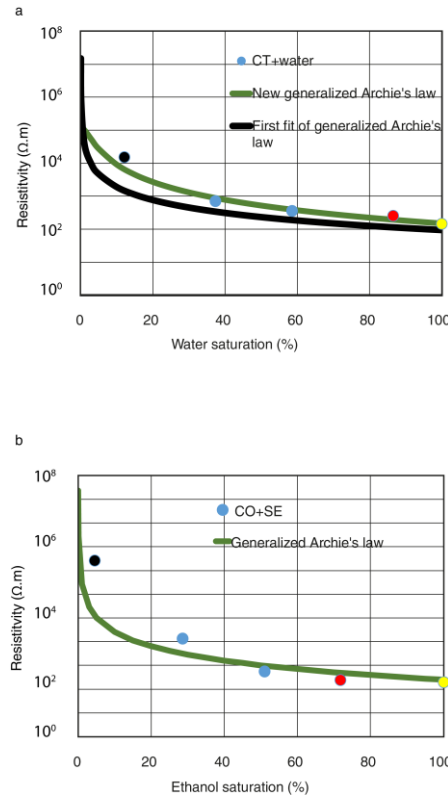


Fig. 60. Correlation curves of resistivity and (a) water saturation and (b) SE saturation fitted by generalized Archie's law.

Yellow point: beginning of experiment (beginning of the first drainage), red point: residual saturation and black point: irreducible saturation

According to our results, at the frequency of 1.46 Hz (see Fig. 60a,b), Generalized Archie's law fits rather well to experimental data of resistivity in both cells (CT+water with $R^2=0.9845$ and CO+SE with $R^2=0.9996$). After analyzing data, we found that the CT that we used for this study has almost 10-15% of water inside. It became obvious when we left the bottle of pure CT for a month and surprisingly found that a layer of water appeared at the top of the bottle. The other clue was that the measured resistivity of the medium saturated with 100% CT was less compare to true resistivity of CT and GB. With assuming conductivity of CT equals 10^{-3} , better fitting (with $R^2=0.9945$) of experimental data was obtained and new equation of generalized Archie's law for CT+water is:

$$\text{CT+water: } \sigma_{mixed} = 0.0345\theta_w^{1.8} + 10^{-3}(0.4 - \theta_w)^{5.2} + 10^{-14}(0.6)^{2.34}$$

As shown in Fig. 57, the evolution of phase is regular for CT+water compared to the cell of CO+SE which the variation of phase is quite chaotic. This phenomenon can be attributed to the extremely high resistivity of CO. In the cell of CT+water, the “-phase” increased after injecting CT.

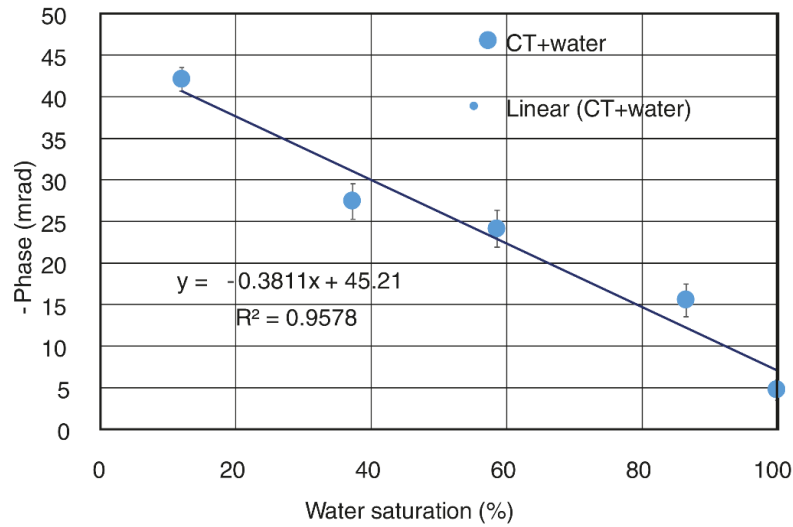


Fig. 61. Correlation curve of phase and water saturation with linear fitting at 1.46 Hz

In Fig. 61 for CT+water, a linear fitting equation was suggested for experimental data of -phase at frequency 1.46 Hz:

$$-Phase (mrad) = -0.4049 S_w + 46.124 \quad \text{Equation 5-10}$$

This linear equation give us a good fitting with coefficient of determination of $R^2=0.97$. The phase variation for different saturations of CO and SE did not investigated in this work due to irregularities of its behavior. For instance in Fig. 57, the phase variation as a function of SE saturation at 1.46 Hz is oscillating and for each saturation, the trend of variation is different. when Se=100% and there is no CO inside the medium, the curve has a trend of variation like any conductive fluids like water with minimum error and the peak point at 187.5 Hz. In this

figure, the maximum measurement error recorded at the minimum SE saturation ($S_e=4.5\%$) is what we expected, more CO saturation, more measurement error.

5.6.2 Empirical models of relative permittivity

. Some previous works focused on the mutual effects of fluid saturation and dielectric properties of a mixture (e.g., Carcione et al., 2003) for a saturated soil with NAPL and Santamarina and Fam (1997) for a contaminated soil with organic contaminations like benzene, xylene, toluene, tetrachloroethylene, trichloroethylene, and chlorobenzene). Endres and Knight (1991) investigated at the pore-scale, the influence of fluids distribution on the relative permittivity on a semi-saturated medium with a simple mixing model. Endres and Redman (1993) have also presented a mixing model for a contaminated soil. They found that geometry and choice of the wetting phase could strongly affect the fluid distribution and its relation to the dielectric properties of the medium. The Complex Refractive Index (CRI) technique as a volumetric mixing law is also used to interpret dielectric characteristics of a medium (Birchak et al., 1974). Persson and Berndtsson (2002) used a method to investigate the relation between dielectric constant of a medium partially saturated with sunflower seed oil. They carried out their measurement with TDR that their method can use for a saturated and partially saturated sandy porous medium. They validated a simple model similar to complex refractive index method (CRIM) model. Lack of consensus among the scientific communities in this subject led us to perform this study

CRIM as a simple and common mixing model in dielectric study of multiphase systems (e.g., Endres and Knight, 1992; Rodriguez and Abreu, 1990; Roth et al., 1990 and Wharton et al., 1980) is one of the mixing models that does not have any geometry dependency. CRIM is a simplified form of Lichtnecker-Rother model (Mavko et al., 2009; Guéguen and Palciauskas, 1994) in which uses simple one layer at ray limits and complex composites (Ajo-Franklin et al., 2004). The general CRIM equation is given by (Birchak et al., 1974; Roth et al., 1990; Endres and Knight, 1992)

$$\varepsilon^* = [\sum_{i=1}^N v_i \varepsilon_i^\alpha]^{1/\alpha} \quad \text{Equation 5-11}$$

where ε^* is the permittivity of the mixture, ε_i is the permittivity of the i th phase, v_i is the volume of the i th phase and α is the empirical constant related to the geometry of the grains and their spatial distribution.

With the hypothesis of α equals 0.5 for a three-phase system (Ajo-Franklin et al., 2004), CRIM equation for a mixture of air, water and solid phase is defined as (Rodriguez and Abreu, 1990):

$$\sqrt{\varepsilon^*} = S_w \Phi \sqrt{\varepsilon_w^*} + (1 - S_w) \Phi \sqrt{\varepsilon_a} + (1 - \Phi) \sqrt{\varepsilon_g} \quad \text{Equation 5-12}$$

where ε^* , ε_w^* , ε_a and ε_g are respectively relative permittivity of saturated porous media, water, air and solid phase, S_w is the water saturation and Φ is the porosity.

Equation 5-12 is a general form of CRIM model for a multiphase porous media with two liquids. This equation for experimental setups of this study can be described by

$$\varepsilon^* = (\theta_w \sqrt{\varepsilon_w^*} + \theta_{DNAPL} \sqrt{\varepsilon_{DNAPL}} + (1 - \Phi) \sqrt{\varepsilon_{GB}})^2 \quad \text{Equation 5-13}$$

where ε_{DNAPL} is relative permittivity of DNAPL, ε_{GB} is relative permittivity of GB, θ_w and θ_{DNAPL} are water and DNAPL contents, respectively. Fig. 59a,b show the evolution of relative permittivity as a function of water saturation. CRIM model has a good fit with experimental data in both cases but for CO+SE an underestimation of CRIM model with the same slope as experimental setup is observed. In contradictory with a previous study (Iravani et al., 2019), experimental data of relative permittivity did not normalized for this study. The relative permittivity of water, SE and CO were measured in the laboratory (with the error less than $\pm 1\%$) and relative permittivity of GB proposed by Louge and Opie (1990) were used to obtain CRIM equations for each setups.

$$\text{CT+water: } \varepsilon_{mixed} = (\Phi_{water} \sqrt{42.7} + \Phi_{CT} \sqrt{6.73} + (1 - 0.4) \sqrt{5.95})^2 \quad \text{Equation 5-14}$$

$$\text{CO+SE: } \varepsilon_{mixed} = (\Phi_{SE} \sqrt{34.5} + \Phi_{CO} \sqrt{3.1} + (1 - 0.4) \sqrt{5.95})^2 \quad \text{Equation 5-15}$$

Fig. 59 shows that drainage in both saturated porous media causes a decrease in the relative permittivity because of the decreasing water/SE saturation that is due to greater magnitude of relative permittivity of water/SE compare to CT/CO. During imbibition, because of replacing CO and CT in the porous media, the relative permittivity of samples were increased.

5.6.3 Effects of saturation on Cole-Cole parameters

The model defined by Pelton et al. (1978) for the complex resistivity is extensively used to investigate SIP response of a medium. The Pelton model is described by

$$\rho(\omega) = \rho_0 \left[1 - m \left(1 - \frac{1}{1 + (i\omega\tau)^c} \right) \right] \quad \text{Equation 5-16}$$

where ρ_0 ($\Omega.m$) is the DC resistivity of the medium, m (in V/V) is the chargeability, τ (s) is the time constant, and c (dimensionless) is the frequency dependence Cole-Cole exponent. The variation of c and m should be between 0 and 1 in all cases. These parameters made this model an adaptable local resistivity model for different laboratory and field experimental setups. A Matlab code, written by Mainault et al. (2017) was used to find the evolution of these four parameters as a function of saturation in the samples of CT+water.

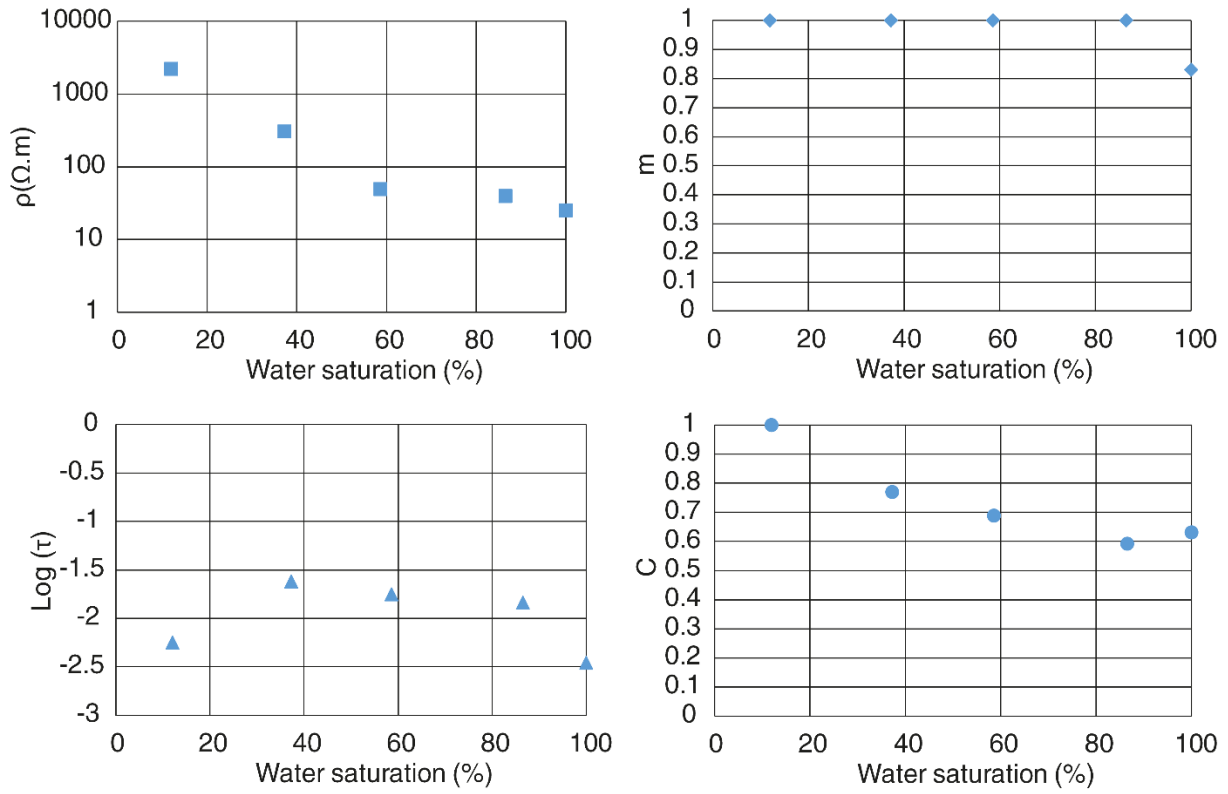


Fig. 62. Evolution of Cole-Cole parameters as a function of water saturation for CT+water

As presented in Fig. 62, water saturation decreasing led to increase in ρ_0 , c and $\log \tau$ with an exception of $\log \tau$ at saturation 13%. m is also increased because of increase in CT saturation but it becomes constant, equal to one, after $S_w=79.6\%$. Decreasing ρ_0 with water saturation is due to higher resistivity of CT compared to water. Increasing in water saturation decreased c and $\log \tau$ because higher water saturation decreases the degree of frequency dependency of ρ_0 , and time constant of the relaxation process. Recently, Mainault et al. (2017) have produced a relationship between the Cole-Cole parameters and the saturation of 2D numerical pore networks. In an unsaturated medium, air as an insulator acts very similar to CT as a DNAPL. There are similarities between the results expressed for evolution of c and ρ_0 in this study and those described by Mainault et al. (2017) but the findings of the current study for m and $\log \tau$ have different trend of variation. Method of Least Square Error (LSE) was used to obtain the magnitude of Cole-Cole parameters for each experiment. As described in session 4.1 unlike CT+water, in cell of CO+SE due to chaotic behavior of phase, the LSE method could not propose us these four parameters with the proper fitting to resistivity and phase figures.

5.6.4 About the second cycle

Laboratory measurements of the complex resistivity showed that the first cycle of drainage and imbibition follow the empirical laws. Evolution of phase in the first cycle was

disordered compared to the second cycle. Since the curves of the capillary pressure and saturation for each drainage and imbibition for both cycles, are different and our experimental data show different curves for each cycle due to hysteresis phenomena, it may justify these inappropriate data for second cycle. The other hypothesis can be due to mistake in calculation of saturation after the first imbibition. After the first cycle of drainage and imbibition, the only sign for us to stop the imbibition was observing water/SE in the tube connected to the bottom of cell. For all experiments, we considered the volume in the tube but maybe mixing of fluids in this tube or human errors to report this volume can be a reason for this mismatching. We believe that precision and accuracy of our measurement is directly related to the existence of water (as a conductive fluid) in the porous media. Not all DNAPL can be removed from porous media after first imbibition; therefore, it can be the reason for the messy geophysical data in the second cycle.

In the first cycle, phase did not show a well-defined variation trend for experiment with CO+SE, but a linear correlation was observed for phase variation in the cell of CT+water. For CT+water, phase and water saturation had an inverse relationship demonstrating that decrease in water saturation led to increase in phase. At higher frequency, the peak part of phase spectra moved to lower frequency due to increase in CT saturation.

5.7 Conclusion

The variation of the complex resistivity and dielectric permittivity in two series of experiments in a glass bead pack saturated with coal tar+water and canola oil+salty ethanol were studied. Results showed that SIP method and TDRs are practical methods and tools to measure the electrical complex resistivity and relative permittivity of a saturated porous media contaminated with CO and CT. The evolution of the magnitude of the complex resistivity with saturation obeys the generalized Archie law. Observations showed that resistivity increased as water/SE saturations decreased.

Increasing in water and SE saturations caused an increase in the relative permittivity that confirms the direct relationship between water/SE saturation and the relative permittivity of a multiphase porous medium. According to these findings, the relative permittivity decreases and increases during drainage and imbibition in a cycle, respectively. Like what we find for the resistivity, the relative permittivity also obeys the CRIM model. The effects of chemical interaction between contaminants and soil grains is not negligible that with using glass beads extrapolation of the results to actual sites remains as an issue.

The correlations between saturation and permittivity and electrical complex resistivity could serve as calibration relationship to interpret measurements in the field scale.

Acknowledgments

This study was performed in the framework of the BIOXYVAL project. The authors would like to thank ADEME for funding part of the project under the “Investissements d'Avenir” program, BRGM, “Hegmatan-Mahar Ab” the Iranian consulting engineers, for providing the PhD thesis scholarship of Mohammad Ali Iravani, and the valuable experimental assistance from Nicolas Philippe from BRGM. Finally, we gratefully acknowledge the financial support provided to the PIVOTS project by the “Région Centre – Val de Loire” and the European Regional Development Fund.

5.8 Appendix C: Detailed figures of chapter 5

The time domain IP responses of different cells were stated in this work. In chapter 5, the time series of resistivity and phase of CT+water was reported but due to facing with the anomalies in phase spectra response of CO+SE, this figure did not show in this chapter. Fig. 63 shows the variation of phase in time domain for the cell of CO+SE. There is no logical trend of variation in this figure. We believe that this disordered data in time and frequency series is because of very high resistivity of CO. Two red cycles in Fig. 63 is the phase spectra responses at the beginning of the first and second drainage in this cell. After injecting CO to the porous media saturated by SE, the phase shift has an immediate change from 0 to the phase between 2000 to 2500 mrad, but after injecting more CO most probably when CO touch the first non-polarizable electrode this phase anomaly in recording phase shift have been started. Future studies with different oils and comparing the results with current data can be interesting.

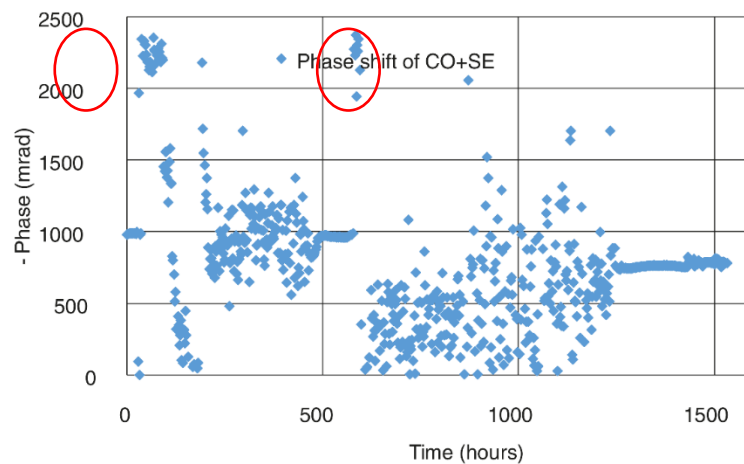


Fig. 63. Time series of phase shift in CO+SE cell

In chapter 5, we carried out the experiments in three different cells with the same dimensions and physical characteristics. Two of them filled with GB, CT and water and one of them with CO and SE. The results concerning one cell with CT+water and the only cell with CO+SE were presented in chapter 5. The second cell of CT+water does not have proper results compared to the other one. As shown in Fig. 64, for the first cycle of drainage and imbibition, the trend of variation of resistivity is logical (increasing during drainage and an inverse change during imbibition), but phase spectra is negative in the first cycle and it is decreasing after starting the second drainage. Phase became close to zero when we should normally have the maximum phase shift. From the beginning of the first cycle, we found a leakage in this cell and we tried to save the experiment but the obtained spectra is not proper for interpreting. It is worth mentioning the highest resistivity in this cell is almost 10 times less than the other cell both saturated with CO and SE.

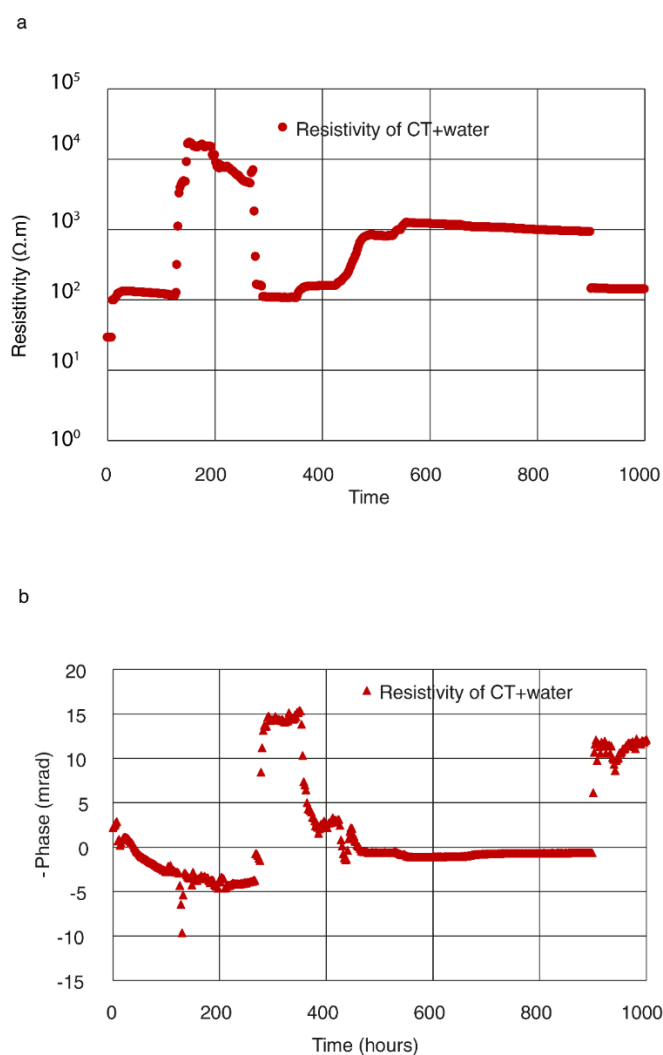


Fig. 64. Time series of SIP response in the second cell of CT+water. a) resistivity and b) phase shift

This page has been intentionally left blank

6 General conclusions and perspective

6.1 Conclusions

The main goal of this thesis was moving one-step closer to execute usage of electro-geophysical methods to monitor the remediation process in the soils contaminated by DNAPLs. In particular, applications of SIP and TDR methods in contaminated porous media were examined experimentally in the laboratory.

The effects of temperature increase on multiple geophysical parameters like complex resistivity and relative permittivity of two types of DNAPL (coal tar and chlorinated solvent) were studied. The experiments were performed for pure DNAPLs and DNAPLs with porous media (DNAPL phase full saturated, after drainage and after imbibition).

We found that whether a solid phase was present or absent in the experiment, results showed that as temperature increased, the real component of the relative permittivity of water and DNAPLs linearly decreased and increased, respectively. Adding solid phase (porous media matrix) to pure products increased and decreased the relative permittivity of DNAPLs and water, respectively. The effect of temperature change on the behavior of relative permittivity of both DNAPLs with porous media was the same as for pure DNAPLs. However, after imbibition (8% DNAPL and 92% water), unlike coal tar, the relative permittivity of chlorinated solvent samples did not conform to the relative permittivity of pure chlorinated solvent.

Temperature increasing decreased both the amplitude and phase shift component of the electrical resistivity of water and both DNAPLs tested in the presence or absence of the solid phase. Our experimental data of electrical complex resistivity and relative permittivity conformed to the empirical models.

How Cole-Cole parameters change as a function of temperature were also discussed in this study. The laboratory spectra showed temperature increases decreased resistivity on the frequency domain for coal tar in the presence or absence of the solid phase. It was found that the difference in resistivity was more significant for low frequencies than for higher frequencies. Laboratory phase spectra of both coal tar with and without solid phase (glass beads) showed that increasing temperature shifted the bell curve of the spectrum to higher frequency.

Soil heating reduces the viscosity of the pollutants, which increase pumping rate of contamination in saturated soil. The study of geophysical parameters during this operation is influenced by two environmental parameters: temperature due to soil heating and saturation change due to contamination pumping. In the first step, the geophysical parameters will be

corrected according to temperature effects. The next step will be finding the relationship between these geophysical parameters and saturation. The obtained correlation curves will be used in the future laboratory studies on a 2D tank (a small model of actual field conditions). Then saturation field in 2D tank will be estimated according to the electro-geophysical measurements and correlation obtained in this study.

Therefore, the next part of this study was an experimental work of electro-geophysical properties in water+DNAPL and a in a simpler fluid couple, salty ethanol+oil multiphase saturated porous media under drainage and imbibition. We attempted to study the effects of saturation changes on electro-geophysical parameters during two cycles of drainage and imbibition with fixed temperature (20°C).

Increasing in water and salty ethanol saturations caused an increase in relative permittivity that confirms the direct relationship between water/salty ethanol saturation and relative permittivity of a multiphase porous medium. According to these findings, relative permittivity linearly decreases and increases during drainage and imbibition in a cycle due to high relative permittivity of water compared to DNAPL, respectively. Relative permittivity conform the CRIM model as a known empirical model to study relationship between saturation and relative permittivity in a multiphase system porous media.

The variation of the complex resistivity and relative permittivity in two series of experiments in a glass bead packed column saturated with coal tar+water and canola oil+salty ethanol was studied. Observations showed that resistivity increased as water/salty ethanol saturations decreased. The evolution of the magnitude of complex resistivity with saturation obeys the generalized Archie law.

Laboratory measurements of complex resistivity showed that first cycle of drainage and imbibition had better results especially for phase, compared to the second cycle. Since the curves of capillary pressure and saturation for each drainage and imbibition for both cycles, are different and our experimental data show different curves for each cycle due to hysteresis phenomena, it can justify these inappropriate data for second cycle. We believe that precision and accuracy of our measurement is directly related to the existence of water (as a conductive fluid) in the porous media. Not all DNAPL can removed from porous media after first imbibition; therefore, it can be the reason for the messy geophysical data in the second cycle.

In the first cycle, phase did not show a well-defined variation trend for experiment with canola oil+salty ethanol, but a linear correlation was observed for phase variation in the cell of coal tar+water. For coal tar+water, phase and water saturation had an inverse relationship

demonstrating that decrease in water saturation led to increase in phase. At higher frequency, the peak part of phase spectra moved to lower frequency due to increase in coal tar saturation.

While the results are encouraging, there may not be a universal usage of them on TDR and SIP responses of different soil types with different characteristics but they could be applicable only to the type of materials studied with same physical characteristic.

It is concluded that SIP and TDR can be successfully applied to follow up variations in electrical resistivity and relative permittivity during the long-term monitoring of soil remediation processes. The glass bead diameter was purposefully selected to simulate the same physical characteristics in laboratory setups and our targeted fieldwork (e.g., same porosity in the lab ($38\% \pm 2\%$) and the field (36% to 42%)). We tried to create similar conditions in the laboratory compared to the field (e.g. same porosity and fluids); therefore, results that was approved with empirical models may be extended to field work. Our findings enhance knowledge on auxiliary remediation techniques (e.g., enhanced thermal DNAPL recovery techniques), which accelerates clean up processes (pump and treat) for sites polluted by DNAPLs.

We believe that these results might be applied to sandy soils and permeable sandstones with close porosity and resistivity but we cannot claim that these findings would be suited to other soils with different texture because the electrical resistivity of soils is related to their composition and corresponding physical indexes like the plasticity index, coarse fraction and more.

Using glass bead instead of soil samples from the project site had some advantages. First, using transparency of glass bead helps to better monitor and report the levels of liquids in the samples to calculate saturations. The use of glass bead also prevents occurrence of unexpected phenomena such as adsorption during the experiment. In the field, the body of porous media are soils with lower resistivity and higher relative permittivity compared to glass bead.

6.2 Perspective

- We recommend extending the measurements and using obtained correlation curves in the future laboratory studies on a 2D tank (a small model of actual field conditions). Saturation field in 2D tank will be determined according to the electro-geophysical measurements. The next part of experiments in the laboratory was carried out in a 2D tank and analyzing data will be the first outlook of this study. The main objective of the experiment on 2D tank will be the validation of the mixing model and calibration curves

obtained from cells and columns using a 2D two-phase flow experimental setup and comparing the results with what we observe from imaging technique. The 2D tank has dimensions of $30 \times 50 \times 7$ cm (height, width, depth). A schematic form of the front, back and top of the tank shows in Fig. 65. There are 12 TDRs and 14 thermocouples to record the relative permittivity of medium in a square network of 5×3 cm² (See Fig. 65). 47 SIP measurements including, 20 Dipole-Dipole and 27 equatorial Dipole-Dipole arrays were performed to find complex electrical resistivity field in the 2D tank. The 2D tank was filled with glass beads, bottom half saturated with DNAPL and top half with water.

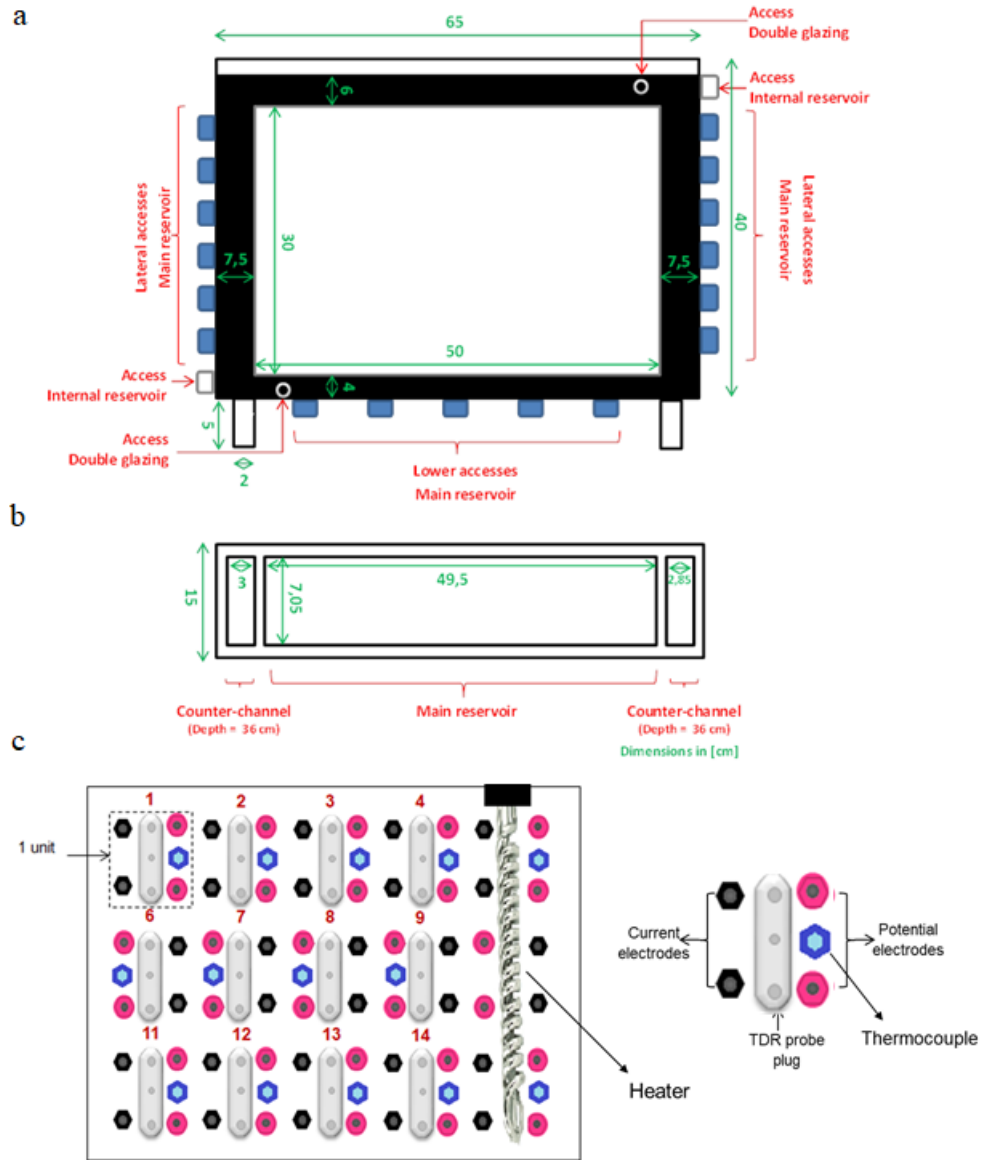


Fig. 65. Schematic of the (a) front, (b) top and (c) back of the 2D tank with the description of each element

In first series of experiments on cells and columns, measurement were performed in four different temperatures (20°C, 30°C, 40°C and 50°C), thereafter, temperature effects on

electro-geophysical parameters were also examined in three different thermal conditions on 2D tank:

1. Isothermal at 20°C
2. Isothermal at 35°C
3. Non-isothermal

Two isothermal experiments were done at 20 and 35°C. Hot water with at a given temperature circulates around the 2D tank to keep the temperature constant in all 2D tank parts. With these temperature conditions, the effect of temperature can be evaluated but in the field, there is no steady state of temperature. Therefore, performing an experiment in non-isothermal condition close to field condition is necessary. Pumping of DNAPL in a non-isothermal condition can simulate real condition in field to study temperature and saturation variations in an experiment in the same time.

In non-isothermal condition, a heater heats from left side of the tank to the right side. Heat loss subsequently happens across the 2D tank. In non-isothermal condition, there is a possibility of studying these parameters based on variation of temperature in different halves of tank and variation of saturation during pumping of DNAPL from bottom middle of the tank. Effect of temperature on electro-geophysical parameters were examined in cells and columns with one and three TDRs, and one and six SIP measurements. Using 2D tank with 15 TDRs, and 47 SIP measurements can yield results that are more accurate.

- Additional research on geophysical characteristics of other DNAPLs to expand the application of this study. Different DNAPL types tend to occur in a separate non-aqueous phase in the subsurface. Their subsurface migration and physical behavior are governed by the physics of multiphase flow in porous or fractured media. Besides chlorinated solvents and coal tar, targeted studies on the other common DNAPLs such as creosote, infiltrated heavy petroleum, polychlorinated biphenyls (PCBs) and pesticides and compare it with presented results can be expanded our understanding in this subject.
- The other important source of contamination in subsurface is light hydrocarbons (LNAPL). Future studies can present a scenario involving LNAPL imbibition and drainage. An experimental setup with modeling describing relationships between relative permittivity and complex electrical resistivity with saturation, and temperature in a three-phase fluid systems consisting of air, LNAPL like oil, and water is proposed to expand this study (LNAPLs in small pores can also be like films on water surfaces).

Evolution of relative permittivity and complex electrical resistivity when LNAPL is pumping will be interesting. LNAPL saturation that remains in the vadose zone after

pumping LNAPL and replacing air (residual LNAPL) can be estimated from electro-geophysical measurements. Then, using geophysical measurements with calculated saturation, coupling with outcome of a multiphase model can be an asset. The main challenge will be distinguishing between LNAPL and air saturation in three phase pumping zone. In fact, the resistivity of air and pure LNAPL are close to each other. However, the phase can be sensitive to air and LNAPL saturation. Stepwise approach in a precisely designed experimental setup is needed for more accurate predictions of field-scale LNAPL behavior.

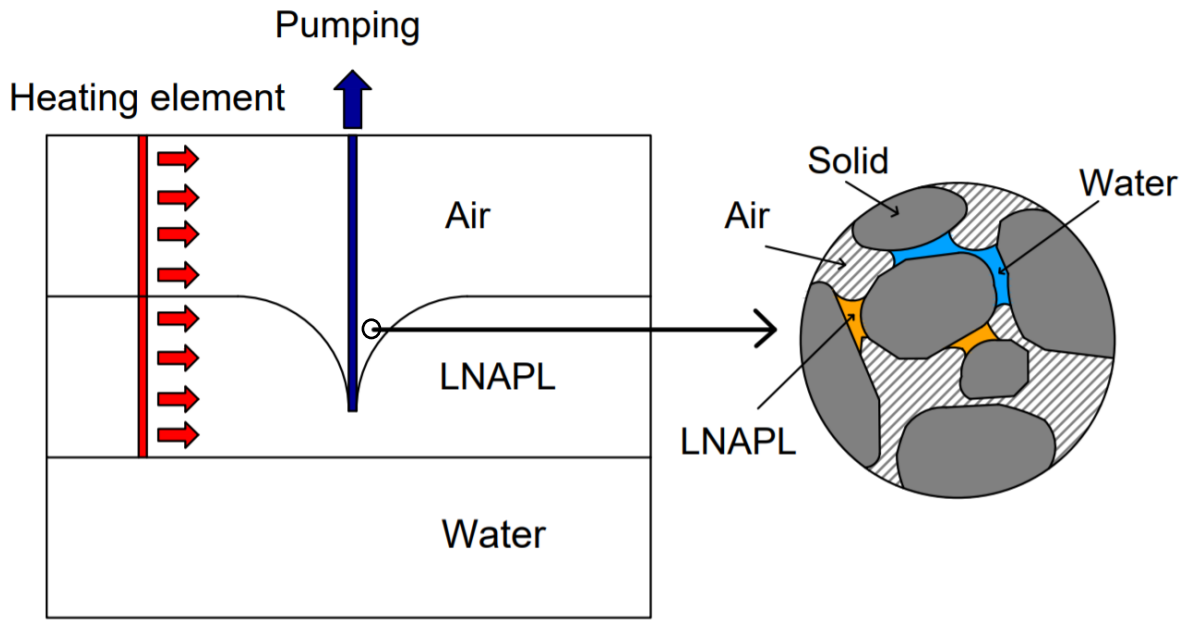


Fig. 66. Schematic of a typical three-phase flow (air, LNAPL and water) during pumping LNAPL in field studies.

- Relative permittivity and electrical resistivity are independently measured but according to the relationship between dielectric constant and conductivity, we can obtain electrical resistivity (inverse of conductivity) from measured relative permittivity from below equation

$$\sigma = \omega \epsilon_0 \epsilon' \tan \delta \quad \text{Equation 6-1}$$

Where ω is the angular frequency and $\epsilon_0 = 8.85 \times 10^{-12}$ and $\tan \delta = \epsilon'' / \epsilon'$. It will give us frequency dependent conductivity (inverse of resistivity) from relative permittivity but if we want to correlate conductivity and dielectric constant, the loss factor (ϵ'') is needed that cannot obtain from our TDR sensor. In the future works, using different type of TDR with ability of measuring loss factor and comparing results obtained from SIP and from Equation 6-1 will be interesting.

- The 5TE type TDR is working in a constant frequency of 70 MHz and as mentioned before this TDR measures real part of relative complex permittivity. Studying the imaginary part of the relative permittivity in depollution programs can be an interesting perspective of this study. It is worth noting that the imaginary component of the relative permittivity, which includes high and low frequency contributions, can be estimated from other kind of TDRs. Maybe we can make a new TDR that works with different frequencies. Frequency domain measurements of the impacts depollution on real and imaginary components of the relative permittivity in remediation programs would be definitely valuable.
- Capacitance sensors such as 5TE are increasingly used for relative permittivity estimation in field. However, their reliability and limitations in soils are demonstrated in different studies but as TDR has a limited zone of influence, we propose to use them after detecting polluted regions in subsurface. After determining the DNAPL source zone, monitoring wells will be installed and TDRs would be used inside them to precisely follow up the soil properties during clean-up process.
- We modeled the real part of the complex resistivity by BERT and COMSOL and the results were remarkable. As far as we dealt with complex resistivity, the results of modeling of amplitude did not present in this study. Modeling of the imaginary part of the complex resistivity could also be fascinating.
- Modelling of the coupled hydraulic and geophysical parameters will be an exciting work for future studies. The simultaneous flow of two phases (DNAPL+water) through a porous medium has different hydraulic (e.g. saturation) and geophysical (e.g. electrical resistivity) characteristic that can be calculated by different tools. For instance, the influence of saturation on the complex electrical resistivity can be modeled by COMSOL Multiphase, a finite element simulator, or other modeling tools and be compared to experimental results. Multiphase Modeling of hydraulic and geophysical parameters can develop discussion and criticizing of the experimental data.
- SIP is the extension of IP method for higher frequency. The usual frequency range for AC current applied during SIP measurements are less than 20 kHz. The need to expand this frequency range in SIP studies is recommended. Working in higher frequency can minimize some salinity and textural effects to obtain data that are more accurate.
- Canola oil is too resistive; using other oils with lower electrical resistivity coupled with salty ethanol can show better results especially for imaginary part of the complex resistivity.

- Performing same experiments with soil sampled from polluted site and comparing new results with current study can clarify effect of using glass bead in this study.
- The main goal of most laboratory studies carried out under controlled condition will be approval of obtained results in the field. While field researches offer contextual data on settings, interactions, controlled laboratory measurements is repeatable with efficient type of studies that can be applied across a variety of disciplines. Validating our results in the electro-geophysical field studies can advance reliability of them on different environmental conditions. Using electrical DC and EM methods (e.g. ground-penetrating radar) can be also effective in monitoring oils and inorganic pollutants due to their high resistivity.

7 References

- Abdel-Shafy, H.I. and Mansour, M.S., 2016. A review on polycyclic aromatic hydrocarbons: source, environmental impact, effect on human health and remediation. *Egyptian Journal of Petroleum*, 25(1), 107-123.
- Abdulsamad, F., Florsch, N., Schmutz, M. and Camerlynck, C., 2016. Assessing the high frequency behavior of non-polarizable electrodes for spectral induced polarization measurements. *Journal of Applied Geophysics*, 135, 449-455.
- Abu-Hassanein, Z.S., Benson, C.H. and Blotz, L.R., 1996. Electrical resistivity of compacted clays. *Journal of geotechnical engineering*, 122(5), 397-406.
- Adamsom, A.W. and Gast, A.P., 1997. *Physical Chemistry of surfaces*, 6th edition, Wiley, New York.
- ADEME, Ernst B.R. and Young C., 2014. Taux d'utilisation et coûts des différentes techniques et filières de traitement des sols et des eaux souterraines polluées en France – Synthèse des données 2012. ADEME (Agence de l'Environnement et de la Maîtrise de l'Energie, Agence de l'Environnement et de la Maîtrise de l'Energie), 148 pages.
- Ajo-Franklin, J. B., Geller, J. T. and Harris, J. M., 2006. A survey of the geophysical properties of chlorinated dnaps. *Journal of Applied Geophysics*, 59(3), 177–189.
- Ajo-Franklin, J.B., Geller, J.T. and Harris, J.M., 2004. The dielectric properties of granular media saturated with DNAPL/water mixtures. *Geophysical Research Letters*, 31(17).
- Amente, G., Baker, J. M. and Reece, C. F., 2000. Estimation of soil solution electrical conductivity from bulk soil electrical conductivity in sandy soils. *Soil Science Society of America Journal*, 64(6), 1931–1939.
- Anderson, W., 1986. Wettability literature survey-part 2: Wettability measurement. *Journal of petroleum technology*, 38(11), 1-246.
- Archer, D.G. and Wang, P., 1990. The dielectric constant of water and Debye-Hückel limiting law slopes. *Journal of physical and chemical reference data*, 19(2), 371-411.
- Archie, G.E., 1942. The electrical resistivity log as an aid in determining some reservoir characteristics. *Transactions of the AIME*, 146(1), 54-62.
- Arps, J., 1953. The effect of temperature on the density and electrical resistivity of sodium chloride solutions. *Journal of Petroleum Technology*, 5(10), 17–20.
- ARTELIA, 2013. Diagnostic environnemental - ancienne cokerie de moyeuivre-grande, Technical Report report n° 8510074, Arcelormittal real estate France, 122 p.

- Atekwana, E. A., Sauck, W. A. and Werkema Jr, D. D., 2000. Investigations of geoelectrical signatures at a hydrocarbon contaminated site. *Journal of Applied Geophysics*, 44(2-3), 167–180.
- Atekwana, E.A. and Slater, L.D., 2009. Biogeophysics: A new frontier in Earth science research. *Reviews of Geophysics*, 47(4), RG4004.
- Attwa, M. and Günther, T., 2013. Spectral induced polarization measurements for predicting the hydraulic conductivity in sandy aquifers. *Hydrology and Earth System Sciences*, 17(10), 4079-4094.
- Baba, K., 2005. Electrical structure in marine tectonic settings. *Surveys in Geophysics*, 26(6), 701-731.
- Bagotsky, V.S. ed., 2005. *Fundamentals of electrochemistry*(Vol. 44). John Wiley & Sons.
- Bai, W., Kong, L. and Guo, A., 2013. Effects of physical properties on electrical conductivity of compacted lateritic soil. *Journal of Rock Mechanics and Geotechnical Engineering*, 5(5), 406–411.
- Bear, J., 1972. *Dynamics of fluids in porous media*. Dover, New York. *Dynamics of fluids in porous media*. Dover, New York.
- Beck, A.E., 1981. *Physical principles of exploration methods*. Macmillan International Higher Education.
- Beekmans, N.M. and Heyne, L., 1976. Correlation between impedance, microstructure and compositions of calcia-stabilised zirconia. *Electrochimica Acta*, 21, 303–310.
- Benson, A.K., Payne, K.L. and Stubben, M.A., 1997. Mapping groundwater contamination using dc resistivity and VLF geophysical methods—A case study. *Geophysics*, 62(1), 80-86.
- Bernabé, Y. and Maineult, A., 2015. Physics of porous media: fluid flow through porous media, in: *Resources in the Near-Surface Earth* (Ed. L. Slater), *Treatise on Geophysics*, 2nd Edition (Ed. G. Schubert), 11, Elsevier, 19-41
- Binley, A. and Kemna, A., 2005. DC resistivity and induced polarization methods. subchapter of *Hydrogeophysics* by Rubin and Hubbard, 129-156.
- Binley, A., Kruschwitz, S., Lesmes, D. and Kettridge, N., 2010. Exploiting the temperature effects on low frequency electrical spectra of sandstone: A comparison of effective diffusion path lengths. *Geophysics*, 75(6), A43–A46.
- Binley, A., Slater, L.D., Fukes, M. and Cassiani, G., 2005. Relationship between spectral induced polarization and hydraulic properties of saturated and unsaturated sandstone. *Water resources research*, 41(12), W12417.

- Birchak, J.R., Gardner, C.G., Hipp, J.E. and Victor, J.M., 1974. High dielectric constant microwave probes for sensing soil moisture. *Proceedings of the IEEE*, 62(1), 93-98.
- Bleil, D.F., 1953. Induced polarization: A method of geophysical prospecting. *Geophysics*, 18(3), 636-661.
- Blondel, A., Schmutz, M., Franceschi, M., Tichané, F. and Carles, M., 2014. Temporal evolution of the geoelectrical response on a hydrocarbon contaminated site. *Journal of Applied Geophysics*, 103, 161-171.
- Börner, F., Gruhne, M. and Schön, J., 1993. Contamination indications derived from electrical properties in the low frequency range 1. *Geophysical Prospecting*, 41(1), 83-98.
- Borner, F.D. and Schon, J.H., 1991. A relation between the quadrature component of electrical conductivity and the specific surface area of sedimentary rocks. *The Log Analyst*, 32(05).
- Breede, K. and Kemna, A., 2012. Spectral induced polarization measurements on variably saturated sand-clay mixtures. *Near Surface Geophysics*, 10(6), 479-489.
- Breede, K., Kemna, A., Esser, O., Zimmermann, E., Vereecken, H. and Huisman, J.A., 2011. Joint measurement setup for determining spectral induced polarization and soil hydraulic properties. *Vadose Zone Journal*, 10(2), 716-726.
- Brewster, M. L. and Annan, A. P., 1994. Ground-penetrating radar monitoring of a controlled DNAPL release: 200 MHz radar. *Geophysics*, 59(8), 1211–1221.
- Briggs, V., Sogade, J., Minsley, B. J., Lambert, M., Reppert, P., Coles, D., Rossabi, J., Riha, B., Shi, W. and Morgan, F. D., 2004. Mapping of TCE and PCE contaminant plumes using a 3-D induced polarization borehole data. *Symposium on the Application of Geophysics to Engineering and Environmental Problems*, Environmental and Engineering Geophysical Society, 472–483.
- Burgess, J., 1978. *Metal Ions in Solution*. First ed, Ellis Horwood (England), ISBN 978-0-85312-027-8.
- Bussian, A.E., 1983. Electrical conductance in a porous medium. *Geophysics*, 48(9), 1258-1268.
- Campbell, R., Bower, C. and Richards, L., 1949. Change of electrical conductivity with temperature and the relation of osmotic pressure to electrical conductivity and ion concentration for soil extracts. *Soil Science Society of America Journal*, 13(C), 66–69.
- Carcione, J.M., Seriani, G. and Gei, D., 2003. Acoustic and electromagnetic properties of soils saturated with salt water and NAPL. *Journal of Applied Geophysics*, 52(4), 177-191.

- Cardarelli, E. and Di Filippo, G., 2009. Electrical resistivity and induced polarization tomography in identifying the plume of chlorinated hydrocarbons in sedimentary formation: a case study in Rho (Milan—Italy). *Waste Management & Research*, 27(6), 595-602.
- Chelidze, T., NoVaramashvili, N., Devidze, M., Tchelidze, Z., Chikhladze, V. and Matcharashvili, T., 2002. Laboratory study of electromagnetic initiation of slip. *Annals of Geophysics*, 45(5).
- Chelidze, T.L. and Gueguen, Y., 1999. Electrical spectroscopy of porous rocks: A review. Theoretical models. *Geophysical Journal International*, 137(1), 1-15.
- Chen, Y. and Or, D., 2006. Effects of Maxwell-Wagner polarization on soil complex dielectric permittivity under variable temperature and electrical conductivity. *Water Resources Research* 42(6), W06424.
- Clavier, C., Coates, G. and Dumanoir, J., 1984. Theoretical and experimental bases for the dual-water model for interpretation of shaly sands. *SPE Journal*, 24, 153–168.
- Clément, R., Descloîtres, M., Gunther, T. and Oxarango, L., 2009. Comparison of three arrays in time-lapse ERT: Simulation of a leachate injection experiment. *ArcheoSciences. Revue d'archéométrie*, 33, 275-278.
- Cohen, R.M. and Mercer, J.W., 1993. DNAPL site investigation. 1st edition, CK Smoley, Boca Raton, Florida, 339 pages.
- Cole, K., S., and Cole, H., 1941. Dispersion and absorption in dielectrics I. Alternating current characteristics. *Journal of Chemical Physics*, 9, 341-351.
- Collett, L.S., 1990. History of the induced-polarization method. In *Induced Polarization Applications and Case Histories*, Society of Exploration Geophysicists, 5-22.
- Colombano, S., 2019. Effects of thermal and chemical enhancements on the recovery efficiency of heavy chlorinated compounds in saturated porous media: experimental and multiphase flows modeling approaches, Université Paris-Est.
- Colombano, S., Davarzani, H., Van Hullebusch, E. D., Ignatiadis, I., Huguenot, D., Guyonnet, D. and Deparis, J., 2017. Drainage-imbibition tests and pumping of heavy chlorinated solvents in saturated porous media: measurements and modeling of the effects of thermal and chemical enhancement. 14th International AquaConSoil Conference-Sustainable Use and Management of Soil, Sediment and Water Resources.
- Colombano, S., Saada, A., Guerin, V., Bataillard, P., Bellenfant, G., Beranger, S., Hube, D., Blanc, C., Zornig, C. and Girardeau, I., 2010. Quelles techniques pour quels traitements—analyse coûts-bénéfices. Rapport final BRGM-RP-58609-FR.

- Comegna, A., Coppola, A., Dragonetti, G. and Sommella, A., 2013. Dielectric response of a variable saturated soil contaminated by non-aqueous phase liquids (NAPLs). *Procedia Environmental Sciences*, 19, 701-710.
- Conrad, S.H., Glass, R.J. and Peplinski, W.J., 2002. Bench-scale visualization of DNAPL remediation processes in analog heterogeneous aquifers: surfactant floods and in situ oxidation using permanganate. *Journal of Contaminant Hydrology*, 58(1-2), 13-49.
- Cosenza, P., Ghorbani, A., Florsch, N. and Revil, A., 2007. Effects of drying on the low-frequency electrical properties of Tournemire argillites. *Pure and Applied Geophysics*, 164(10), 2043-2066.
- Coster, H., 1948. The electrical conductivity of rocks at high temperatures. *Geophysical Journal International* 5, 193–199.
- Dakhnov, V. N., 1962. Geophysical well logging: The application of geophysical methods; electrical well logging. Colorado School of Mines.
- Davidson, D.W. and Cole, R.H., 1951. Dielectric relaxation in glycerol, propylene glycol, and n-propanol. *The Journal of Chemical Physics*, 19(12), 1484-1490.
- Debye, P., 1929. *Polar Molecules*. Chemical Catalog Company, New York.
- Denicol, P.S. and Jing, X.D., 1998. Effects of water salinity, saturation and clay content on the complex resistivity of sandstone samples. Geological Society, London, Special Publications, 136(1), 147-157.
- Di Maio, R. and Patella, D., 1991. Basic theory of electrokinetic effects associated with earthquakes. *Bollettino di Geofisica Teorica ed Applicata*, 33(130–131), 145–154.
- Dias, C., A., 2000. Developments in a model to describe low-frequency electrical polarization of rocks, *Geophysics*, 65(2), 437-451.
- Dihui, L., Jingshan, J., Ji, W., Dehai, Z. and Xiaohui, Z., 2005. Experimental research and statistical analysis on the dielectric properties of lunar soil simulators. *Chinese Science Bulletin*, 50(10), 1034-1044.
- Dissado, L.A. and Hill, R.M., 1984. Anomalous low-frequency dispersion. Near direct current conductivity in disordered low-dimensional materials. *Journal of the Chemical Society, Faraday Transactions 2 (Molecular and Chemical Physics)*, 80(3), 291-319.
- Dullien, F.A., 2012. *Porous media: fluid transport and pore structure*. Academic press.
- Edmondson, T.A., 1965. Effect of temperature on waterflooding. *Journal of Canadian Petroleum Technology*, 4(04), 236-242.

- Endres, A.L. and Knight, R., 1991. The effects of pore-scale fluid distribution on the physical properties of partially saturated tight sandstones. *Journal of Applied Physics*, 69(2), 1091-1098.
- Endres, A.L. and Knight, R., 1992. A theoretical treatment of the effect of microscopic fluid distribution on the dielectric properties of partially saturated rocks 1. *Geophysical Prospecting*, 40(3), 307-324.
- Endres, A.L. and Redman, J.D., 1993, January. Modelling the electrical properties of porous rocks and soils containing immiscible contaminants. In *Symposium on the Application of Geophysics to Engineering and Environmental Problems 1993*. Society of Exploration Geophysicists, 21-38.
- Fatt, I., 1956. The network model of porous media. 1, 2 and 3, *Trans. AIME*, 144-181.
- Friedrichs, B., Matzander, U., Large, D. and Davies, M., 1999. Controlled Source Electro-Magnetic Mapping development and evaluation of its application to mineral exploration. *Transactions of the Institution of Mining and Metallurgy. Section B. Applied Earth Science*, 108.
- Gazoty, A., Fiandaca, G., Pedersen, J., Auken, E. and Christiansen, A.V., 2012. Mapping of landfills using time-domain spectral induced polarization data: the Eskelund case study. *Near Surface Geophysics*, 10(6), 575-586.
- Gerhard, J.I., Pang, T. and Kueper, B.H., 2007. Time scales of DNAPL migration in sandy aquifers examined via numerical simulation. *Groundwater*, 45(2), 147-157.
- Ghorbani, A., 2007. Contribution au développement de la résistivité complexe et à ses applications en environnement. Mémoire de thèse de doctorat. Université Pierre-et-Marie-Curie, Paris (France).
- Glover, P. W. J., 2009. What is the cementation exponent? A new interpretation. *The Leading Edge*, 28, 82–85.
- Glover, P. W. J., Hole, P. J. and Pous J., 2000. A modified Archie's law for two conducting phases. *Earth and Planetary Science Letters*, 180(3–4), 369–383.
- Glover, P.W., 2010. A generalized Archie's law for n phases. *Geophysics*, 75(6), E247-E265.
- Glover, P.W.J., 1996. Graphite and electrical conductivity in the lower continental crust: a review. *Physics and Chemistry of the Earth*, 21(4), 279-287.
- Glover, P.W., Meredith, P.G., Sammonds, P.R. and Murrell, S.A., 1994. Ionic surface electrical conductivity in sandstone. *Journal of Geophysical Research: Solid Earth*, 99(B11), 21635-21650.

- Glover, P.W.J., 2015. Geophysical properties of the near surface Earth: Electrical properties. In *Treatise on Geophysics*, Schubert, G. (Editor-in-chief). Elsevier: Oxford, Vol. 11, 89-137.
- Gourry, J., Jeannot, R. and Proust E., 2001. Coupling of geophysical measurements and gas analyzes for the detection of pollutants organic on a former coking, resreport RP-50856-FR, BRGM.
- Grellier, S., Robain, H., Bellier, G. and Skhiri, N., 2006. Influence of temperature on the electrical conductivity of leachate from municipal solid waste. *Journal of Hazardous Materials*, 137(1), 612–617.
- Griffiths, D., 1999. *Introduction to Electrodynamics* (3rd edition ed.). Upper Saddle River, New Jersey, Prentice Hall, 286.
- Grimm, R. E. and Olhoeft, G. R., 2004. Cross-hole complex resistivity survey for PCE at the SRS A-014 outfall. *Symposium on the Application of Geophysics to Engineering and Environmental Problems*, 455–464.
- Guéguen, Y. and Palciauskas, V., 1994. *Introduction to the Physics of Rocks*. Princeton University Press.
- Hallof, P. and Pelton, W., 1980. The removal of inductive coupling effects from spectral ip data, 50th Annual International Meeting of the Society of Exploration Geophysicists, 2681.
- Hashin, Z. and Shtrikman, S., 1962. A variational approach to the theory of the effective magnetic permeability of multiphase materials. *Journal of applied Physics*, 33(10), 3125-3131.
- Hayashi, M., 2004. Temperature-electrical conductivity relation of water for environmental monitoring and geophysical data inversion. *Environmental monitoring and assessment* 96(1-3), 119–128.
- Hayley, K., Bentley, L., Gharibi, M. and Nightingale, M., 2007. Low temperature dependence of electrical resistivity: Implications for near surface geophysical monitoring. *Geophysical Research Letters* 34(18), L18402.
- Heimovaara, T., Focke, A., Bouten, W. and Verstraten, J., 1995. Assessing temporal variations in soil water composition with time domain reflectometry. *Soil Science Society of America Journal*, 59(3), 689–698.
- Heimovaara, T.J., Bouten, W. and Verstraten, J.M., 1994. Frequency domain analysis of time domain reflectometry waveforms. A four-component complex dielectric mixing model for soils. *Water Resources Research*, 30(2), 201-209.

- Helba, A.A., Sahimi, M., Scriven, L.E. and Davis, H.T., 1992. Percolation theory of two-phase relative permeability. *SPE Reservoir Engineering*, 7(1), 123-132.
- Helmig, R., 1997. Multiphase flow and transport processes in the subsurface: a contribution to the modeling of hydrosystems. Springer-Verlag.
- Horton, R.J., Smith, B.D. and Washburne, J.C., 1985. Electrical geophysical investigations of massive sulfide deposits and their host rocks. West Shasta copper-zinc district. *Economic Geology*, 80(8), 2213-2229.
- Hwang, Y. K., Endres, A. L., Piggott, S. D. and Parker, B. L., 2008. Long-term ground penetrating radar monitoring of a small volume DNAPL release in a natural groundwater flow field. *Journal of Contaminant Hydrology*, 97(1-2), 1–12.
- International Agency for Research on Cancer and World Health Organization, 2013. IARC: Outdoor air pollution a leading environmental cause of cancer deaths. No. 221. World Health Organization.
- Iordache, D., Niculae, D. and Hathazi, F. I., 2010. Utilization of microwave energy for decontamination of oil polluted soils. *Journal of Microwave Power and Electromagnetic Energy*, 44(4), 213–221.
- Iravani, M. A., Deparis, J., Davarzani H., Colombano S., Guérin R. and Mainault A. 2020. The influence of temperature on the dielectric permittivity and complex electrical resistivity of porous media saturated with DNAPLs: A laboratory study, *Journal of Applied Geophysics*, 172, 103921.
- Ishido, T. and Mizutani, H., 1981. Experimental and theoretical basis of electrokinetic phenomena in rock-water systems and its applications to geophysics. *Journal of Geophysical Research: Solid Earth*, 86(B3), 1763-1775.
- Jackson, P.D., Northmore, K.J., Meldrum, P.I., Gunn, D.A., Hallam, J.R., Wambura, J., Wangusi, B. and Ogutu, G., 2002. Non-invasive moisture monitoring within an earth embankment - a precursor to failure. *Ndt & E International*, 35(2), 107-115.
- Jougnot, D., Ghorbani, A., Revil, A., Leroy, P. and Cosenza, P., 2010. Spectral induced polarization of partially saturated clay-rocks: A mechanistic approach. *Geophysical Journal International*, 180(1), 210-224.
- Kalmykov, Y. P., Coffey, W. T., Crothers, D. S. and Titov, S. V., 2004. Microscopic models for dielectric relaxation in disordered systems. *Physical Review E* 70(4), 041103.
- Kavanaugh, M.C., Suresh, P. and Rao, C., 2003. The DNAPL remediation challenge: Is there a case for source depletion?. Environmental protection agency Washington DC, EPA/600/R-03/143.

- Keller, G. V. and Frischknecht, F. C., 1966. Electrical methods in geophysical prospecting. Pergamon Press, Oxford.
- Keller, G.V., 1989. Electrical properties; in, Practical Handbook of Physical Properties of Rocks and Minerals, RS Carmichael.
- Kemna, A., Binley, A., Cassiani, G., Niederleithinger, E., Revil, A., Slater, L., Williams, K.H., Orozco, A.F., Haegel, F.H., Hoerdt, A. and Kruschwitz, S., 2012. An overview of the spectral induced polarization method for near-surface applications. *Near Surface Geophysics*, 10(6), 453-468.
- Kemna, A., Binley, A., Ramirez, A. and Daily, W., 2000. Complex resistivity tomography for environmental applications. *Chemical Engineering Journal*, 77(1-2), 11-18.
- Kessouri, P., 2012. Mesure simultanée aux fréquences moyennes et cartographie de la permittivité diélectrique et de la conductivité électrique du sol (Doctoral dissertation), Sorbonne Université (UPMC).
- Kizito, F., Campbell, C.S., Campbell, G.S., Cobos, D.R., Teare, B.L., Carter, B. and Hopmans, J.W., 2008. Frequency, electrical conductivity and temperature analysis of a low-cost capacitance soil moisture sensor. *Journal of Hydrology*, 352(3-4), 367-378.
- Korvin, G., 1982. Axiomatic characterization of the general mixture rule. *Geoexploration*, 19(4), 267-276.
- Kraszewski, A.W., 1996. Microwave Aquametry: Introduction to the workshop. *Microwave Aquametry, Electromagnetic wave interaction with water-containing materials*, 38-45.
- Kueper, B.H., Redman, D., Starr, R.C., Reitsma, S. and Mah, M., 1993. A field experiment to study the behavior of tetrachloroethylene below the water table: Spatial distribution of residual and pooled DNAPL. *Groundwater*, 31(5), 756-766.
- Lakrari, K., El Moudane, M., Hassanain, I., Ellouzi, I., Kitane, S. and El Belghiti, M. A., 2013. Study of electrical properties of vegetable oils for the purpose of an application in electrical engineering. *African Journal of Food Science*, 7(11), 404–407.
- Le Méhauté, A. and Crepy, G., 1983. Introduction to transfer and motion in fractal media: the geometry of kinetics. *Solid State Ionics*, 9, 17-30.
- Ledieu, J., De Ridder, P., De Clerck, P. and Dautrebande, S., 1986. A method of measuring soil moisture by time-domain reflectometry. *Journal of Hydrology*, 88(3-4), 319-328.
- Lenormand, R., Zarcone, C. and Sarr, A., 1983. Mechanisms of the displacement of one fluid by another in a network of capillary ducts. *Journal of Fluid Mechanics*, 135, 337-353.

- Lerner, D.N., Kueper, B.H., Wealhall, G.P., Smith, J.W.N. and Leharne, S.A., 2003. An illustrated handbook of DNAPL transport and fate in the subsurface, R&D Publication 133, Environment Agency, Almondsbury, Bristol.
- Lesmes, D. P., and Morgan, F. D., 2001. Dielectric spectroscopy of sedimentary rocks. *Journal Geophysical. Research*, 106, 13392-13346.
- Lesparre, N., Gibert, D., Nicollin, F., Nussbaum, C. and Adler, A., 2013. Monitoring the excavation damaged zone by three-dimensional reconstruction of electrical resistivity. *Geophysical Journal International*, 195(2), 972-984.
- Li, C. and Suzuki, K., 2010. Resources, properties and utilization of tar. *Resources, Conservation and Recycling*, 54(11), 905-915.
- Lichtenecker, K. and Rother, K., 1936. Die Herleitung des logarithmischen Mischungsgesetzen als allgemeinen Prinzipien der statonaren Stromung, *Physikalische Zeitschrift*, 32, 256–660.
- Lichtenecker, K., 1931. Die Herleitung des logarithmischen Mischungsgesetzes aus allgemeinen Prinzipien der stationaren Stromung. *Physikalische Zeitschrift*, 32, 255-260.
- Lide, D.R. (Ed), 2008. *Handbook of Chemistry and Physics*, 89th Ed., CRC Press, Boca Raton, NY, 6/154.
- Llera, F. J., Sato, M., Nakatsuka, K. and Yokoyama, H., 1990. Temperature dependence of the electrical resistivity of water-saturated rocks. *Geophysics* 55(5), 576–585.
- Lockner, D.A. and Byerlee, J.D., 1985. Complex resistivity measurements of confined rock. *Journal of Geophysical Research (Solid Earth)*, 90(B9), 7837-7847.
- Louge, M. and Opie, M., 1990. Measurements of the effective dielectric permittivity of suspensions. *Powder Technology*, 62(1), 85-94.
- Luo, M., Wood, J. R. and Cathles, L. M., 1994. Prediction of thermal conductivity in reservoir rocks using fabric theory. *Journal of Applied Geophysics*, 32(4), 321–334.
- Maineult, A., Bernabé, Y. and Ackerer, P., 2004. Electrical response of flow, diffusion, and advection in a laboratory sand box. *Vadose Zone Journal*, 3(4), 1180-1192.
- Maineult, A., Jougnot, D. and Revil, A., 2017. Variations of petrophysical properties and spectral induced polarization in response to drainage and imbibition: a study on a correlated random tube network. *Geophysical Journal International*, 212(2), 1398-1411.
- Maineult, A., Revil, A., Camerlynck, C., Florsch, N. and Titov, K., 2017. Upscaling of spectral induced polarization response using random tube networks. *Geophysical Journal International*, 209(2), 948-960.

- Malmberg, C. and Maryott, A., 1956. Dielectric constant of water from 0 to 100°C. *Journal of Research of the National Bureau of Standards* 56, 1–8.
- Malvankar, N.S., Lau, J., Nevin, K.P., Franks, A.E., Tuominen, M.T. and Lovley, D.R., 2012. Electrical conductivity in a mixed-species biofilm. *Applied and Environmental Microbiology*, 78(16), 5967-5971.
- Mao, D., Lu, L., Revil, A., Zuo, Y., Hinton, J. and Ren, Z.J., 2016. Geophysical monitoring of hydrocarbon-contaminated soils remediated with a bioelectrochemical system. *Environmental science & technology*, 50(15), 8205-8213.
- Marshall, D.J. and Madden, T.R., 1959. Induced polarization, a study of its causes. *Geophysics*, 24(4), 790-816.
- Martín-Alfonso, M.J., Martínez-Boza, F.J., Navarro, F.J., Fernández, M. and Gallegos, C., 2007. Pressure–temperature–viscosity relationship for heavy petroleum fractions. *Fuel*, 86(1-2), 227-233.
- Martinho, E., Almeida, F. and Matias, M.S., 2006. An experimental study of organic pollutant effects on time domain induced polarization measurements. *Journal of Applied Geophysics*, 60(1), 27-40.
- Mathews, P., and K. Zonge, L., 2003. 50 years State of the art in IP and complex resistivity, in *KEGS 50th Anniversary Symposium Mining and Environmental Geophysics - Past, Present & Future*. Toronto, Ontario.
- Mavko, G., Mukerji, T. and Dvorkin, J., 2009. *The rock physics handbook: Tools for seismic analysis of porous media*. Cambridge university press.
- Maxwell, J.C., 1891. *Conduction through heterogeneous media. A treatise on electricity and magnetism*, 1, 435-441.
- Mayer, A.S., 2005. *Soil and groundwater contamination: Nonaqueous phase liquids* (No. 17). American Geophysical Union.
- Mendelson, K.S. and Cohen, M.H., 1982. The effect of grain anisotropy on the electrical properties of sedimentary rocks. *Geophysics*, 47(2), 257-263.
- Nabighian, M.N. ed., 1991. *Electromagnetic Methods in Applied Geophysics: Volume 1, Theory*, Society of Exploration Geophysicists (USA).
- Nath, J. and Dubey, S., 1980. Binary systems of trichloroethylene with benzene, toluene, p-xylene, carbon tetrachloride, and chloroform. ultrasonic velocities and adiabatic compressibilities at 303.15 and 313.15 k, and dielectric properties and refractive indexes at 303.15 k. *The Journal of Physical Chemistry* 84(17), 2166–2170.

- Nath, J., 1995. Ultrasonic velocities, relative permittivities and refractive indices for binary liquid mixtures of trichloroethene with pyridine and quinoline. *Fluid Phase Equilibria* 109(1), 39–51.
- Nathanail, J., Bardos, P. and Nathanail, C.P., 2011. Contaminated land management: ready reference. EPP Publications.
- Naudet, V., Revil, A., Bottero, J.Y. and Bégassat, P., 2003. Relationship between self-potential (SP) signals and redox conditions in contaminated groundwater. *Geophysical research letters*, 30(21), 2091.
- Noel, C., 2014. Suivi de la biodégradation des hydrocarbures par le couplage des mesures géophysiques électriques du sol (polarisation provoquée) et des analyses des gaz (concentration du CO₂ et isotopie du carbone) (Doctoral dissertation), Université d'Orléans.
- Nordsiek, S. and Weller, A., 2008. A new approach to fitting induced-polarization spectra. *Geophysics*, 73(6), F235-F245.
- Noritomi, K., 1958. Migration of charged carrier in the case of electric conduction of rocks, *Science Reports of the Tohoku University, Ser. 5, Geophysics* 9(3), 120–127.
- Nouveau, M., Grandjean, G., Leroy, P., Philippe, M., Hedri, E. and Boukcim, H., 2016. Electrical and thermal behavior of unsaturated soils: experimental results. *Journal of Applied Geophysics*, 128, 115-122.
- Olhoeft, G.R., 1984. Clay-organic reactions measured with complex resistivity. *SEG Technical Program Expanded Abstracts, Society of Exploration Geophysicists*, 356-358.
- Olhoeft, G.R., 1985. Low-frequency electrical properties. *Geophysics*, 50(12), 2492-2503.
- Orlando, L. and Palladini, L., 2019. Time-lapse laboratory tests to monitor multiple phases of DNAPL in a porous medium. *Near Surface Geophysics*, 17(1), 55-68.
- Pankow, J.F. and Cherry, J.A., 1996. Dense chlorinated solvents and other DNAPLs in groundwater: History, behavior, and remediation.
- Pearce, J.A. and Zuluaga, A., 2004. Electrical properties of soils at ism radio frequencies, from 1 to 40 MHz. *Journal of Microwave Power and Electromagnetic Energy*, 39(3-4), 179-190.
- Pelton, W.H., Ward, S.H., Hallof, P.G., Sill, W.R. and Nelson, P.H., 1978. Mineral discrimination and removal of inductive coupling with multifrequency IP. *Geophysics*, 43(3), 588-609.
- Pelton, W.H. and Smith, P.K., 1976. Mapping porphyry copper deposits in the Philippines with IP. *Geophysics*, 41(1), 106-122.

- Persson, M. and Berndtsson, R., 2002. Measuring nonaqueous phase liquid saturation in soil using time domain reflectometry. *Water Resources Research* 38(5), 22–1-22-8.
- Petiau, G. and Dupis, A., 1980. Noise, temperature coefficient, and long time stability of electrodes for telluric observations. *Geophysical Prospecting*, 28(5), 792-804.
- Petiau, G., 2000. Second generation of lead-lead chloride electrodes for geophysical applications. *Pure and applied geophysics*, 157(3), 357-382.
- Pierson, H.O., 1993. Handbook of carbon, graphite, diamond and fullerenes. Properties, processing and applications, William Andrew Publishing/Noyes.
- Power, C., Gerhard, J.I., Karaoulis, M., Tsourlos, P. and Giannopoulos, A., 2014. Evaluating four-dimensional time-lapse electrical resistivity tomography for monitoring DNAPL source zone remediation. *Journal of contaminant hydrology*, 162, 27-46.
- Powers, S.E., Anckner, W.H. and Seacord, T.F., 1996. Wettability of NAPL-contaminated sands. *Journal of Environmental Engineering*, 122(10), 889-896.
- Purcell, E.M. and Morin, D.J., 2013. Electricity and magnetism. Cambridge University Press.
- Quist, A. S. and Marshall, W. L., 1968. Electrical conductances of aqueous sodium chloride solutions from 0 to 800° and at pressures to 4000 bars. *The Journal of Physical Chemistry* 72(2), 684–703.
- Raju, G.G. 2003. Dielectrics in electric fields. Dekker. 578p.
- Raythatha, R. and Sen, P.N., 1986. Dielectric properties of clay suspensions in MHz to GHz range. *Journal of Colloid and Interface Science*, 109(2), 301-309.
- Razafindratsima, S., Guérin, R., Bendjoudi, H. and de Marsily, G., 2014. Hydrogeological modeling constraints provided by geophysical and geochemical mapping of a chlorinated ethenes plume in northern France. *Hydrogeology journal*, 22(6), 1433-1446.
- Revil, A. and Florsch, N., 2010. Determination of permeability from spectral induced polarization in granular media. *Geophysical Journal International*, 181(3), 1480-1498.
- Revil, A., Binley, A., Mejus, L. and Kessouri, P., 2015. Predicting permeability from the characteristic relaxation time and intrinsic formation factor of complex conductivity spectra. *Water Resources Research*, 51(8), 6672-6700.
- Revil, A., Hermitte, D., Spangenberg, E. and Cochémé, J.J., 2002. Electrical properties of zeolitized volcanoclastic materials. *Journal of Geophysical Research. Solid Earth*, 107(B8), ECV-3.
- Revil, A., Schmutz, M. and Batzle, M.L., 2011. Influence of oil wettability upon spectral induced polarization of oil-bearing sands. *Geophysics*, 76(5), A31-A36.

- Rew, A., 2007. Phytoremediation: an environmentally sound technology for pollution prevention, control and remediation in developing countries. *Educational Research and Reviews*, 2(7), 151-156.
- Reynolds, J.M., 2011. An introduction to applied and environmental geophysics. John Wiley & Sons.
- Richards, L.A., 1954. Diagnosis and Improvement of Saline and Alkali Soils. United States Salinity Laboratory Staff. Agriculture Handbook No. 60, USDA and IBH Pub. Coy Ltd., New Delhi, 98-99.
- Riley, F., 1988, The Electronics Assembly Handbook, Springer, Berlin.
- Robinson, D.A., Gardner, C.M.K. and Cooper, J.D., 1999. Measurement of relative permittivity in sandy soils using TDR, capacitance and theta probes: comparison, including the effects of bulk soil electrical conductivity. *Journal of Hydrology*, 223(3-4), 198-211.
- Robinson, D.A., Jones, S.B., Wraith, J.M., Or, D. and Friedman, S.P., 2003. A review of advances in dielectric and electrical conductivity measurement in soils using time domain reflectometry. *Vadose Zone Journal*, 2(4), 444-475.
- Rocha, M.D.S. and Simões-Moreira, J.R., 2005. A simple impedance method for determining ethanol and regular gasoline mixtures mass contents. *Fuel*, 84(4), 447-452.
- Rodriguez, A. and Abreu, R., 1990, January. A mixing law to model the dielectric properties of porous media. In SPE Latin America Petroleum Engineering Conference. Society of Petroleum Engineers.
- Rojo, A., Hansen, H.K. and Monárdez, O., 2014. Electrokinetic remediation of mine tailings by applying a pulsed variable electric field. *Minerals Engineering*, 55, 52-56.
- Romig, P., 2000. Seeing Into the Earth: Noninvasive Characterization of the Shallow Subsurface for Environmental and Engineering Application, National Academies Press, Washington, D. C.
- Rosenbaum, U., Huisman, J., Vrba, J., Vereecken, H. and Boga, H., 2011. Correction of temperature and electrical conductivity effects on dielectric permittivity measurements with ech 2 o sensors. *Vadose Zone Journal* 10(2), 582–593.
- Roth, K., Schulin, R., Flühler, H. and Attinger, W., 1990. Calibration of time domain reflectometry for water content measurement using a composite dielectric approach. *Water Resources Research*, 26(10), 2267-2273.
- Ruffet, C., Gueguen, Y. and Darot, M., 1991a. Complex conductivity measurements and fractal nature of porosity. *Geophysics*, 56(6), 758-768.

- Ruffet, C., Gueguen, Y. and Darot, M., 1991b. Rock conductivity and fractal nature of porosity. *Terra Nova*, 3(3), 265-275.
- Sadowski, R.M., 1988. Clay-organic interactions. M.Sc. thesis, Colorado School of Mines.
- Santamarina, J.C. and Fam, M., 1997. Dielectric permittivity of soils mixed with organic and inorganic fluids (0.02 GHz to 1.30 GHz). *Journal of Environmental and Engineering Geophysics*, 2(1), 37-51.
- Sauck, W.A., 2000. A model for the resistivity structure of LNAPL plumes and their environs in sandy sediments. *Journal of Applied Geophysics*, 44(2-3), 151-165.
- Schilling, F.R., Partzsch, G.M., Brasse, H. and Schwarz, G., 1997. Partial melting below the magmatic arc in the central Andes deduced from geoelectromagnetic field experiments and laboratory data. *Physics of the Earth and Planetary Interiors*, 103(1-2), 17-31.
- Schmutz, M., Blondel, A. and Revil, A., 2012. Saturation dependence of the quadrature conductivity of oil-bearing sands. *Geophysical Research Letters*, 39(3), L03402.
- Schmutz, M., Revil, A., Vaudelet, P., Batzle, M., Viñao, P.F. and Werkema, D.D., 2010. Influence of oil saturation upon spectral induced polarization of oil-bearing sands. *Geophysical Journal International*, 183(1), 211-224.
- Schwartz, R.C., Casanova, J.J., Pelletier, M.G., Evett, S.R. and Baumhardt, R.L., 2013. Soil permittivity response to bulk electrical conductivity for selected soil water sensors. *Vadose Zone Journal*, 12(2), vzj2012.0133.
- Schon J.H., 2004. Fundamentals and Principles of Petrophysics. *Physical Properties of Rocks*. Elsevier (Amsterdam, Netherlands), 18, ISBN: 008044346X.
- Schweitzer, P. A., 2004. Corrosion resistance tables: metals, nonmetals, coatings, mortars, plastics, elastomers and linings, and fabrics. CRC Press.
- Scott, W. and Kay, A. E., 1988. Earth resistivities of Canadian soils, Canadian Electrical Association.
- Seigel, H., Nabighian, M., Parasnis, D.S. and Vozoff, K., 2007. The early history of the induced polarization method. *The Leading Edge*, 26(3), 312-321.
- Sen, P. N. and Goode, P. A., 1992. Influence of temperature on electrical conductivity on shaly 725 sands. *Geophysics*, 57(1), 89-96.
- Sen, P.N., Scala, C. and Cohen, M.H., 1981. A self-similar model for sedimentary rocks with application to the dielectric constant of fused glass beads. *Geophysics*, 46(5), 781-795.
- Seyfried, M. S. and Grant, L. E., 2007. Temperature effects on soil dielectric properties measured at 50 MHz. *Vadose Zone Journal*, 6(4), 759-765.

- Shah, Z. and Tahir, Q., 2011. Dielectric properties of vegetable oils. *Journal of Scientific Research* 3(3), 481–492.
- Sherrod, L., Sauck, W. and Werkema Jr, D. D., 2012. A low-cost, in situ resistivity and temperature monitoring system. *Groundwater Monitoring & Remediation* 32(2), 31–39.
- Sims, R.C., 1990. Soil remediation techniques at uncontrolled hazardous waste sites. *Journal of the Air & Waste Management Association*, 40(5), 704-732.
- Slater, L., Barrash, W., Montrey, J. and Binley, A., 2014. Electrical-hydraulic relationships observed for unconsolidated sediments in the presence of a cobble framework. *Water Resources Research*, 50(7), 5721-5742.
- Slater, L.D., Choi, J. and Wu, Y., 2005. Electrical properties of iron-sand columns: Implications for induced polarization investigation and performance monitoring of iron-wall barriers. *Geophysics*, 70(4), G87-G94.
- Sleep, B.E. and Ma, Y., 1997. Thermal variation of organic fluid properties and impact on thermal remediation feasibility. *Soil and Sediment Contamination*, 6(3), 281-306.
- Smith, B.D., Tippens, C.L., Flanigan, V.J. and Sadek, H., 1983. Preliminary results of spectral induced polarization measurements, Wadi Bidah District, Kingdom of Saudi Arabia (No. 83-612). US Geological Survey.
- Snieder, R., Hubbard, S., Haney, M., Bawden, G., Hatchell, P., Revil, A. and DOE Geophysical Monitoring Working Group, 2007. Advanced noninvasive geophysical monitoring techniques. *Annual Review of Earth and Planetary Sciences*, 35, 653-683.
- Sogade, J. A., Scira-Scappuzzo, F., Vichabian, Y., Shi, W., Rodi, W., Lesmes, D. P. and Morgan, F. D., 2006. Induced-polarization detection and mapping of contaminant plumes. *Geophysics*, 71(3), B75–B84.
- Somerton, W.H., 1992. Thermal properties and temperature-related behavior of rock/fluid systems (Vol. 37). Elsevier.
- Stegemeier, G.L. and Vinegar, H.J., 2001. Thermal conduction heating for in-situ thermal desorption of soils. *Hazardous and radioactive waste treatment technologies handbook*, 1-37.
- Stogryn, A., 1971. Equations for calculating the dielectric constant of saline water (correspondence). *IEEE Transactions on Microwave Theory and Techniques* 19(8), 733–736.
- Sumner, J.S., 1976. Principles of induced polarization for geophysical exploration. Elsevier Publishing Co.

- Susanto, A., Koleva, D.A., Copuroglu, O., van Beek, K. and van Breugel, K., 2013. Mechanical, electrical and microstructural properties of cement-based materials in conditions of stray current flow. *Journal of Advanced Concrete Technology*, 11(3), 119-134.
- Tarasov, A. and Titov, K., 2013. On the use of the Cole–Cole equations in spectral induced polarization. *Geophysical Journal International*, 195(1), 352-356.
- Tiab, D., and Donaldson, E. C., 2004. Theory and practice of measuring reservoir rock and fluid transport properties. *Petrophysics*, Gulf Publishing Company.
- Titov, K., Kemna, A., Tarasov, A. and Vereecken, H., 2004. Induced polarization of unsaturated sands determined through time domain measurements. *Vadose Zone Journal*, 3(4), 1160-1168.
- Topp, G.C., Davis, J.L. and Annan, A.P., 1980. Electromagnetic determination of soil water content: Measurements in coaxial transmission lines. *Water resources research*, 16(3), 574-582.
- Tsonos, C., 2019. Comments on frequency dependent AC conductivity in polymeric materials at low frequency regime. *Current Applied Physics*, 19(4), 491-497.
- Vacquier, V., Holmes, C.R., Kintzinger, P.R. and Lavergne, M., 1957. Prospecting for ground water by induced electrical polarization. *Geophysics*, 22(3), 660-687.
- Valenti, M., 1994. Cleaning soil without incineration. *Mechanical Engineering*, 116(5), 50.
- Van Voorhis, G.D., Nelson, P.H. and Drake, T.L., 1973. Complex resistivity spectra of porphyry copper mineralization. *Geophysics*, 38(1), 49-60.
- Vanhala, H., 1997a. Laboratory and field studies of environmental and exploration applications of the spectral induced-polarization. Geological Survey of Finland (Geologian tutkimuskeskus).
- Vanhala, H., 1997b. Mapping oil-contaminated sand and till with the spectral induced polarization (SIP) method. *Geophysical prospecting*, 45(2), 303-326.
- Vanhala, H., Soininen, H. and Kukkonen, I., 1992. Detecting organic chemical contaminants by spectral-induced polarization method in glacial till environment. *Geophysics*, 57(8), 1014-1017.
- Vaudelet, P., Schmutz, M., Pessel, M., Franceschi, M., Guerin, R., Atteia, O., Blondel, A., Ngomseu, C., Galaup, S., Réjiba, F. and Bégassat, P., 2011. Mapping of contaminant plumes with geoelectrical methods. A case study in urban context. *Journal of Applied Geophysics*, 75(4), 738-751.

- Vidonish, J.E., Zygourakis, K., Masiello, C.A., Sabadell, G. and Alvarez, P.J., 2016. Thermal treatment of hydrocarbon-impacted soils: a review of technology innovation for sustainable remediation. *Engineering*, 2(4), 426-437.
- Villaume, J.F., Lowe, P.C. and Unites, D.F., 1983. Recovery of coal gasification wastes: An innovative approach. In *Proceedings of the Third National Symposium on Aquifer Restoration and Ground-Water Monitoring*. National Water Well Association, Worthington OH (USA), 434-445.
- Vinegar, H.J. and Waxman, M.H., 1984. Induced polarization of shaly sands. *Geophysics*, 49(8), 1267-1287.
- Vogel, H.J., 2002. Topological characterization of porous media. In *Morphology of condensed matter*. Springer, Berlin, Heidelberg, 75-92.
- Vouillamoz, J.M., 2003. La caractérisation des aquifères par une méthode non invasive: les sondages par résonance magnétique protonique (Doctoral dissertation, Paris 11).
- Waff, H. S., 1974. Theoretical consideration of electrical conductivity in a partially molten mantle and implications for geothermometry. *Journal of Geophysical Research*, 79(26), 4003–4010.
- Wagner, P.A., 1924. On Magmatic nickel deposits of the Bushveld complex in the Rustenburg district, Transvaal. The Government Printing and Stationery Office, 21-27.
- Wait, J.R., 1959. A phenomenological theory of overvoltage for metallic particles. In *Overvoltage research and geophysical applications*. Pergamon, 22-28.
- Wang, J.R. and Schmugge, T.J., 1980. An empirical model for the complex dielectric permittivity of soils as a function of water content. *IEEE Transactions on Geoscience and Remote Sensing*, (4), 288-295.
- Waxman, M. M., and Smits, L. J. M., 1968. Electrical conductivity in oil-bearing shaly sand. *SPE Journal*, 8, 107–122.
- Waxman, M. H. and Thomas, E., 1974. Electrical conductivities in shaly sands-i. the relation between hydrocarbon saturation and resistivity index; ii. the temperature coefficient of electrical conductivity. *Journal of Petroleum Technology* 26(02), 213–225.
- Weast, R. C., 1986. *Handbook of physics and chemistry*. CRC Press, Boca Raton, 1983–1984.
- Weiss, J., Snyder, K., Bullard, J. and Bentz, D., 2012. Using a saturation function to interpret the electrical properties of partially saturated concrete. *Journal of Materials in Civil Engineering*, 25(8), 1097-1106.
- Weller, A. and Börner, F.D., 1996. Measurements of spectral induced polarization for environmental purposes. *Environmental Geology*, 27(4), 329-334.

- Weller, A., Nordsiek, S. and Debschütz, W., 2010. Estimating permeability of sandstone samples by nuclear magnetic resonance and spectral-induced polarization. *Geophysics*, 75(6), E215-E226.
- Wharton, R.P., Rau, R.N. and Best, D.L., 1980, January. Electromagnetic propagation logging: Advances in technique and interpretation. In *SPE Annual Technical Conference and Exhibition*. Society of Petroleum Engineers.
- Whelan, M.P., Voudrias, E.A. and Pearce, A., 1994. DNAPL pool dissolution in saturated porous media: Procedure development and preliminary results. *Journal of Contaminant Hydrology*, 15(3), 223-237.
- Whitney, M. and Briggs, L. J., 1897. An electrical method of determining the temperature of soils. *USDA Division of Soils Bulletin 7*, U.S. Government Printing Office, Washington, D.C.
- Wightman, W., Jalinoos, F., Sirles, P. and Hanna, K., 2004. Application of geophysical methods to highway related problems. Technical report No. FHWA-IF-04-021.
- Wilson, L.G., 1983. Monitoring in the vadose zone: Part III. *Groundwater Monitoring & Remediation*, 3(1), 155-166.
- Wischkaemper, H. K., Beliveau, A. F. and Henderson, R. W., 2013. USEPA Regional 4 Technical Services Issue Paper for Polychlorinated Biphenyl Characterization at Region 4 Superfund and RCRA Sites.
- Wong, P. and Horn, P.M., 1979. Magnetic phase-diagram of $(\text{Fe}_{1-x}\text{Co}_x)\text{Cl}_2$, *American Physical Society*, 24(3), 363-363.
- Wong, P.Z., 1987. Fractal surfaces in porous media. In *AIP Conference Proceedings*, 154(1), 304-317.
- Wraith, J.M. and Or, D., 1999. Temperature effects on soil bulk dielectric permittivity measured by time domain reflectometry: Experimental evidence and hypothesis development. *Water Resources Research*, 35(2), 361-369.
- Zehnder, A.J. ed., 1995. *Soil and Groundwater Pollution: Fundamentals, Risk Assessment and Legislation (Vol. 4)*. Springer Science & Business Media, ISBN 978-94-015-8587-3.
- Zhu, H., Wang, W., Wang, H., Zhao, H. and Xin, M., 2018. Study on electrical properties of coal at spontaneous combustion characteristic temperature. *Journal of Applied Geophysics* 159, 707-714.

This page has been intentionally left blank

List of Figures

Fig. 1. Organic contaminants, like petroleum fuels and solvents may be present as a free liquid, dissolved liquid (in water) and as vapor (ref: https://www.heroninstruments.com/news/dnapl-and-lnapl).	1
Fig. 2. Pollutants treated in 2012 on groundwater remediation sites located in France (ADEME, Ernest and Young, 2014)	2
Fig. 3. Schematic of a gas extraction well (Sims, 1990)	5
Fig. 4. Effect of moisture on VOC adsorption and desorption in soil —VOC adsorption with two moisture regimes (Sims, 1990)	5
Fig. 5. In situ Bioremediation System Configurations (https://semspub.epa.gov/work/11/171054.pdf)	6
Fig. 6. Thermal enhanced technique for a) shallow contamination (0-3') with thermal blankets and b) deep contamination with thermal wells (>3')	7
Fig. 7. Ex situ TD includes the excavation of contaminated soils, which are heat-treated in a desorption unit (gas flow conditions may vary). Off-gases are collected for reuse or disposal (Vidonish et al., 2016).	8
Fig. 8. In situ TD utilizes dual heater/vacuum wells to heat soils and remove contaminants. Off-gases are collected for reuse or disposal (Vidonish et al., 2016).	9
Fig. 9. In situ smoldering utilizes a self-sustaining smoldering wave to destroy hydrocarbons without excavation. The smoldering reactions are started at a central ignition well. Off-gases are collected for reuse or disposal (Vidonish et al., 2016).	9
Fig. 10. Aerial view of the polluted site	15
Fig. 11. Hydrogeological porosity. a) Representation of the saturation profile and b) Comparison of the hydrogeological porosities (Vouillamoz, 2003).	21
Fig. 12. Cross section of interface between soil particles, wetting phase and non-wetting phase (Mayer, 2005)	24
Fig. 13. Contact angle and typical fluid relationship (Cohen and Mercer, 1993)	25
Fig. 14. A generic example of capillary pressure curves (i.e., nonwetting fluid pressure plotted against wetting fluid saturation). During the first drainage, a nonwetting fluid (represented as black in the insets) is gradually injected into a porous body initially saturated with a wetting fluid (light gray). This stage is followed by imbibition–drainage cycles that all follow the same curves. The insets illustrate the pore-scale distribution of the phases at various stages during the drainage–imbibition cycles. (a) In the initial state, only the wetting fluid is present. (b) A small nonwetting fluid meniscus appears on the left side, indicating the onset of penetration by the nonwetting fluid. (c) The irreducible wetting fluid saturation is shown as a film of wetting fluid along the pore walls (implying that y is zero). (d) At the residual nonwetting fluid saturation, some amount of nonwetting fluid is trapped in the pore space. (e) A small nonwetting fluid meniscus appears on the left side, indicating the onset of penetration by the nonwetting fluid at the beginning of a new drainage cycle (Bernabé and Maineult, 2015).	27
Fig. 15. The general solution consists of linear combinations of sinusoidal components (Purcell and Morin, 2013)	29
Fig. 16. V , I , and R , the parameters of Ohm's law	29

Fig. 17. Electrical resistivity of several geomaterials (Glover, 2015).....	31
Fig. 18. Transient decay of electric field strength in a rock sample. (b) Transient decay of voltage in an RC circuit (Keller and Frischknecht, 1966).....	34
Fig. 19. Schematic form of membrane polarization (ref: https://bit.ly/2mdLFVy)	35
Fig. 20. Illustration of elements of electrode polarization (Beck, 1981).....	36
Fig. 21. The behavior of the Debye (solid blue) and Cole and Cole (dashed red) dispersion models shown as a function of frequency for each of the in-phase (upper) and out-of-phase (middle) components and as an are Argand diagram (bottom). An arbitrary value of $\alpha=0.22$ has been used for the Cole and Cole model (Glover, 2015).	47
Fig. 22. Example of configuration of an electrical device. a and b are the electrodes injection (current) and m and n are measuring electrodes (potential) (Noel, 2014). ...	50
Fig. 23. Most common electrical acquisition arrays (Noel, 2014).	50
Fig. 24. Data acquisition in spectral-induced polarization. (a) A sinusoidal electric current I of period T in a single frequency pis imposed on a medium and the resulting voltage V is measured. The measured voltage is characterized by a phase lag in time relative to the excitation current. (b) Resistivity and phase spectrum. The ratio of voltage $ V $ to current $ I $ multiplied by the geometric factor, K , expresses the magnitude (amplitude) of the complex resistivity of the medium, where both its magnitude and the phase depend on the specific electrical properties of the sample (Ghorbani, 2007).	51
Fig. 25. Data acquisition in the time domain induced polarization (TDIP) method. The voltage decay after excitation by a current pulse is measured (Ghorbani, 2007).	52
Fig. 26. Sketch of the distribution of the ionic species in the pore space of a charged porous medium at equilibrium (Revil and Florsch, 2010).	52
Fig. 27. Preliminary tests to find the best solution portions for non-polarizable electrodes, a) top view of the test box, b) position of different non-polarizable electrodes in a glass tray, c) one of the injection points and d) electrodes portions written in an electrode	60
Fig. 28. Length of copper wire and cap position.....	61
Fig. 29. Position of cutting of the narrow part of the pipette cone.....	61
Fig. 30. The different steps to make Cu/CuSO ₄ electrodes (see text for details).....	62
Fig. 31. The frequency series of resistivity before and after an experiment in a cell	62
Fig. 32. SIP lab IV and connected cables.....	63
Fig. 33. Schematic of experimental setup (lengths are in cm). a) Geometry of a cell and a column with the position of TDRs, current (A and B) and potential (M and N) electrodes. Each bracket indicates a measurement in a sample. b) Experimental setup including water and DNAPL reservoirs and sample.....	64
Fig. 34. a) Schematic of a cross section of a cell with exact positioning of TDR and the other elements and b) a photo from inside a cell.....	65
Fig. 35. Sets of test cells and columns	66
Fig. 36. Experimental setup for determining water and DNAPL saturation and geophysical parameters inside the samples (cells or columns) (Mayer, 2005)	69
Fig. 37. 5TE components (5TE manual “METER group”).....	70
Fig. 38. Pigtail wiring and wiring diagram of a TDR 5TE (5TE manual “METER group”)...	72
Fig. 39. The TDR calibration curve according to the air and water relative permittivity.....	73
Fig. 40. Schematic of experimental setup (lengths are in cm). a) Geometry of a cell and a column with the position of TDRs, current (A and B) and potential (M and N)	

electrodes. Each bracket indicates a measurement in a sample. b) Experimental setup including water and DNAPL reservoirs and sample.....	87
Fig. 41. Variations of relative permittivity as a function of temperature for pure products: CS, CT, water, GB+CS, GB+CT and GB+water.	90
Fig. 42. Change in relative permittivity as a function of temperature for a) CS and b) CT after drainage (80% DNAPLs and 20% water) and imbibition (92% water and 8% DNAPLs) compared to the pure products.	91
Fig. 43. Variation of (a) resistivity and (b) phase as a function of temperature at 1.46 Hz for pure products: CS, CT, water, GB+CS, GB+CT and GB+water.	93
Fig. 44. Changes in electrical resistivity (a and b) and phase (c and d) as a function of temperature at 1.46 Hz for CS and CT after drainage (80% DNAPLs and 20% water) and after imbibition (92% water and 8% DNAPLs) compared to the pure products.	97
Fig. 45. SIP response and comparison between resistivity and phase spectra of samples with (a) CT and (b) GB+CT as a function of temperature.	98
Fig. 46. Fitting of experimental data of relative permittivity with three empirical models (Lide, 2008; Weast, 1986; Malmberg and Maryott, 1956)	99
Fig. 47. Mixing model of experimental data of relative permittivity for different multiphase systems.....	101
Fig. 48. (a) An example of using linear regression to obtain α value for water (b) comparison between α values obtained for water ($R^2=0.9964$), GB+water ($R^2=0.9937$), CT ($R^2=0.9522$), GB+CT ($R^2=0.9538$), CS ($R^2=0.9824$) and GB+CS ($R^2=0.9734$) for $f=1.46$ Hz.	102
Fig. 49. Cole-Cole parameters as a function of temperature for CT, with and without GB. .	103
Fig. 50. Schematic cross-section of a site polluted by DNAPL during DNAPL pumping....	106
Fig. 51. Time domain of relative permittivity and temperature for pure products for a) water and GB+water, b) CT and GB+CT and c) CS and GB+CS.	108
Fig. 52. Time domain of relative permittivity and temperature after imbibition for a) GB+CS and b) GB+CT.	109
Fig. 53. Time domain of relative permittivity and temperature after drainage for a) GB+CS and b) GB+CT.	109
Fig. 54. Evolution of resistivity with time for pure products, a) water and GB+water, b) CS and GB+CS and.....	110
Fig. 55. Evolution of resistivity with time after drainage for a) GB+CT and b) GB+CS at 1.46 Hz	111
Fig. 56. Evolution of resistivity with time after imbibition for a) GB+CS and b) GB+CT at 1.46 Hz	111
Fig. 57. SIP response of resistivity and phase spectra of samples with (a and b) CT+water and (c and d) CO+SE as a function of saturation change, for the first cycle of drainage and imbibition.....	124
Fig. 58. Time series of SIP responses of cells with a and b) for resistivity and phase of CT+water and c) resistivity of CO+SE at $f=1.46$ Hz	125
Fig. 59. Correlation curves of relative permittivity and (a) water saturation and (b) SE saturation fitted by CRIM model. Yellow point: beginning of experiment (beginning of the first drainage), red point: residual saturation and black point: irreducible saturation.....	126

Fig. 60. Correlation curves of resistivity and (a) water saturation and (b) SE saturation fitted by generalized Archie's law. Yellow point: beginning of experiment (beginning of the first drainage), red point: residual saturation and black point: irreducible saturation.....	128
Fig. 61. Correlation curve of phase and water saturation with linear fitting at 1.46 Hz	129
Fig. 62. Evolution of Cole-Cole parameters as a function of water saturation for CT+water	132
Fig. 63. Time series of phase shift in CO+SE cell	134
Fig. 64. Time series of SIP response in the second cell of CT+water. a) resistivity and b) phase shift.....	135
Fig. 65. Schematic of the (a) front, (b) top and (c) back of the 2D tank with the description of each element.....	140
Fig. 66. Schematic of a typical three-phase flow (air, LNAPL and water) during pumping LNAPL in field studies.	142

List of Tables

Table 1: Some of the most common mixing models for electrical conductivity in porous media (Glover, 2015).	44
Table 2. Models, equivalent circuits and complex resistivity proposed for SIP (in chronological order) (Dias, 2000).	55
Table 3. Dimensions of 5TE	70
Table 4. Range of variations and resolutions of measuring parameters.....	73
Table 5. All experiments were done for this study	74
Table 6. Physical characteristics of the DNAPL (CT and CS) used in experiments at 20°C ..	86
Table 7. SIP spectra elements of resistance (Ω), phase ($^{\circ}$), error resistance (%) and error phase ($^{\circ}$) for CT.....	95
Table 8. The number of samples and measurements for each stage	96
Table 9. Relative permittivity at 20°C (ϵ_{20}^{\prime}) and coefficients of a, b and (R2) (Equation 4-5) for different multiphase media used in this study.....	100

This page has been intentionally left blank

8 Appendix A: Experimental protocol

8.1 Procedure to switch the column to the tank

At first SIP-LAB-III software should be turned off if there will be a problem, using task manager is the best way to solve it! Then, please follow the below steps respectively,

- 1) On the folder c:\Program Files\SIP-LAB-IV280616
 - a. **Select the five following files :** “SIP-LAB-IV.dat“ ; “SIP-LAB-IV.txt“ ; “SIP-LAB-IV.ini“; “SIP-LAB-IV.res“; “SIP-LAB-III.err“
 - b. **CUT these files**
- 2) Go to the folder c:\Program Files\SIP-LAB-IV280616\tmpmeasurecolumn
- 3) Paste these files.
- 4) Rename the file “SIP-LAB-IV.dat“ to “SIP-LAB-IVYYMMDD.dat“ with **YY** = Years (17), **MM** current month and **DD** current day, for example for the first day of September it will be: “SIP-LAB-IV170901.dat”
- 5) Go to c:\Program Files\SIP-LAB-IV280616\tmpmeasuretank folder
 - a. **select the following files :**“SIP-LAB-IV.txt“ ; “SIP-LAB-IV.ini“; “SIP-LAB-IV.res“; “SIP-LAB-IV.err“
 - b. **CUT these files**
- 6) Go to c:\Program Files\SIP-LAB-IV280616 folder
- 7) Paste these files
- 8) Turn on SIP-LAB-III software, click on the executer button. (Figure A- 1)

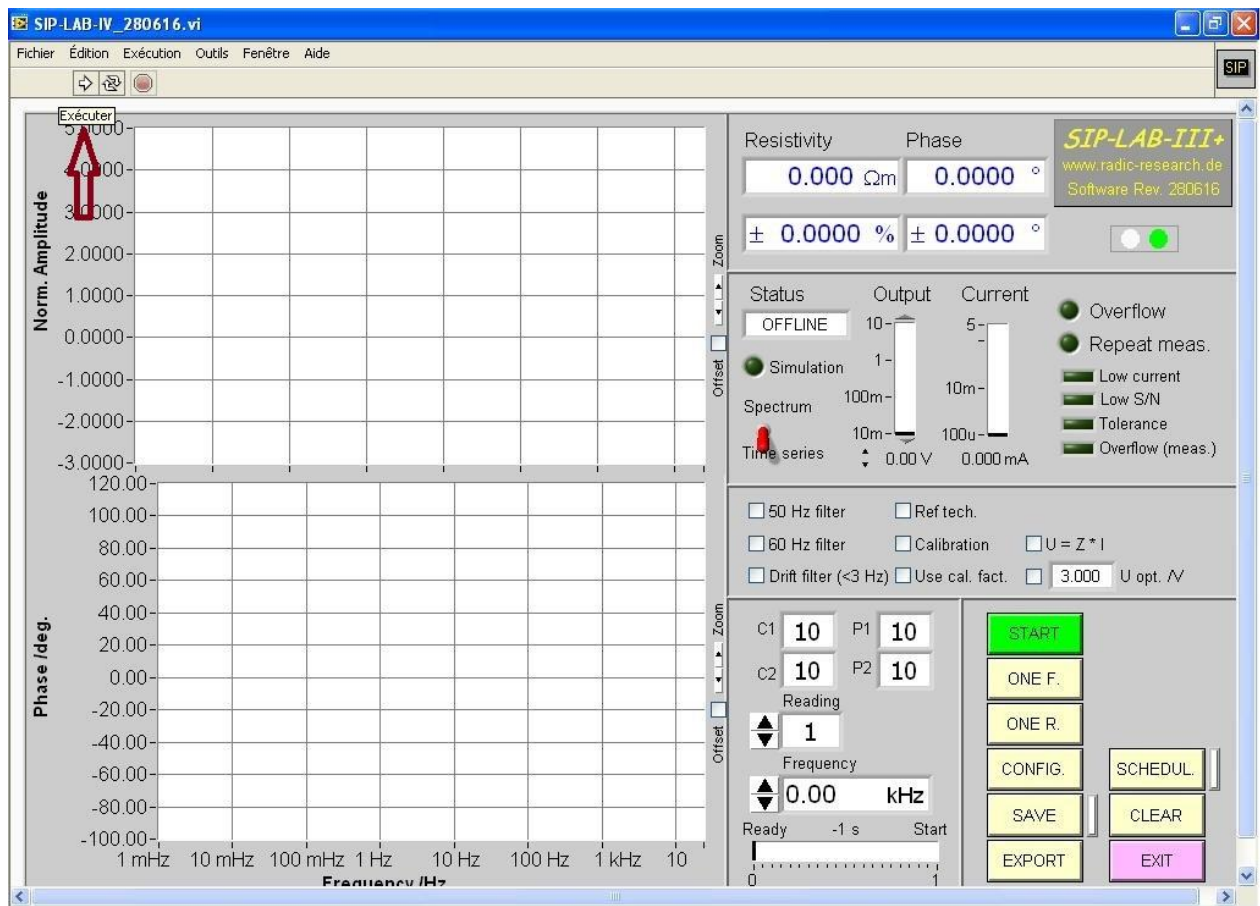


Figure A- 1: Position of executer button

9) On the configuration menu (Figure A- 2)

- a. Select $f_{min}=730$ mHz and $f_{max} = 20$ kHz ($f_{min}=1.46$ Hz and $f_{max}=2.93$ Hz for fast procedure).
- b. Be sure that the save time filter is on

Fichier Édition Exécution Outils Fenêtre Aide

CONFIGURATION

<div> <div>20.00 kHz FMAX</div> <div>732.42 mHz FMIN</div> </div>	<div>0.6002 Rel. amplitude</div> <div>300.00 Shunt resistor /Ω</div> <div>10.000 MaxOutputVoltage /V</div> <div>1.0000 K factor /m</div> <div>5.0000 I_{max} /mA</div> <div>2.5000 U_{opt} /V</div>	<div>5 COMPort</div> <div>1 RRU</div> <div>10 MUX</div> <div>Simulation</div>																				
<div>1.00 Tol. N*dr</div> <div>0.10 Min. current /mA</div> <div>10.00 Amplitude tolerance /Ohm</div> <div>0.00 Phase tolerance /°</div>	<div>1 Reading</div> <table border="1"> <thead> <tr> <th></th> <th></th> <th>z /m</th> <th>Phi /°</th> </tr> </thead> <tbody> <tr> <td>C1</td> <td>61</td> <td>61.00</td> <td>0.00</td> </tr> <tr> <td>C2</td> <td>91</td> <td>91.00</td> <td>0.00</td> </tr> <tr> <td>P1</td> <td>10</td> <td>10.00</td> <td>10.00</td> </tr> <tr> <td>P2</td> <td>20</td> <td>20.00</td> <td>0.00</td> </tr> </tbody> </table>			z /m	Phi /°	C1	61	61.00	0.00	C2	91	91.00	0.00	P1	10	10.00	10.00	P2	20	20.00	0.00	<div>Comment</div> <div>Spectral Induced Polarization</div> <div>ON Save time series</div> <div>ON 50 Hz filter</div> <div>OFF 60 Hz filter</div> <div>OFF Drift filter</div> <div>SCHEDULE</div> <div>EXIT</div>
		z /m	Phi /°																			
C1	61	61.00	0.00																			
C2	91	91.00	0.00																			
P1	10	10.00	10.00																			
P2	20	20.00	0.00																			

Export

Figure A- 2: Configuration menu

- c. On Schedule (Figure A- 3), time interval is equal to 25 minutes (it is 1 for fast procedure)

SCHEDULER

<div>Start time /d.m.y h:m:s</div> <div>07.09.17 16:57:00</div>	<div>Present time /d.m.y h:m:s</div> <div>08/12/2017 13:35:00</div>	<div>Start times /d.m.y h:m:s</div> <div>07/09/2017 16:57:</div> <div>07/09/2017 17:22:</div> <div>07/09/2017 17:47:</div> <div>07/09/2017 18:12:</div> <div>07/09/2017 18:37:</div> <div>07/09/2017 19:02:</div> <div>07/09/2017 19:27:</div> <div>07/09/2017 19:52:</div>
<div>8000 Number of cycles</div> <div>25.00 First interval /min</div> <div>1.00 Interval growth</div> <div>0.00 Delay frequency /s</div> <div>0.00 Delay reading /s</div>	<div>08/12/2017 13:32:00</div> <div>0.10 Length of cycle /min</div>	

EXIT

Figure A- 3: Schedule menu

- 10) Click on the exit to go to the configuration menu, then click on the exit button

- 11) On SIP-measurement mode (Figure A- 4)
 - a. Unselect all option (50 Hz, 60 Hz, ...)
 - b. Click on the “schedule” button
 - c. Choose 6 V as the output voltage
 - d. Click on the schedule button

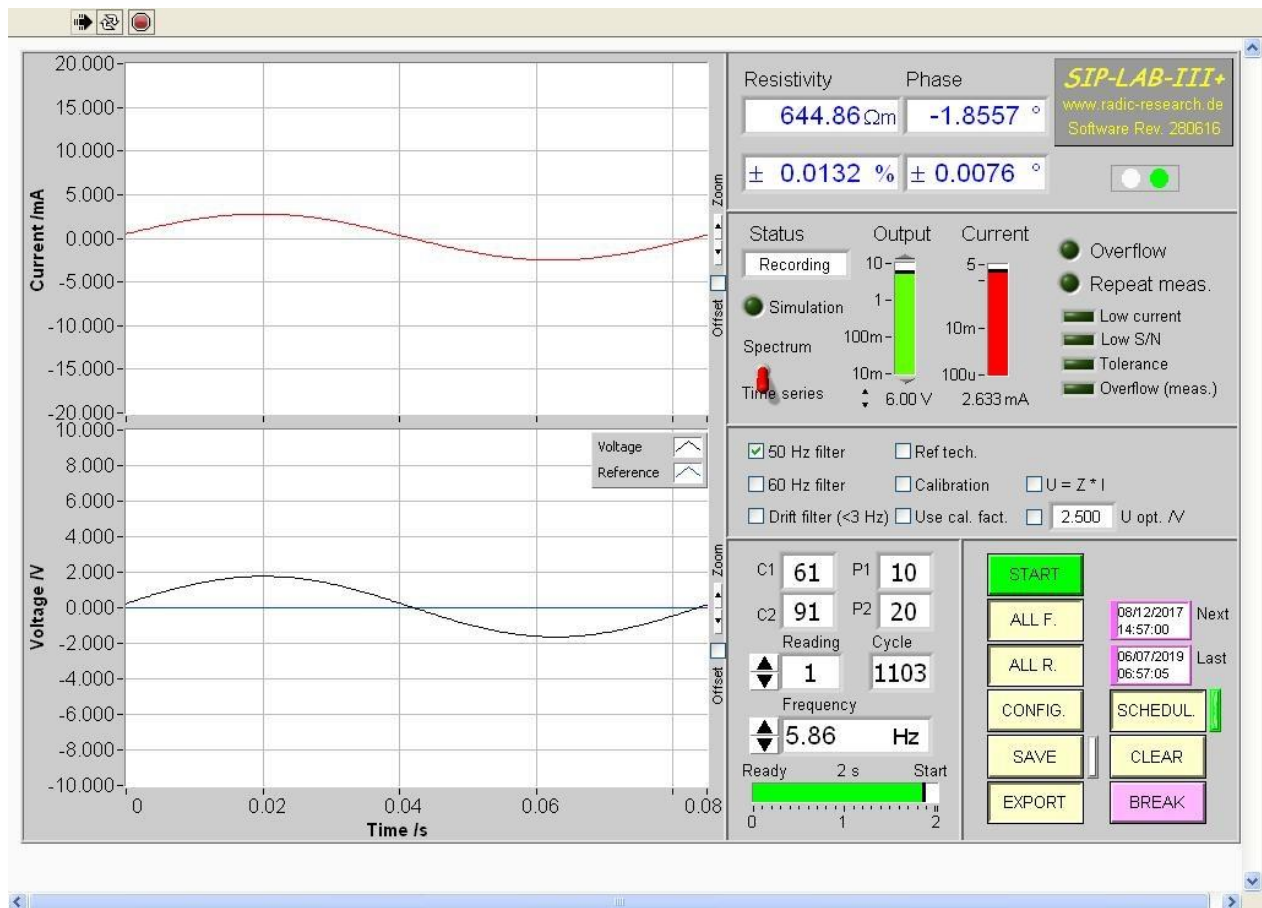


Figure A- 4: SIP main window

8.2 Procedure to switch the tank to the columns

At first SIP-LAB-III software should be turned off if there will be a problem, using task manager is the best way to solve it! Then, please follow the below steps respectively,

- 1) On the folder c:\Program Files\SIP-LAB-IV280616
 - a. **Select at least the five following files :** “SIP-LAB-IV.dat“ ; “SIP-LAB-IV.txt“ ; “SIP-LAB-IV.ini“; “SIP-LAB-IV.res“; “SIP-LAB-III.err“
 - b. **CUT these files**
- 2) Go to the folder c:\Program Files\SIP-LAB-IV280616\2Dtank_expX_YYMMDD
- 3) Paste these files.

- 4) Rename the file “SIP-LAB-IV.dat”to “SIP-LAB-IVYYMMDD.dat”with **YY** = Years (17), **MM** current month and **DD** current day, for example for the first day of September it will be: “SIP-LAB-IV170901.dat”.
- 5) Go to c:\Program Files\SIP-LAB-IV280616\ tmpmeasurecolumn folder
 - a. **select the following files** : “SIP-LAB-IV.txt” ; “SIP-LAB-IV.ini” ; “SIP-LAB-IV.res” ; “SIP-LAB-IV.err”
 - b. **CUT these files**
- 6) Go to c:\Program Files\SIP-LAB-IV280616 folder
- 7) Paste these files
- 8) Turn on SIP-LAB-IV software, click on Executer button. (Figure A- 5)

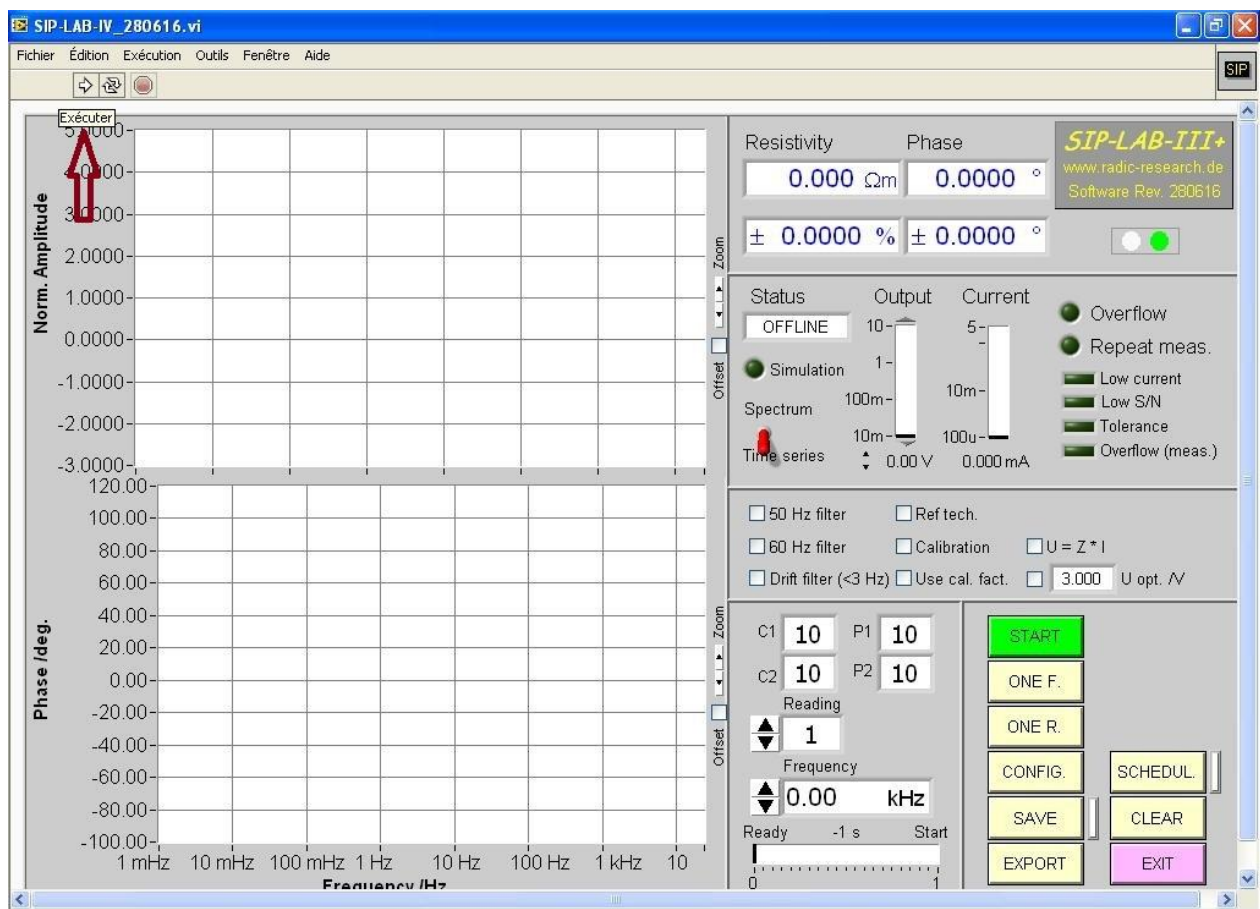


Figure A- 5: Position of executer button

- 9) on the configuration menu (Figure A- 6)
 - a. Select fmin=183.11 mHz and fmax = 20 kHz
 - b. Be sure that Save time filter is on

Fichier Édition Exécution Outils Fenêtre Aide

CONFIGURATION

20.00 kHz FMAX 183.11 mHz FMIN	0.6002 Rel. amplitude 300.00 Shunt resistor / Ω 10.000 MaxOutputVoltage /V 1.0000 K factor /m 5.0000 I _{max} /mA 2.5000 U _{opt} /V	5 COMPort 1 RRU 10 MUX Simulation																				
1.00 Tol. N*dr 0.10 Min. current /mA 10.00 Amplitude tolerance /Ohm 0.00 Phase tolerance /°	1 Reading <table border="1"> <thead> <tr> <th></th> <th></th> <th>z /m</th> <th>Phi /°</th> </tr> </thead> <tbody> <tr> <td>C1</td> <td>61</td> <td>61.00</td> <td>0.00</td> </tr> <tr> <td>C2</td> <td>91</td> <td>91.00</td> <td>0.00</td> </tr> <tr> <td>P1</td> <td>10</td> <td>10.00</td> <td>10.00</td> </tr> <tr> <td>P2</td> <td>20</td> <td>20.00</td> <td>0.00</td> </tr> </tbody> </table>			z /m	Phi /°	C1	61	61.00	0.00	C2	91	91.00	0.00	P1	10	10.00	10.00	P2	20	20.00	0.00	Comment Spectral Induced Polarization ON Save time series ON 50 Hz filter OFF 60 Hz filter OFF Drift filter SCHEDULE EXIT
		z /m	Phi /°																			
C1	61	61.00	0.00																			
C2	91	91.00	0.00																			
P1	10	10.00	10.00																			
P2	20	20.00	0.00																			

Export

Figure A- 6: Configuration menu

c. On the schedule (Figure A- 7), time interval is equal to 120 minutes

SCHEDULER

Start time /d.m.y h:m:s 07.09.17 16:57:00 8000 Number of cycles 120.00 First interval /min 1.00 Interval growth 0.00 Delay frequency /s 0.00 Delay reading /s	Present time /d.m.y h:m:s 08/12/2017 13:36:43 Present time /d.m.y h:m:s 08/12/2017 12:57:00 0.10 Length of cycle /min	Start times /d.m.y h:m:s 07/09/2017 16:57: 07/09/2017 18:57: 07/09/2017 20:57: 07/09/2017 22:57: 08/09/2017 00:57: 08/09/2017 02:57: 08/09/2017 04:57: 08/09/2017 06:57: EXIT
---	---	--

Figure A- 7: Schedule menu

10) Click on the exit to go to the configuration menu, then click on the exit button

- 11) On the SIP-measurement mode (Figure A- 8)
 - a. Unselect all option (50 Hz, 60 Hz, ...)
 - b. Click on “Schedule” button
 - c. Choose 6 V as the output voltage

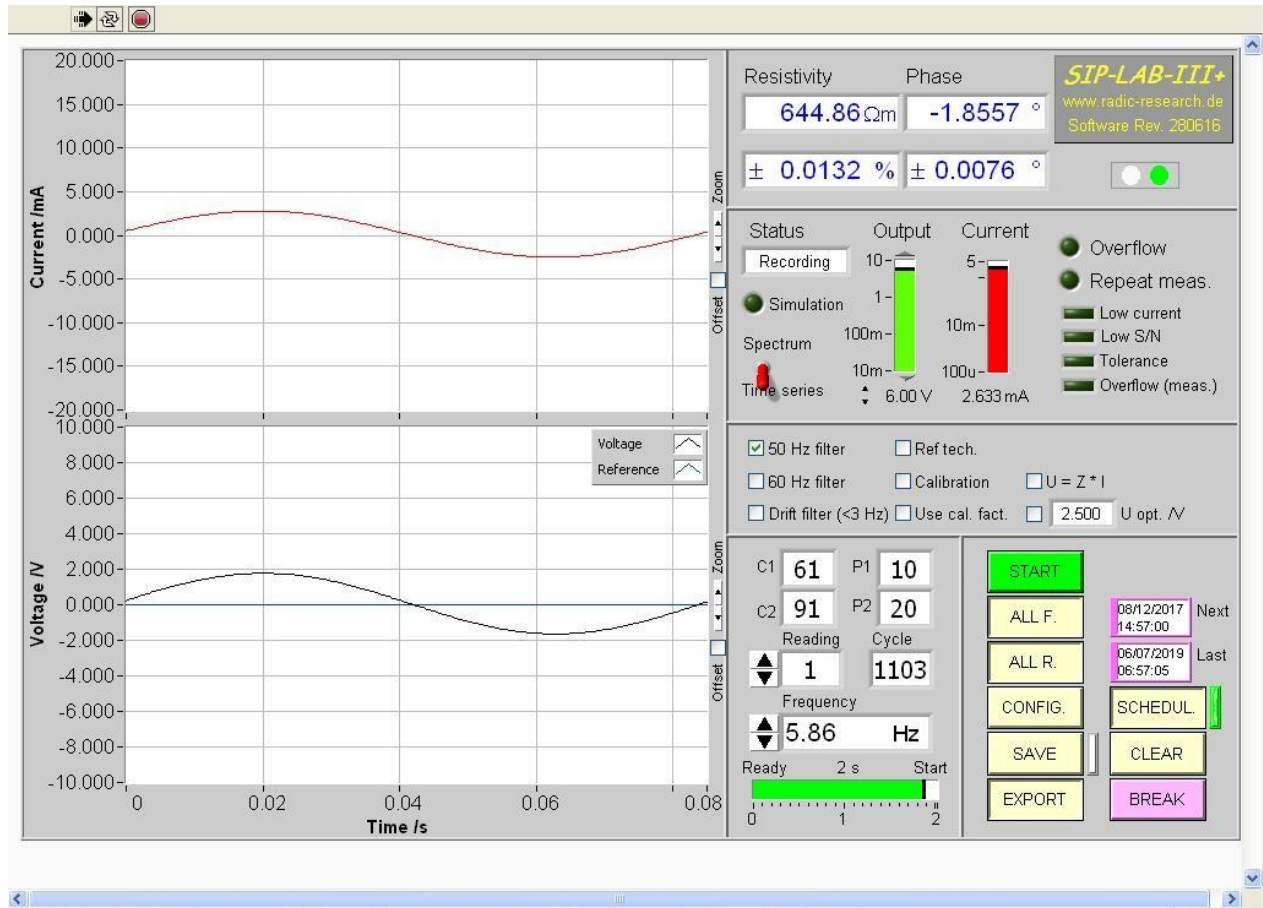


Figure A- 8: SIP main window

8.3 TDRs' Numbers

Table A- 1 is the Number of TDRs and the number of the permittivity on the Loggernet software for the columns.

Columns' name	TDR wire Number	Permittivity on the Loggernet
Wyoming	679	K(22)
Alaska	828	K(21)
Robert	681	K(23)
Pierre	676	K(24)
Dakota (Down to top)	652	K(25)
Dakota (Down to top)	823	K(26)
Dakota (Down to top)	807	K(27)
Nunavut (Down to top)	655	K(28)
Nunavut (Down to top)	814	K(29)
Nunavut (Down to top)	680	K(30)

Table A- 1: TDRs' information for the columns

8.4 Connecting the tank to SIP-lab IV

Figure A- 9 is the number of wires to be connected to the tank,

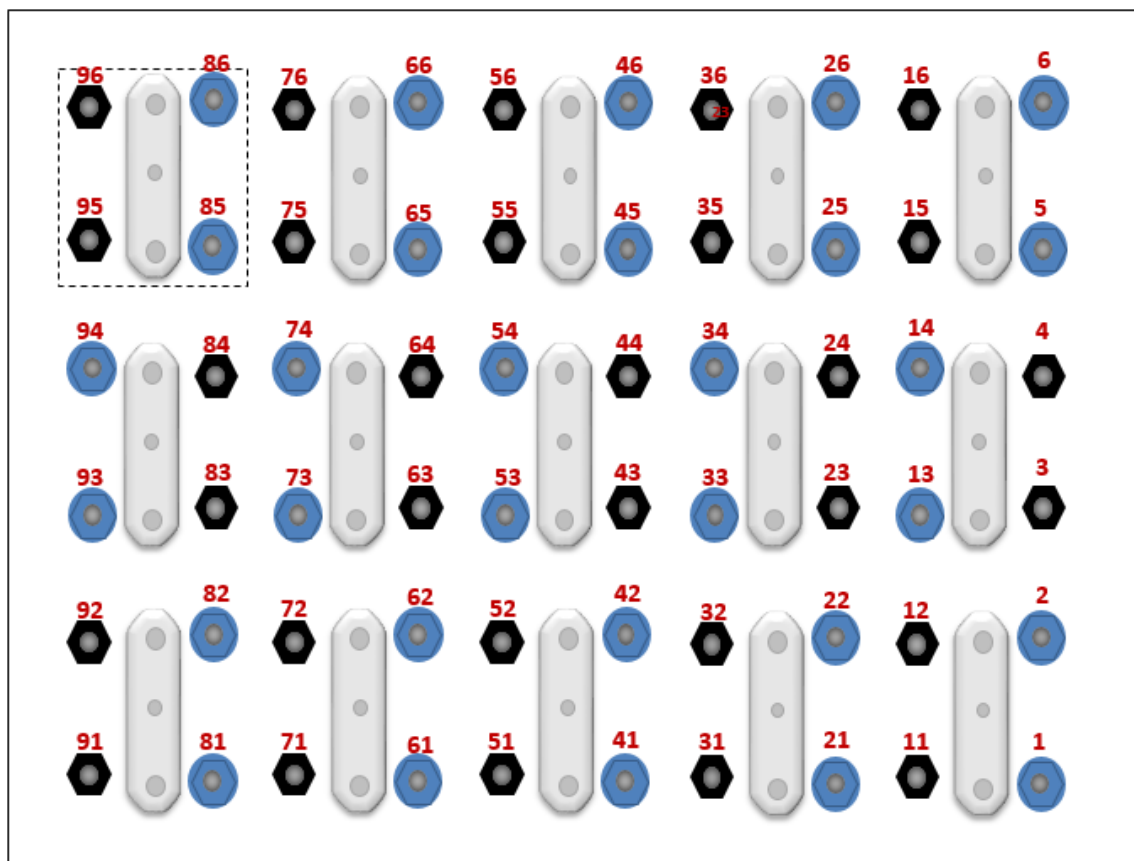


Figure A- 9: number of wires for the tank (back view)

Table A- 2 is the equivalent SIP number for each wire number,

Number of wires	Number of SIP plug	Number of wires	Number of SIP plug	Number of wires	Number of SIP plug
1	1	11	22	21	3
2	11	12	32	22	13
3	21	13	42	23	23
4	31	14	52	24	33
5	41	15	62	25	43
6	51	16	72	26	53

Number of wires	Number of SIP plug	Number of wires	Number of SIP plug	Number of wires	Number of SIP plug
31	24	41	5	51	26
32	34	42	15	52	36
33	44	43	25	53	46
34	54	44	35	54	56
35	64	45	45	55	66
36	74	46	55	56	76

Number of wires	Number of SIP plug	Number of wires	Number of SIP plug	Number of wires	Number of SIP plug
61	7	71	28	81	9
62	17	72	38	82	19
63	27	73	48	83	29
64	37	74	58	84	39
65	47	75	68	85	49
66	57	76	78	86	59

Number of wires	Number of SIP plug
91	30
92	40
93	50
94	60
95	70
96	80

Table A- 2: Proper SIP and wire numbers

8.5 Some important points:

1. For the tank, (fast procedure)

- i. During the pumping and injecting of DNAPL because of the rapid changes, f_{min} and f_{max} should change respectively to 1.46 Hz and 2.93 Hz and first interval is 1 min.
- ii. In many cases there is no “SIP-LAB-III.err” file.
- iii. Before the first white test, the conductivity value and the temperature should be reported on readme file.

2. For the columns,

- i. The number of wires for each column increase from bottom to the top
- ii. Be sure that all columns works well. The right sequence numbers are:

```
1 61 91 10 20 1.000000E+0 -> Column 1 (Wyoming)
2 63 93 73 83 1.000000E+0 -> Column 2 (Alaska)
3 65 95 75 85 1.000000E+0 -> Column 3 (Robert)
4 67 97 77 87 1.000000E+0 -> Column 4 (Pirès)
5 69 79 88 98 1.000000E+0 -> Column 5 (Dakota), the first measurement
6 69 79 98 89 1.000000E+0 -> Column 5 (Dakota), the second measurement
7 69 79 89 99 1.000000E+0 -> Column 5 (Dakota), the third measurement
8 69 79 99 90 1.000000E+0 -> Column 5 (Dakota), the fourth measurement
9 69 79 90 100 1.000000E+0 -> Column 5 (Dakota), the fifth measurement
10 69 79 98 90 1.000000E+0 -> Column 5 (Dakota), the sixth measurement
11 8 12 92 81 1.000000E+0 -> Column 6 (Nunavut), the first measurement
11 8 12 81 94 1.000000E+0 -> Column 6 (Nunavut), the second measurement
11 8 12 94 82 1.000000E+0 -> Column 6 (Nunavut), the third measurement
11 8 12 82 96 1.000000E+0 -> Column 6 (Nunavut), the fourth measurement
11 8 12 96 89 1.000000E+0 -> Column 6 (Nunavut), the fifth measurement
11 8 12 81 96 1.000000E+0 -> Column 6 (Nunavut), the sixth measurement
```

- iii. If one column does not work well, please replace the sequence of the given column with one another with well performance on .ini file.
- iv. Table (3a to 3f) is the equivalent SIP number for each wire number for the columns,
- v. For Wyoming:
- vi.

Number of wires	Number of SIP plug
17	61
18top	91
7	10
8	20

For Alaska:

Number of wires	Number of SIP plug
57t	63
58	93
39	73
40	83

For Robert:

Number of wires	Number of SIP plug
27	65
30t	95
28	75
29	85

For Pirès:

Number of wires	Number of SIP plug
70	67
100t	97
79	77
80	87

For Dakota:

Number of wires	Number of SIP plug
9	69
99t	79
10	88
59	98
60	89
69	99
97	90
98	100

For Nunavut:

Number of wires	Number of SIP plug
50	8
88t	12
38	18
37	6
19	16
20	4
67	14
47	2

Table A- 3: Numbers of SIP plugs and their wires'

3. For the tank and the columns,

- i. The experiments have 4 steps,
 - a. White test (Just water) for 12 hours
 - b. White test (Water + glass beads) for 12 hours
 - c. Main experiment (water + glass beads + DNAPL)
 - d. White test (Just water) for 12 hours
- ii. Plugging the proper SIP wire with the correct number and also the correct TDR are the most important point to get the precise and true results.

- iii. All the work, data and the useful details of the work should be noted on **readme.txt** file in the folder c:\Program Files\SIP-LAB-IV280616.

4. **For TDR,**

- i. The Loggernet software should be launched during all the steps of the experiment that mentioned above.
- ii. The Campbell can collect the TDR data for maximum 10 days, so please collect data at least in the period of less than 10 days.
- iii. Before starting the experiment, correctness of performance of each TDR should be checked.
- iv. Please check the TDR results every day.